Nucleic acid-based recognition events in hydrogel array systems

McMaster University
Chemical Engineering Department

Nucleic acid-based recognition events in hydrogel array systems

By Milana Pikula (B.Sc., M.Sc., Spec. Ind. Pharm.)

A Thesis Submitted to the School of Graduate Studies
in Partial Fulfillment of the Requirements for the Degree
Doctor of Philosophy
McMaster University

DOCTOR OF PHILOSOPHY (2024)

McMaster University
Chemical Engineering
Hamilton, Ontario

TITLE: Nucleic acid-based recognition events in hydrogel array systems

AUTHOR: Milana Pikula, B.Sc., M.Sc., Spec. Ind. Pharm. (University of Belgrade, Serbia)

SUPERVISOR: Professor Carlos Filipe and Professor Todd Hoare

NUMBER OF PAGES: XX, 162

Lay Abstract

This thesis describes the integration of hydrogel material with nucleic acids for the development of biosensing platforms in the detection of small molecules. First, a DNA hybridization microarray was developed by integrating printable hydrogel with long-chain DNA sensing material based on a rolling circle amplification (RCA) product. Assembled hydrogel microarray was investigated on the ability to physically encapsulate sensing material and allow for hybridization events with fluorophore-tagged complementary oligonucleotides. The study revealed that a hydrogel-based system improves the hybridization efficiency and detection potential of very short oligonucleotides, a functional benefit that was further investigated in improving the thermodynamic stability of FRET-based structure switching aptamer constructs. The ability of hydrogel microarray to reinforce very short quencher stems while promoting solution-like affinity interactions enabled an enhanced affinity and sensitivity towards the cognate ligands, relative to hydrogel free-system.

Thesis Abstract

Nucleic acids play an important role in the construction of novel biosensing units. Integrating nucleic-acid-diagnostic tools with polymeric assemblies can enhance selectivity and sensitivity and protect them from nuclease digestion. In this thesis, DNA-based sensing molecules are incorporated into hydrogel films based on poly(oligoethylene glycol methacrylate) (POEGMA) to fabricate printable DNA hybridization and DNA aptamer microarrays to detect small molecules.

Firstly, a printable hydrogel microarray incorporating long-chain-sensing DNA generated via a rolling circle amplification reaction was developed to exploit the benefits of isothermal nucleic acid amplification technology and the non-covalent immobilization potential of POEGMA-hydrogel films on a nitrocellulose substrate. Fluorophore-labelled nucleic acid analytes of varying sizes were spotted on hydrogel-trapped RCA sensing units and assessed on their ability to detect specific DNA hybridization events. Compared to hydrogel-free sensors, the developed sensors provided greater detection potential for small oligonucleotides while also enabling uniform spot-to-spot fluorescence signal distribution from the sensing analytes.

The hydrogel's ability to increase base-pairing affinity in short DNA duplexes was further investigated using fluorescence resonance energy transfer (FRET)-based structure-switching aptamers that bind adenosine triphosphate (ATP). Moderate thermal stabilization was observed in the hydrogel matrices embedding FRET-based structure-switching aptamer constructs (SSAC) assembled with quencher stems having lengths of $\leq$ 10-bp. The combination of a water-swollen/flexible matrix and the thermal stabilization capabilities of the POEGMA polymeric matrix endowed the hydrogel-immobilized aptamer reporters with greater sensitivity compared to hydrogel-free systems.

The developed hydrogel-based aptamer sensor was then translated into a printable nitrocellulose-supported microarray format, with additional modulation of the SSAC configuration. DNA microarrays with even greater sensitivity were produced by rationally positioning and further shortening the quencher-stems to 7-bp using the optimized assay conditions. In addition to effective immobilization and ligand-binding affinity comparable to the native aptamer, the hydrogel interface provided protection against nucleases and supported applications using real biological samples (*i.e.,* in human serum).

Acknowledgment

I would like to thank Professors Carlos Filipe and Todd Hoare, for giving me the opportunity to do what I love and providing me with the support and guidance over the entire course of my PhD program.
I highly appreciate all your advice and recommendations that helped me become a better scientist and improve my scientific writing and presentation skills, while as well, teaching me patience, humbleness and kindness, throughout different challenging situations along the way.

Dr. Yingfu Li is highly appreciated for supporting us at supervisory committee meetings and offering us precious recommendations for our project, empowered by his great experience and expertise in the field.

Dr. Monsur Ali is acknowledged for helpful suggestions in development of our first experimental chapter, designing the RCA product-DNA sequences and for the technical support in the lab over the years. Mrs. Marcia Reid is acknowledged for her kindness, helpful discussions and acquiring the SEM images, while Mitchel Johnson from Dr. Stover's Lab for assistance in confocal microscopy data acquisition, used in our first experimental chapter.

I also highly acknowledge the current and former Biointerfaces Institute personnel for providing technical support and facilities in conducting the majority of the experimental work, in particular, Dr. Marta Prinz, Mrs. Dawn White, Mrs. Leanne Brown, Dr. Mehdi Keramane and my dear friend Dr. Julijana Milojević.

Former and current members of Filipe Lab and Hoare Lab are highly appreciated for their in-lab generous help over the years. In particular, I would like to acknowledge AlexandreD'Sousa for kindly providing necessary training for the experimental procedures, sharing detailed insights into performing various DNA-purification and amplification assays, including the help in programming the PCR machine for DNA melting assays; Dr. Zhicheng Pan for assistance with polymer characterization and synthetic protocols; Dr. Fei Xu for helpful discussions on hydrogels stability; Dr. Rabia Mateen for training me on hydrogel printing, use of high-throughput equipment and troubleshooting discussions on our first experimental chapter; Dr. Matt Campea for his kindness and continuous help in acquiring NMR data, as well as Ridhdhi Dave for assistance in acquiring GPC data; Nahieli Preciado Rivera for acquiring hydrogel rheological data and Dr. Lisha Zhao for being a lovely office-mate.

Finally, I would like to thank my family and my friends for loving me, believing in me, and supporting me through some of the hardest of times.
In particular I would highly acknowledge my friends Dr. Darko Ljubić and Marina (Ilinka) Mirković for their support at the beginning of my program, and for being one of the kindest of souls; Dr. Ivana Poštić for her cheerful spirit and optimism, as well as many other members of our Serbian community in Canada (especially to my dear Duško Janjić) who welcomed and supported me throughout the years.

Thank you!

I dedicate this thesis to my beloved family (my father Milenko, my late mother Radmila, my sister Petra Paovica and my late brother Anđelko) who are my true soulmates for a lifetime!

"Слава нашем Богу, због свега и за све."

Table of Contents

List of Figures

Chapter 1.

Chapter 2.

Chapter 2 Supporting Information – Appendix

Chapter 3.

Chapter 3 Supporting Information – Appendix

Chapter 4.

Chapter 4 Supporting Information – Appendix

List of Tables

Abbreviations

A:	Aldehyde
AA:	Acrylic acid
ADH:	Adipic acid dihydrazide
AFQ	Tripartite aptamer reporter (*i.e.,* Duplexed aptamer construct)
AIBME:	2,2-Azobisisobutryic acid dimethyl ester
ATP	Adenosine 5'-triphosphate
BHQ	Black hole quencher
BSA:	Bovine serum albumin
CT-DNA:	Circular DNA template
CTP:	Cytidine 5’-triphosphate
DIW:	Deionized water
DMAEMA:	N,N-dimethylaminoethyl methacrylate
DMSO:	Dimethyl sulfoxide
DNA:	Deoxyribonucleic acid
DNase:	Deoxyribonuclease
dNTPs:	2'-deoxyribonucleoside 5'-triphosphates
dPAGE:	Denaturing polyacrylamide gel electrophoresis
dsDNA:	Double-stranded DNA
EDC:	N-3-dimethylaminopropyl-N-ethyl carbodiimide
FA	Fluorescent Aptamer Construct
F-DNA:	Fluorophore-labeled DNA
FITC:	Fluorescence isothiocyanate
FNAs:	Functional nucleic acids
FRET:	Fluorescence resonance energy transfer
GO:	Graphene oxide
GPC:	Gel permeation chromatography
GTP:	Guanosine 5’-triphosphate
H:	Hydrazide
HCl:	Hydrochloric acid
HG:	Hydrogel
HF:	Hydrogel Film
HPLC:	High performance liquid chromatography
ITC:	Isothermal titration calorimetry
Kd:	Dissociation constant
LT-DNA	Linear DNA Template
Mn:	Number average molecular weight
Mw:	Mass average molecular weight
NaCl:	Sodium chloride
NaOH:	Sodium hydroxide

NMR:	Nuclear magnetic resonance spectrometry
nt:	Nucleotide
OEG:	Oligo(ethylene glycol)
PBS:	Phosphate buffered saline
PBST:	Phosphate buffered saline with Tween-20
PCR:	Polymerase chain reaction
PEG:	Poly(ethylene glycol)
PNIPAM:	Poly(N-isopropylacrylamide)
PNK:	Polynucleotide kinase
PO:	Poly(oligoethylene glycol methacrylate)
POA:	Aldehyde-functionalized poly(oligoethylene glycol methacrylate)
POH:	Hydrazide-functionalized poly(oligoethylene glycol methacrylate)
Pr-DNA:	Primer-DNA
Q-DNA:	Quencher-labeled DNA
RCA:	Rolling circle amplification
RNA:	Ribonucleic acid
RNase:	Ribonuclease
S:	Solution
SELEX	Systematic evolution of ligands by exponential enrichment
SEM	Scanning electron microscopy
TGA:	Thioglycolic acid
T_m	Melting Temperature
UTP	Uridine 5’-triphosphate
UV:	Ultraviolet
µPAD	Microfluidic paper analytical device

Declaration of Academic Achievement

The work described in this thesis was performed by the author in consultation with Dr. Carlos Filipe and Dr. Todd Hoare.

In the Chapter 2, we collaborated with:

Dr. Monsur M. Ali (Bio Interfaces Institute, McMaster University) who designed the sequences for rolling circle amplification (RCA) product synthesis, suggested the use of fluorophore-tagged complementary oligonucleotides in RCA product detection and suggested the protocol for RCA product purification and with Mrs. Marcia Reid (Canadian Center for Electron Microscopy, McMaster University) who was in charge of acquiring the SEM images.

In the Chapter 3 and 4, we collaborated with:

Dr. Yingfu Li (Department of Biochemistry and Biomedical Sciences, McMaster University) who proposed utilization of FRET structure switching aptamer constructs assembled with shorter quencher stems for improved sensing of small molecules.

Chapter 1. Introduction

1.1. Biomolecular recognition fundamentals

Biomolecular recognition refers to the process of association between two biological molecules: a macromolecule, or molecular assembly (Receptor, R), and a target molecule, or analyte (Ligand, L). The R-L complexation is driven by many weak, non-covalent interactions working in concert, including hydrogen bonding, hydrophobic interactions, van der Waals forces, and π-π and electrostatic interactions.[1]

Biomolecules associate when the attractive forces generated by two interacting species outweigh the repulsive forces, and the entropic penalty to loss in conformational freedom associated with the formation of the R-L assembly. From a thermodynamic perspective, molecular recognition occurs *because* the free energy of the receptor-ligand complex is lower than the sum of free energies of unbound individual species.[2,3] The binding process is reversible and, typically, highly specific, as only "perfect-match" ligands will support a sufficient number of favourable weak interactions for affinity binding.

The specificity of the R-L association is governed by the structure complementarity and binding domain uniqueness in both interacting species, while the affinity of the R-L association is the function of the thermodynamic properties of the binding event.[1] The binding affinity between two molecules, expressed as a dissociation constant (K_d), represents the strength of the molecular interaction, which is determined based on the differences in the relative energy (enthalpy) and entropy in their bound and the unbound state, and not the absolute free energy of the formed complex.[4]

The binding reaction of a ligand (L) to a receptor (R) is described by the following equation:

$$R + L \rightleftarrows R \cdot L \quad (1.1)$$

The binding affinity can be determined as,

$$K_d = \frac{[R][L]}{[R \cdot L]} \quad (1.2)$$

where [R] is the concentration of the free receptor, [L] is the concentration of the free ligand, and [R·L] is the concentration of the receptor-ligand complex upon achieving equilibrium.[5]

Binding affinity as a function of standard Gibbs free energy change upon binding is expressed as,

$$\Delta G^{\circ}_{binding} = RT ln K_d = \Delta H^{\circ}_{binding} - T\Delta S^{\circ}_{binding} \quad (1.3)$$

where R is the gas constant, T is the temperature, $\Delta H^{\circ}_{binding}$ is the change in enthalpy, and $\Delta S^{\circ}_{binding}$ is the change in the entropy component of the binding reaction.[6]

At equilibrium, products are favoured over reactants when $\Delta G°bind < 0$, while reactants are favoured over products when $\Delta G°bind > 0$. A more negative $\Delta G°bind$ value corresponds to stronger spontaneous L-R complexation events. In biological molecular recognition systems, the $\Delta G°$ values are typically -50 kJ/mole for stronger interactions (*e.g.*, enzyme-inhibitor binding) and approximately -17 kJ/mole for the weakest interactions (*e.g.*, protein kinase-ATP binding).[7] Analyzing the changes in the Gibbs free energy reveals the changes in the enthalpy ($\Delta H°_{bind}$) and entropy components ($T\Delta S°_{bind}$) of the binding reaction, thus providing important structural insights into the receptor-ligand interactions.[4]

The environment in which the recognition event occurs plays a critical role in determining the affinity of the binding event.[2] Most biorecognition events occur in aqueous media, as water environments tend to reduce the impact of electrostatic and induction interactions (screening the R-L interactions at distances

greater than the Debye length), thereby positioning hydrophobic effects as the dominant acting force. Hydrophobic effects refer to the entropy-driven complexation of hydrophobic species governed by the desolvation and minimization of interactions between hydrophobic domains and water molecules. Typically, hydrophobic interactions are considered to be the major stabilizing force in biomolecular R-L complexation, while Coulombic electrostatic, hydrogen, and van der Waals forces determine the specificity between the R-L complementary domains, mostly by destabilizing incorrect binding events.[1,2,8]

The binding affinity constant is experimentally obtained *via* a *binding isotherm*, which is a curve that represents the amount of ligand associated with the receptor as a function of the concentration (or partial pressure) of the ligand at a constant temperature.[9] In order to generate a binding isotherm, it is necessary to obtain the signal for the R-L complex concentration, typically *via* spectroscopic, colorimetric, fluorometric or functional assays. The binding isotherm is defined by the fractional saturation, Y, which represents the fraction of the receptor (R) bound with ligand (L) at equilibrium,

$$(1.4) \quad Y = \frac{[R{\cdot}L]}{[R] + [R{\cdot}L]} = \frac{[L]}{K_d + [L]}$$

where [R·L] is the concentration of the receptor-ligand complex, [R] is the concentration of the receptor, [L] is the concertation of the free ligand, and K_d is the binding constant.[10] The binding constant is determined by fitting the obtained data to the theoretical equation model that best fits the complexation system. This equation gives a hyperbolic curve that reveals the point at which the receptor is half saturated with the ligand (*i.e.*, when the ligand concentration is equal to K_d (fractional saturation = 0.5)).[9]

The binding affinity can be measured using one of two methods. The first method entails conducting an equilibrium experiment to determine the extent to which the reaction is a function of the concentration of one of the reactants and analyzing the resultant data to obtain the equilibrium constant, which is used to derive the binding constant.[10] In the second method, a kinetic experiment is conducted to determine the rates of the forward and reverse reactions as functions of the concentration of one of the reactants. Here, the equilibrium—and, subsequently, the binding constant—are obtained by analyzing the ratio between the forward and reverse reactions.[11] Of the two methods, the kinetic approach provides greater insight into the complexation event, revealing the thermodynamic parameter and dynamics of the R-L complex generation. Most of the binding reactions are monitored *via* optical measurements based on absorbance or fluorescence, as the obtained signals are directly proportional to the concentrations of interacting molecules. Conventional binding assays typically rely on monitoring differences in the fluorescence, fluorescence anisotropy, and fluorescence resonance energy transfer (FRET) intensity of the products relative to the reactants.[12–14]

Spectroscopic or calorimetric assay can be used to estimate the thermodynamic parameters of the complexation event.[15] The van't Hoff method allows the indirect spectroscopic calculation of changes in the enthalpy and entropy of binding by measuring the binding constant at different temperatures. According to the van't Hoff equation:

$$(1.5) \quad ln(K_d) = \frac{\Delta H^{\circ}_{binding}}{RT} - \frac{\Delta S^{\circ}_{binding}}{R} = \frac{\Delta G^{\circ}_{binding}}{RT}$$

The linear relationship obtained by plotting ln(K_d) as a function of the reciprocal temperature allows $\Delta H^{\circ}_{binding}$ and $\Delta S^{\circ}_{binding}$ to be calculated based on the slope and *y*-intercept, respectively. The main limitation of van't Hoff analysis is its assumption that the thermodynamic parameters are independent of the temperature, which limits its applicability across biorecognition systems.[16] This issue can be circumvented by employing more precise, calorimetric methods (*e.g.*, isothermal titration calorimetry,

ITC) that allow the independent estimation of $\Delta H^{\circ}_{binding}$ and $\Delta G^{\circ}_{binding}$ based on the non-linear relationship between the heat generated (absorbed or released) in a molecular binding event as a function of the molar ratio of the ligand titrated into the receptor.[17] The change in enthalpy is subsequently determined as:

(1.6) $$- T\Delta S^{\circ}_{binding} = \Delta G^{\circ}_{binding} - \Delta H^{\circ}_{binding}$$

The primary limitation of calorimetric analysis, specifically ITC, is its assumption that the receptor does not undergo ligand-induced conformational change or self-association, thus creating the need for independent single-site or two-site binding mechanism models to fit the experimental data.[18] Furthermore, low-throughput data collection and the consumption of high sample volumes are two additional notable disadvantages of calorimetric measurements compared to spectroscopic van't Hoff based assays.

1.1.1. Molecular recognition in biosensing

Molecular recognition phenomena govern numerous biological processes (*e.g.*, gene expression, enzyme-substrate complexation, and immune response); as such, they have found practical applications across a range of biosensing diagnostic technologies.[19] The sensitive and accurate determination of small molecules (*i.e.*, toxins, drugs, antibiotics, molecular markers, heavy metals, and ions) is particularly important and is becoming a growing need in the pharmaceutical, food safety, and medical diagnostics industries. Conventional small-molecule-detection methods are either based on spectroscopy (*e.g.*, fluorescence polarization or UV absorption), separation (*e.g.*, HPLC, equilibrium dialysis, affinity chromatography), or thin-layer chromatography (TLC) and typically require sophisticated and expensive instrumentation followed by labour-intensive and time-consuming procedures.[20,21]
The use of biosensor devices is an alternative approach that enables cost-efficient, simple, and portable detection, along with high sensitivity and specificity. Biosensors are analytical devices that exploit biomolecular recognition phenomena and utilize biological molecules to detect a target analyte by converting the recognition event into a detectable signal. A basic biosensor assembly consists of a biological receptor, a signal transducer, and a signal processor.[2,20] Biological receptors are typically macromolecules such as enzymes, antibodies, or oligonucleotides that recognize the analyte of interest with high affinity and selectivity and generate an optical, electrochemical, or electrical signal read-out.[20]
Although enzymatic sensors are highly specific, sensitive, and provide rapid and quantitative analyte detection, even in complex biological fluids (through the measurement of catalysis or the inhibition of enzyme activity by a target analyte substrate), they also lack generalizability, as only a limited number of target molecules can serve as a substrate for enzymes applicable in biosensing diagnostics.[20,22]
Immunoassay biosensors use antibodies as bioreceptors to enable high affinity and specific molecular recognition, which has led to their adoption in a wide range of research and clinical areas for the quantification of proteins, biological toxins, and biomarkers.[23] The main limitations of antibodies as molecular recognition elements are their time-consuming and labour-intensive generation process and their lack of specificity for small-molecular targets. Moreover, their high batch-to-batch variability, high production costs, and relatively short shelf life make antibodies non-ideal for on-site diagnostics.[20,24]
Nucleic acids are chemically and thermally more stable than antibodies, particularly deoxyribonucleic acid (DNA)-based recognition elements, which typically exhibit greater resistance to harsh application conditions (e.g., elevated temperatures or pH-values). Furthermore, nucleic acid probes can be easily chemically modified to achieve proper anchoring onto biosensing surfaces or labelled to generate effective signaling read-out when being converted into a molecular recognition tool.[24–26]

1.1.2. Nucleic acids as biosensing diagnostic tools

Nucleic acids, including RNA (ribonucleic acids) and DNA (deoxyribonucleic acids), perform vital biological functions in cells and can act as recognition elements for a variety of molecules.[27] DNA is generally responsible for the storage of hereditary information (*i.e.*, genetic material) and, as such, serves as the template for guiding protein synthesis. RNA is involved in multiple functions in living organisms, including protein synthesis and gene expression regulation. Although single-stranded nucleic acids consist of only four types of structurally similar nucleotides, they are folded into specific three-dimensional structures possessing an array of functionalities (functional oligonucleotides) as a result of different intramolecular interactions (*e.g.*, Watson-Crick type of hydrogen bonding combined with electrostatic forces, π-π stacking, and hydrophobic forces).[2,24,28] These distinct functions are determined by a combination of the basic primary, secondary, and tertiary structure of the oligonucleotides, resulting in large variations even amongst short nucleic acid sequences.[24] Functional nucleic acids can be harnessed as recognition elements against a variety of targets—for example, in nucleic acid sequence analysis and recognition, protein-based manipulations involving nucleic acid amplification, the catalysis of chemical reactions (*e.g.*, DNAzymes), and the recognition of molecules ranging from small ions to proteins or cells (*e.g.*, DNA aptamers)—rendering them a suitable alternative to antibody-based probes in the development of diagnostic devices for experimental and clinical applications.[21,29]
The most common DNA molecular recognition events for biosensing technology are DNA hybridization, DNA isothermal amplification, and DNA ligand binding (Figure 1.1). Therefore, these recognition events will be addressed in this thesis.

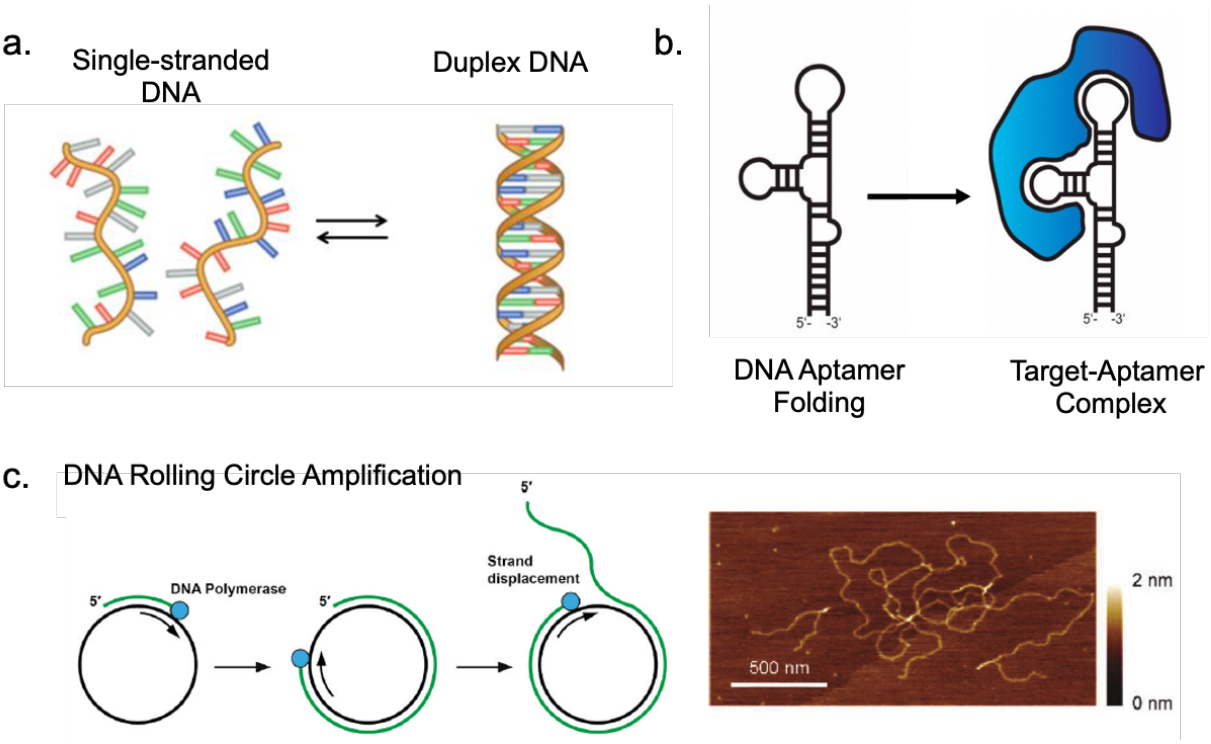

Figure 1.1 Different Nucleic Acid Recognition Events. (a) Nucleic acid hybridization *via* base-pairing, reproduced from Kuriyan *et al.*[7] (b) Nucleic acid aptamer ligand binding, reproduced from Wolter *et al.*[30] (c) Isothermal nucleic acid amplification *via* rolling circle amplification (RCA) reaction, reproduced from Beyer *et al.*[31]

1.1.2.1. Nucleic acid hybridization

Nucleic acid hybridization refers to the process whereby the complementary bases of two single-stranded molecules form a hybrid helical complex following the rule of Watson-Crick base pairing, which entails the formation of hydrogen bonds between the adenine:thymine and cytosine:guanine (A-T and C-G) nitrogen bases.[32,33] Hybridization is a dynamic process that involves many intermediate states that continue until the most energetically favourable hybrid form is achieved. Moreover, since the nitrogen bases are non-polar structures, they may also associate due to a combination of base stacking and hydrogen bonding and electrostatic or van der Waals forces, thereby reducing the area exposed to polar solvents and producing more complex and stabilized structures.[2,34,35] Thus, the stability of DNA hybridizing structures is considered to be a function of several factors, including: (1) the hydrogen bonds between nucleobases, (2) stacking between neighbouring base pairs, (3) entropic penalty due to conformational loss, (4) counterion condensation by the cations from the solvent, and (5) the hydration of the DNA strands.

The stability of the formed DNA hybrids is defined by a melting temperature, T_m, which refers to the temperature at which half of the hybridizing strands are annealed.[34,36] The T_m is quantified from theoretically fitted melting curves obtained from data collected *via* optical UV or fluorescence spectroscopy measurements. The estimated T_m values can be linked to the thermodynamic parameters of hybridization using the van't Hoff equation, which relates the reciprocal melting temperature in Kelvins ($1/T_m$) and the total strand concentration (Ct)[35,37] as follows:

$$(1.7) \quad \frac{1}{Tm} = \frac{R}{\Delta H^\circ} \ln\frac{Ct}{4} + \frac{\Delta S^\circ}{\Delta H^\circ} \quad ; \quad \Delta G^\circ = \Delta H^\circ - T\Delta S^\circ$$

The hybridization conditions that determine the hybridization efficiency and the thermal stability of the corresponding double-stranded DNA complexes are pH, temperature, and ionic strength, as well as the length and degree of complementarity between the annealing strands.[38]

Complementary DNA base pairing is the foundational element of hybridization biosensors. In DNA sensors, sensing probes function as molecular recognition elements with a known nucleotide sequence, typically 20-40 bases long.[26,28,39] DNA hybridization assays can be performed under solid-phase or solution-phase conditions, depending on whether the sensing probe is surface-tethered or randomly distributed in the solution. Since both hybridization assays are distinct in terms of their thermodynamic and kinetic behaviors, the development of new interfacial hybridization technologies requires a robust understanding of the differences between the two assays and their optimized conditions.

1.1.2.2. Nucleic acid amplification

Most diagnostic platforms that rely on nucleic acid hybridization or ligand binding require the preamplification of the target nucleic acid sequence or analyte enrichment to achieve lower detection limits and the desired assay sensitivity.[2]

Polymerase chain reaction (PCR) is a commonly used DNA amplification technique that relies on the exponential accumulation of specific DNA fragments through a series of cycles involving template denaturation, primer annealing, and the extension of annealed primers by the enzyme DNA polymerase. The products generated in one cycle can serve as a template in the next one, thus doubling the number of copies produced in each cycle.[40] Although widely utilized, PCR technology is limited by its complexity, potential for non-specific amplification, and high cost. The isothermal amplification of nucleic acids, which involves rapidly accumulating nucleic acid products at a constant temperature, has become an efficient alternative strategy for enhancing the sensitivity of bioanalytical devices. Unlike PCR, which requires complex thermocycling instrumentation and thermostable polymerases, isothermal

amplification is typically performed at 30°C or room temperature, thus significantly simplifying signal enhancement in DNA-based diagnostics.[41]

Rolling circle amplification (RCA) has emerged as one of the most utilized isothermal amplification strategies in biosensing platforms due to the high processivity (generating tens to hundreds of thousands of nucleotides over a single amplification reaction) and low amplification errors of RCA-enzymes. The RCA reaction amplifies the primer-template recognition event into a detectable, long, single-stranded DNA molecule comprised of repeating complementary copies of the template (*i.e.*, concatemers).[42] More precisely, if the DNA or RNA primer specifically hybridizes to the circular template (ct-DNA), the polymerase will initiate ct-DNA replication using deoxynucleotide triphosphates (dNTPs) as building blocks. Soon after reaching a primer binding site and completing the first round of ct-DNA replication, the polymerase displaces the synthesized strand and continues "rolling," generating an end-product that is hundreds of nanometers to micron-sized in length.

Besides DNA, isothermal amplification can be performed using other biomolecules as an input signal (*e.g.*, RNA strands, proteins, small DNA ligands *etc.*), after converting a molecular recognition event to priming DNA molecules for the amplification reaction.[43] Moreover, by customizing the circular template, RCA-based assays can be adapted to include functional nucleic acid motifs (FNAs) such as DNA aptamers or DNAzymes, thus enabling them to detect diverse non-nucleic acid targets with improved sensitivity.[42,44,45] Furthermore, FNA-encoded RCA can serve as a template for the nano assembly of highly ordered multivalent DNA nanostructures (*e.g.*, nanoflowers),[46] utilized for improved cell-internalization in targeted chemotherapeutic drug delivery, biosensing, and cancer cell bioimaging.[42,47]

The RCA process can be monitored using various probes (*e.g.,* dual-labelled molecular beacons, fluorogenic dyes, or complementary DNA molecules labelled with fluorophores) that enable rapid signal read-outs that are compatible with a range of biosensing platforms. The generated RCA product can be visually inspected via gel electrophoresis by incorporating fluorophore-conjugated dNTPs or colorimetric agents (*e.g.,* gold-nanoparticle (Au-NP) tags and peptide-nucleic acid (PNA) modified strands).[48,49]

RCA is particularly useful in genetic research, which requires ultrasensitive and specific DNA or RNA sequence detection at the level of single nucleotide polymorphism (SNP)[50] or epigenetic modification (*e.g.*, DNA methylation).[51] For example, to discriminate SNP, the target nucleic acids can be employed as a ligation template to join the ends of a circularizable DNA oligonucleotide (''padlock probe''), followed by an RCA reaction.[52] The circularization of the padlock is strictly target-dependent, as even a single mismatch in the ligation junction will preclude template ligation and subsequent RCA initiation.

Although advantageous, the adaptation and commercialization of RCA into sensing technology remains hampered by several technical challenges. While some of these challenges relate to the need for highly purified and well-optimized circular templates,[53] others relate to the difficulties of scaling-up production handling, as high-molecular-weight RCA products tend to aggregate due to a combination of nonspecific inter- and intra-molecular crosslinking.[54] Thus, fine tuning the reaction time, template sequence, and content and composition of reagents is necessary to achieve optimal performance for RCA molecules.

1.1.2.3. Nucleic acid ligand binding – DNA aptamers

Nucleic acid aptamers are single-stranded ligand-binding oligonucleotides (typically sequences comprised of 20 to 80 bases) that can fold into distinct three-dimensional (3D) secondary structures with high affinity and specificity towards a binding partner.[55,56] The high affinity and specificity of aptamer molecules is attributable to highly organized ligand-binding sites and ligand-stabilized conformations, which allow multiple non-covalent interactions (electrostatic attraction, bases-stacking, hydrogen bonding and van der Waals forces) to take place between the aptamer and ligand, thus preventing off-target recognition due to steric and ionic factors.[57] Aptamers are generated from a large library of RNA or DNA molecules (*i.e.*, combinatorial oligonucleotides ~10^{10}–10^{16}) via *in vitro* selection using a process

known as Systematic Evolution of Ligands by Exponential Enrichment (SELEX), which is predicated on the principle of "survival of the fittest. Over multiple rounds (typically 16-20) of selection, separation, and amplification high-affinity aptamers are isolated, identified, and synthesized with high reproducibility.[56]

Since the 1990s, numerous aptamers have been isolated against a variety of targets ranging from small molecules (*e.g.*, amino acids, cofactors, and nucleotides) to peptides, proteins, and even supramolecular complexes.[55,58,59] The binding affinities of selected aptamers are highly target dependent, with dissociation constants (K_d) ranging in scale from picomolar (10^{-12} M) to nanomolar (10^{-9} M) for protein ligands and micromolar (10^{-6} M) to millimolar (10^{-3} M) for small molecules, depending on the number of interactions molecules can initiate with their respective aptamers. Aptamer-ligand interactions tend to be highly specific, regardless of affinity, and able to discriminate between closely related single-molecule compounds or enantiomers.[58]

Aptamers also offer significant benefits over antibodies concerning production costs and simplicity, as their selection does not involve the immunization of animals or cell lines followed by complicated protein purification procedures.[24] In addition, SELEX can isolate the aptamers of targets (including families of non-immunogenic toxins and small molecules) that are unsuccessfully targeted by *in vivo* isolated antibodies due to low specificity and batch-to-batch variability.

Once selected, aptamers can be synthesized with high reproducibility and high purity. Additionally, various functionalities can be introduced post-SELEX *via* sequence engineering, allowing the synthesis of aptamers with greater resistance to nucleolytic attack.[21] Moreover, post-synthesis modification with different functional groups, linkers, and signal-reporting molecules can enable the facile adaptation of selected aptamers into ready-to-use biosensing tools.[14,60]

Different readout strategies, including electrochemical, fluorescent, or enzymatic, have been proposed to enable aptasensors to simultaneously bind and report the concentration of a specific ligand. Optical fluorescent signaling remains a prominent transduction study due to its facile conjugation of fluorophores to nucleic acids, the convenience of fluorescence signal detection, its overall high sensitivity, and the availability of numerous dyes for molecular labelling.[58,61]

1.1.2.3.1. Fluorescence signal transduction with DNA aptamers

To fabricate the aptamer-based analytical devices, nucleic acid aptamers were first selected *in vitro* and then subjected to signaling-transduction modification.

Structural studies have shown that aptamers undergo significant conformational change upon ligand binding,[57,62] a feature which can be utilized in the signal transduction mechanism. Initially, a single fluorescent label is integrated into the conformationally labile regions of the aptamers (*e.g.,* near the ligand-binding pocket) *via* the covalently linked fluorophore of a fluorescent nucleotide analogue.[63] The alterations in the aptamer structure caused by ligand binding trigger changes in the electronic environment around the fluorophore tags appended to the aptamer, which are typically detected *via* changes in the fluorescent anisotropy or fluorescence intensity. Although this strategy provides affinities similar to the native aptamer, it is hampered by low signal gain and limited generalization across a broad range of aptamers, as the design requires an in-depth analysis of the native aptamer's structure.

More effective signaling was achieved utilizing two reporters based on FRET signal transduction. The design of these FRET aptamer sensors was inspired by "molecular beacon" assembly featuring a stem-loop structure (*i.e.*, aptamer beacons)[64] with a covalently linked fluorophore on one end (FRET donor) and a quencher on the other (FRET acceptor). The FRET pair comprising the final aptamer sensors were situated approximately 2-6 nm apart *via* self-annealing.[65] Notably, the overlapping emission and excitation spectra of the FRET donor and acceptor result in fluorescence quenching in the absence of a target. Ligand addition triggers an interaction with the aptamer-sequence-containing loop region, which in turn disrupts the self-annealed stem. This reaction alters the structure from a hairpin to an open

configuration wherein the fluorophore is separated from the quencher, thus resulting in increased fluorescence. In 2000, Hamaguchi *et al.* utilized this approach to develop a thrombin aptamer sensor[66] that was assembled from a canonical aptamer DNA sequence extended at the 5'-end with a short sequence complementary to the 3'-end of the aptamer. Furthermore, the developed sensor was dual-labelled such that the absence of a ligand forced the aptamer to adopt a closed conformation, thus quenching fluorescence. In contrast, when the ligand is present, the complementary sequence is de-hybridized and signaling is enabled. To increase the generalizability of this signaling approach, Li *et al.*, introduced a "structure-switching model" based on a bimolecular design and "duplex-to-complex" conversion.[67,68] In a typical structure-switching FRET design, the 5'-end of the aptamer sequence is extended and labelled with a fluorescent moiety, while the complementary oligonucleotide is quencher-labelled at the 3'-end and hybridized to the aptamer-containing sequence, partially covering both the extension and the aptamer native domain. As illustrated in Figure 1.2, the fluorescent moiety can be covalently attached to the aptamer sequence extension (*i.e.*, bipartite aptamer construct) or affixed to a portion of the extension (*i.e.*, tripartite aptamer construct) through the hybridization of fluorophore-labelled oligonucleotides. The hybridization of quencher-labeled DNA (Q-DNA) to a portion of the aptamer sequence simultaneously denatures and unfolds the native aptamer while quenching fluorescence. Thus, the absence of a target results in low fluorescence due to the proximity of the FRET pair. After the ligand is added, it competes with the Q-DNA to bind to the aptamer, causing the ligand-binding-induced dissociation of the complementary oligonucleotides (*i.e.*, strand displacement) and fluorescence signal recovery. This approach has been adapted for both DNA and RNA aptamers using a variety of analytes (*e.g.*, adenosine, thrombin, etc.).[67,69] Although the resultant aptamer constructs are adaptable to different ligands and enable low fluorescence background and high signal gain, they possess significantly lower binding affinities for the native aptamers, as the quencher strands compete with, and thus inhibit, ligand binding. For instance, after being converted into a sensor, an ATP aptamer will display a K_d value 60-100-fold lower compared to the native aptamer (K_d: 6-10 μM), suggesting that the high signal increase (typically 10-fold) and low background in such designs comes at the cost of reduced binding affinity.[67,70]

In addition to the use of FRET pairs, fluorescence signal enhancement *via* energy transfer or dequenching mechanisms can also be achieved using polymers such as graphene oxide (GO),[71] carbon nanotubes (CNT),[72] or polythiophene polymer.[73] For example, the use of electrostatic interactions and π- π stacking to adsorb single-stranded fluorophore-labelled aptamers onto GO surfaces results in fluorescence quenching. Upon target binding, the aptamer folds into a native tertiary structure and dissociates from the material, allowing an increase in fluorescence signal. While the incorporation of nanoparticle reporters and dye displacement assays are viable alternatives to FRET signaling transduction, their applicability is limited due to their inherent low stability, which is the result of their propensity for aggregation and high background.[58]

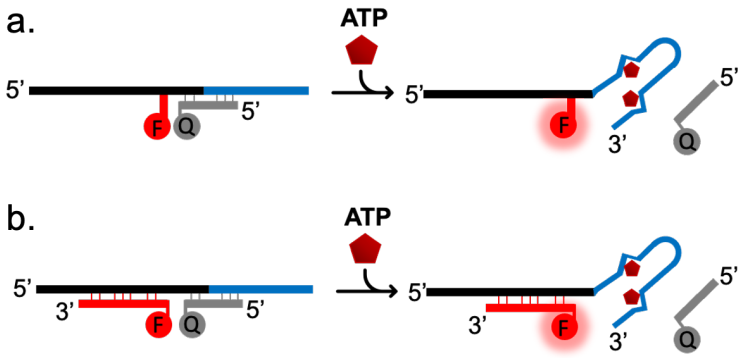

Figure 1.2 Different Designs of Structure-Switching Signaling Aptamers on the Example of an ATP ligand**.** Aptamer sequence (blue) is extended at the 5'-end (black) and tagged by a fluorophore (red) either (a) covalently (F) in a bipartite structure-switching design, or (b) by hybridization with a fluorophore-labeled strand (F-DNA) in a tripartite structure-switching design. In both images, fluorescence is quenched through hybridization with a quencher-labeled strand (Q) that is complementary to the portion of aptamer and the 5'extension. Ligand addition causes the aptamer to refold and displace the Q-DNA strands, thus recovering the fluorescence.

1.2. Nucleic Acid at Surfaces

To facilitate the practical application of nucleic acid sensors, molecular recognition assays are adapted from solution phase-based to solid phase-based. Biosensing performance on surfaces strongly depends on the interfacial properties of the immobilized DNA, with the sensor's sensitivity, specificity, and signal magnitude being significantly influenced by three key factors: (1) the ability to immobilize bioreceptors while preserving their native activity; (2) the availability of ligand-binding sites within immobilized bioreceptors; and (3) the degree of non-specific adsorption to the immobilizing substrate.[74]

Microarray solid-phase formats that enable multiple analyses in a single assay (*i.e.*, high throughput assays) are particularly attractive diagnostic platforms. Microarrays consist of a large collection of immobilized biomolecules that act as miniaturized sensors, enabling the simultaneous collection of large amounts of data. In addition, solid phase-based microarrays consume significantly lower amounts of reagent and can be used to perform multi-step reactions that are not possible with solution-phase systems (*e.g.*, washing steps). DNA microarray technology specifically exploits oligonucleotides that are surface-tethered to glass slides, plastic slides, or polymeric sheets (*e.g.*, nylon or nitrocellulose membranes).[75–77]

While microarray-based sensors have many beneficial properties, attaining optimal performance when using nucleic acids in solid-phase-based microarrays can be challenging given that certain steric requirements must be met if proper functionality is to be achieved. However, the ability to meet these steric requirements is often complicated by various factors associated with the microarray production process including the surface density, the surface charge, and the proximity of the anchored molecules to the surface, although these challenges can in many cases be mitigated through the use of different immobilization methods.[78]

Typically, DNA is anchored to the microarray surface using one of three main immobilization strategies: physical adsorption, chemical grafting through covalent or affinity binding, and physical entrapment into polymeric assemblies (*i.e.*, hydrogels, microgel particles or inorganic porous materials).[79,80] These methods will be described in more detail in the subsequent section.

1.2.1. Two-dimensional (2D) immobilization formats

2D immobilization typically involves grafting one or more bioreceptor molecule(s) onto a planar surface in a monolayer. For immobilization via physical adsorption, the biomolecules bind to the solid substrate through non-specific interactions such as hydrogen bonding, π-π stacking, hydrophobic interactions, electrostatic interactions, or van der Waals interactions.[2,81] The number of adsorbed molecules usually varies from spot-to-spot, as reaction conditions such as pH, temperature, or ionic strength can cause anchored molecules to disperse into the solution during application leading to cross-contamination and signal loss. Moreover, physical adsorption allows minimal if any control over the conformation of the oligonucleotides, leading them to adopt random orientations that may alter the native functional folding and reduce the activity and accessibility of analytes.[82] In contrast, chemical grafting exploits covalent bonding to attach biomolecules to the sensor surface. The greater specificity and strength of covalent bonding ensures the sensing molecules remain anchored and (if properly designed) oriented toward binding, even under varying assay conditions.[81] However, such grafting groups are not typically available on aptamers and other DNA-based sensing ligands, thus requiring the chemical modification of both the sensor surface and biomolecules to introduce one nucleophilic (e.g. primary amine-, thiol-, or hydrazide) and one electrophilic (e.g. aldehyde-, epoxide-, or activated ester) component respectively on the DNA ligand and the target surface(s).[83]

The large-scale manufacturing of DNA microarrays typically consists of spotting amino-modified DNA probes onto aldehyde-activated glass slides *via* micro-deposition techniques using contact or non-contact printers.[75,81] When anchoring the DNA to the sensor surface, it is critical to prevent any interaction between the nucleobases and the surface; indeed, even at concentrations as low as 3% of nucleobases present during covalent linkage can render the immobilized molecules inaccessible for hybridization.[84] As such, the insertion of molecular spacers containing reactive groups is necessary to facilitate DNA attachment and prevent surface-induced DNA inactivation. Furthermore, careful tuning of the DNA loading is encouraged, as this can prevent the electrostatic and/or steric hindrance that occurs at higher surface densities in addition to lowering the signal due to the reduced mobility and accessibility of sensing sites. Similar to covalent binding, affinity interactions based on a biotin-streptavidin system (known as the strongest non-covalent interaction with $K_a = 10^{15}$ M^{-1})[85] can also be employed to anchor biotinylated sensing probes to solid substrates with high stability *via* selective and highly oriented bonds. Although this method can be used with RNA and DNA species, it has limited practical value due to the presence of protein linkers that are prone to denaturation.[2]

Collectively, the immobilization chemistry used in 2D formats must be optimized to attain site-specific and -oriented DNA attachment with proper biosensing activity. In addition, such methods also require complex synthetic procedures to achieve effective anchoring. This latter concern is particularly challenging in microarray manufacturing, in which the immobilization chemistry should be simple and reproducible to enable larger-scale production. Non-equilibrium drying, a common observation when using automatic dispensers, can also be a concern, leading to convection-flow-induced drying artefacts (*i.e.*, "coffee rings") that can produce variability in or within the spot-to-spot DNA distribution.[86] Furthermore, dehydration can act as a source of non-specific adsorption, which if it occurs can further challenge signal generation and increase the background noise (particularly in fluorescence-based systems). Therefore, alternative routes for immobilization have been introduced.

1.2.2. Three-dimensional (3D) immobilization formats

In 2D biosensing surfaces, the loading capacity of the biomolecules is limited by the surface area, which limits signal intensity and sensitivity. One strategy to increase the specific area—and thus, the number of sensing biomolecules—is to immobilize the biomolecules within thick 3D substrates such as organic polymeric coatings, crosslinked polymeric matrices, or inorganic sol-gel materials, either *via* chemical attachment or physical entrapment.[87,88] The sensing activity in such platforms is dependent on the diffusion efficiency of the analytes, on the level of stability of the immobilized bioreceptors and the degree to which the bioreceptors leach into the surrounding solution during the application. Inorganic polymeric assemblies, especially sol-gels composites, have been particularly exploited in this way for DNA and protein entrapment.[89] Although this approach is relatively easy and inexpensive, pore size control can be challenging and in many cases the entrapped DNA can leach out *via* diffusion. As such, it is critical to consider the porosity of the sol-gel matrix, the length of the DNA, the gel concentration, and even the inclusion of charged groups (*e.g.*, cationic monomers) within the polymeric backbone in order to optimize overall sensor performance. Alternately, materials with more controllable morphologies that can still stably encapsulate biomolecules may offer advantages for advanced biosensor fabrication.

1.2.2.1. Hydrogels

Hydrogels are crosslinked water-swollen polymer networks that can exhibit high transparency and biocompatibility, making them important functional interfaces in biosensing devices. Water-soluble synthetic polymers such as polyacrylic acid (PAA), polyethylene glycol (PEG), or polyvinyl alcohol (PVA)[90,91] are widely used in the design of biomedical hydrogels due to their low toxicity and non-fouling properties. The polymeric assemblies are crosslinked either chemically (involving covalent bonds formed between complementary reactive groups[90,92] or by thermal- and photo-induced radical polymerization processes) or physically (utilizing hydrogen bonding, electrostatic interactions, hydrophobic interactions, or other physical interactions). Chemically crosslinked hydrogels are advantageous for stabilizing encapsulated molecules, as they typically provide more resistant networks under a broader variety of environmental conditions[93] (temperature, pH, or ionic strength), thereby minimizing the likelihood of denaturation and the leaching of valuable ingredients.

Two main strategies are employed to prepare chemically crosslinked hydrogels: (1) the polymerization of small hydrophilic molecules (*i.e.,* monomers) in the presence of multifunctional crosslinkers, and (2) the direct crosslinking of hydrophilic polymers.[91] Since the *in situ* polymerization is typically followed by the removal of unreacted and toxic species,[92] the direct crosslinking of hydrogel precursor polymers is deemed more favorable, as it often eliminates the need for extensive purification processes. The success of the direct crosslinking method depends on the choice of the chemistry, with click or click-like chemistries particularly attractive given the absence of (or at least inert nature of) any byproducts and the many options of such chemistries that can proceed under room temperature conditions.[94] Schiff base reactions[94] (*e.g.*, *aldehyde + amine*) are one such bond that can be generated *in situ* under physiological aqueous conditions without the release of toxic byproducts, thus offering an efficient, yet mild, fabrication method. A related bond is the hydrazone bond (*aldehyde + hydrazide*), which can also form quickly but demonstrates greater hydrolytic stability compared to other Schiff bases without significantly denaturing a range of encapsulated biomolecules.[95,96]

One important benefit of hydrogel technology is the ability to immobilize fragile biomolecules that must be kept in aqueous media to remain active. The hydrated "solution-like" microenvironment inside the hydrogel matrix can preserve the conformation and activity of biological molecules, which is particularly

important when assembling biomolecular microarrays given that it is difficult to prevent droplets from drying on surfaces (even under conditions with 100% humidity and with the use of humectants and additives).[2] The tunable pore size of hydrogels (based on the crosslinking density and the water affinity of the constituent chains) also permits high loading capacities and the ability to accommodate more recognition binding sites with enhanced accessibility and less steric hindrance;[97,98] at the same time, pore size control can also impede the diffusion of biomolecules in or out of the hydrogel depending on the molecular diameter of the biomolecule, offering potential for selective uptake and/or effective capture of biomolecules depending on the pore size selected. The hydrophilicity of hydrogel coatings can also suppress the non-specific adsorption of proteins and off-target molecules, thus supporting greater sensing selectivity.[99,100]

Hydrogel matrices used in DNA biosensing are typically based on polyacrylamide or polysaccharides (*e.g.*, agarose, dextran).[88,101] In these cases, DNA molecules are typically chemically immobilized onto the hydrogel by forming amide linkages between the amino-modified oligonucleotides[88] and succinimidyl ester groups within the polymeric backbone[101] or by co-polymerizing acrydite-modified DNA into polyacrylamide hydrogels.[102] These reactions can take place during or after the formation of the hydrogel, resulting in either the uniform distribution of DNA throughout the matrix or the grafting of the DNA molecules onto the hydrogel surface.[101] In addition to forming covalent linkages, DNA can be physically entrapped within polymeric networks. For example, Nielsen et al. embedded DNA aptamer into polyacrylamide nanoparticles for in vivo metabolite sensing.[99] The 30 nm polyacrylamide nanoparticles were prepared by inverse microemulsion polymerization, containing structure switching aptamer probes trapped in the hydrogel matrix that allows diffusion of small molecules but prevents nuclease instability.

1.2.2.2. Hydrogel films

The use of hydrogels as interfacial coatings in biosensing devices can reduce mass transfer limitations and response times to ligand addition, as well as protect biological receptors from a variety of detrimental surface-effects during fabrication and application conditions.[103] Hydrogel films even have the potential to reduce fluorescence background, which when combined with their enhanced immobilization capacity and accessibility of recognition sites can lead to lower limits of detection, better selectivity, and higher signal-to-noise ratios.[88,104] For example, a FRET molecular beacon DNA assembly immobilized onto aldehyde-activated planar slides can generate high fluorescence background and a relatively low increase in fluorescence upon hybridization.[105] Once immobilized inside agarose films, the same DNA assembly exhibits improved quenching efficiency and excellent discrimination against SNP, likely due to the suppression of hydrophobic and electrostatic interactions between the molecular beacons and the underlying surface, which tend to destabilize delicate stem-loop conformations.

Different strategies are available for producing hydrogel microarray chips, including dip-coating,[106] spray deposition,[107] spin-coating,[108] and drop-on-demand printing.[109,110] Printing offers a number of benefits compared to other fabrication techniques, most notably allowing the relatively facile deposition of small volumes in specific patterns in a localized manner and the potential for scaled-up production. Consequently, the use of printing has become a topic of particular interest in biomaterial research. To date, hydrogel films have been employed to immobilize a variety of bioreceptor molecules,[111,112] and to act as size-selective separation membranes,[113] thus demonstrating their wide functional potential within the development of diagnostic systems.

1.2.3. Molecular crowding influence on the DNA base pairing

DNA is a complex molecule that can take part in many competing non-covalent interactions with a surface or immobilizing substrate.[114,115] Therefore, the design of platforms that can encourage DNA base pairing and specific nucleic acid recognition reactions while also inhibiting irreversible non-specific adsorption is not straightforward. One phenomenon of particular relevance to this thesis is the stabilization of double-stranded DNA within macromolecular crowding systems, such as polymeric matrices.[116,117] Researchers have identified two distinct effects that alter the thermodynamics and kinetics of DNA duplex formation in crowded and confined systems: the volume-excluded effect[118], which is caused by macromolecules, and the osmotic stress effect[117], which is caused by small crowders that alter the water activity and dielectric environment of DNA containing solutions. For example, with a PEG-based molecular crowder, the larger PEG molecules decrease the reaction volume by generating an area that is inaccessible to other molecules while also increasing the solution viscosity, thus enabling higher thermodynamic activity among biomolecules with pronounced association rates (although with somewhat reduced diffusion). In contrast, smaller PEG molecules along with other small cosolutes (glycerol, ethylene glycol, or sucrose), act by decreasing the water activity *due to* accumulation around the single-stranded helixes *via* preferential interactions that alter the DNA reactivity and may decrease the base-paring affinity.[118] From a thermodynamic point of view, large steric crowders favor reactions that reduce the net volume and promote the formation of more compact and ordered structures, thus demonstrating the potential to stabilize complementary matched DNA duplexes; in contrast, small crowders that can preferentially bind to single-stranded DNA have greater potential to destabilize the double helix and even alter the kinetics of hybridization reactions, as they disrupt the spine of the water molecules around the minor DNA grooves and thus modulate the affinity between the two interacting DNA species compared to one species in bulk solutions.[119]

Several studies have investigated using molecular crowding in this context. For example, an increase of up to 5°C was observed in the T_m of poly(dA)-poly(dT) DNA duplexes when surrounded by PEG 8000 while a decrease of 1–5 °C was observed when surrounded with smaller osmolytes (*e.g.*, ethylene glycols and small molecular weight PEGs) in a buffer containing 300 mM NaCl.[120] The selective nature of PEG-molecules with respect to DNA stabilization was further confirmed and quantified using 12-bp-long DNA duplexes based on the free energy change of hybridization. In contrast to samples not containing cosolutes, the addition of small glycols such as EG, diEG, triEG, and PEG 200 (approximately tetraEG) produced a destabilizing effect, with one order of magnitude increase moving from EG to triEG. A slight reversal of the destabilizing effect was observed with the introduction of the PEG 200 molecules, while significantly greater duplex stabilization was observed after the introduction of the PEG 600 that further increased alongside the PEG chain length. Apart from changing the thermodynamics, the use of PEG molecules with different weights may also interfere with the kinetics of the DNA base pairing, with smaller PEG crowders decreasing the forward pairing rate and increasing the dissociation rate.[121]
Another study on DNA base pairing dynamics[117] indicated that similar hybridization efficiency can be achieved in buffers with higher ionic strength (the formation of a spine of water and ions within the minor DNA groove increases the pairing rate of complementary strands) or under increasing molecular crowding at low salt concentrations. The authors discussed the latter phenomena in relation to hydrophobic interactions induced under a regimen featuring lower concentrations of counter-ions; specifically, they argued that promoting the release of the water molecules bound to the hydrophobic sites of the nucleobases yields higher base-pairing efficiency.

In addition to base-pairing, hydrophobic interactions and surface hydrophobicity may influence the interfacial dynamics of single-stranded oligonucleotides—particularly the residence time and surface diffusion—in sometimes non-intuitive ways[122] and thus are particularly relevant in microarray

production. Surfaces based on oligoethylene glycol (OEG) are more hydrophilic and characterized by increased surface residence time for single-stranded DNA (especially longer DNA strands) due to the greater number of molecule-surface interactions. The residence time of DNA on hydrophobic surfaces decreases as its length increases, which has been attributed to the adoption of conformations that minimize hydrophobic interactions, (*e.g.*, the internal sequestration of hydrophobic nucleobases). Furthermore, the OEG surfaces exhibited larger mean surface diffusion coefficients and, thus, more rapid surface exploration by DNA molecules compared to less hydrophilic or hydrophobic surfaces, a key property that dictates the DNA-target molecule's ability to locate a tethered sensing DNA for specific base pairing in hybridization sensors.

Overall, the above-discussed studies strongly indicate that choosing the most appropriate polymeric immobilization matrix configuration is critical to the success of solid-phase DNA assays, as doing so can enable enhanced molecular recognition and effective anchoring.

1.3. Nucleic Acid Hybridization Microarrays

The detection of specific segments of nucleic acids *via* hybridization with complementary sequences is a foundational function of DNA microarray technology that is applicable in a wide range of areas, including the monitoring of infectious diseases and gene expressions, the discovery of drug and clinical biomarkers, and environmental and food analysis.[26,75,76]
DNA microarray hybridization is based on the immobilization of DNA oligonucleotides with known sequences onto a variety of solid substrates; in contrast to traditional hybridization or PCR assays, this approach allows researchers to obtain sequence-specific information in a rapid, miniaturized, and parallel format. The specificity of DNA hybridization relies on the ability of the interacting oligonucleotides to form hydrogen bonds.

Conventional 2D DNA hybridization microarrays typically suffer from slow hybridization kinetics and low signaling enhancement and sensitivity due to the limited number of DNA molecules that can be immobilized onto their relatively small surface area.[83,123] However, this limitation can be overcome by developing microarrays using 3D hydrogel interfaces, as such interfaces can immobilize up to 100x more sensing DNA per unit area compared to planar glass,[97] support accelerated diffusional transport and hybridization kinetics, and sterically prevent entrapped DNA from nucleolytic degradation. Moreover, the use of 3D hydrogel interfaces also eliminates the need for synthetically challenging covalent reactions.[97,111]

Typically, microarrays are designed using polyacrylamide-, agarose-, and polyethylene glycol-based hydrogels and fabricated using nano- or microliter-scale inkjet printers. For example, Le Goff *et al.* developed a DNA hydrogel microarray by covalently immobilizing amino-modified oligonucleotides onto a poly(dimethylacrylamide) hydrogel and depositing the hydrogel onto a shrinkable polystyrene-based substrate using a piezoelectric spotter.[124] The developed sensor exhibited a significant signal increase in samples having low target analyte concentrations, thus demonstrating the hydrogel network's ability to provide superior sensitivity by enhancing analyte diffusion within the DNA probes. To achieve greater swelling and even better analyte diffusion, Soto *et al.* fabricated a DNA microarray by casting a sugar-polyacrylate-based hydrogel film onto aldehyde-functionalized glass,[125], first copolymerizing acrylated galactopyranoside with *N*-(3-aminopropyl)methacrylamide and the crosslinker N,N'-methylenebisacrylamide and then conjugating the amine-terminated oligonucleotides to the amine-functionalized carbohydrate network *via* bis(sulfosuccinimidyl)suberate (an amine-to-amine homobifunctional crosslinker). The resultant hydrogel was printable, had a water content of 84%,

allowed the free diffusion of the fluorophore-labeled target DNA, and could be successfully hybridized with the immobilized oligonucleotides. To simplify the polymerization process and reduce the effect of UV irradiation on the incorporated DNA, Beyer *et al.* developed an acrylamide-based hydrogel functionalized with amino-modified sensing DNA, using a photoinitiator that enables radical polymerization under visible light within 20 min.[126] The fabricated hydrogel offered effective analyte diffusion and annealing of DNA molecules, allowing it to be adapted for use in colorimetric assays based on naked-eye DNA hybridization monitoring *via* color changes induced by the addition of silver nanoparticles.[127]

Although conducive to successful hybridization assays, neither of these examples nor any other similar reports on hydrogel-based microarrays offer the joint benefits of facile fabrication and enhanced functional characteristics such as hybridization kinetics, low background signal, and high assay sensitivity. Therefore, the development of new hydrogel matrices is strongly incentivized.

1.4. Nucleic Acid Amplification Microarrays

As earlier noted, to achieve the desired sensitivity, most nucleic acid hybridization assays require a certain level of preamplification. However, it is difficult to configure conventional PCR technology on-chip due to a lack of signal accumulation at the amplification site and the detrimental effect of temperature cycling on the reaction components and microarray substrate. In light of these challenges, isothermal amplification assays based on RCA can be employed. RCA microarrays offer better performance compared to solution-based or other solid-phase RCA formats with respect to providing increased sensitivity while also maintaining their parallel analytical nature. RCA microarrays can be particularly beneficial in enhancing RCA-enzyme processivity, as the localization of the reaction within a confined space under saturating concentrations of all reagents and buffer components induces stronger and more frequent annealing between the circular template and primer and thus higher RCA efficiency.[128] Additionally, the use of 3D supporting materials (hydrogels or polymers) can enable higher immobilization efficiency and probe stability, further increasing the overall sensing performance of the developed DNA microarray.[129]

Multiple published examples describe the fabrication of DNA microarrays for sensing. Nallur *et al.*[130] prepared gel-coated planar glass microarrays for RCA-assisted SNP discrimination that were able to detect as few as ~150 molecules of DNA per microzone. In their approach, biotinylated or amino-modified primer-DNA molecules were immobilized onto streptavidin-coated glass slides or glutaraldehyde-activated polyacrylamide gel elements *via* printing or hand-spotting. Compared to direct hybridization, the developed method enabled 8000-fold and 1000-fold RCA signal enhancements in the planar glass and gel-coated arrays respectively, with the possibility for further signal amplification using a circle-independent branched RCA reaction. Attempts to adapt the hydrogel-based RCA platform for immunoassays and the ultrasensitive detection of biotin achieved a 3000-fold improvement in sensitivity relative to direct-hybridization and as high as an 8-fold signal-to-noise ratio at the limit of detection due to the presence of the hydrogel and RCA-induced signal amplification.[131] Mirzabekov's group[132] developed hydrogel microarrays with uniform DNA distribution for SNP analytics by co-polymerizing the DNA within polyacrylamide-based gel microarrays applied to glass slides[133], combining RCA with a ligase detection reaction using padlock probes. The proposed assay achieved fmol-scale sensitivity with the potential for further improvement using hydrogels with different configurations and the consequent suppression of the fluorescent background generated by non-specifically-bound signaling oligonucleotides.

Functional nucleic acids have also been employed in RCA-on-a-chip platforms to improve the sensing of non-nucleic acid analytes. For example, Ellington's group developed a DNA aptazyme-supported RCA sensor on a glass substrate that enabled the reproducible detection of ATP molecules with 1 μM sensitivity.[82] Their analytical approach was based on ATP-molecular recognition transduced into circular probes governed by an anti-ATP-aptamer appended to the selected deoxyribozyme ligase. Although the developed approach enabled rapid signal accumulation, the activation of functional nucleic acids on planar surfaces requires the further optimization of the already somewhat complex anchoring chemistry, and the inclusion of linkers and streptavidin-avidin bridges. To simplify the preparation of RCA-sensors, Ali *et al*. prepared paper strips containing DNA-conjugated poly(N-isopropylacrylamide) microgels capable of RCA synthesis.[134] In this approach, the microgels were spotted onto paper strips that served as substrates for RCA-template formation in the presence of the target DNA and T4 DNA ligase. After ligation, the paper strips were washed and placed into the RCA reaction solution to allow the formation of long ssDNA, which was visualized using complementary fluorophore-labeled DNA probes. Ali *et al.*'s method achieved a limit of detection of 100 pM, representing a low-throughput but reliable quantitative method for DNA analysis. To enable multiplex analysis utilizing paper substrates, Liu *et al.* developed a printable microarray-based RCA sensor for miRNA detection in which biotinylated DNA-streptavidin conjugate was bound to a nitrocellulose surface having the sequence complementary to the circular template, and as such capable of acting as a primer for an RCA reaction.[128] The RCA reaction on paper was initiated by placing a mixture of circular DNA template, phi29 DNA polymerase, dNTPs and reaction buffer on a microzone, and allowed to incubate for 40 min at room temperature. The results showed that using a paper-bound DNA-primer as a biotinylated-streptavidin conjugate enhances the RCA reaction efficiency by at least 2 to 3 fold compared to the solution. Moreover, integrating pullulan into paper sensors can protect RCA reagents from thermal and chemical denaturation at room temperature, simplifying the storage and handling of DNA-sensing devices. In subsequent work, Liu *et al.* extended their sensor's applicability to the detection of bacterial biomarkers by employing a graphene oxide-DNA/RNA-aptamer mixture for analyte recognition and triggering amplification, thus offering a potential solution for rapid and low-cost diagnostics.[135]

Although RCA technology holds promise for enhancing sensitivity, the efficient detection and quantification of RCA products remain challenging given that the tendency of concatemeric DNA molecules to aggregate and cluster, thus rendering them inaccessible for labeling and investigation. Additionally, non-specific amplification or amplification suppression in RCA assays[136] can affect the sensor's specificity and further inhibit target detection, particularly in crude biological samples that may contain DNA binding or polymerase inhibitory components.[137] However, the wider adoption of this powerful diagnostic tool remains hampered by the need for multi-step reaction processes (including blocking steps, intermediate washing/drying cycles, and post-reaction processing) as well as the specific anchoring chemistry required for effective DNA immobilization and annealing.

To address the aforementioned challenges, a strategy based on the physical entrapment of pre-amplified RCA products inside hydrogel matrices for application in an on-chip format was explored. In this approach, the size of the RCA product enhances the immobilization efficiency without requiring affinity/covalent attachment, while the RCA product's concatemeric nature increases the likelihood of hybridization/FNA-recognition events without the need for enzymatic processing; both these advantages significantly simplify the application and preparation of the device. In one such work, Brennan *et al.* fabricated sol-gel monoliths with meso- and macro-porous morphologies containing RCA-derived concatemeric aptamers able to detect both small and large analytes (*i.e.,* ATP metabolites and PDGF proteins).[138] The authors pre-formed the RCA molecules and then physically entrapped them in the sol-gel material, achieving improved retention capacity (more than 80%) and signaling gain compared to a monomeric aptamer assembly while also delaying nucleolytic degradation. However, the translation of

this technology to the microarray format remains delayed, mostly because the dynamic nature of the sol-gel transition affects the dispensing process[139] by clogging the ink-jet printheads.

1.5. Nucleic Acid Aptamer Microarrays

Given their high affinity and specificity, nucleic acid aptamer microarrays are becoming increasingly popular diagnostic tools, particularly in the detection of small molecules.
Aptamer microarrays evolved from DNA hybridization microarrays and consist of numerous surface-immobilized aptamer capture probes that have been functionalized to detect target molecules. Typically, aptamer microarrays are fabricated by applying signaling-modified aptamers onto functionalized microarray substrates *via* contact or non-contact printing, thus combining facile production with high throughput analysis.[78,140]

1.5.1. Microarrays utilizing FRET aptamer constructs

FRET aptamer constructs provide signal-on sensing with low background and high signal increases; however, this comes at the cost of decreased binding affinity, which creates challenges in transitioning from solution-phase to solid-phase assays. Strategies for enhancing the surface affinity of aptamer constructs strongly rely on ligand-binding mechanisms and the stability of the assembled aptamer construct.[141] Surface-based assays involving structure-switching aptamer constructs are subject to three main requirements: (1) minimization of the spontaneous dissociation rate of aptamer duplexes (*i.e.*, off-target fluorescence recovery), thereby suppressing the background fluorescence; (2) promotion of the ligand-binding pathway associated with enhanced signaling; and (3) maximization of on-target signaling, (*i.e.*, the ligand-induced dissociation rate of aptamer duplexes).

Ligand-binding systems have been described using conformational selection models and induced fit models.[142–144] A conformational selection model assumes that a ligand binder exists at equilibrium between a binding-competent and binding non-competent state and that cognate ligand only binds to the competent state to form an aptamer-ligand complex. In contrast, an induced fit model assumes that the ligand interacts with the non-competent binder state, catalytically inducing the fit and formation of the aptamer-ligand complex. Notably, ligand-binding pathways are not mutually exclusive and may co-exist in parallel between ligand-unbound and ligand-bound states.

With regards to structure-switching aptamer constructs, conformational selection suggests that the aptamer senses the ligand after the quencher-strand has become dehybridized and the native aptamer has refolded. As such, the binder's affinity must be tuned by regulating the quencher strand's hybridization affinity. This is typically achieved by adjusting the quencher-strand length, concentration, or GC-content or by altering assay conditions such as temperature, buffer content, or even FRET pair type (i.e. certain fluorophore-quencher combinations may affect the stability of the DNA duplexes *via* contact quenching phenomena[145,146]). In contrast, the induced fit model postulates that ligands can directly bind to the aptamer construct to form a tertiary complex that induces quencher-strand departure and the formation of an aptamer-ligand complex. In this model, the hybridization affinity and the quencher strand location both influence the binding affinity of the aptamer construct, with the response to a catalytic ligand being a function the 3D aptamer structure, the native ligand's binding affinity, and the availability of bases within ligand-binding pocket.[141,144,147,148]

Modeling of surface aptamer sensors based on strand-displacement must assume factors that influence both ligand-binding pathways. Hybridization thermodynamics based on quencher-strand length is the

first and most straightforward parameter to tune. This is typically achieved by following the "Rule of 7 in Watson-Crick base pairing," which suggests that effective annealing requires the complementarity of at least seven consecutive bases.[149] The hybridization thermodynamics should provide balance such that the aptamer-ligand complex is favorable in the presence of the target and the quenching strand is displaced to allow for dose-dependent fluorescence recovery. In contrast, in the absence of the target, the aptamer duplex is favorable to achieving low fluorescence background.[68] In general, shorter competitors with weaker hybridization potential are more favorable to switching in the presence of ligands while longer and more stable quencher stems generate slower sensor responses and lower the binding affinities. Another key parameter to consider is the location of the quencher stem, which determines the degree of quencher-sequence hybridization to the ligand-binding pocket. Prior work has shown that the interfacing of competitor oligonucleotides with the bases inside the ligand-binding pocket promotes an induced fit binding mechanism associated with enhanced signaling. Furthermore, reduced interaction with biding site bases can change the cooperativity between ligand-binding sites (if more than one) to a non-co-operative relationship.[144]

The literature contains several studies that adapt these principles. For example, Scheper *et al*. covalently anchored aptamers to aldehyde-modified glass slides to develop an ethanolamine aptamer-based microarray that relies on competition between ligands and signaling of complementary oligonucleotides.[150] The aptamer construct was assembled *via* the simultaneous hybridization of fluorophore-tagged complementary oligonucleotides and addition of ligand, allowing the construct to identify the presence of ethanolamine based on competitor strand displacement and signal loss (*i.e.*, an off-signal sensor). Hybridization strength was regulated by varying the length of the complementary oligonucleotides between 10 and 16 bases and by adjusting the position of hybridization within the ligand-binding sequence. This approach not only enabled ligand sensing but also enabled the determination of the optimal location and length of competitive sequences to interfere with the binding site, maximizing the sensitivity of the assay. Munzar *et al*. employed a similar approach to analyze RNA ATP aptamer, DNA ATP aptamer, and cocaine aptamer,[147] immobilizing a fluorescent aptamer sequence on a 2D array *via* hybridization with oligonucleotide competitors covalently anchored on aldehyde-functionalized glass slides. The array contained 7-32-bp-long competitor DNAs that were complementary to various regions of the aptamer in order to map the entire aptamer sequence. Incubating the ligand will cause the aptamer to dissociate, thereby reducing fluorescence that can be translated into information about the ligand-binding mechanism and the most suitable sequences for sensor development. As observed with ethanolamine, most of the responsive aptamer reporters adaptable to surface biosensors were built with signaling oligonucleotides that were between 9- and 12-bp in length and positioned to interface with a ligand-binding site.[141] Importantly, in the case of the DNA ATP aptamer, signaling oligonucleotides that were < 9-nt and rationally positioned did not improve the aptamer construct's affinity and demonstrated high off-target dissociation rates with little or no response to the cognate ligand. These results indicate that this approach is limited by the hybridization efficiency of short DNA strands on typical 2D surfaces.[144]

Alternatively, 3D arrays have also been used in aptamer sensing technology. One of the most well-explored designs involves the integration of sol-gel materials[89] and DNA or RNA aptamer reporters for various small-molecules.[112,151–154] Bipartite or tripartite FRET aptamer reporters have been immobilized in 96-well plates by incubating pre-formed aptamer constructs with sol-gel (*i.e.,* affinity immobilization) or by entrapping them within a porous matrix. Depending on the sol-gel's hydrophilicity, the immobilizing microenvironment can result in a thermodynamic stabilizing or destabilizing effect on the quencher stems that impacts the performance of the sensor. Although encapsulated aptamer constructs retain their structure-switching ability, sol-gel matrices strongly influence the binding kinetics and end-point signal resolution, which typically requires 60 min compared to 1 min in solution.[152] The authors

thus tuned the quencher stems to lengths between 15- and 10-nt; while the shortest sequences imparted enhanced signal resolution kinetics but at the cost of high fluorescent background due to impaired hybridization. Ultimately, the authors suggested the use of quencher oligonucleotides with a minimum length of 11-nt to obtain the most effective signaling inside sol-gel composites.[151]

1.5.2. Integration of hydrogel materials with aptamers

Hydrogel materials have also been employed in the assembly of aptamer-responsive matrices. Some examples of such matrices include colorimetric stimuli-responsive "gel-to-sol" hydrogels based on aptamer-crosslinked polyacrylamide gels[155] and FRET-based aptamer-incorporated graphene-oxide hydrogels.[156,157] For example, Tan *et al.* immobilized fluorescently labeled aptamers designed to selectively bind tetracycline onto a graphene oxide-based hydrogel monolith.[158] The fluorescence quenching properties of graphene oxide cause the aptamers to lose their fluorescence signal upon being entrapped in the hydrogel, which was physically crosslinked with adenosine as a gel-forming promoter agent *via* electrostatic interactions; however, when exposed to tetracycline, the aptamer recovered its fluorescence signal to enable the high sensitivity detection of the tetracycline concentration in a dose-dependent manner.

Another type of hydrogel assembly based on molecular imprinted polymers (MIP) has also been proposed for affinity enhancement. The MIPs were prepared by mixing different monomers with the target molecules, polymerizing the matrix, and then washing the imprinted ligands from the polymeric matrix, leaving a cavity that served as a recognition site.[159] Using DNA aptamers as one of the macromonomers enhances the hydrogel's binding affinity towards the cognate ligand; for example, incorporating a FRET-based split adenosine aptamer into an acrylamide MIP network can yield an 18-fold increase in the adenosine binding affinity (vs. a DNA-free MIP system) while also achieving a K_d value comparable to the wild aptamer and a 2-fold increase compared to the free-aptamer.[160]

Although fabricable as monolithic gels, bulk nanoparticles, or surface substrates, the use of hydrogel materials in DNA aptamer sensing is limited by their laborious preparation, often harsh polymerization conditions, and post-polymerization processing. As a result, the scaled-up and high-throughput production of hydrogel materials for DNA aptamer sensing remains a challenge. For instance, MIP systems require specific alkene or allyl polymer modifications to sufficiently incorporate monomers into the MIP matrix and multiple DNA anchoring points to ensure correct orientation under the confined system.[161] Furthermore, aptamer incorporation is moderate for sol-gel and MIP systems (typically ranging between 30-55%) and kinetic response is often delayed due to diffusion restrictions, particularly in high-volume hydrogel monolith-assemblies.
As such, while the integration of hydrogel materials in aptamer sensing technologies offers potential for facilitating immobilization, providing a solution-like microenvironment, and stabilizing the sensing units, the development of hydrogels within a microarray format that exhibit enhanced ligand-binding affinity and signaling kinetics is rarely addressed.

1.6. Nitrocellulose-based DNA sensors

Paper has become a popular substrate for the fabrication of biosensors because it is abundant, inexpensive, and biodegradable compared to plastic, metallic, or glass materials. As such, paper substrates enable the development of portable, affordable, and rapid assays for on-site monitoring under resource-limited conditions.[162] In addition, paper can be coated or printed on, can be chemically or physically modified to possess various interfacial properties (*e.g.,* wettability and reactivity), and

possesses a porous structure that facilitates liquid transport *via* capillary forces without the need for external power. Paper substrates also support the use of inkjet printing to create hydrophobic barriers and microzones for microarray fabrication, typically by heating a solid wax upon deposition to cause it to melt through the paper to create defined patterns for the subsequent deposition of bioreceptors.[163,164]

The main methods used to immobilize DNA on paper are physical adsorption and covalent linking. Physical adsorption is simple in that it requires no pre-treatment of the paper; however, the recognition elements are not stably coupled onto the paper surface, resulting in often low reproducibility and reduced test accuracy. Li's group investigated the simple adsorption of DNA aptamers compared to covalent attachment and found that physical adsorption was too weak for aptamer immobilization, as the aptamer molecules get easily desorbed from the paper during the liquid flow.[165] To overcome this limitation, the physisorption immobilization technique was improved by linking DNA molecules with carriers such as streptavidin, colloidal particles, and microgels *via* covalent coupling followed by deposition and adsorption on paper.[128,166] In another example, DNA aptamers were coupled to poly(N-isopropylacrylamide) (PNIPAM) microgels, with the aptamer-microgel conjugates being entrapped on paper following drying.[167] Although the fluorescence-based structure-switching mechanism did not provide remarkable sensitivity, the large size of the complex ensured steady immobilization within the paper without significantly affecting the recognition ability of the aptamer or the hydrophilicity of the paper substrate to allow wetting during the sample flow.

As an alternative approach, the same group explored another strategy for simplifying immobilization that involved assembling the DNA aptamers into RCA-derived amplicons and printing the resultant megadalton-sized concatemers directly onto unmodified paper surfaces.[168] The RCA-based concatemers not only remained immobilized on the paper after a liquid flow but also retained their structure-switching ligand-binding ability to generate fluorescence signals. To further increase the DNA surface density, RCA-based long-chain-DNA molecules were assembled into flower-shaped superstructures and then printed onto cellulose and nitrocellulose membranes.[169] Compared to monomeric and concatemeric unassembled RCA products, the 3D nano-flower DNA provided better retention efficiency, enhanced resistance to nuclease degradation, and suppressed nonspecific protein adsorption. Nonetheless, the practical application of this technology remains limited due to its high DNA consumption.

Covalent immobilization has also been investigated as a strategy for increasing the stability and uniformity of paper-anchored DNA-sensing probes. In one such work, an amine-terminated ATP-binding DNA aptamer was covalently coupled to a cellulose membrane that had been oxidized to generate aldehyde groups on the surface. Compared to physical adsorption, the covalent binding of the DNA aptamer enabled more stable retention while maintaining its affinity and specificity; however, the coupling efficiency to the cellulose membrane was only about 25%.[165]

The integration of hydrogel film biosensing interfaces and DNA bioreceptors on cellulose-based substrates is still in its infancy and is currently mainly focused on stimuli-responsive matrices. For example, Yang *et al.* developed a paper-based microfluidic analytical device (μPADs) for the detection of small molecules by combining a microfluidic platform with a target-responsive DNA hydrogel placed in the flow channel as the flow regulator.[170] The polyacrylamide polymers grafted with DNA aptamers were physically crosslinked with another short DNA strand with a complementary sequence *via* hybridization, thus forming a dense DNA hydrogel network capable of undergoing a target-induced gel-to-sol phase transition. In the presence of the target, aptamer-target binding, induces hydrogel network dissociation inducing flow of the colored indicator; conversely, in the absence of ligands, flow stops due to the blocking action of the hydrogel. This developed microfluidic detection system can be applied for

a variety of target-molecules including cocaine, adenosine, and Pb^{2+} by simply modifying the aptamer component.[163,164,170]

The integration of interfacial hydrogel coatings with cellulose-based substrates further facilitates the inexpensive preparation of portable sensing platforms with enhanced functional benefits. Thus, there is considerable research on new hydrogel compositions that are adaptable on paper substrates currently ongoing, including the work in this thesis.

1.6.1. Introducing POEGMA hydrogel chemistry into biosensing technology

Poly (oligoethylene glycol methacrylate) (POEGMA) hydrogels recently synthesized by our group have emerged as promising candidates for a variety of biomedical applications due to their low cytotoxicity and excellent antifouling properties.[96,171] In particular, relative to other anti-fouling hydrogel systems (e.g. conventional PEG-based hydrogels), POEGMA hydrogels have tunable chemistries via facile free radical copolymerization with other functional monomer(s) in addition to varying the length of the oligo(ethylene glycol) side chain on the different monomer units, allowing for the production of hydrogels with different mechanical strengths, porosities, thermo-responsivities, and charge densities.[172] While many strategies can thus be used to gel POEGMA-based hydrogels, dynamic covalent chemistry leveraging hydrazone-based crosslinking of hydrazide- and aldehyde-functionalized polymers is beneficial given that hydrazone bonds are stable, quick-forming (enabling printing), and reversible upon changes in pH conditions.

The macrostructure of POEGMA hydrogels can be controlled by adjusting the polymerization and crosslinking conditions.[96,171] For example, the crosslinking density (and thus the hydrogel's porosity) can be controlled by tuning the concentration (mol%) of the crosslinking functional groups in one or both precursor polymers and/or the concentration of pre-hydrogel polymers during crosslinking. The properties of the hydrogel network can be further modulated at the interface by controlling the length of the oligoethylene glycol integrated within the side chain of each polymer. In the specific hydrazone-crosslinked system used in this work, co-polymerization of a short-chain PEG monomer (diethylene glycol methacrylate ($M(EO)_2MA$, n= 2)) with a long-chain PEG monomer (oligoethylene glycol methacrylate ($OEGMA_{500}$, n = 8–9)) and either an aldehyde or hydrazide functional monomer is used to produce the two complementary reactive polymers PO_xA_y and PO_xH_y, where x indicates the mole fraction of the long-chain monomer-$OEGMA_{500}$ and y indicates the mole fraction of the aldehyde and hydrazide reactive groups. The gelation kinetics, crosslinking density, and mechanical and interfacial properties of the resultant hydrogel can be adjusted by tuning the $M(EO)_2MA$: $OEGMA_{500}$ ratio within the polymer precursors. For example, $PO_{10}A_{30}$/$PO_{10}H_{30}$ hydrogels (prepared with precursor polymers containing 10 mol% of long-chain PEG-monomer) gel significantly faster and exhibit 3-fold higher crosslink densities compared to $PO_{100}A_{30}$/$PO_{100}H_{30}$ hydrogels (prepared with precursor polymers containing 100 mol% of long-chain PEG-monomer) due to the steric hindrance of the longer and bulkier OEG groups, which reduce the availability of functional groups with which to react and crosslink. Small-angle neutron scattering analysis confirmed that PO_{100} hydrogels form more homogenous polymeric networks and larger mesh sizes than PO_{10} hydrogels despite both precursor polymers being functionalized with the same crosslinkable functional group content,[173] while protein adsorption studies showed improved steric hindrance of protein deposition in PO_{100} relative to PO_{10} hydrogels.[171] In this context, the optical transparency (linked to network homogeneity) and the improved anti-fouling properties of PO_{100} hydrogels are optimal for use in optical biosensors. Moreover, PO_{100} hydrogels swell significantly more than PO_{10} hydrogels, promoting higher swelling ratios when exposed to buffer (up to a 215±20% weight increase) and increased mesh size from 2.5 nm to 4.5 nm (with 13 wt % precursor polymer concentrations), suggesting their potential for enabling faster mass transport. However, PO_{100} hydrogels

possess comparatively lower mechanical strength and stability relative to the more highly crosslinked PO_{10} hydrogels. One solution to this challenge is to prepare hydrogels using precursor polymers with dissimilar PEG side-chain lengths.[174] For example, mechanical stability can be increased and the gelation time decreased by mixing $PO_{10}A_{30}$ with $PO_{100}H_{30}$ precursors, which also preserves the gel's homogenous internal morphology and transparency that is beneficial for optical biosensing applications.

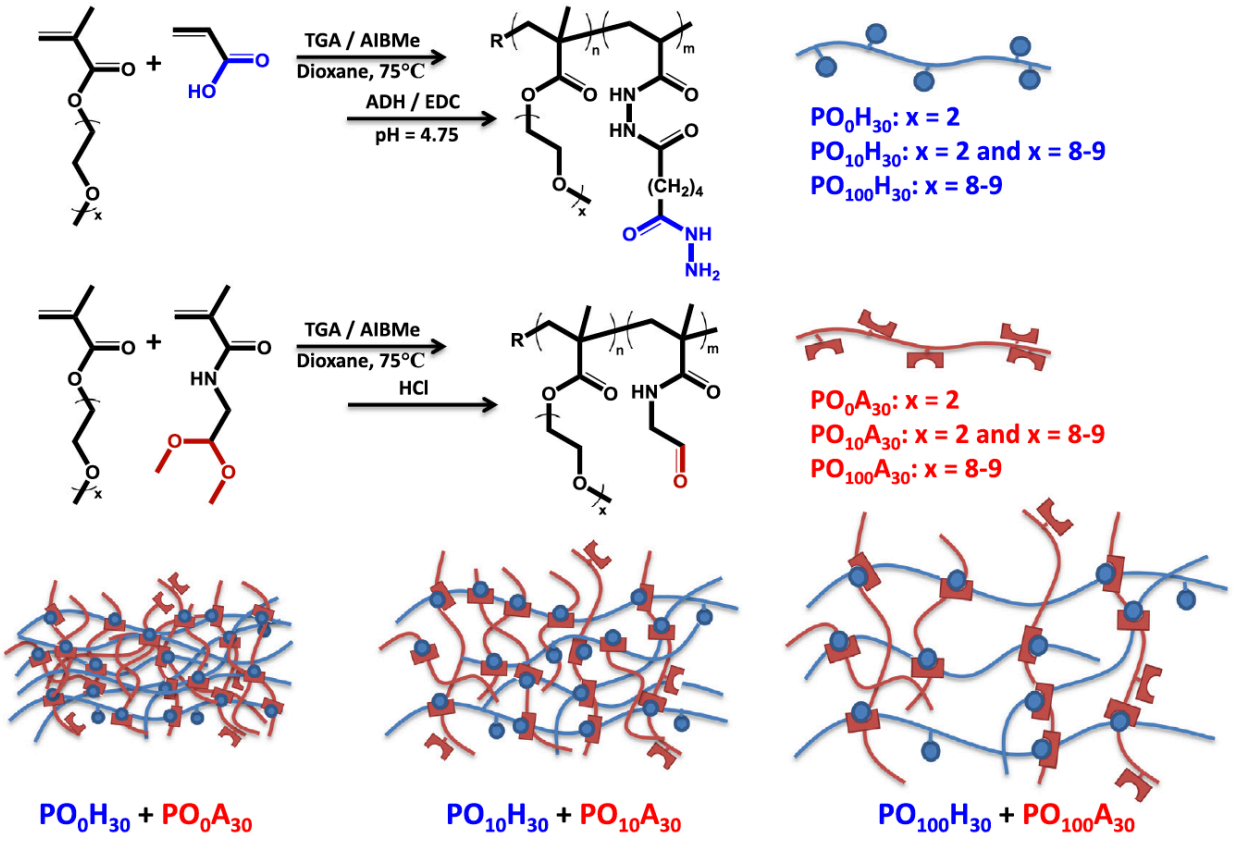

Figure 1.3 Schematic of the synthesis of POEGMA precursors. Top and middle images: Hydrazide-functionalized hydrogel precursor (blue; POH) and aldehyde-functionalized hydrogel precursor (red; POA) prepared with varying hydrophilicities. Lower images: the resultant hydrogel networks. Adapted from Smeets *et al.*[171]

1.6.2. Nitrocellulose-based POEGMA hydrogel films in biosensing

POEGMA hydrogel films can be affixed to nitrocellulose substrates using a layer-by-layer approach wherein small volumes of diluted aldehyde and hydrazide-functionalized polymer precursors (typically starting with the aldehyde-functionalized polymer to promote hemiacetal formation with any surface-bound aldehyde groups on the nitrocellulose) are sequentially deposited onto the surface of the film. The polymer can be applied using various fabrication methods, including spin coating,[175,176] non-contact printing,[177] and dip-coating.[178]

Deng *et al.* developed an enzyme-linked immunosorbent assay (ELISA) platform consisting of a dip-coated paper-based sensing device with a POEGMA hydrogel film interface.[178] The POEGMA-based hydrogel interface demonstrated the ability to resist the non-specific adsorption of IgG antibodies,

resulting in more effective sensor passivation compared to traditional blocking agents like bovine serum albumin or skim milk. Notably, the designed platform was also amenable to microarray fabrication. Building on this promise, a printable POEGMA hydrogel-film microarray was fabricated *via* the sequential deposition of aldehyde-functionalized polymer and hydrazide-functionalized polymer co-dissolved with various enzymes, with the fabrication process enabling effective physical entrapment of valuable bioreceptor compounds without significantly impacting their bioactivity[177]. Of note, the tunability of the pore size in the hydrogel enabled the microarray to effectively discriminate between true and aggregating enzyme inhibitors, facilitating the rapid (< 25min) and inexpensive (using 95% less sample compared to a solution-assay) identification of molecules with true inhibitory potential to minimize the number of false hits in stage one of drug screening. Furthermore, the water binding capacity of the hydrogel enables the stabilization and protection of physically trapped enzymes against drying and protease degradation, which significantly increases its commercial potential.

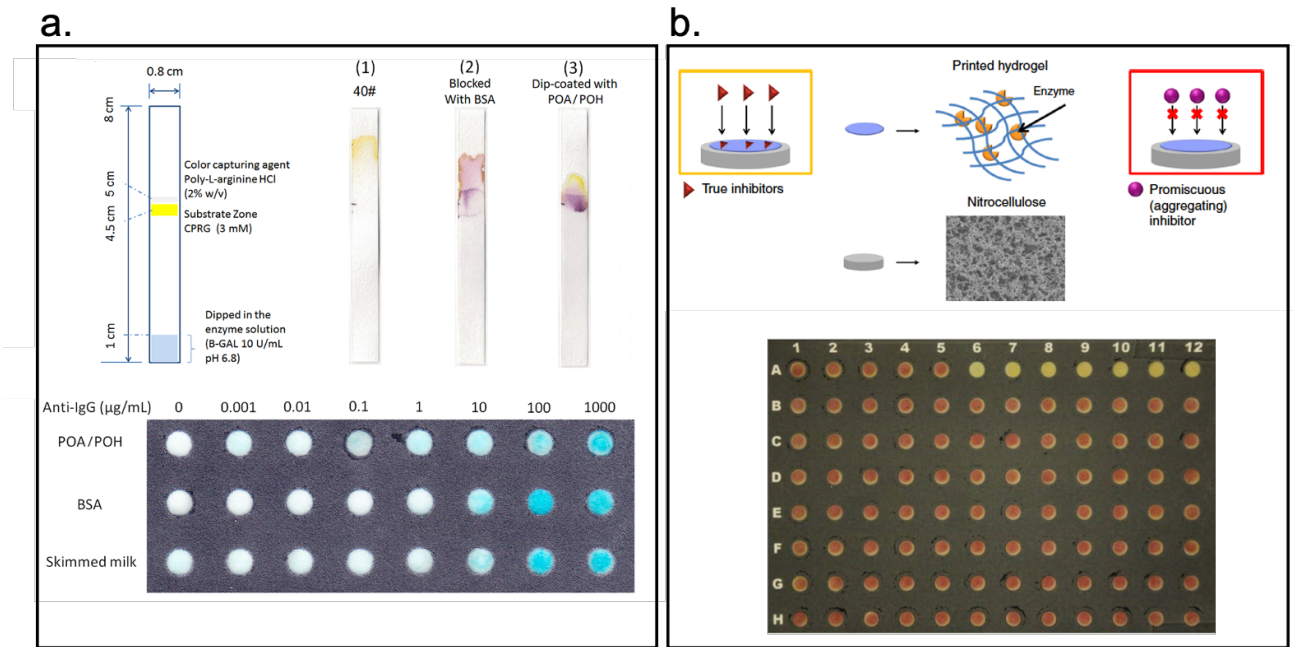

Figure 1.4 Application of POEGMA hydrogel films in protein-based assays. **(a)** Dip-coated nitrocellulose-based ELISA assay adapted from *Deng et al.*[178] **(b)** Printed microarray sensor for screening true enzyme inhibitors, adapted from Mateen *et al.*[177]

1.7. Thesis Objectives

The development of facile, low-cost, and portable devices capable of sensitive and rapid small-molecule detection remains a significant challenge for researchers focusing on clinical and academic biosensing technology. Given the diagnostic potential of nucleic acids and the benefits of hydrogel interfaces in fabricating solid-phase assays, the work in this thesis investigates a new class of polymeric materials that integrates different nucleic acid affinity tags to achieve improved biosensing performance. More precisely, the goal of this research is to design a facile fabrication protocol for printable POEGMA hydrogel-film microarrays capable of physically entrapping DNA oligonucleotides, including DNA aptamers, without the need for complex conjugation and immobilization procedures. Moreover, the resultant microarrays should possess the ability to stabilize the sensing molecules against chemical and physical denaturing conditions while exercising antifouling properties and exhibiting enhanced binding affinity, sensitivity, and selectivity, thus improving the ability of the nucleic acid bioreceptors to recognize a target cognate ligand without the need for laborious on-chip signal-amplification procedures.

While the literature contains several reports of hydrogel-based DNA microarrays, research focusing on the application of surface-affixed hydrogel films in DNA-hybridization technology is still limited. This research gap is largely due to the lack of a strategy for synthesizing biohybrid hydrogel-film materials that enable both reproducible and reliable fabrication as well as enhanced sensing performance. To fill this gap, our group previously developed a hydrogel film material based on an *in situ*-gelling POEGMA chemistry that does not require external gelation initiators and is adaptable to a printing fabrication format. In this approach, the hydrogel film is affixed to a nitrocellulose membrane *via* a sequential "layer-by-layer" deposition of covalently cross-linkable aldehyde- and hydrazide-functionalized precursor polymers. The developed POEGMA hydrogel films were subsequently adapted to fabricate protein-based microarrays designed to discriminate between true and aggregating enzyme inhibitors based on the hydrogel pore sizes.

Building on this prior work, Chapter 2 focuses on incorporating the POEGMA chemistry into a DNA-sensing application. To meet the requirement for DNA hybridization microarrays, we configured a new hydrogel film based on more hydrophilic hydrogel precursors. Pre-amplified long-chain DNA molecules, produced *via* RCA reactions, were used as sensing materials to increase the incidence of hybridization events. The material's ability to envelop the RCA product, detect fluorophore-tagged oligonucleotides of varying sizes, reduce non-specific adsorption on nitrocellulose, and improve the signaling capacity of short oligonucleotides (< 30-nt DNA strands) was then assessed and compared to that of hydrogel-free systems. In addition, the microstructure of the developed hydrogel film and the co-localization of the RCA product within the hydrogel matrix were also investigated to assess the film's capacity to provide more uniform fluorescence signal distribution, stabilize newly formed hybridized complexes, and support the development of more specific and size-selective hybridization assays relative to hydrogel-free systems. We demonstrate that combining RCA-product-based DNA sensing with optimal POEGMA hydrogel films enables the facile fabrication of printable sensors featuring more uniformly distributed surface-immobilized DNA-sensing molecules with higher retention capacities, thus providing superior detection capacity for small nucleic acids targets compared to hydrogel-free systems. The production of such films would address some of the key challenges associated with the fabrication and application of conventional 2D hybridization microarrays.

To expand the applicability of POEGMA hydrogels to the detection of non-nucleic-acid targets, DNA-based aptamers were introduced as a sensing element. Chapter 3 describes the incorporation of an ATP-binding FRET-based structure-switching aptamer construct that identifies cognate ligands through quencher-labeled oligonucleotide strand displacement into a hydrogel system prepared in a 96-well

microtiter plate *via* physical entrapment. The POEGMA hydrogel and structure-switching aptamer designs were optimized with respect to their ability to provide sufficient capacity to immobilize the sensing molecules, protect against nucleolytic attack, and enable enhanced ligand-induced signaling ability. In addition, the effectiveness of the overall sensitivity of the assay was assessed and compared to that of hydrogel-free systems. More specifically, this chapter presents a high-throughput investigation of the ability of hydrogels to thermally stabilize structure-switching aptamer constructs assembled with quencher stems of decreasing length (≤ 12-nt). Aptamer assemblies with shorter quencher strands are typically more responsive to ligands, as they leave more of the aptamer sequence free for ligand binding; however, they are also characterized by lower hybridization strength and FRET efficiency that results in higher background fluorescence and lower signaling gain. The developed hydrogel-based aptamer arrays are characterized with respect to FRET efficiency, changes in the Gibbs free energy of the hybridization, ligand-binding affinity, and the sensitivity of aptamer constructs composed with different quencher strand lengths. Given the improved hybridization efficiency achieved by embedding short DNA duplexes inside POEGMA hydrogel microarrays (demonstrated in Chapter 2), we demonstrate that the optimal POEGMA hydrogel film will not only facilitate the effective immobilization of nucleic acid aptamer reporters but also reinforce aptamer constructs assembled with shorter quencher stems, thus facilitating more sensitive assays with a lower trade-off in background signal. Moreover, the optimized POEGMA hydrogel film possessed solution-like kinetics in ligand response enabled by the swollen and deformable polymeric networks.

Chapter 4 details the translation of the developed hydrogel-based aptamer sensor into a printable microarray format in addition to implementing several improvements to the assay conditions aimed at further enhancing the device's sensitivity. First, the aptamer construct was assembled with shorter quencher stems (≤ 9-nt) rationally positioned to trigger a ligand-binding mechanism associated with enhanced signaling, thereby implementing quencher stem thermodynamic and location considerations, both to the design of more responsive aptamer reporters. Additionally, parameters such as hydrogel concentration and aptamer surface density were examined and compared to those in hydrogel-free systems to support the development of optimal ligand-binding conditions. Combining an optimal hydrogel configuration and aptamer constructs assembled from even shorter rationally positioned oligonucleotides (9-nt and 7-nt) was observed to significantly improve the sensor's ligand biding affinity based on more effective ligand-induced aptamer renaturation, offering a solution to the low sensitivity and reduced affinity following signaling modification typically observed with FRET aptamer constructs. The developed aptamer microarray was assessed in both pure and complex media to confirm its applicability for use with real biological samples (e.g. human serum).

Collectively, this thesis documents a unique strategy entailing the integration of nucleic-acid-sensing elements into a hydrogel-based system. In this configuration, the hydrogel-based system acts not only serves an immobilization substrate but also as a tool to enhance a variety of affinity interactions driven by the nucleic acid binders, enabling effective detection of complementary oligonucleotides and small biological analytes in diverse potential sample types.

1.8. References

(1) Clegg, J. R.; Peppas, N. A. Molecular Recognition with Soft Biomaterials. *Soft Matter* **2020**, *16* (4), 856–869. https://doi.org/10.1039/C9SM01981B.

(2) *Recognition Receptors in Biosensors*; Zourob, M., Ed.; Springer New York: New York, NY, 2010. https://doi.org/10.1007/978-1-4419-0919-0.

(3) Stauffer, D. A.; Barrans, R. E.; Dougherty, D. A. Concerning the Thermodynamics of Molecular Recognition in Aqueous and Organic Media. Evidence for Significant Heat Capacity Effects. *J. Org. Chem.* **1990**, *55* (9), 2762–2767. https://doi.org/10.1021/jo00296a038.

(4) Williams, D. H.; Stephens, E.; O'Brien, D. P.; Zhou, M. Understanding Noncovalent Interactions: Ligand Binding Energy and Catalytic Efficiency from Ligand-Induced Reductions in Motion within Receptors and Enzymes. *Angew Chem Int Ed* **2004**, *43* (48), 6596–6616. https://doi.org/10.1002/anie.200300644.

(5) Corzo, J. Time, the Forgotten Dimension of Ligand Binding Teaching. *Biochem Molecular Bio Educ* **2006**, *34* (6), 413–416. https://doi.org/10.1002/bmb.2006.494034062678.

(6) Bongrand, P. Ligand-Receptor Interactions. **2008**. https://doi.org/10.48550/ARXIV.0809.1926.

(7) Kuriyan, J.; Konforti, B.; Wemmer, D. *The Molecules of Life*, 0 ed.; W.W. Norton & Company, 2012. https://doi.org/10.1201/9780429258787.

(8) Yang, L.; Adam, C.; Nichol, G. S.; Cockroft, S. L. How Much Do van Der Waals Dispersion Forces Contribute to Molecular Recognition in Solution? *Nature Chem* **2013**, *5* (12), 1006–1010. https://doi.org/10.1038/nchem.1779.

(9) Ben-Naim, A. The Binding Isotherm. In *Cooperativity and Regulation in Biochemical Processes*; Springer US: Boston, MA, 2001; pp 25–49. https://doi.org/10.1007/978-1-4757-3302-0_2.

(10) Hulme, E. C.; Trevethick, M. A. Ligand Binding Assays at Equilibrium: Validation and Interpretation. *British J Pharmacology* **2010**, *161* (6), 1219–1237. https://doi.org/10.1111/j.1476-5381.2009.00604.x.

(11) Meyer-Almes, F.-J. Kinetic Binding Assays for the Analysis of Protein–Ligand Interactions. *Drug Discovery Today: Technologies* **2015**, *17*, 1–8. https://doi.org/10.1016/j.ddtec.2015.08.004.

(12) Ma, W.; Yang, L.; He, L. Overview of the Detection Methods for Equilibrium Dissociation Constant KD of Drug-Receptor Interaction. *Journal of Pharmaceutical Analysis* **2018**, *8* (3), 147–152. https://doi.org/10.1016/j.jpha.2018.05.001.

(13) De Jong, L. A. A.; Uges, D. R. A.; Franke, J. P.; Bischoff, R. Receptor–Ligand Binding Assays: Technologies and Applications. *Journal of Chromatography B* **2005**, *829* (1–2), 1–25. https://doi.org/10.1016/j.jchromb.2005.10.002.

(14) Yu, H.; Alkhamis, O.; Canoura, J.; Liu, Y.; Xiao, Y. Advances and Challenges in Small-Molecule DNA Aptamer Isolation, Characterization, and Sensor Development. *Angew. Chem. Int. Ed.* **2021**, *60* (31), 16800–16823. https://doi.org/10.1002/anie.202008663.

(15) Stepanov, I. A. The Heats of Chemical Reactions: The Van't-Hoff Equation and Calorimetry. *Zeitschrift für Physikalische Chemie* **2005**, *219* (8), 1089–1097. https://doi.org/10.1524/zpch.2005.219.8.1089.

(16) Krug, R. R.; Hunter, W. G.; Grieger, R. A. Enthalpy-Entropy Compensation. 1. Some Fundamental Statistical Problems Associated with the Analysis of van't Hoff and Arrhenius Data. *J. Phys. Chem.* **1976**, *80* (21), 2335–2341. https://doi.org/10.1021/j100562a006.

(17) Freire, E.; Mayorga, O. L.; Straume, M. Isothermal Titration Calorimetry. *Anal. Chem.* **1990**, *62* (18), 950A-959A. https://doi.org/10.1021/ac00217a002.

(18) Freyer, M. W.; Lewis, E. A. Isothermal Titration Calorimetry: Experimental Design, Data Analysis, and Probing Macromolecule/Ligand Binding and Kinetic Interactions. In *Methods in Cell Biology*; Elsevier, 2008; Vol. 84, pp 79–113. https://doi.org/10.1016/S0091-679X(07)84004-0.

(19) Gellman, S. H. Introduction: Molecular Recognition. *Chem. Rev.* **1997**, *97* (5), 1231–1232. https://doi.org/10.1021/cr970328j.

(20) Justino, C. I. L.; Freitas, A. C.; Pereira, R.; Duarte, A. C.; Rocha Santos, T. A. P. Recent Developments in Recognition Elements for Chemical Sensors and Biosensors. *TrAC Trends in Analytical Chemistry* **2015**, *68*, 2–17. https://doi.org/10.1016/j.trac.2015.03.006.

(21) Ruscito, A.; DeRosa, M. C. Small-Molecule Binding Aptamers: Selection Strategies, Characterization, and Applications. *Front. Chem.* **2016**, *4*. https://doi.org/10.3389/fchem.2016.00014.

(22) Meng, X.; Wei, J.; Ren, X.; Ren, J.; Tang, F. A Simple and Sensitive Fluorescence Biosensor for Detection of Organophosphorus Pesticides Using H2O2-Sensitive Quantum Dots/Bi-Enzyme. *Biosensors and Bioelectronics* **2013**, *47*, 402–407. https://doi.org/10.1016/j.bios.2013.03.053.

(23) Luo, X.; Davis, J. J. Electrical Biosensors and the Label Free Detection of Protein Disease Biomarkers. *Chem. Soc. Rev.* **2013**, *42* (13), 5944. https://doi.org/10.1039/c3cs60077g.

(24) Yu, X.; Zhang, S.; Guo, W.; Li, B.; Yang, Y.; Xie, B.; Li, K.; Zhang, L. Recent Advances on Functional Nucleic-Acid Biosensors. *Sensors* **2021**, *21* (21), 7109. https://doi.org/10.3390/s21217109.

(25) Du, Y.; Dong, S. Nucleic Acid Biosensors: Recent Advances and Perspectives. *Anal. Chem.* **2017**, *89* (1), 189–215. https://doi.org/10.1021/acs.analchem.6b04190.
(26) V, K. DNA Biosensors-A Review. *J Bioengineer & Biomedical Sci* **2017**, *07* (02). https://doi.org/10.4172/2155-9538.1000222.
(27) Wang, H.; Yang, R.; Yang, L.; Tan, W. Nucleic Acid Conjugated Nanomaterials for Enhanced Molecular Recognition. *ACS Nano* **2009**, *3* (9), 2451–2460. https://doi.org/10.1021/nn9006303.
(28) Hua, Y.; Ma, J.; Li, D.; Wang, R. DNA-Based Biosensors for the Biochemical Analysis: A Review. *Biosensors* **2022**, *12* (3), 183. https://doi.org/10.3390/bios12030183.
(29) Walter, J.-G.; Heilkenbrinker, A.; Austerjost, J.; Timur, S.; Stahl, F.; Schepe, T. Aptasensors for Small Molecule Detection. *Zeitschrift für Naturforschung B* **2012**, *67* (10), 976–986. https://doi.org/10.5560/znb.2012-0147.
(30) Wolter, O.; Mayer, G. Aptamers as Valuable Molecular Tools in Neurosciences. *J. Neurosci.* **2017**, *37* (10), 2517–2523. https://doi.org/10.1523/JNEUROSCI.1969-16.2017.
(31) Beyer, S.; Nickels, P.; Simmel, F. C. Periodic DNA Nanotemplates Synthesized by Rolling Circle Amplification. *Nano Lett.* **2005**, *5* (4), 719–722. https://doi.org/10.1021/nl050155a.
(32) Anderson, M. L. M. *Nucleic Acid Hybridization*, 1st ed.; Rickwood, D., Ed.; Garland Science, 2020. https://doi.org/10.1201/9781003076780.
(33) Marky, L. A.; Garcia, A. Watson–Crick Base Pairs. In *Encyclopedia of Life Sciences*; Wiley, 2002. https://doi.org/10.1038/npg.els.0003126.
(34) Kessler, C. Overview on Factors Influencing Nucleic Acid Hybridization. In *Nonradioactive Analysis of Biomolecules*; Kessler, C., Ed.; Springer Berlin Heidelberg: Berlin, Heidelberg, 2000; pp 437–442. https://doi.org/10.1007/978-3-642-57206-7_37.
(35) Sugimoto, N.; Nakano, S.; Katoh, M.; Matsumura, A.; Nakamuta, H.; Ohmichi, T.; Yoneyama, M.; Sasaki, M. Thermodynamic Parameters To Predict Stability of RNA/DNA Hybrid Duplexes. *Biochemistry* **1995**, *34* (35), 11211–11216. https://doi.org/10.1021/bi00035a029.
(36) Wu, P.; Nakano, S.; Sugimoto, N. Temperature Dependence of Thermodynamic Properties for DNA/DNA and RNA/DNA Duplex Formation: Temperature Dependence of Thermodynamic Properties. *European Journal of Biochemistry* **2002**, *269* (12), 2821–2830. https://doi.org/10.1046/j.1432-1033.2002.02970.x.
(37) You, Y.; Tataurov, A. V.; Owczarzy, R. Measuring Thermodynamic Details of DNA Hybridization Using Fluorescence. *Biopolymers* **2011**, *95* (7), 472–486. https://doi.org/10.1002/bip.21615.
(38) Owczarzy, R.; You, Y.; Moreira, B. G.; Manthey, J. A.; Huang, L.; Behlke, M. A.; Walder, J. A. Effects of Sodium Ions on DNA Duplex Oligomers: Improved Predictions of Melting Temperatures. *Biochemistry* **2004**, *43* (12), 3537–3554. https://doi.org/10.1021/bi034621r.
(39) Peter, C.; Meusel, M.; Grawe, F.; Katerkamp, A.; Cammann, K.; Börchers, T. Optical DNA-Sensor Chip for Real-Time Detection of Hybridization Events. *Fresenius J Anal Chem* **2001**, *371* (2), 120–127. https://doi.org/10.1007/s002160101006.
(40) Green, M. R.; Sambrook, J. Polymerase Chain Reaction. *Cold Spring Harb Protoc* **2019**, *2019* (6), pdb.top095109. https://doi.org/10.1101/pdb.top095109.
(41) Zhao, Y.; Chen, F.; Li, Q.; Wang, L.; Fan, C. Isothermal Amplification of Nucleic Acids. *Chem. Rev.* **2015**, *115* (22), 12491–12545. https://doi.org/10.1021/acs.chemrev.5b00428.
(42) Ali, M. M.; Li, F.; Zhang, Z.; Zhang, K.; Kang, D.-K.; Ankrum, J. A.; Le, X. C.; Zhao, W. Rolling Circle Amplification: A Versatile Tool for Chemical Biology, Materials Science and Medicine. *Chem. Soc. Rev.* **2014**, *43* (10), 3324. https://doi.org/10.1039/c3cs60439j.
(43) Gu, L.; Yan, W.; Liu, L.; Wang, S.; Zhang, X.; Lyu, M. Research Progress on Rolling Circle Amplification (RCA)-Based Biomedical Sensing. *Pharmaceuticals* **2018**, *11* (2), 35. https://doi.org/10.3390/ph11020035.
(44) Liu, M.; Zhang, Q.; Chang, D.; Gu, J.; Brennan, J. D.; Li, Y. A DNAzyme Feedback Amplification Strategy for Biosensing. *Angew. Chem. Int. Ed.* **2017**, *56* (22), 6142–6146. https://doi.org/10.1002/anie.201700054.
(45) Ali, M. M.; Li, Y. Colorimetric Sensing by Using Allosteric-DNAzyme-Coupled Rolling Circle Amplification and a Peptide Nucleic Acid-Organic Dye Probe. *Angew. Chem. Int. Ed.* **2009**, *48* (19), 3512–3515. https://doi.org/10.1002/anie.200805966.
(46) Pei, H.; Zuo, X.; Pan, D.; Shi, J.; Huang, Q.; Fan, C. Scaffolded Biosensors with Designed DNA Nanostructures. *NPG Asia Mater* **2013**, *5* (6), e51–e51. https://doi.org/10.1038/am.2013.22.
(47) Zhao, W.; Ali, M. M.; Brook, M. A.; Li, Y. Rolling Circle Amplification: Applications in Nanotechnology and Biodetection with Functional Nucleic Acids. *Angew. Chem. Int. Ed.* **2008**, *47* (34), 6330–6337. https://doi.org/10.1002/anie.200705982.
(48) Linck, L.; Reiß, E.; Bier, F.; Resch-Genger, U. Direct Labeling Rolling Circle Amplification as a Straightforward Signal Amplification Technique for Biodetection Formats. *Anal. Methods* **2012**, *4* (5), 1215. https://doi.org/10.1039/c2ay05760c.

(49) Linck, L.; Resch-Genger, U. Identification of Efficient Fluorophores for the Direct Labeling of DNA via Rolling Circle Amplification (RCA) Polymerase Φ29. *European Journal of Medicinal Chemistry* **2010**, *45* (12), 5561–5566. https://doi.org/10.1016/j.ejmech.2010.09.005.
(50) Qi, X. L-RCA (Ligation-Rolling Circle Amplification): A General Method for Genotyping of Single Nucleotide Polymorphisms (SNPs). *Nucleic Acids Research* **2001**, *29* (22), 116e–1116. https://doi.org/10.1093/nar/29.22.e116.
(51) Leung, A.; Schones, D. E.; Natarajan, R. Using Epigenetic Mechanisms to Understand the Impact of Common Disease Causing Alleles. *Current Opinion in Immunology* **2012**, *24* (5), 558–563. https://doi.org/10.1016/j.coi.2012.07.004.
(52) Jain, S.; Dandy, D. S.; Geiss, B. J.; Henry, C. S. Padlock Probe-Based Rolling Circle Amplification Lateral Flow Assay for Point-of-Need Nucleic Acid Detection. *Analyst* **2021**, *146* (13), 4340–4347. https://doi.org/10.1039/D1AN00399B.
(53) Mao, Y.; Liu, M.; Tram, K.; Gu, J.; Salena, B. J.; Jiang, Y.; Li, Y. Optimal DNA Templates for Rolling Circle Amplification Revealed by In Vitro Selection. *Chem. Eur. J.* **2015**, *21* (22), 8069–8074. https://doi.org/10.1002/chem.201500994.
(54) Clausson, C.-M.; Arngården, L.; Ishaq, O.; Klaesson, A.; Kühnemund, M.; Grannas, K.; Koos, B.; Qian, X.; Ranefall, P.; Krzywkowski, T.; Brismar, H.; Nilsson, M.; Wählby, C.; Söderberg, O. Compaction of Rolling Circle Amplification Products Increases Signal Integrity and Signal-to-Noise Ratio. *Sci Rep* **2015**, *5* (1), 12317. https://doi.org/10.1038/srep12317.
(55) Ellington, A. D.; Szostak, J. W. In Vitro Selection of RNA Molecules That Bind Specific Ligands. *Nature* **1990**, *346* (6287), 818–822. https://doi.org/10.1038/346818a0.
(56) Irvine, D.; Tuerk, C.; Gold, L. Systematic Evolution of Ligands by Exponential Enrichment with Integrated Optimization by Non-Linear Analysis. 23.
(57) Hermann, T.; Patel, D. J. Adaptive Recognition by Nucleic Acid Aptamers. *Science* **2000**, *287* (5454), 820–825. https://doi.org/10.1126/science.287.5454.820.
(58) Cho, E. J.; Lee, J.-W.; Ellington, A. D. Applications of Aptamers as Sensors. *Annual Rev. Anal. Chem.* **2009**, *2* (1), 241–264. https://doi.org/10.1146/annurev.anchem.1.031207.112851.
(59) Huizenga, D. E.; Szostak, J. W. A DNA Aptamer That Binds Adenosine and ATP. *Biochemistry* **1995**, *34* (2), 656–665. https://doi.org/10.1021/bi00002a033.
(60) Yoo, H.; Jo, H.; Oh, S. S. Detection and beyond: Challenges and Advances in Aptamer-Based Biosensors. *Mater. Adv.* **2020**, *1* (8), 2663–2687. https://doi.org/10.1039/D0MA00639D.
(61) Song, S.; Wang, L.; Li, J.; Fan, C.; Zhao, J. Aptamer-Based Biosensors. *TrAC Trends in Analytical Chemistry* **2008**, *27* (2), 108–117. https://doi.org/10.1016/j.trac.2007.12.004.
(62) Lin, C. H.; Patei, D. J. Structural Basis of DNA Folding and Recognition in an AMP-DNA Aptamer Complex: Distinct Architectures but Common Recognition Motifs for DNA and RNA Aptamers Complexed to AMP. *Chemistry & Biology* **1997**, *4* (11), 817–832. https://doi.org/10.1016/S1074-5521(97)90115-0.
(63) Jhaveri, S. D.; Kirby, R.; Conrad, R.; Maglott, E. J.; Bowser, M.; Kennedy, R. T.; Glick, G.; Ellington, A. D. Designed Signaling Aptamers That Transduce Molecular Recognition to Changes in Fluorescence Intensity. *J. Am. Chem. Soc.* **2000**, *122* (11), 2469–2473. https://doi.org/10.1021/ja992393b.
(64) Wang, K.; Tang, Z.; Yang, C. J.; Kim, Y.; Fang, X.; Li, W.; Wu, Y.; Medley, C. D.; Cao, Z.; Li, J.; Colon, P.; Lin, H.; Tan, W. Molecular Engineering of DNA: Molecular Beacons. *Angew. Chem. Int. Ed.* **2009**, *48* (5), 856–870. https://doi.org/10.1002/anie.200800370.
(65) *Principles of Fluorescence Spectroscopy*; Lakowicz, J. R., Ed.; Springer US: Boston, MA, 2006. https://doi.org/10.1007/978-0-387-46312-4.
(66) Hamaguchi, N.; Ellington, A.; Stanton, M. Aptamer Beacons for the Direct Detection of Proteins. *Analytical Biochemistry* **2001**, *294* (2), 126–131. https://doi.org/10.1006/abio.2001.5169.
(67) Nutiu, R.; Li, Y. Structure-Switching Signaling Aptamers. *J. Am. Chem. Soc.* **2003**, *125* (16), 4771–4778. https://doi.org/10.1021/ja028962o.
(68) Feagin, T. A.; Maganzini, N.; Soh, H. T. Strategies for Creating Structure-Switching Aptamers. *ACS Sens.* **2018**, *3* (9), 1611–1615. https://doi.org/10.1021/acssensors.8b00516.
(69) Lau, P. S.; Lai, C. K.; Li, Y. Quality Control Certification of RNA Aptamer-Based Detection. *ChemBioChem* **2013**, *14* (8), 987–992. https://doi.org/10.1002/cbic.201300134.
(70) Li, Y.; Liu, J. Aptamer-Based Strategies for Recognizing Adenine, Adenosine, ATP and Related Compounds. *Analyst* **2020**, *145* (21), 6753–6768. https://doi.org/10.1039/D0AN00886A.
(71) Lu, C.; Yang, H.; Zhu, C.; Chen, X.; Chen, G. A Graphene Platform for Sensing Biomolecules. *Angew Chem Int Ed* **2009**, *48* (26), 4785–4787. https://doi.org/10.1002/anie.200901479.
(72) Zheng, M.; Jagota, A.; Semke, E. D.; Diner, B. A.; Mclean, R. S.; Lustig, S. R.; Richardson, R. E.; Tassi, N. G. DNA-Assisted Dispersion and Separation of Carbon Nanotubes. *Nature Mater* **2003**, *2* (5), 338–342. https://doi.org/10.1038/nmat877.

(73) Béra Abérem, M.; Najari, A.; Ho, H. -A.; Gravel, J. -F.; Nobert, P.; Boudreau, D.; Leclerc, M. Cover Picture: Protein Detecting Arrays Based on Cationic Polythiophene–DNA-Aptamer Complexes (Adv. Mater. 20/2006). *Advanced Materials* **2006**, *18* (20), adma.200690082. https://doi.org/10.1002/adma.200690082.
(74) Scheller, F. W.; Wollenberger, U.; Warsinke, A.; Lisdat, F. Research and Development in Biosensors. *Current Opinion in Biotechnology* **2001**, *12* (1), 35–40. https://doi.org/10.1016/S0958-1669(00)00169-5.
(75) Sassolas, A.; Leca-Bouvier, B. D.; Blum, L. J. DNA Biosensors and Microarrays. *Chem. Rev.* **2008**, *108* (1), 109–139. https://doi.org/10.1021/cr0684467.
(76) Debouck, C.; Goodfellow, P. N. DNA Microarrays in Drug Discovery and Development. **1999**, *21*, 3.
(77) Wheelan, S. J.; Martínez Murillo, F.; Boeke, J. D. The Incredible Shrinking World of DNA Microarrays. *Mol. BioSyst.* **2008**, *4* (7), 726. https://doi.org/10.1039/b706237k.
(78) Witt, M.; Walter, J.-G.; Stahl, F. Aptamer Microarrays—Current Status and Future Prospects. *Microarrays* **2015**, *4* (2), 115–132. https://doi.org/10.3390/microarrays4020115.
(79) Wittmann, C.; Marquette, C. DNA Immobilization. In *Encyclopedia of Analytical Chemistry*; Meyers, R. A., Ed.; Wiley, 2012. https://doi.org/10.1002/9780470027318.a9210.
(80) Rupcich, N.; Nutiu, R.; Shen, Y.; Li, Y.; Brennan, J. D. The Use of Functional Nucleic Acids in Solid-Phase Fluorimetric Assays. In *Functional Nucleic Acids for Analytical Applications*; Yingfu, L., Yi, L., Eds.; Springer New York: New York, NY, 2009; pp 309–342. https://doi.org/10.1007/978-0-387-73711-9_12.
(81) Nimse, S.; Song, K.; Sonawane, M.; Sayyed, D.; Kim, T. Immobilization Techniques for Microarray: Challenges and Applications. *Sensors* **2014**, *14* (12), 22208–22229. https://doi.org/10.3390/s141222208.
(82) Belosludtsev, Y.; Iverson, B.; Lemeshko, S.; Eggers, R.; Wiese, R.; Lee, S.; Powdrill, T.; Hogan, M. DNA Microarrays Based on Noncovalent Oligonucleotide Attachment and Hybridization in Two Dimensions. *Analytical Biochemistry* **2001**, *292* (2), 250–256. https://doi.org/10.1006/abio.2001.5088.
(83) Bilgic, T.; Klok, H.-A. Oligonucleotide Immobilization and Hybridization on Aldehyde-Functionalized Poly(2-Hydroxyethyl Methacrylate) Brushes. *Biomacromolecules* **2015**, *16* (11), 3657–3665. https://doi.org/10.1021/acs.biomac.5b01116.
(84) Bünemann, H. Immobilization of Denatured DNA to Macroporous Supports: II. Steric and Kinetic Parameters of Heterogeneous Hybridization Reactions. *Nucl Acids Res* **1982**, *10* (22), 7181–7196. https://doi.org/10.1093/nar/10.22.7181.
(85) Balzer, A. H. A.; Whitehurst, C. B. An Analysis of the Biotin–(Strept)Avidin System in Immunoassays: Interference and Mitigation Strategies. *CIMB* **2023**, *45* (11), 8733–8754. https://doi.org/10.3390/cimb45110549.
(86) Rao, A. N.; Grainger, D. W. Biophysical Properties of Nucleic Acids at Surfaces Relevant to Microarray Performance. *Biomater. Sci.* **2014**, *2* (4), 436–471. https://doi.org/10.1039/C3BM60181A.
(87) Jung, I. Y.; Kim, J. S.; Choi, B. R.; Lee, K.; Lee, H. Hydrogel Based Biosensors for In Vitro Diagnostics of Biochemicals, Proteins, and Genes. *Adv. Healthcare Mater.* **2017**, *6* (12), 1601475. https://doi.org/10.1002/adhm.201601475.
(88) Herrmann, A.; Haag, R.; Schedler, U. Hydrogels and Their Role in Biosensing Applications. *Adv. Healthcare Mater.* **2021**, *10* (11), 2100062. https://doi.org/10.1002/adhm.202100062.
(89) Monton, M. R. N.; Forsberg, E. M.; Brennan, J. D. Tailoring Sol–Gel-Derived Silica Materials for Optical Biosensing. *Chem. Mater.* **2012**, *24* (5), 796–811. https://doi.org/10.1021/cm202798e.
(90) Bi, X.; Liang, A. In Situ-Forming Cross-linking Hydrogel Systems: Chemistry and Biomedical Applications. In *Emerging Concepts in Analysis and Applications of Hydrogels*; Majee, S. B., Ed.; InTech, 2016. https://doi.org/10.5772/63954.
(91) Caló, E.; Khutoryanskiy, V. V. Biomedical Applications of Hydrogels: A Review of Patents and Commercial Products. *European Polymer Journal* **2015**, *65*, 252–267. https://doi.org/10.1016/j.eurpolymj.2014.11.024.
(92) Ahmed, E. M. Hydrogel: Preparation, Characterization, and Applications: A Review. *Journal of Advanced Research* **2015**, *6* (2), 105–121. https://doi.org/10.1016/j.jare.2013.07.006.
(93) Patenaude, M.; Smeets, N. M. B.; Hoare, T. Designing Injectable, Covalently Cross-Linked Hydrogels for Biomedical Applications. *Macromol. Rapid Commun.* **2014**, *35* (6), 598–617. https://doi.org/10.1002/marc.201300818.
(94) Hydrogels Based on Schi_ Base Linkages for Biomedical Applicationsmolecules-24-03005.Pdf.
(95) Patenaude, M.; Smeets, N. M. B.; Hoare, T. Designing Injectable, Covalently Cross-Linked Hydrogels for Biomedical Applications. *Macromol. Rapid Commun.* **2014**, *35* (6), 598–617. https://doi.org/10.1002/marc.201300818.
(96) Smeets, N. M. B.; Bakaic, E.; Patenaude, M.; Hoare, T. Injectable and Tunable Poly(Ethylene Glycol) Analogue Hydrogels Based on Poly(Oligoethylene Glycol Methacrylate). *Chem. Commun.* **2014**, *50* (25), 3306. https://doi.org/10.1039/c3cc48514e.
(97) Zubtsov, D. A.; Savvateeva, E. N.; Rubina, A. Yu.; Pan'kov, S. V.; Konovalova, E. V.; Moiseeva, O. V.; Chechetkin, V. R.; Zasedatelev, A. S. Comparison of Surface and Hydrogel-Based Protein Microchips. *Analytical Biochemistry* **2007**, *368* (2), 205–213. https://doi.org/10.1016/j.ab.2007.04.040.

(98) Zlatanova and Mirzabekov - 2001 - Gel-Immobilized Microarrays of Nucleic Acids and P.Pdf.
(99) Nielsen, L. J.; Olsen, L. F.; Ozalp, V. C. Aptamers Embedded in Polyacrylamide Nanoparticles: A Tool for *in Vivo* Metabolite Sensing. *ACS Nano* **2010**, *4* (8), 4361–4370. https://doi.org/10.1021/nn100635j.
(100) Rubina, A. Y.; Pan'kov, S. V.; Dementieva, E. I.; Pen'kov, D. N.; Butygin, A. V.; Vasiliskov, V. A.; Chudinov, A. V.; Mikheikin, A. L.; Mikhailovich, V. M.; Mirzabekov, A. D. Hydrogel Drop Microchips with Immobilized DNA: Properties and Methods for Large-Scale Production. *Analytical Biochemistry* **2004**, *325* (1), 92–106. https://doi.org/10.1016/j.ab.2003.10.010.
(101) Liu, J. Oligonucleotide-Functionalized Hydrogels as Stimuli Responsive Materials and Biosensors. *Soft Matter* **2011**, *7* (15), 6757. https://doi.org/10.1039/c1sm05284e.
(102) Helwa, Y.; Dave, N.; Froidevaux, R.; Samadi, A.; Liu, J. Aptamer-Functionalized Hydrogel Microparticles for Fast Visual Detection of Mercury(II) and Adenosine. *ACS Appl. Mater. Interfaces* **2012**, *4* (4), 2228–2233. https://doi.org/10.1021/am300241j.
(103) Kuckling, D. Responsive Hydrogel Layers—from Synthesis to Applications. *Colloid Polym Sci* **2009**, *287* (8), 881–891. https://doi.org/10.1007/s00396-009-2060-x.
(104) Zhu, C.; Yang, G.; Li, H.; Du, D.; Lin, Y. Electrochemical Sensors and Biosensors Based on Nanomaterials and Nanostructures. *Anal. Chem.* **2015**, *87* (1), 230–249. https://doi.org/10.1021/ac5039863.
(105) Wang, H. Label-Free Hybridization Detection of a Single Nucleotide Mismatch by Immobilization of Molecular Beacons on an Agarose Film. *Nucleic Acids Research* **2002**, *30* (12), 61e–661. https://doi.org/10.1093/nar/gnf061.
(106) Liu, J.; Qu, S.; Suo, Z.; Yang, W. Functional Hydrogel Coatings. *National Science Review* **2021**, *8* (2), nwaa254. https://doi.org/10.1093/nsr/nwaa254.
(107) Shundo, A.; Hoshino, Y.; Higuchi, T.; Matsumoto, Y.; Penaloza Jr, D. P.; Matsumoto, K.; Ohno, M.; Miyaji, K.; Goto, M.; Tanaka, K. Facile Microcapsule Fabrication by Spray Deposition of a Supramolecular Hydrogel. *RSC Adv.* **2014**, *4* (68), 36097–36100. https://doi.org/10.1039/C4RA04636F.
(108) Chollet, B.; Li, M.; Martwong, E.; Bresson, B.; Fretigny, C.; Tabeling, P.; Tran, Y. Multiscale Surface-Attached Hydrogel Thin Films with Tailored Architecture. *ACS Appl. Mater. Interfaces* **2016**, *8* (18), 11729–11738. https://doi.org/10.1021/acsami.6b00446.
(109) Zhang, R.; Liberski, A.; Khan, F.; Diaz-Mochon, J. J.; Bradley, M. Inkjet Fabrication of Hydrogel Microarrays Using in Situ Nanolitre-Scale Polymerisation. *Chem. Commun.* **2008**, No. 11, 1317. https://doi.org/10.1039/b717932d.
(110) Ooi, H. W.; Mota, C.; ten Cate, A. T.; Calore, A.; Moroni, L.; Baker, M. B. Thiol–Ene Alginate Hydrogels as Versatile Bioinks for Bioprinting. *Biomacromolecules* **2018**, *19* (8), 3390–3400. https://doi.org/10.1021/acs.biomac.8b00696.
(111) Tanase, C. P.; Albulescu, R.; Neagu, M. Application of 3D Hydrogel Microarrays in Molecular Diagnostics: Advantages and Limitations. *Expert Review of Molecular Diagnostics* **2011**, *11* (5), 461–464. https://doi.org/10.1586/erm.11.30.
(112) Carrasquilla, C.; Li, Y.; Brennan, J. D. Surface Immobilization of Structure-Switching DNA Aptamers on Macroporous Sol−Gel-Derived Films for Solid-Phase Biosensing Applications. *Anal. Chem.* **2011**, *83* (3), 957–965. https://doi.org/10.1021/ac102679r.
(113) Ikeda, M.; Ochi, R.; Hamachi, I. Supramolecular Hydrogel-Based Protein and Chemosensor Array. *Lab Chip* **2010**, *10* (24), 3325. https://doi.org/10.1039/c004908e.
(114) Rao, A. N.; Grainger, D. W. Biophysical Properties of Nucleic Acids at Surfaces Relevant to Microarray Performance. *Biomater. Sci.* **2014**, *2* (4), 436–471. https://doi.org/10.1039/C3BM60181A.
(115) Monserud, J. H.; Schwartz, D. K. Effects of Molecular Size and Surface Hydrophobicity on Oligonucleotide Interfacial Dynamics. *Biomacromolecules* **2012**, *13* (12), 4002–4011. https://doi.org/10.1021/bm301289n.
(116) Nakano, S.; Yamaguchi, D.; Sugimoto, N. Thermal Stability and Conformation of DNA and Proteins under the Confined Condition in the Matrix of Hydrogels. *Mol Biol Rep* **2018**, *45* (4), 403–411. https://doi.org/10.1007/s11033-018-4174-z.
(117) Markarian, M. Z.; Schlenoff, J. B. Effect of Molecular Crowding and Ionic Strength on the Isothermal Hybridization of Oligonucleotides. *J. Phys. Chem. B* **2010**, *114* (32), 10620–10627. https://doi.org/10.1021/jp103213w.
(118) Nakano, S.; Miyoshi, D.; Sugimoto, N. Effects of Molecular Crowding on the Structures, Interactions, and Functions of Nucleic Acids. *Chem. Rev.* **2014**, *114* (5), 2733–2758. https://doi.org/10.1021/cr400113m.
(119) Schmitt, T. J.; Knotts, T. A. Thermodynamics of DNA Hybridization on Surfaces. *J. Chem. Phys.* **2011**, *134* (20), 205105. https://doi.org/10.1063/1.3592557.
(120) Spink, C. H.; Chaires, J. B. Selective Stabilization of Triplex DNA by Poly(Ethylene Glycols). *J. Am. Chem. Soc.* **1995**, *117* (51), 12887–12888. https://doi.org/10.1021/ja00156a038.
(121) Gu, X.-B.; Nakano, S.; Sugimoto, N. Consecutive GC Base Pairs Determine the Energy Barrier of DNA Duplex Formation under Molecularly Crowded Conditions. *Chem. Commun.* **2007**, No. 26, 2750. https://doi.org/10.1039/b702865b.

(122) Monserud, J. H.; Schwartz, D. K. Effects of Molecular Size and Surface Hydrophobicity on Oligonucleotide Interfacial Dynamics. *Biomacromolecules* **2012**, *13* (12), 4002–4011. https://doi.org/10.1021/bm301289n.
(123) Bilgic, T.; Klok, H.-A. Surface-Initiated Controlled Radical Polymerization Enhanced DNA Biosensing. *European Polymer Journal* **2015**, *62*, 281–293. https://doi.org/10.1016/j.eurpolymj.2014.07.037.
(124) Le Goff, G. C.; Blum, L. J.; Marquette, C. A. Shrinking Hydrogel-DNA Spots Generates 3D Microdots Arrays: Shrinking Hydrogel-DNA Spots Generates 3D Microdots Arrays. *Macromol. Biosci.* **2013**, *13* (2), 227–233. https://doi.org/10.1002/mabi.201200370.
(125) Soto, C. M.; Patterson, C. H.; Charles, P. T.; Martin, B. D.; Spector, M. S. Immobilization and Hybridization of DNA in a Sugar Polyacrylate Hydrogel. *Biotechnol. Bioeng.* **2005**, *92* (7), 934–942. https://doi.org/10.1002/bit.20665.
(126) Beyer, A.; Cialla-May, D.; Weber, K.; Popp, J. Hydrogel Decorated Chips for Convenient DNA Test. *Macromol. Chem. Phys.* **2016**, *217* (8), 959–965. https://doi.org/10.1002/macp.201500439.
(127) Beyer, A.; Pollok, S.; Berg, A.; Weber, K.; Popp, J. Easy Daylight Fabricated Hydrogel Array for Colorimetric DNA Analysis: Daylight Fabricated Hydrogel Array. *Macromol. Biosci.* **2014**, *14* (6), 889–898. https://doi.org/10.1002/mabi.201300487.
(128) Liu, M.; Hui, C. Y.; Zhang, Q.; Gu, J.; Kannan, B.; Jahanshahi-Anbuhi, S.; Filipe, C. D. M.; Brennan, J. D.; Li, Y. Target-Induced and Equipment-Free DNA Amplification with a Simple Paper Device. *Angew. Chem.* **2016**, *128* (8), 2759–2763. https://doi.org/10.1002/ange.201509389.
(129) Buenger, D.; Topuz, F.; Groll, J. Hydrogels in Sensing Applications. *Progress in Polymer Science* **2012**, *37* (12), 1678–1719. https://doi.org/10.1016/j.progpolymsci.2012.09.001.
(130) Nallur, G. Signal Amplification by Rolling Circle Amplification on DNA Microarrays. *Nucleic Acids Research* **2001**, *29* (23), 118e–1118. https://doi.org/10.1093/nar/29.23.e118.
(131) Nallur, G.; Marrero, R.; Luo, C.; Krishna, R. M.; Bechtel, P. E.; Ray, M.; Wiltshire, S.; Fang, L.; Huang, H.; Liu, C.-G.; Sun, L.; Sawyer, J. R.; Kingsmore, S. F.; Xia, J. Protein and Nucleic Acid Detection by Rolling Circle Ampli®cation on Gel-Based Microarrays. 9.
(132) Kashkin, K. N.; Strizhkov, B. N.; Gryadunov, D. A.; Surzhikov, S. A.; Grechishnikova, I. V.; Kreindlin, E. Ya.; Chupeeva, V. V.; Evseev, K. B.; Turygin, A. Yu.; Mirzabekov, A. D. Detection of Single-Nucleotide Polymorphisms in the P53 Gene by LDR/RCA in Hydrogel Microarrays. *Mol Biol* **2005**, *39* (1), 26–34. https://doi.org/10.1007/s11008-005-0004-1.
(133) Strizhkov, B. N.; Drobyshev, A. L.; Mikhailovich, V. M.; Mirzabekov, A. D. PCR Amplification on a Microarray of Gel-Immobilized Oligonucleotides: Detection of Bacterial Toxin- and Drug-Resistant Genes and Their Mutations. *BioTechniques* **2000**, *29* (4), 844–857. https://doi.org/10.2144/00294rr01.
(134) Ali, M. M.; Aguirre, S. D.; Xu, Y.; Filipe, C. D. M.; Pelton, R.; Li, Y. Detection of DNA Using Bioactive Paper Strips. *Chem. Commun.* **2009**, No. 43, 6640. https://doi.org/10.1039/b911559e.
(135) Hui, C. Y.; Liu, M.; Li, Y.; Brennan, J. D. A Paper Sensor Printed with Multifunctional Bio/Nano Materials. *Angew. Chem. Int. Ed.* **2018**, *57* (17), 4549–4553. https://doi.org/10.1002/anie.201712903.
(136) Bialy, R. M.; Ali, M. M.; Li, Y.; Brennan, J. D. Protein-Mediated Suppression of Rolling Circle Amplification for Biosensing with an Aptamer-Containing DNA Primer. *Chem. Eur. J.* **2020**, *26* (22), 5085–5092. https://doi.org/10.1002/chem.202000245.
(137) Wang, L.; Tram, K.; Ali, M. M.; Salena, B. J.; Li, J.; Li, Y. Arrest of Rolling Circle Amplification by Protein-Binding DNA Aptamers. *Chem. Eur. J.* **2014**, *20* (9), 2420–2424. https://doi.org/10.1002/chem.201304292.
(138) Carrasquilla, C.; Kapteyn, E.; Li, Y.; Brennan, J. D. Sol-Gel-Derived Biohybrid Materials Incorporating Long-Chain DNA Aptamers. *Angew. Chem. Int. Ed.* **2017**, *56* (36), 10686–10690. https://doi.org/10.1002/anie.201702859.
(139) Li, Y.; Dahhan, O.; Filipe, C. D. M.; Brennan, J. D.; Pelton, R. H. Optimizing Piezoelectric Inkjet Printing of Silica Sols for Biosensor Production. *J Sol-Gel Sci Technol* **2018**, *87* (3), 657–664. https://doi.org/10.1007/s10971-018-4762-3.
(140) Collett, J. R.; Cho, E. J.; Ellington, A. D. Production and Processing of Aptamer Microarrays. *Methods* **2005**, *37* (1), 4–15. https://doi.org/10.1016/j.ymeth.2005.05.009.
(141) Munzar, J. D.; Ng, A.; Juncker, D. Duplexed Aptamers: History, Design, Theory, and Application to Biosensing. *Chem. Soc. Rev.* **2019**, *48* (5), 1390–1419. https://doi.org/10.1039/C8CS00880A.
(142) Boehr, D. D.; Nussinov, R.; Wright, P. E. The Role of Dynamic Conformational Ensembles in Biomolecular Recognition. *Nat Chem Biol* **2009**, *5* (11), 789–796. https://doi.org/10.1038/nchembio.232.
(143) Prinz, H. Hill Coefficients, Dose–Response Curves and Allosteric Mechanisms. *J Chem Biol* **2010**, *3* (1), 37–44. https://doi.org/10.1007/s12154-009-0029-3.
(144) Munzar, J. D.; Ng, A.; Corrado, M.; Juncker, D. Complementary Oligonucleotides Regulate Induced Fit Ligand Binding in Duplexed Aptamers. *Chem. Sci.* **2017**, *8* (3), 2251–2256. https://doi.org/10.1039/C6SC03993F.
(145) Marras, S. A. E.; Kramer, F. R.; Tyagi, S. Ef®ciencies of ¯uorescence Resonance Energy Transfer and Contact-Mediated Quenching in Oligonucleotide Probes. *Nucleic Acids Research* **2002**, *30* (21), 8.

(146) Algar, W. R.; Hildebrandt, N.; Vogel, S. S.; Medintz, I. L. FRET as a Biomolecular Research Tool — Understanding Its Potential While Avoiding Pitfalls. *Nat Methods* **2019**, *16* (9), 815–829. https://doi.org/10.1038/s41592-019-0530-8.
(147) Munzar, J. D.; Ng, A.; Juncker, D. Comprehensive Profiling of the Ligand Binding Landscapes of Duplexed Aptamer Families Reveals Widespread Induced Fit. *Nat Commun* **2018**, *9* (1), 343. https://doi.org/10.1038/s41467-017-02556-3.
(148) Wilson, B. D.; Hariri, A. A.; Thompson, I. A. P.; Eisenstein, M.; Soh, H. T. Independent Control of the Thermodynamic and Kinetic Properties of Aptamer Switches. *Nat Commun* **2019**, *10* (1), 5079. https://doi.org/10.1038/s41467-019-13137-x.
(149) Cisse, I. I.; Kim, H.; Ha, T. A Rule of Seven in Watson-Crick Base-Pairing of Mismatched Sequences. *Nat Struct Mol Biol* **2012**, *19* (6), 623–627. https://doi.org/10.1038/nsmb.2294.
(150) Heilkenbrinker, A.; Reinemann, C.; Stoltenburg, R.; Walter, J.-G.; Jochums, A.; Stahl, F.; Zimmermann, S.; Strehlitz, B.; Scheper, T. Identification of the Target Binding Site of Ethanolamine-Binding Aptamers and Its Exploitation for Ethanolamine Detection. *Anal. Chem.* **2015**, *87* (1), 677–685. https://doi.org/10.1021/ac5034819.
(151) Rupcich, N.; Nutiu, R.; Li, Y.; Brennan, J. D. Entrapment of Fluorescent Signaling DNA Aptamers in Sol−Gel-Derived Silica. *Anal. Chem.* **2005**, *77* (14), 4300–4307. https://doi.org/10.1021/ac0506480.
(152) Hui, C. Y.; Li, Y.; Brennan, J. D. Fluorescence Analysis of the Properties of Structure-Switching DNA Aptamers Entrapped in Sol–Gel-Derived Silica Materials. *Chem. Mater.* **2014**, *26* (5), 1896–1904. https://doi.org/10.1021/cm404114g.
(153) Hui, C. Y.; Lau, P. S.; Li, Y.; Brennan, J. D. Investigation of RNA Structure-Switching Aptamers in Tunable Sol–Gel-Derived Materials. *J Sol-Gel Sci Technol* **2019**, *89* (1), 234–243. https://doi.org/10.1007/s10971-018-4588-z.
(154) Carrasquilla, C.; Lau, P. S.; Li, Y.; Brennan, J. D. Stabilizing Structure-Switching Signaling RNA Aptamers by Entrapment in Sol–Gel Derived Materials for Solid-Phase Assays. *J. Am. Chem. Soc.* **2012**, *134* (26), 10998–11005. https://doi.org/10.1021/ja304064a.
(155) Murtaza, G.; Rizvi, A. S.; Qiu, L.; Xue, M.; Meng, Z. Aptamer Empowered Hydrogels: Fabrication and Bio-sensing Applications. *J of Applied Polymer Sci* **2022**, *139* (26). https://doi.org/10.1002/app.52441.
(156) Abune, L.; Davis, B.; Wang, Y. Aptamer-functionalized Hydrogels: An Emerging Class of Biomaterials for Protein Delivery, Cell Capture, Regenerative Medicine, and Molecular Biosensing. *WIREs Nanomed Nanobiotechnol* **2021**, *13* (6). https://doi.org/10.1002/wnan.1731.
(157) Chen, M.; Wang, Y.; Zhang, J.; Peng, Y.; Li, S.; Han, D.; Ren, S.; Qin, K.; Li, S.; Gao, Z. Stimuli-Responsive DNA-Based Hydrogels for Biosensing Applications. *J Nanobiotechnol* **2022**, *20* (1), 40. https://doi.org/10.1186/s12951-022-01242-x.
(158) Tan, B.; Zhao, H.; Du, L.; Gan, X.; Quan, X. A Versatile Fluorescent Biosensor Based on Target-Responsive Graphene Oxide Hydrogel for Antibiotic Detection. *Biosensors and Bioelectronics* **2016**, *83*, 267–273. https://doi.org/10.1016/j.bios.2016.04.065.
(159) Zhang, Z.; Liu, J. Molecular Imprinting with Functional DNA. *Small* **2019**, *15* (26), 1805246. https://doi.org/10.1002/smll.201805246.
(160) Zhang, Z.; Liu, J. Molecularly Imprinted Polymers with DNA Aptamer Fragments as Macromonomers. *ACS Appl. Mater. Interfaces* **2016**, *8* (10), 6371–6378. https://doi.org/10.1021/acsami.6b00461.
(161) Poma, A.; Brahmbhatt, H.; Pendergraff, H. M.; Watts, J. K.; Turner, N. W. Generation of Novel Hybrid Aptamer-Molecularly Imprinted Polymeric Nanoparticles. *Adv. Mater.* **2015**, *27* (4), 750–758. https://doi.org/10.1002/adma.201404235.
(162) Liu, R.; McConnell, E. M.; Li, J.; Li, Y. Advances in Functional Nucleic Acid Based Paper Sensors. *J. Mater. Chem. B* **2020**, *8* (16), 3213–3230. https://doi.org/10.1039/C9TB02584G.
(163) Tian, T.; Wei, X.; Jia, S.; Zhang, R.; Li, J.; Zhu, Z.; Zhang, H.; Ma, Y.; Lin, Z.; Yang, C. J. Integration of Target Responsive Hydrogel with Cascaded Enzymatic Reactions and Microfluidic Paper-Based Analytic Devices (μPADs) for Point-of-Care Testing (POCT). *Biosensors and Bioelectronics* **2016**, *77*, 537–542. https://doi.org/10.1016/j.bios.2015.09.049.
(164) Wei, X.; Tian, T.; Jia, S.; Zhu, Z.; Ma, Y.; Sun, J.; Lin, Z.; Yang, C. J. Microfluidic Distance Readout Sweet Hydrogel Integrated Paper-Based Analytical Device (μDiSH-PAD) for Visual Quantitative Point-of-Care Testing. *Anal. Chem.* **2016**, *88* (4), 2345–2352. https://doi.org/10.1021/acs.analchem.5b04294.
(165) Su, S.; Nutiu, R.; Filipe, C. D. M.; Li, Y.; Pelton, R. Adsorption and Covalent Coupling of ATP-Binding DNA Aptamers onto Cellulose. *Langmuir* **2007**, *23* (3), 1300–1302. https://doi.org/10.1021/la060961c.
(166) Zhao, W.; Ali, M. M.; Aguirre, S. D.; Brook, M. A.; Li, Y. Paper-Based Bioassays Using Gold Nanoparticle Colorimetric Probes. *Anal. Chem.* **2008**, *80* (22), 8431–8437. https://doi.org/10.1021/ac801008q.
(167) Su, S.; Ali, Md. M.; Filipe, C. D. M.; Li, Y.; Pelton, R. Microgel-Based Inks for Paper-Supported Biosensing Applications. *Biomacromolecules* **2008**, *9* (3), 935–941. https://doi.org/10.1021/bm7013608.
(168) Carrasquilla, C.; Little, J. R. L.; Li, Y.; Brennan, J. D. Patterned Paper Sensors Printed with Long-Chain DNA Aptamers. *Chem. Eur. J.* **2015**, *21* (20), 7369–7373. https://doi.org/10.1002/chem.201500949.

(169) Liu, M.; Zhang, Q.; Kannan, B.; Botton, G. A.; Yang, J.; Soleymani, L.; Brennan, J. D.; Li, Y. Self-Assembled Functional DNA Superstructures as High-Density and Versatile Recognition Elements for Printed Paper Sensors. *Angew Chem Int Ed* **2018**, *57* (38), 12440–12443. https://doi.org/10.1002/anie.201806489.

(170) Wei, X.; Tian, T.; Jia, S.; Zhu, Z.; Ma, Y.; Sun, J.; Lin, Z.; Yang, C. J. Target-Responsive DNA Hydrogel Mediated "Stop-Flow" Microfluidic Paper-Based Analytic Device for Rapid, Portable and Visual Detection of Multiple Targets. *Anal. Chem.* **2015**, *87* (8), 4275–4282. https://doi.org/10.1021/acs.analchem.5b00532.

(171) Smeets, N. M. B.; Bakaic, E.; Patenaude, M.; Hoare, T. Injectable Poly(Oligoethylene Glycol Methacrylate)-Based Hydrogels with Tunable Phase Transition Behaviours: Physicochemical and Biological Responses. *Acta Biomaterialia* **2014**, *10* (10), 4143–4155. https://doi.org/10.1016/j.actbio.2014.05.035.

(172) Bakaic, E.; Smeets, N. M. B.; Hoare, T. Injectable Hydrogels Based on Poly(Ethylene Glycol) and Derivatives as Functional Biomaterials. *RSC Adv.* **2015**, *5* (45), 35469–35486. https://doi.org/10.1039/C4RA13581D.

(173) Smeets, N. M. B.; Bakaic, E.; Yavitt, F. M.; Yang, F.-C.; Rheinstädter, M. C.; Hoare, T. Probing the Internal Morphology of Injectable Poly(Oligoethylene Glycol Methacrylate) Hydrogels by Light and Small-Angle Neutron Scattering. *Macromolecules* **2014**, *47* (17), 6017–6027. https://doi.org/10.1021/ma5011827.

(174) Bakaic, E.; Smeets, N. M. B.; Dorrington, H.; Hoare, T. "Off-the-Shelf" Thermoresponsive Hydrogel Design: Tuning Hydrogel Properties by Mixing Precursor Polymers with Different Lower-Critical Solution Temperatures. *RSC Adv.* **2015**, *5* (42), 33364–33376. https://doi.org/10.1039/C5RA00920K.

(175) Sivakumaran, D.; Bakaic, E.; Campbell, S. B.; Xu, F.; Mueller, E.; Hoare, T. Fabricating Degradable Thermoresponsive Hydrogels on Multiple Length Scales via Reactive Extrusion, Microfluidics, Self-Assembly, and Electrospinning. *JoVE* **2018**, No. 134, 54502. https://doi.org/10.3791/54502.

(176) De France, K. J.; Xu, F.; Hoare, T. Structured Macroporous Hydrogels: Progress, Challenges, and Opportunities. *Adv. Healthcare Mater.* **2018**, *7* (1), 1700927. https://doi.org/10.1002/adhm.201700927.

(177) Mateen, R.; Ali, M. M.; Hoare, T. A Printable Hydrogel Microarray for Drug Screening Avoids False Positives Associated with Promiscuous Aggregating Inhibitors. *Nat Commun* **2018**, *9* (1), 602. https://doi.org/10.1038/s41467-018-02956-z.

(178) Deng, X.; Smeets, N. M. B.; Sicard, C.; Wang, J.; Brennan, J. D.; Filipe, C. D. M.; Hoare, T. Poly(Oligoethylene Glycol Methacrylate) Dip-Coating: Turning Cellulose Paper into a Protein-Repellent Platform for Biosensors. *J. Am. Chem. Soc.* **2014**, *136* (37), 12852–12855. https://doi.org/10.1021/ja507372v.

2. Chapter 2.

A Single-Step Printable Hydrogel Microarray Integrating Long-Chain DNA for the Discriminative and Size-Specific Sensing of Nucleic Acids

Preface

This chapter and its supporting information-appendix are reproduced from the publication describing the development of printable hydrazone-cross-linked hydrogel microarray integrating rolling circle amplification (RCA) product as the sensing material for DNA hybridization assay. The sensor was characterized on printing reproducibility, RCA product immobilization efficiency and co-localization within hydrogel microarray, the microstructure of hydrogel anchored on nitrocellulose substrate and the ability of miniaturized sensor to allow effective hybridization reaction with complementary fluorescent-oligonucleotides.

Of note, this chapter followed an extensive study performed on development of optimal hydrazone cross-linked hydrogel configuration supporting nucleic acids based diagnostic tests, the optimization of assay conditions for effective signaling, design of hybridization protocols for minimizing non-specific DNA adsorption/absorption, printability and stability of different hydrogel configuration against varying denaturation agents including the investigation on optimal fluorescent detection techniques for DNA microarray hybridization assays. In addition, a separate study was conducted on assessment of hydrogel microarray ability to support on-chip RCA reaction as the alternative method for signal amplification, collectively suggesting the capacity of hydrogel microarray to be employed in various DNA-based molecular recognition assays (Data not shown in the current report).

Milana Pikula,[1] M. Monsur Ali,[2] Carlos Filipe,[1,*] and Todd Hoare[1,*]

[1]Department of Chemical Engineering, McMaster University, Hamilton, ON L8S 4K1, Canada;

[2]Biointerfaces Institute, McMaster University, Hamilton, ON L8S 4L8, Canada

In *ACS Applied Materials and Interfaces (2021)* 13, 2: 2360–2370; Reproduced with permission from American Chemical Society Publications.

Abstract

A simple approach to fabricating hydrogel-based DNA microarrays is reported by physically entrapping rolling circle amplification (RCA) product inside printable *in situ*-gelling hydrazone cross-linked poly(oligoethylene glycol methacrylate) hydrogels. The hydrogel-printed RCA microarray facilitates improved RCA immobilization (>65% even after vigorous washing) and resistance to denaturation relative to RCA-only printed microarrays in addition to size-discriminative sensing of DNA probes (herein, 27 or fewer nucleotides) depending on the internal porosity of the hydrogel. Furthermore, the high number of sequence repeats in the concatemeric RCA product enables high sensitivity detection of complementary DNA probes without the need for signal amplification, with signal:noise ratios of 10 or more achieved over a short 30-minute assay time followed by minimal washing. The inherent anti-fouling properties of the hydrogel enable discriminative hybridization in complex biological samples, particularly for short (~10-nt) oligonucleotides whose hybridization in other assays tends to be transient and low-affinity. The scalable manufacturability and efficient performance of these hydrogel-printed RCA microarrays thus offers potential for rapid, parallel, and inexpensive sensing of short DNA/RNA biomarkers and ligands, a critical current challenge in diagnostic and affinity screening assays.

2.1. Introduction

DNA microarrays that can quantify the binding of complementary nucleic acids are powerful tools in a range of applications including genetic analysis,[1] drug discovery[2] and disease detection[3] given their capacity to rapidly collect large volumes of data while using fewer reagents.[4] However, the presence of an interface in microarray-based sensors introduces multiple challenges that can limit their signal:noise and thus sensitivity, including: (1) higher mass transfer resistances associated with the diffusion of the probe to the binding site; (2) potential condensation/reconformation of the DNA recognition sequences due to surface-DNA interactions;[5,6] (3) limited maximum DNA concentrations due to the limited surface area associated with 2D assays;[7,8] and (4) enhanced non-specific interactions between non-target ligands and the sensor interface.[9]

To overcome such challenges, multiple efforts have been pursued to engineer the surface geometry, surface chemistry, DNA conformation, and DNA packing density on a microarray chip.[10–13] Among these strategies, the creation of hydrogel-based DNA microarrays[14] has attracted particular interest given the multiple beneficial properties of hydrogels[15,16] in addressing the key drawbacks associated with conventional DNA microarrays.[17,18] The hydrated microenvironment of a hydrogel minimizes both conformational changes of the sensing DNA upon drying[16] and non-specific protein adsorption on the sensor surface.[19] The porosity of a hydrogel can be tuned to enable stable physical entrapment of the sensing DNA, avoiding the need for expensive chemically-modified oligonucleotides that are required for covalent[20–22] or high-affinity non-covalent DNA immobilization[23] while facilitating improved sensor stability relative to DNA immobilization *via* physical adsorption.[24,25] Concurrently, the 3D (or at least "2.5D") dimensionality of a hydrogel enables the immobilization of two to three orders of magnitude higher DNA loadings per unit surface area than are achievable with 2D systems,[3,4] in most cases more than offsetting any enhanced mass transfer resistance associated with transport of the probe (i.e. the target to be detected) into the hydrogel.[26] While photopolymerization is most commonly used to fabricate hydrogel-based microarrays,[3,4] the potential for UV-induced DNA damage[27,28] has motivated the investigation of new gelation chemistries for DNA microarray fabrication, including visible light-induced polymerization[29,30] or the use of homo-bifunctional covalent crosslinkers that can crosslink hydrogels *via* non-radical mechanisms under ambient or near-ambient conditions.[31] While such approaches avoid potentially denaturing UV exposure, they also still require covalent tethering of the sensing DNA to the hydrogel to ensure long-term immobilization.

Herein, we report an alternative DNA microarray fabrication strategy based on the combination of covalently *in situ*-gelling hydrogels with megadalton-sized concatemeric DNA molecules generated via rolling circle amplification (RCA) that significantly simplifies the production of DNA microarray sensors while enabling rapid and high-sensitivity oligonucleotide detection. In an RCA reaction, isothermal DNA polymerase (Phi29 polymerase) continuously adds nucleotides to a short DNA primer to create a long (up to micrometer length scales) single stranded DNA molecule[32] *via* repeated copying of a circular DNA template. The repeating sequence can be customized through encoding the template with different functional sequences (e.g. DNA aptamers, DNAzymes, or spacer domains) to detect different functional targets[33] and/or promote self-assembly of the RCA product into programmable nano- or micro-scaled architectures,[34] facilitating the design of solid phase sensors with high densities of sensing DNA.[35,36] Paper-based sensors formed by ink jet printing of RCA-based concatemers or functional RCA-based "nanoflowers" have been produced by exploiting the strong adsorption (and thus immobilization) of the RCA product on cellulose substrates while preserving sufficient target-induced structure-switching for signal generation[37] and enhanced resistance to nuclease degradation.[38] However, the tendency of RCA product to aggregate over time[34] represents a limitation to its independent use as a nitrocellulose-immobilized sensing element.[13] Inclusion of the RCA product within a macroporous PEG-doped silica sol-gel results in high retention efficiency and better RCA product stability[39] without substantially

reducing DNA binding activity; however, the dynamic nature of silica sol-gels and the challenges around printing silica-based sol-gel systems remain limitations.[40]

In contrast, *in situ*-gelling chemistry enables the direct formation of hydrogel films on an interface by sequentially depositing aldehyde and hydrazide-functionalized precursor polymers (POA and POH, respectively) on a cellulose-based substrate using a "drop-on-demand" solenoid-controlled ink jet printer. As the deposited polymers diffuse together upon printing the second (or any subsequent) layer, dynamic hydrazone crosslinking occurs to form a covalently crosslinked hydrogel film on the cellulose surface. Such a "covalent layer-by-layer" gelation strategy (mimicking in operation polyelectrolyte layer-by-layer processes) does not require external initiation while also being easily adaptable to printing-based fabrication.[41] Our group has previously demonstrated that when highly protein-repellent and hygroscopic poly(oligoethylene glycol methacrylate) (POEGMA) is used as the base polymer, low non-specific adsorption coupled with effective stabilization of entrapped proteins can be achieved.[42] Building on that result, herein we adapt this printable hydrogel system to immobilize RCA product and thus create a DNA microarray sensor in a single printing step. The printed gel can retain the sensing RCA product on nitrocellulose at up to 5-fold higher efficacy relative to direct printing (i.e., without polymer entrapment) while maintaining high uniformity and resistance to vigorous denaturation treatments. Furthermore, the confined DNA molecules remain functional, enabling size and sequence-specific detection of complementary DNA probes; the efficiency of the platform for detecting short-length nucleic acids in particular addresses a critical drawback with standard hybridization-based detection assays[43] given the typically low binding efficiency and duplex stability observed with oligonucleotides of less than 25 bases.[44] Coupled with the anti-fouling properties enabled by the POEGMA hydrogel, discrimination of specific hybridization events from both simple and complex media with S:N (signal to noise) ratios up to 11× can be achieved, with particular benefits observed for the detection of short (10-nt) oligonucleotides that bind weakly in the solution and are thus challenging to detect by conventional hybridization microarrays.

2.2. Experimental Section

2.2.1. Materials.

Glycerol (Sigma-Aldrich, ≥99%), acrylic acid (AA, Sigma-Aldrich, 99%), 2,2-azobisisobutryic acid dimethyl ester (AIBMe, Wako Chemicals, 98.5%), N'-ethyl-N-(3-dimethylaminopropyl)-carbodiimide (EDC, Carbosynth, Compton CA, commercial grade), thioglycolic acid (TGA, Sigma Aldrich, 98%), fluorescein isothiocyanate (FITC, Sigma-Aldrich, 90%), adipic acid dihydrazide (ADH, Alfa Aesar, 98%), nitrocellulose backed-membrane (GE Healthcare, FF120HP Plus), polyoxyethylene sorbitan monolaurate (Tween® 20, Sigma-Aldrich), human serum (Normal, containing 4% trisodium citrate, Sigma-Aldrich), QuantiFluor® dsDNA System (Promega Corporation), and Phi29 DNA polymerase (Phi29P, BioLabs Inc.) were all used as received. N-(2,2-dimethoxyethyl)methacrylamide (DMEMAm) was synthesized as previously reported.[45] Diethylene glycol methyl ether methacrylate ($M(EO)_2MA$, Sigma Aldrich, 98%) and oligo(ethylene glycol) methyl ether methacrylate ($OEGMA_{500}$, M_n = 500 g/mol, Sigma Aldrich, 95%) were purified on a column of basic aluminum oxide (Sigma Aldrich, type CG-20) to remove the inhibitors methyl ether hydroquinone (MEHQ) and butylated hydroxytoluene (BHT) respectively. All DNA oligonucleotides were purchased from Integrated DNA Technologies (Supporting Table S2.1). Ulysis™ Alexa Fluor™ 647 Nucleic Acid Labeling Kit, T4 DNA ligase, dNTP mix, and FITC-labeled bovine serum albumin (BSA) were all purchased from ThermoFisher Scientific. Magnesium chloride hexahydrate ($MgCl_2 \cdot 6H_2O$, 99%), ammonium sulfate ($(NH_4)_2SO_4$, 99.8%), tris-HCl ($C_4H_{11}NO_3HCl$, 99.5%), sodium hydroxide (NaOH, >98%), and phosphate-buffered saline (PBS, 10× liquid concentrate) were purchased from Bioshop Canada Inc. Milli-Q grade distilled deionized water (DIW) was used for all experiments.

2.2.2. RCA product synthesis and characterization.

The circular DNA template (CT) was synthesized via ligation of the primer-linear template LT (sequence: 5' - AAG GCG AAG ACA TGC TTA GTC GAAA – 3') to the phosphorylated linear precursor of the circular template, pre-CT (sequence: 5' /5Phos/ TGT CTT CGC CTT CTT GTT TCC TTT CCT TGA AAC TTC TTC CTT TCT TTC TTT CGA CTA AGCA – 3'). 100 µL of LT (10 µM in DIW solution) was mixed with 11 µL of pre-CT (100 µM) via repeated pipetting, heated at 90°C for 1 min, and then cooled back to room temperature. Ligation was initiated by adding 1× T4 DNA ligase buffer with 5U T4 DNA into the LT-pre-CT complex. The reaction mixture (total volume 300 µL) was incubated at room temperature for 2 h, followed by heating at 90°C for 5 min to deactivate the enzyme. The ligated circular DNA product was precipitated with 3M sodium-acetate in 100% ethanol, washed in 70% ethanol, and purified using 10% denaturing polyacrylamide gel electrophoresis (dPAGE) as per standard techniques for circular DNA separation.[39] Circular DNA was eluted from the polyacrylamide gel and ethanol-precipitated as already described. Purified circular DNA pellets were re-suspended in DIW, quantified using a Nano-Quant spectrophotometer operating at 260 nm and stored at -20°C.

The circular DNA was then used as a template to conduct the RCA reaction by heating 10 pmol of CT with 10 pmol of primer-LT in sterile deionized water (DIW, 100 µL total volume) at 90°C for 1 min. The mixture was cooled to 25°C, after which 2.5 µL of 10 mM dNTPs, 10 U of Phi29 polymerase, 10 µL of 10× RCA reaction buffer, and 10 µL of 10× BSA solution was added. The amplification proceeded for 1 h at 30°C, conditions previously demonstrated to achieve sufficient RCA yields while minimizing the formation of RCA nanoflowers that could render the RCA product less printable;[37–39,46] following, the reaction mixture was diluted 5-fold in sterile DIW and heated at 90°C for 10 min to deactivate the enzyme. The RCA product was recovered into DIW from the reaction mixture by centrifugation using a 100 kDa Nanosep® spin column and quantified using a Nano-Quant spectrophotometer operating at 260

nm. The approximate molar concentration of RCA product was calculated based on the obtained DNA quantity, while the expected molecular weight of the RCA product was calculated based on a previously reported RCA reaction efficiency[46] using the average repeating units (ARU) number and the molecular weight of a monomeric circular precursor.

2.2.3. Polymer Precursors Synthesis and Characterization.

The synthesis and characterization of hydrazide-functionalized (POH) and aldehyde-functionalized (POA) hydrogel precursor polymers was conducted based on previous reports[45,47,48] with some modifications (Supporting Information, Figure S2.1).

Briefly, **Hydrazide-functionalized poly(oligoethylene glycol methacrylate) (POH)** was prepared by adding AIBMe (37 mg, 0.14 mmol), $OEGMA_{500}$ (4 g, 8.4 mmol), AA (0.25 g, 3.5 mmol), TGA (1 µL, 0.12 mmol) and 20 mL dioxane to a 50 mL Schlenk flask. Following the purging of the solution with nitrogen for at least 30 min, the flask was heated to 75 °C for 4 h under magnetic stirring to complete the polymerization. The solvent was then removed by rotary evaporation and the polymer was redissolved in water, dialyzed against DIW for a minimum of six (6+ h) cycles, and lyophilized to dryness. The carboxylic acid groups on the acrylic acid residues in the polymer product were subsequently converted to hydrazide groups by dissolving the purified polymer (3.8 g) and ADH (2.65 g, 15.2 mM, 5× molar excess to polymer-bound -COOH groups) in 100 mL DIW in a 500 mL round-bottom flask and adjusting the pH to 4.75 using 0.1 M HCl. EDC (1.18 g, 7.6 mmol) was then added, and the pH was maintained at pH = 4.75 by the dropwise addition (as required) of 0.1 M HCl over 4 h. The solution was left to stir overnight, dialyzed against DIW for a minimum of six (6+ h) cycles, and lyophilized. The degree of functionalization was determined via conductometric base-into-acid titration (ManTech Associates) using 50 mg of polymer dissolved in 50 mL of 3 mM NaCl as the analysis sample and 0.1 M NaOH as the titrant. The polymer was stored as a 20 w/w % solution in DIW at 4 °C. Fluorescence labeling of POH (FITC-POH) was achieved by reacting 1 g of POH with 1.5 mg of FITC in water at pH=8 and stirring overnight at room temperature (targeting FITC labeling of 2 mol% of the hydrazide groups). Labeled polymer was dialyzed against DIW for 6 cycles (6+ hours/cycle) in the dark to avoid photobleaching, lyophilized to dryness, dissolved in DIW at 15 % w/w, and stored at 4°C in the dark.

Aldehyde-functionalized poly(oligoethylene glycol methacrylate) (POA) was prepared by adding AIBMe (50 mg, 0.22 mmol), $M(EO)_2MA$ (1.13 g, 6.0 mmol), $OEGMA_{500}$ (2.85 g, 5.7 mmol), N-(2,2-dimethoxyethyl) methacrylamide (DMEMAm; 0.364 g, 2.1 mmol), TGA (4 µL, 0.08 mmol) and 20 mL dioxane to a 100 mL Schlenk flask, as per a previous report.[2] Following N_2 purge, the flask was heated at 75°C for 4 h under magnetic stirring to enable polymerization. After polymerization, the solvent was removed by rotary evaporation and the polymer was dissolved in DIW, purified by dialysis against DIW for a minimum of six (6+ h) cycles, and lyophilized to dryness. The acetal groups of POA were subsequently converted to aldehydes by dissolving 3.5 g of the purified polymer in 75 mL DIW and 25 mL 1.0 M HCl in a 250 mL round-bottom flask. The solution was stirred for 24 h, dialyzed for a minimum of six (6+ h) cycles, and lyophilized to dryness. The aldehyde content of the resulting polymer was measured using ^1H NMR as previously reported[45,47,48]. The polymer was stored as a 20 w/w% solution in DIW at 4°C.

For both precursor polymers, size exclusion chromatography (SEC) was performed to measure molecular weight using a Waters 2695 separations module equipped with a Waters 2996 photodiode array detector, a Waters 2414 refractive index detector, a Waters 2475 multi λ fluorescence detector and four Polymer Labs PLgel individual pore size columns maintained at 40°C, using a 5 µm bead size and pore sizes of

100, 500, 103 and 105 Å. DMF was used as the eluent at a flow rate of 1.0 mL/min, and poly(methyl methacrylate) standards were used for calibration. ^{1}H-NMR was performed using a Bruker AVANCE 600 MHz spectrometer using deuterated chloroform as the solvent. A rheometer (DHR-2, TA Instruments) was used to measure the viscosity of the precursor polymer hydrogel inks.

2.2.4. Printing RCA product microarrays.

RCA product microarrays were fabricated by printing hydrophobic wax barriers onto plastic-backed nitrocellulose membranes (FF-120 GE Healthcare) using a Xerox ColorQube 8570N solid wax printer and a 96-well-plate template (4 mm diameter wells with a 7 mm inter-well distance). The wax-printed paper was cured in the oven at 110°C for 2 min to melt the wax through the paper and create defined microzone spots. To print hydrogel-based RCA product microarrays (HF-RCP), one line of the BioJet printer was charged with 6 wt.% of POA in DIW while the other line was charged with 6 wt.% of POH and 0.006 μM (0.015 pmol/microzone) of purified RCA product, also in DIW; 5 wt.% of glycerol was also added to both precursor solutions as a humectant and viscosity modifier to facilitate printing. The solenoid dispenser valve was programmed to stay open for 6 ms, and the frequency was set to 100 Hz. Microarrays were fabricated by dispensing 2.5 μL of POA ink onto each microzone followed by 2.5 μL of POH/RCA ink. The printed multi-well plate was stored at 4°C overnight to ensure completion of cross-linking and then dried for a further 2 hr under ambient temperature. Control hydrogel-only microarrays were fabricated using the same method but excluding the RCA product, while control RCA product-only microarrays (henceforth referred to as rolling circle product, RCP) were printed using the same strategy without including the precursor polymers.

2.2.5. Printing Reproducibility.

RCA product was labeled with Alexa Fluor 647 according to the manufacturer's instructions (Ulysis™ Alexa Fluor™ 647 Nucleic Acid Labeling Kit, ThermoFisher Scientific). Labeled RCA product was purified via centrifugation using a 100kDa Nanosep® spin column. The purified labeled RCA product was heated for 15 min at 90°C to redissolve/resuspend the Alexa Fluor 647-RCA DNA complex following the labeling protocol, after which the product was cooled to room temperature and printed in hydrogel or alone at a concentration of 0.0012 μM or 0.006 μM (0.003 pmol/microzone or 0.015 pmol/microzone) as described in section 2.2.4. The uniformity of RCA product printing was assessed by using a Chemidoc™ MP System (BioRad) operating at 650 nm excitation/665 nm emission, with the resulting image processed using the round-based volume tool in ImageLab™ software (BioRad) to enable quantitative comparisons of the fluorescence signals.

2.2.6. Quantification of Immobilized RCA product.

Hydrogel-based RCA microarrays or single-RCA microarrays were printed with Alexa Fluor 647-labeled RCA at a surface density of 0.003 or 0.015 pmol/microzone and then washed using two different strategies: (1) 1× PBS containing 0.05% Tween 20 for 2 hours under shaking at 150 RPM, refreshing the washing buffer every 30 min; (2) 0.2 M NaOH (pH=12.3) for 10 min under shaking at 150 RPM followed by 3× rinses with 1× PBST washing buffer (1× PBS containing Tween 20 0.05%) over 5 min to re-adjust the pH. The amount of residual immobilized RCA product was determined by imaging the hydrated samples pre- and post- wash through the Alexa Fluor 647 channel of the Chemidoc™ MP System and quantifying the measured fluorescence intensity via Image Lab™ software using the round-based volume tool; fluorescence measurements were normalized based on the background auto-fluorescence of the printed hydrogel or bare nitrocellulose, depending on the platform. Each reported value represents the

ratio between pre-wash and post-wash fluorescence intensities (n=3), with the error bar representing the standard deviation.

2.2.7. Localization of Immobilized RCA product.

To assess the relative localization of RCA product within the printed hydrogel, Alexa Fluor 647-labeled RCA product was printed at a concentration of 0.015 pmol/microzone but using FITC-POH as the hydrazide-functionalized ink. The distribution of FITC-POH and Alexa Fluor 647-labeled RCA product within the printed hydrogel was visualized via confocal laser scanning microscopy (CLSM, Nikon) using laser excitation/emission wavelengths of 488/522 nm (FITC-POH) and 650/670 nm (Alexa-Fluor-647 RCA) to acquire the images. Washed (30 min in 1× PBST) and air-dried samples were positioned on a glass slide facing the objective and scanned in the bottom-to-top z-direction. The 3D z-stack images were collected at 2 μm intervals to a depth of 100 μm (800 × 800 μm probed area). The RCA-only printed microarrays were scanned using the same experimental set-up using 650/670 nm excitation/emission wavelengths. The acquired images were processed using Fiji (ImageJ) software version 2.0.0.

2.2.8. Microstructure of Printed Interfaces.

Hydrogel microarrays and hydrogel-based RCA microarrays were prepared as described in section 2.2.4. Along with control nitrocellulose array, prepared samples were sputter coated with a thin layer of gold and imaged using a Tescan Vega scanning electron microscope (SEM) with secondary electron (SE) detector and an acceleration voltage of 10 kV at 4000x magnification.

2.2.9. Non-specific Adsorption Assay.

RCA and hydrogel-based RCA arrays were prepared at 0.002 pmol/microzone and 0.02 pmol/microzone of RCA product (n=4 per microarray). The samples were equilibrated in 25 mL of 1× PBS buffer (pH=7.50) over 2 hours at ambient temperature, after which the arrays were incubated with 10 μL of a 100 μg/mL solution of FITC-BSA containing 20 vol.% of glycerol over 1 hour. The samples were imaged before and after a one-hour wash in 1× PBST under 150 RPM shaking using the fluorescein channel of the Chemidoc™ MP System (BioRad), with images subsequently processed using the round-based volume tool in Image Lab™ software.

2.2.10. DNA Hybridization Assay.

RCA and hydrogel-based RCA arrays were prepared at a density of 0.015 pmol/microzone (n=3 per microarray). The samples were hydrated in sterilized hybridization buffer (10 mM $MgCl_2$, 50 mM tris-HCl, 10 mM $(NH_4)_2SO_4$, pH 7.5, with the aim of screening the anionic charge of concatemeric RCA) for 30 min followed by 10 min of air-drying. In-gel hybridization was performed on five different sizes of AlexaFluor 647-labeled DNA probes with molecular weights ranging from 4-20 kDa (10-61 base pairs). Both complementary and non-complementary DNA probe sequences were tested at each molecular weight to assess the specificity of the probe binding (Supporting Table S2.1). Hybridization assays were conducted by dispensing 5 μL of a 2 μM DNA probe solution (corresponding to 10 pmol of DNA probe per array spot) dissolved in sterile DIW containing 20 vol.% of glycerol and incubating for 30 min at ambient temperature. The assay was repeated in complex media consisted of 20 wt.% human serum, with the remaining volume consisting of DIW containing 20 vol.% of glycerol. Non-specifically bound probe was washed from the microarray by soaking in 1× PBST over 60 min under 110 RPM shaking. The

samples were imaged before and after washing using the Alexa Fluor 647 channel of the Chemidoc™ MP Imaging System (BioRad). Image processing was performed using Image Lab™ software using the round-based volume tool, after which the ratio between specific and non-specific hybridization (Signal:Noise ratio) was calculated (n=3 replicates per sample).

2.2.11. Statistics.

The statistical analysis of the hybridization efficiency data in both sample groups (RCP and HF-RCP) was performed using GraphPad-Prism software version 8.4.2. The Welch's t-test was used to determine significance ($p \leq 0.05$ implying statistical significance) given that this test is specifically designed to handle small sample groups with unequal variances.[49]

2.3. Results and Discussion

2.3.1. Printing fabrication and reproducibility of RCA microarrays.

Hydrogel-based arrays (HF-RCP) were fabricated by sequentially printing these aldehyde and hydrazide-functionalized polymers together with RCA product on a nitrocellulose substrate, as shown in Figure 2.1a. Due to the previously demonstrated strong adhesion of aldehyde-functionalized precursor polymer to nitrocellulose,[41,42] the nitrocellulose substrate (with wax printed regions) was used as-is, avoiding the need for the additional surface pre-treatment or blocking steps required with other printed DNA microarray fabrication techniques.[50–52] 5 wt.% glycerol was added to each precursor polymer solution to tune the shear viscosity profile of the ink to be appropriate for printing (Supporting Table S2.2) and avoid premature evaporation of the small droplet on the printing nozzle. The 6 wt.% concentrations of polymer ink solutions ensured slow gelation kinetics and relatively lower cross-link densities, both of which promote more internally homogenous hydrogel morphologies with enhanced optical clarity beneficial in colorimetric or fluorometric biosensing applications.[53] The control RCA-only microarrays (RCP) were prepared by directly printing a 5 wt.% glycerol in DIW solution of RCA product, exploiting previous observations that concatemeric DNA can self-immobilize on nitrocellulose *via* physiosorption.[37]

To assess the spot-to-spot uniformity of the printing process (and thus the suitability of the technique for making uniform microarrays), AlexaFluor 647-labeled RCA product was mixed at a concentration of 0.003 pmol/microzone with the POH ink, printed, and fluorescently imaged. Relatively uniform fluorescence is observed across each microzone (coefficient of variation = 9.5% over 60 replicates) for the hydrogel-based DNA microarray (Figure 2.1b, Supporting Figure S2.2a); in contrast, RCA product printed alone yielded more zone-to-zone variation (coefficient of variation = 11.4% over 60 replicates (Figure 2.1d, Supporting Figure S2.2b). Additionally, the fluorescence intensity in hydrogel-printed microarrays is evenly spread over the full spot area while in RCA-only microarrays the distinctive doughnut or coffee-ring artefact often associated with microarray printing[5,30] is observed (Figure 2.1c-d). The coffee-ring effect in RCA-only microarrays becomes even more pronounced when a higher concentration of RCA product is printed (0.015 pmol/microzone), while hydrogel arrays containing the same RCA concentration maintain relatively uniform RCA product distributions within each printed spot (Figure 2.1c,e-lower inset; Supporting Figure S2.3). We attribute this improved printing uniformity to the gelation process suppressing the mobility of RCA (and thus inhibiting the formation of self-assembled RCA structures upon drying[54]) as well as avoiding drying artefacts by maintaining a more hydrated microenvironment around the RCA product.

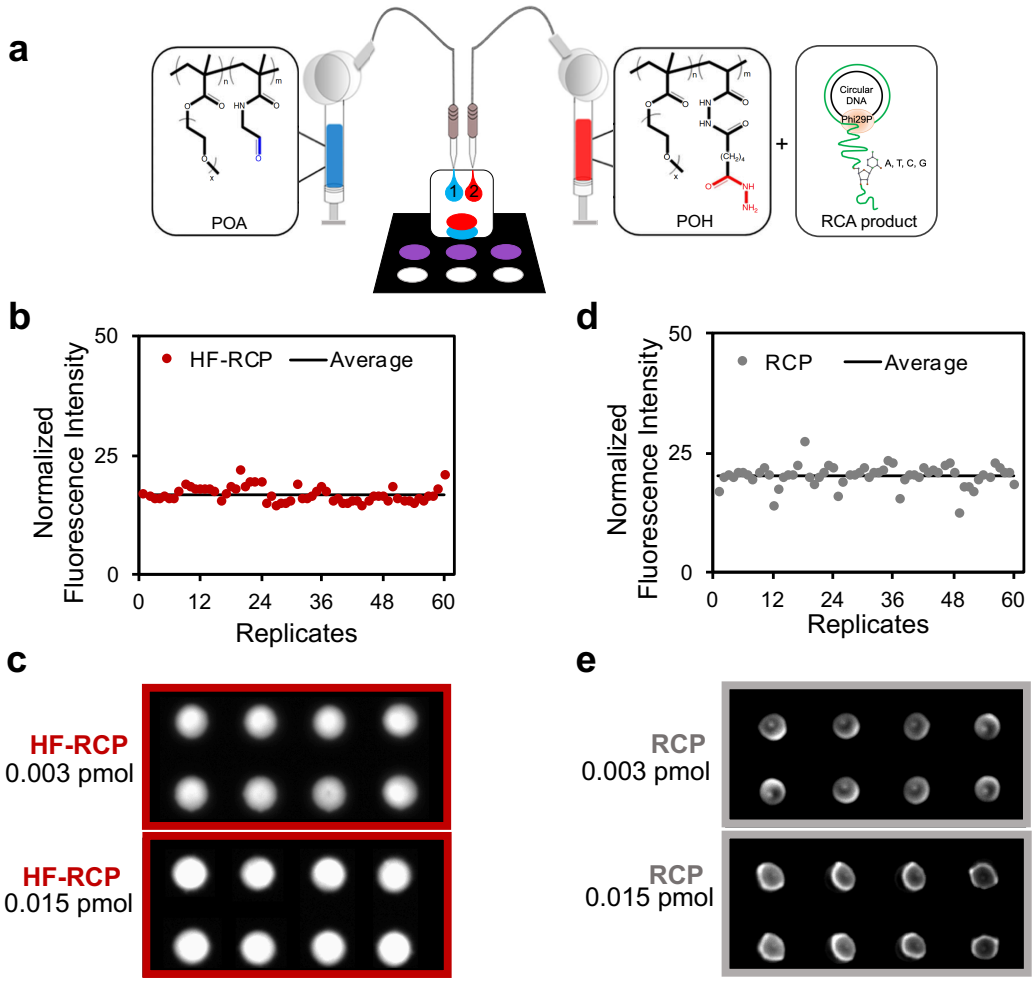

Figure 2.1 Printing fabrication and reproducibility of RCA microarrays. (a) Schematic illustration of hydrogel-based RCA microarray fabrication (HF-RCP) using the BioJet non-contact solenoid printer. Hydrogel precursor POA was printed first on the nitrocellulose substrate, followed by the mixture of RCA product with POH precursor. The RCA product was physically immobilized via *in situ* covalent cross-linking of the gel. The RCA-only microarray (RCP) was fabricated by direct printing of the RCA product that physically adsorbs on nitrocellulose. (b) Normalized fluorescence intensity of printed spots in a hydrogel-printed RCA product microarray (0.003 pmol/microzone in each of the 60 wells, coefficient of variation = 9.5%); (c) Uniformity of fluorescence intensity within the each single microzone printed at low (0.003 pmol/microzone) and high (0.015 pmol/microzone) RCA product concentrations; (d) Normalized fluorescence intensity of printed spots in an RCA product-only microarray (0.003 pmol/microzone in each of the 60 wells, coefficient of variation = 11.4%); (e) Uniformity of fluorescence intensity within each single microzone printed at low (0.003 pmol/microzone) and high (0.015 pmol/microzone) RCA product concentrations.

2.3.2. Stability of printed RCA microarrays to washing and denaturation treatment.

To investigate the effect of the hydrogel on the efficiency of RCA product immobilization, the samples were vigorously washed in 1x PBST (1× PBS containing 0.05% of Tween 20) washing buffer at pH=7.5 over 2 hours under shaking and the retained fluorescence signals were measured. Hydrogel-printed RCA microarrays enable high and consistent retention of the printed RCA product (67 ± 7%, Figure 2.2a,

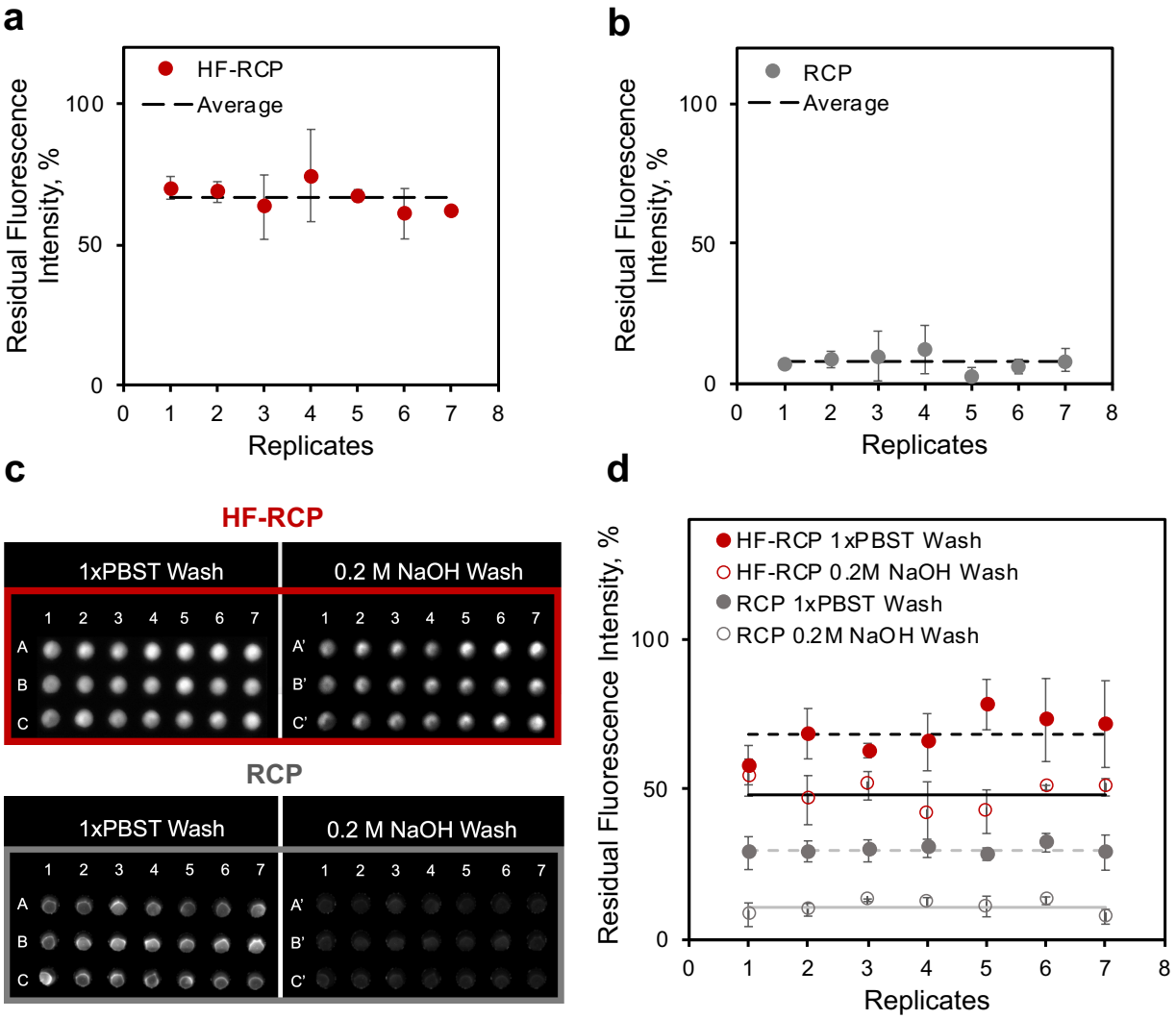

Figure 2.2 Stability of printed RCA microarrays to washing and denaturation. (a, b) Retention of fluorescence intensity (corresponding to retained RCA product concentration) in a hydrogel-printed RCA product microarray (a) compared to a RCA product-only printed microarray (b) following washing in 1× PBST, pH=7.5 for 2 hours (0.003 pmol RCA/microzone); the dashed lines represent the average fluorescence retention of the replicates tested; (c) Qualitative analysis of 3×7 microarray samples washed under different conditions, with rows A, B, C representing the samples after 1× PBST wash and rows A', B', C' representing the samples after a 0.2 M NaOH wash; (d) Quantitative retention of fluorescence intensity in hydrogel-printed (red points) and RCA-only printed (grey points) microarrays containing 0.015 pmol RCA/microzone after 1× PBST, pH=7.5 washing for 15 min (filled points) followed by 0.2 M NaOH, pH=13.0 washing for 10 minutes (unfilled points). Dashed lines (1× PBST washing) and solid lines (0.2 M NaOH washing) represent averages of the replicate samples tested.

Supporting Figure S2.2c) while the RCA-only printed microarrays exhibit >7-fold lower immobilization (8 ± 3%, Figure 2.2b, Supporting Figure S2.2d). Of note, even printing the RCA product at a ten-fold higher concentration at which self-assembly into nanoflowers is strongly favored[38] cannot achieve the same immobilization efficiency as the lower RCA concentration printed hydrogel (Supporting Figure S2.4). Furthermore, the hydrogel maintains a uniform RCA distribution throughout the matrix even after washing; in comparison, RCA-only printed microarrays show a further amplification of the coffee-ring effect (particularly when printed in concentrations >0.01 pmol/microzone) that would make imaging-based signal quantification more challenging (Supporting Figure S2.4b-inset).

Exposure of the hydrogel-printed microarrays to more vigorous washing under denaturing conditions shows even clearer advantages of the hydrogel printing approach. Working at a higher RCA concentration

of 0.015 pmol/microzone at which substantial retention of direct-printed RCA can still be achieved (Supporting Figure S2.4b, S2.5, S2.6), washing with 1× PBST retained 68 ± 9% of the hydrogel-printed RCA microarray signal and 30 ± 4% of RCA-only printed microarray signal. Following an additional wash with an aggressive denaturing agent (0.2 M NaOH, pH=13.0 for 10 minutes), only 11 ± 2% of the original fluorescence of the RCA-only printed microarray was maintained while hydrogel-printed microarray retained 48 ± 6% of its original fluorescence (Figure 2.2c,d). This result, achieved even for a very small denaturing agent that can freely diffuse into the hydrogel network, shows the substantially higher stability the RCA product inside the printed hydrogel relative to the direct-printed RCA, which is protected only by intramolecular cross-linking/self-assembly driving forces that can be disrupted via pH or salt addition.[38]

2.3.3. Co-localization of immobilized RCA product.

To assess the 3D distribution and orientation of the RCA product within the printed hydrogel, confocal fluorescence microscopy was used to image the 3D localization of FITC-POH (representing the hydrogel) and AlexaFluor 647-labeled RCA product (see Figure 2.3 for 2D slices or Supporting Figure S2.7 for the corresponding 3D stacks). Confocal z-slices indicate relatively homogeneous distributions of polymer and/or RCA product within each x-y slice, suggesting efficient entrapment of the RCA product without substantial phase separation. However, a clear z-gradient is observed in the RCA product concentration, with no significant RCA product signal observed at the hydrogel-solution interface (Figure 2.3a-i) but substantial RCA signal observed at depths of ~20-50 μm below the interface (Figure 2.3a-ii to iii). This result suggests that the RCA is fully entrapped within the hydrogel, consistent with the high degree of RCA retention observed upon washing (Figure 2.2a) and resistance of the hydrogel-printed RCA product against denaturation (Figure 2.2d). The apparent complete entrapment of RCA product also suggests the potential for the hydrogel-printed RCA microarrays to enable size-selective detection of complementary probes, as probe binding can only occur if the probe diffuses through the hydrogel to interact with the sensing RCA. In comparison, the RCA-only sample (Figure 2.3b) shows a much less uniform RCA distribution consistent with the presence of locally concentrated self-assembled supramolecular structures. Scanning electron microscopy (Figure 2.4a) further supports the uniformity of printed gel microarray. Hydrogel-printed microarrays prepared with or without RCA product show a smooth and highly uniform surface without any evidence of macroscopic pores that can be observed within bulbous structure of bare nitrocellulose membrane or other printed hydrogel systems.[29,31] This apparent small and uniform porosity is a particular advantage of the dynamic covalent crosslinking chemistry used herein in terms of effectively entrapping the high molecular weight RCA product within the gel to promote high surface immobilization and stability under rigorous washing conditions.

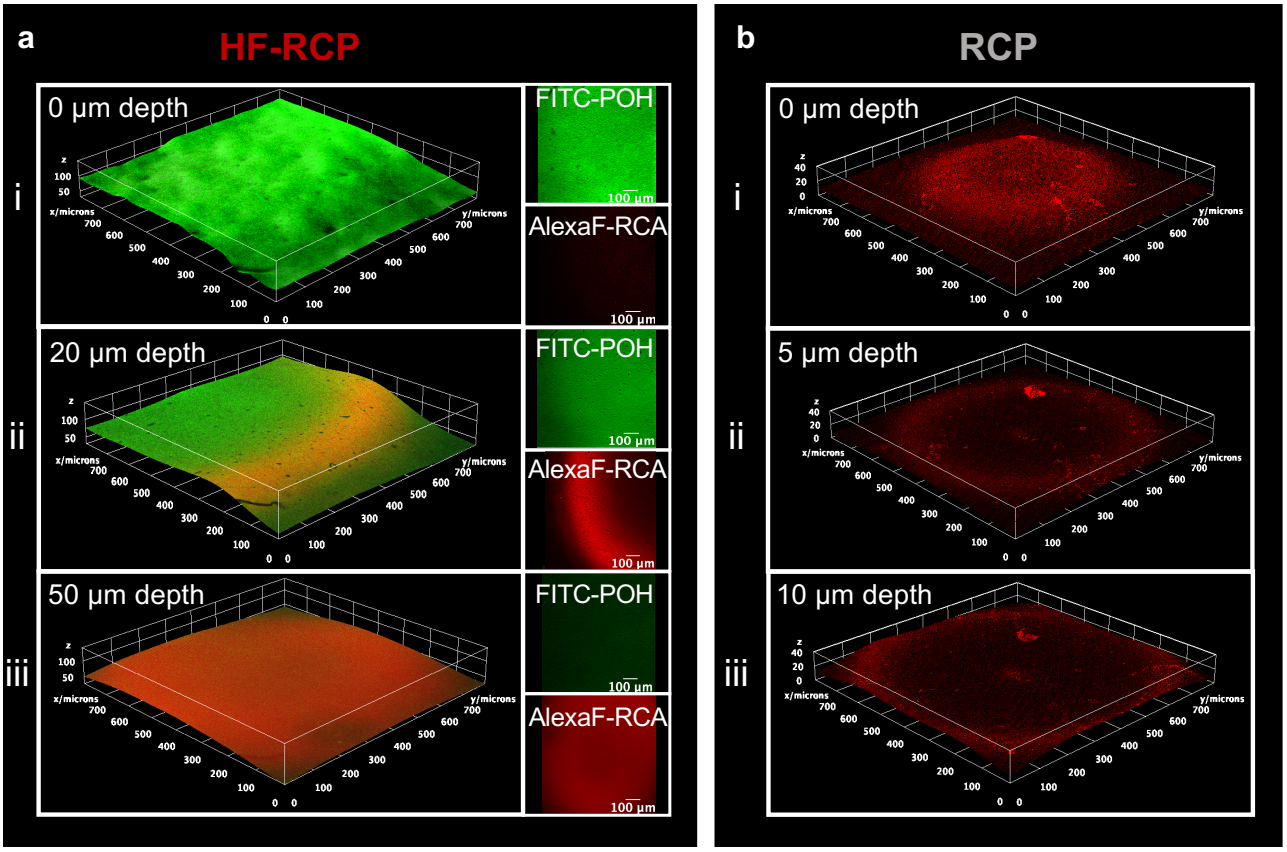

Figure 2.3 Confocal 3D z-stacks of AlexaFluor 647-labeled RCA product distribution following printing (0.015 pmol RCA/microzone RCA density, 800×800 µm area per slice). (a) Hydrogel-printed RCA product microzones prepared using FITC-POH as a hydrogel ink (green = hydrogel, red = RCA product); the right inset images at each different height from the nitrocellulose interface represent the individual channel 2D signals while the central left image represents the overlay of the two signals; (b) RCA-only printed microzones.

2.3.4. Anti-fouling properties of RCA microarrays.

To assess the capacity of hydrogel-printed RCA microarrays to reduce non-specific protein adsorption to the printed DNA microarray, the adsorption of FITC-labeled bovine serum albumin (BSA) to hydrogel-printed and RCA-only printed microzones was measured (Figure 2.4b). At both RCA concentrations tested (0.002 and 0.02 pmol/microzone), hydrogel-printed RCA microarrays suppressed FITC-BSA adsorption by almost one order of magnitude relative to RCA-only printed microarrays following a standard washing cycle (1× PBST, 60 min), with the RCA-only printed microarray exhibiting similar protein adsorption to unmodified nitrocellulose. This result is consistent with the hydrogel-rich interface observed via confocal microscopy (Figure 2.3a) as well as the inherently protein-repellent nature of POEGMA.[41,42] Given that non-specific adsorption of non-complementary DNA probes or other biomolecules (e.g. proteins) in complex samples is known to reduce both reproducibility and accuracy in DNA microarray sensing assays,[12] suppressing fouling offers promise for improving signal:noise ratios.

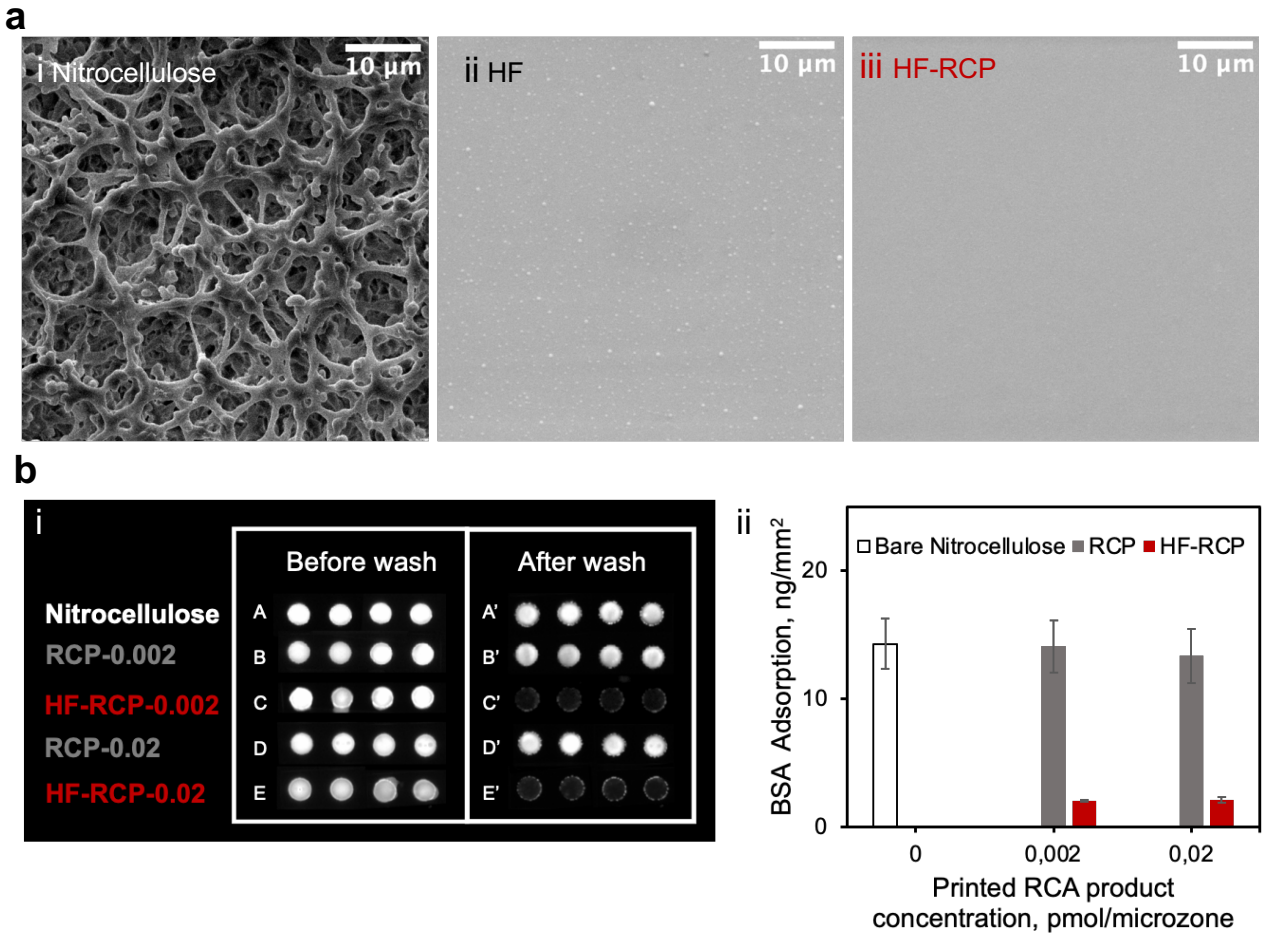

Figure 2.4 Microstructure (a) and anti-fouling properties (b) of hydrogel-printed RCA microarrays. (a) Scanning electron microscopy images of bare nitrocellulose (i) compared to a control printed hydrogel microarray (ii, HF, without encapsulated RCA product) and a hydrogel-based RCA printed microarray (iii, HF-RCP). SEM images were acquired at 4000× magnification; scale bar = 10 µm. (b) Reduction in non-specific protein adsorption to hydrogel-printed RCA microarrays. (i) Visual representation of adsorbed FITC-BSA to bare nitrocellulose (NC, row A'), RCA-only microarrays printed at 0.002 pmol RCA/microzone (row B') and 0.02 pmol RCA/microzone (row C'), hydrogel-printed RCA microarrays printed at 0.002 pmol RCA/microzone (row D') and 0.02 pmol RCA/microzone (row E'). Rows A, B, C, D, E correspond to the same samples immediately after FITC-BSA incubation but before the washing cycle; (ii) Quantitative comparison of FITC-BSA adsorption following washing in 1× PBST between bare nitrocellulose microzones, RCA-only microzones, and hydrogel-printed RCA microzones printed with 0.002 pmol RCA/microzone and 0.02 pmol RCA/microzone (n=4 per sample).

2.3.5. Hybridization efficiency of printed RCA microarrays.

In light of the complex interplay of the effects of the gel configuration, hybridization protocol and post-reaction processing on the hybridization efficiency of a DNA sensor,[12,55,56] we assessed whether our hydrogel-printed RCA microarray can simplify the sensing protocol while still enabling reproducible and sensitive DNA detection. To evaluate the size-screening potential of the printed hydrogel, five different fluorescently-labeled oligonucleotides with molecular weights between 4-20 kDa (Supporting Table S2.1) were tested against both complementary and non-complementary oligonucleotide sequences to discriminate between specific hybridization events and non-specific binding; given the equivalent lengths

and similar chemistries of the complementary and non-complementary probe sequences, the "noise" measurement using the non-complementary probe explicitly accounts for any non-specific retention of the probe in the hydrogel network that may cause a "false" positive signal. The oligonucleotides were dispensed at a concentration of 10 pmol/microzone to ensure saturation of the sensing RCA product (Supporting Figure S2.8). In order to facilitate the removal of non-specifically bound DNA probe (often related to altered chemical reactivity of oligonucleotides on surfaces due to the drop-drying effect[57]), we included 20 vol.% of glycerol in the salt-free DNA probe solution that, coupled with the highly hydrophilic nature of the printed hydrogel, enabled the assay to be conducted with minimal post-hybridization washing-steps on the benchtop without the use of a humidity chamber.

To account, however, for the mass transport limitations of removing non-specifically bound probe from the hydrogel film, 4 × 15 min washes were instituted to ensure complete removal of any unbound probe (see Supporting Figure S2.9).

Figure 2.5a and Figure 2.5b show that the hydrogel-printed RCA microarray facilitates high-throughput discrimination of specific hybridization events for DNA probes up to 27-nt, with significantly higher signal:noise ratios achieved for very short probes (10-nt, $p = 0.0127$) and comparable signal:noise ratios achieved for probes with up to 27 nucleotides. The improved sensitivity for very short probes that, in solution, typically have high dissociation rate constants and too much conformational entropy to remain hybridized[58,59] suggests that the hydrogel assists in stabilizing hybridization interactions; indeed, signal:noise ratios of >5 could be maintained in the presence of as little as 5 pmol (1 μM concentration) of complementary 10-nt probe while a statistically significant signal was still observed at concentrations as low as 0.2 μM (Figure 2.5c). Such detection limits are on par with those of previously reported microarrays but relevant to the sensing of significantly longer minimum reported oligonucleotide sequences (Supporting Table S2.3), demonstrating a key advantage of our printed microarray strategy. In addition, given the ~7-fold higher thickness of the printed hydrogels relative to the direct RCA printed microarrays (as per Figure 2.3a,b), the comparable or better hybridization specificity observed in this shorter probe molecular weight range suggests that the hydrogel can facilitate sufficient diffusional mobility of oligonucleotides in and out of the gel interior even at the relatively short assay time used (30 minutes). However, when using probes longer than 27-nt (molecular weight ~10 kDa), no significant signal above the baseline was observed using the hydrogel printed microarray; this observation persisted even when printing lower concentrations of RCA product (0.003 pmol/microzone and 0.01 pmol/microzone) that promote a less crowded microenvironment and thus better probe diffusion. This result is consistent with the porosity of the printed hydrogel allowing relatively unrestricted diffusion of smaller probes but sterically excluding larger probes; the specific cut-off observed here is consistent with the previously reported pore sizes of POEGMA-based bulk gels prepared with similar precursor polymers (5 - 7 nm).[53] Signal:noise ratios also increase with the concentration of printed RCA product in the microarrays (Supporting Figure S2.10), with RCA product concentrations of > 0.01 pmol/microzone providing the highest signal:noise values performance. In contrast, RCA-only printed microarrays hybridize with complementary oligonucleotides of any molecular weight, with similar signal:noise ratios achieved with nucleotide sequences of 20 bases and above.

To assess the potential combined benefits of the hydrogel in terms of RCA entrapment and suppression of non-specific protein adsorption (Figure 2.4b), the same hybridization assay was conducted in the presence of 20% serum as a fouling agent (Figure 2.5d,e). Under these conditions, the hydrogel-printed RCA microarrays show significantly improved performance versus the RCA-only printed microarray for any DNA probe small enough to penetrate into the hydrogel mesh size (27 nucleotides or less), with a particularly notable >2-fold higher signal:noise achieved with the very short 10-nt sequence ($p=0.004$). Comparing the signal:noise ratios between the DIW-only (Figure 2.5b) and 20% serum (Figure 2.5e) hybridization data, no significant change in signal:noise was observed for the hydrogel-printed RCA

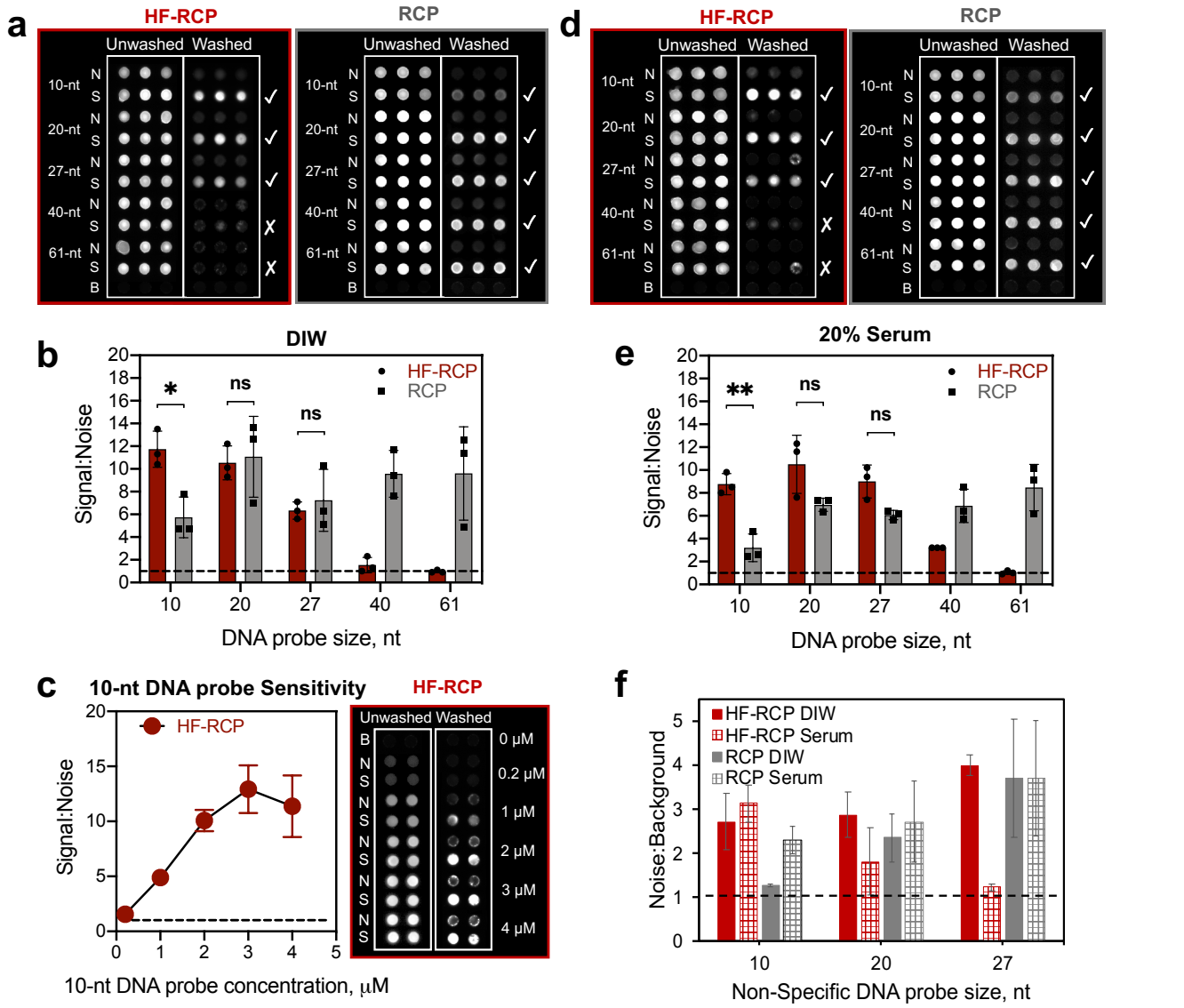

Figure 2.5 Hybridization efficiency of printed RCA microarrays as a function of DNA probe length (0.015 pmol RCA/microzone of RCA density). (a) Qualitative hybridization between specific (S) and non-specific (N) AlexaFluor 647-labeled DNA probes of different lengths in DIW before (left) and after (right) washing in 1× PBST for hydrogel-printed RCA microarrays (left series) and RCA-only printed microarrays (right series) relative to a control hydrogel without RCA product or bare nitrocellulose (B). Columns for each sample correspond to replicate samples; (b) Signal:noise ratio (i.e. binding of specific versus non-specific DNA probe) for DNA hybridization to a hydrogel-printed RCA microarray (red bars) and an RCA-only microarray (grey bars) in DIW after washing (n=3, *=p<0.05 in a pairwise comparison between the hydrogel-printed and RCA-only printed microarrays at a specific DNA probe length, dashed line represents S:N = 1); (c) Signal (complementary probe signal) : noise (non-complementary probe signal) ratio associated with the hybridization of 10-nt DNA probes to HF-RCP array (0.015 pmol RCA/microzone) at varying probe concentrations from 0.2 µM (1 pmol) - 4 µM (20 pmol) in DIW; the figure on the right shows the corresponding qualitative data; (d) Qualitative hybridization between specific (S) and non-specific (N) AlexaFluor 647-labeled DNA probes of different lengths in 20% serum before (left) and after (right) washing in 1× PBST for hydrogel-printed RCA microarrays (left series) and RCA-only printed microarrays (right series) relative to an unloaded control hydrogel or bare nitrocellulose (B). Columns for each sample correspond to replicate tests; (e) Signal:noise ratio for DNA hybridization to a hydrogel-printed RCA microarray (red bars) and an RCA-only microarray (grey bars) in 20% serum after washing (n=3, **=p<0.05 in a pairwise comparison between the hydrogel-printed and RCA-only printed microarrays at a specific DNA probe length, dashed line represents S:N = 1); (f) Normalized residual fluorescence for non-specific DNA probes of different molecular weights following washing for hydrogel-printed RCA microarrays and RCA-only microarrays. The fluorescence intensity was normalized against the background of a hydrogel-only or nitrocellulose-only microarray as appropriate.

microarray at any probe molecular weight when serum was added; in contrast, the signal:noise ratio for the RCA-only printed microarray consistently decreases between 10-35% across all nucleotide chain lengths consistent with non-specific adsorption of serum proteins to the microarray inhibiting effective hybridization. Residual fluorescence measurements from mismatched DNA probes non-specifically interacting with the hydrogel-printed RCA microarray (Figure 2.5f) suggest nearly complete suppression of non-specific adsorption (to background levels) for probes of 20-nt and 27-nt in size; in comparison, RCA-only microarrays showed significant retained fluorescence (i.e. non-specific signal) for these same probe lengths despite the base pair mismatch that would prevent hybridization. Lower background signals in hydrogel-printed microarrays resulting in serum relative to pure hybridization solution (DIW), we attribute to charge and/or hydrophobic interactions between serum proteins and non-hybridized DNA (particularly longer DNA)[60,61] creating weak nanoscale complexes that do not penetrate into the gel and thus can be easily washed from the anti-fouling gel surface. In contrast, in the pure hybridization solution DNA probes can more freely interact with, and penetrate into, the hydrogel. Given the proximity of the hydrodynamic diameter of the larger probes tested with the gel pore size, subsequent high-throughput post-reaction washing results in imperfect removal of unbound molecules and thus similar or slightly higher noise values obtained for each tested DNA targets. However, considering that all the sensing data reported are normalized for these noise values that even though present are still substantially lower from the signal values, the high sensitivity of the assay is sustained while detecting target molecules in pure and complex hybridization solutions.

2.4. Conclusions

In summary, the hydrazone crosslinked hydrogel microarray technology described herein enables improved RCA product immobilization (Figure 2.2a,b), improved resistance to washing/denaturation (Figure 2.2c) and lower fouling (Figure 2.4b) relative to direct RCA-printed microarrays. Such functional benefits ultimately result in better discriminative hybridization potential for DNA probes in complex media, with the added advantage of size selectivity enabling detection of specific sizes of oligonucleotides based on the printed hydrogel layer porosity. Of particular note, even though the free diffusion of target molecules to the RCA-only printed microarray would in principle be beneficial to enable faster hybridization and lower background signals (although, interestingly, not in the presence of serum proteins, as evidenced by Figure 2.5e-f), the confined hydrogel environment is highly beneficial for stabilizing the relatively fragile hybridization interactions between DNA probes and the RCA product, enabling the detection of shorter nucleic acids that typically suffer from low hybridization stability and thus poor sensing capacity.[60,62,63] As such, the hydrogel microarray reported herein offers particular promise to address sensing situations requiring discrimination between targets of different sizes but similar affinity in addition to stabilizing short double-stranded DNA complexes often targeted for the development of high-performing functional nucleic acid sensors. These functional benefits can be accomplished while preserving short assay times (30 min) and simple protocols for performing both the fabrication (one-step printing, without the need for blocking agents, on the benchtop) and the assay itself (requiring only automated reagents dispensing and four PBST washes).

2.5. References

(1) Wheelan, S. J.; Martínez Murillo, F.; Boeke, J. D. The Incredible Shrinking World of DNA Microarrays. *Mol. BioSyst.* 2008, *4* (7), 726.

(2) Evans, W. E.; Relling, M. V. Moving towards Individualized Medicine with Pharmacogenomics. *Nature* 2004, *429* (6990), 464–468.

(3) Gryadunov, D.; Dementieva, E.; Mikhailovich, V.; Nasedkina, T.; Rubina, A.; Savvateeva, E.; Fesenko, E.; Chudinov, A.; Zimenkov, D.; Kolchinsky, A.; Zasedatelev, A. Gel-Based Microarrays in Clinical Diagnostics in Russia. *Expert Review of Molecular Diagnostics* 2011, *11* (8), 839–853.

(4) Zlatanova, J.; Mirzabekov, A. Gel-Immobilized Microarrays of Nucleic Acids and Proteins: Production and Application for Macromolecular Research. In *DNA Arrays*; Humana Press: New Jersey, 2001; Vol. 170, pp 17–38.

(5) Rao, A. N.; Grainger, D. W. Biophysical Properties of Nucleic Acids at Surfaces Relevant to Microarray Performance. *Biomater. Sci.* 2014, *2* (4), 436–471.

(6) Monserud, J. H.; Schwartz, D. K. Effects of Molecular Size and Surface Hydrophobicity on Oligonucleotide Interfacial Dynamics. *Biomacromolecules* 2012, *13* (12), 4002–4011.

(7) Sorokin, N. V.; Chechetkin, V. R.; Pan'kov, S. V.; Somova, O. G.; Livshits, M. A.; Donnikov, M. Y.; Turygin, A. Y.; Barsky, V. E.; Zasedatelev, A. S. Kinetics of Hybridization on Surface Oligonucleotide Microchips: Theory, Experiment, and Comparison with Hybridization on Gel-Based Microchips. *Journal of Biomolecular Structure and Dynamics* 2006, *24* (1), 57–66.

(8) Draghici, S.; Khatri, P.; Eklund, A.; Szallasi, Z. Reliability and Reproducibility Issues in DNA Microarray Measurements. *Trends in Genetics* 2006, *22* (2), 101–109.

(9) Yalçın, A.; Damin, F.; Özkumur, E.; di Carlo, G.; Goldberg, B. B.; Chiari, M.; Ünlü, M. S. Direct Observation of Conformation of a Polymeric Coating with Implications in Microarray Applications. *Anal. Chem.* 2009, *81* (2), 625–630.

(10) Tang, J.; Xiao, P. Polymerizing Immobilization of Acrylamide-Modified Nucleic Acids and Its Application. *Biosensors and Bioelectronics* 2009, *24* (7), 1817–1824.

(11) Rubina, A. Y.; Pan'kov, S. V.; Dementieva, E. I.; Pen'kov, D. N.; Butygin, A. V.; Vasiliskov, V. A.; Chudinov, A. V.; Mikheikin, A. L.; Mikhailovich, V. M.; Mirzabekov, A. D. Hydrogel Drop Microchips with Immobilized DNA: Properties and Methods for Large-Scale Production. *Analytical Biochemistry* 2004, *325* (1), 92–106.

(12) Han, T.; Melvin, C. D.; Shi, L.; Branham, W. S.; Moland, C. L.; Pine, P. S.; Thompson, K. L.; Fuscoe, J. C. Improvement in the Reproducibility and Accuracy of DNA Microarray Quantification by Optimizing Hybridization Conditions. *BMC Bioinformatics* 2006, *7* (S2), S17.

(13) Pei, H.; Zuo, X.; Pan, D.; Shi, J.; Huang, Q.; Fan, C. Scaffolded Biosensors with Designed DNA Nanostructures. *NPG Asia Mater* 2013, *5* (6), e51–e51.

(14) Tavakoli, J.; Tang, Y. Hydrogel Based Sensors for Biomedical Applications: An Updated Review. *Polymers* 2017, *9* (12), 364.

(15) Dominguez, M. M.; Wathier, M.; Grinstaff, M. W.; Schaus, S. E. Immobilized Hydrogels for Screening of Molecular Interactions. *Anal. Chem.* 2007, *79* (3), 1064–1066.

(16) Tanase, C. P.; Albulescu, R.; Neagu, M. Application of 3D Hydrogel Microarrays in Molecular Diagnostics: Advantages and Limitations. *Expert Review of Molecular Diagnostics* 2011, *11* (5), 461–464.

(17) Gurevitch, D.; Dongs, X. F.; Pircher, T. J.; Matsumoto, S. S.; Roycroft, P.; Tsinberg, P.; Falcovitz, Y. H.; Hahn, S. A Novel Three-Dimensional Hydrogel-Based Microarray Platform. *J. Lab. Autom.* 2001, *6* (4), 87–91.

(18) Kowalczyk, A.; Fau, M.; Karbarz, M.; Donten, M.; Stojek, Z.; Nowicka, A. M. Hydrogel with Chains Functionalized with Carboxyl Groups as Universal 3D Platform in DNA Biosensors. *Biosensors and Bioelectronics* 2014, *54*, 222–228.

(19) Jung, I. Y.; Kim, J. S.; Choi, B. R.; Lee, K.; Lee, H. Hydrogel Based Biosensors for In Vitro Diagnostics of Biochemicals, Proteins, and Genes. *Adv. Healthcare Mater.* 2017, *6* (12), 1601475.

(20) Hook, A. L.; Voelcker, N. H.; Thissen, H. Patterned and Switchable Surfaces for Biomolecular Manipulation. *Acta Biomaterialia* 2009, *5* (7), 2350–2370.

(21) Bilgic, T.; Klok, H.-A. Oligonucleotide Immobilization and Hybridization on Aldehyde-Functionalized Poly(2-Hydroxyethyl Methacrylate) Brushes. *Biomacromolecules* 2015, *16* (11), 3657–3665.

(22) Bilgic, T.; Klok, H.-A. Surface-Initiated Controlled Radical Polymerization Enhanced DNA Biosensing. *European Polymer Journal* 2015, *62*, 281–293.

(23) Belosludtsev, Y.; Iverson, B.; Lemeshko, S.; Eggers, R.; Wiese, R.; Lee, S.; Powdrill, T.; Hogan, M. DNA Microarrays Based on Noncovalent Oligonucleotide Attachment and Hybridization in Two Dimensions. *Analytical Biochemistry* 2001, *292* (2), 250–256.

(24) Sassolas, A.; Leca-Bouvier, B. D.; Blum, L. J. DNA Biosensors and Microarrays. *Chem. Rev.* 2008, *108* (1), 109–139.

(25) Sethi, D.; Gandhi, R. P.; Kuma, P.; Gupta, K. C. Chemical Strategies for Immobilization of Oligonucleotides. *Biotechnol. J.* 2009, *4* (11), 1513–1529.

(26) Zubtsov, D. A.; Savvateeva, E. N.; Rubina, A. Yu.; Pan'kov, S. V.; Konovalova, E. V.; Moiseeva, O. V.; Chechetkin, V. R.; Zasedatelev, A. S. Comparison of Surface and Hydrogel-Based Protein Microchips. *Analytical Biochemistry* 2007, *368* (2), 205–213.

(27) Friedberg, E. C.; McDaniel, L. D.; Schultz, R. A. The Role of Endogenous and Exogenous DNA Damage and Mutagenesis. *Current Opinion in Genetics & Development* 2004, *14* (1), 5–10.

(28) Yang, W. Surviving the Sun: Repair and Bypass of DNA UV Lesions. *Protein Science* 2011, *20* (11), 1781–1789.

(29) Beyer, A.; Pollok, S.; Berg, A.; Weber, K.; Popp, J. Easy Daylight Fabricated Hydrogel Array for Colorimetric DNA Analysis: Daylight Fabricated Hydrogel Array. *Macromol. Biosci.* 2014, *14* (6), 889–898.

(30) Beyer, A.; Cialla-May, D.; Weber, K.; Popp, J. Hydrogel Decorated Chips for Convenient DNA Test. *Macromol. Chem. Phys.* 2016, *217* (8), 959–965.

(31) Soto, C. M.; Patterson, C. H.; Charles, P. T.; Martin, B. D.; Spector, M. S. Immobilization and Hybridization of DNA in a Sugar Polyacrylate Hydrogel. *Biotechnol. Bioeng.* 2005, *92* (7), 934–942.

(32) Zhao, W.; Ali, M. M.; Brook, M. A.; Li, Y. Rolling Circle Amplification: Applications in Nanotechnology and Biodetection with Functional Nucleic Acids. *Angew. Chem. Int. Ed.* 2008, *47* (34), 6330–6337.

(33) Tang, L.; Liu, Y.; Ali, M. M.; Kang, D. K.; Zhao, W.; Li, J. Colorimetric and Ultrasensitive Bioassay Based on a Dual-Amplification System Using Aptamer and DNAzyme. *Anal. Chem.* 2012, *84* (11), 4711–4717.

(34) Ali, M. M.; Li, F.; Zhang, Z.; Zhang, K.; Kang, D.-K.; Ankrum, J. A.; Le, X. C.; Zhao, W. Rolling Circle Amplification: A Versatile Tool for Chemical Biology, Materials Science and Medicine. *Chem. Soc. Rev.* 2014, *43* (10), 3324.

(35) Nallur, G. Signal Amplification by Rolling Circle Amplification on DNA Microarrays. *Nucleic Acids Research* 2001, *29* (23), 118e–1118.

(36) Gu, L.; Yan, W.; Liu, L.; Wang, S.; Zhang, X.; Lyu, M. Research Progress on Rolling Circle Amplification (RCA)-Based Biomedical Sensing. *Pharmaceuticals* 2018, *11* (2), 35.

(37) Carrasquilla, C.; Little, J. R. L.; Li, Y.; Brennan, J. D. Patterned Paper Sensors Printed with Long-Chain DNA Aptamers. *Chem. Eur. J.* 2015, *21* (20), 7369–7373.

(38) Liu, M.; Zhang, Q.; Kannan, B.; Botton, G. A.; Yang, J.; Soleymani, L.; Brennan, J. D.; Li, Y. Self-Assembled Functional DNA Superstructures as High-Density and Versatile Recognition Elements for Printed Paper Sensors. *Angew. Chem.* 2018, *130* (38), 12620–12623.

(39) Carrasquilla, C.; Kapteyn, E.; Li, Y.; Brennan, J. D. Sol-Gel-Derived Biohybrid Materials Incorporating Long-Chain DNA Aptamers. *Angew. Chem. Int. Ed.* 2017, *56* (36), 10686–10690.

(40) Li, Y.; Dahhan, O.; Filipe, C. D. M.; Brennan, J. D.; Pelton, R. H. Optimizing Piezoelectric Inkjet Printing of Silica Sols for Biosensor Production. *J Sol-Gel Sci Technol* 2018, *87* (3), 657–664.

(41) Deng, X.; Smeets, N. M. B.; Sicard, C.; Wang, J.; Brennan, J. D.; Filipe, C. D. M.; Hoare, T. Poly(Oligoethylene Glycol Methacrylate) Dip-Coating: Turning Cellulose Paper into a Protein-Repellent Platform for Biosensors. *J. Am. Chem. Soc.* 2014, *136* (37), 12852–12855.

(42) Mateen, R.; Ali, M. M.; Hoare, T. A Printable Hydrogel Microarray for Drug Screening Avoids False Positives Associated with Promiscuous Aggregating Inhibitors. *Nat Commun* 2018, *9* (1), 602.

(43) Cai, S.; Lau, C.; Lu, J. Sequence-Specific Detection of Short-Length DNA via Template-Dependent Surface-Hybridization Events. *Anal. Chem.* 2010, *82* (17), 7178–7184.

(44) Goldman, J. M.; Zhang, L. A.; Manna, A.; Armitage, B. A.; Ly, D. H.; Schneider, J. W. High Affinity γPNA Sandwich Hybridization Assay for Rapid Detection of Short Nucleic Acid Targets with Single Mismatch Discrimination. *Biomacromolecules* 2013, *14* (7), 2253–2261.

(45) Smeets, N. M. B.; Bakaic, E.; Patenaude, M.; Hoare, T. Injectable and Tunable Poly(Ethylene Glycol) Analogue Hydrogels Based on Poly(Oligoethylene Glycol Methacrylate). *Chem. Commun.* 2014, *50* (25), 3306.

(46) Liu, M.; Hui, C. Y.; Zhang, Q.; Gu, J.; Kannan, B.; Jahanshahi-Anbuhi, S.; Filipe, C. D. M.; Brennan, J. D.; Li, Y. Target-Induced and Equipment-Free DNA Amplification with a Simple Paper Device. *Angew. Chem.* 2016, *128* (8), 2759–2763.

(47) Smeets, N. M. B.; Bakaic, E.; Patenaude, M.; Hoare, T. Injectable Poly(Oligoethylene Glycol Methacrylate)-Based Hydrogels with Tunable Phase Transition Behaviours: Physicochemical and Biological Responses. *Acta Biomaterialia* 2014, *10* (10), 4143–4155.

(48) Bakaic, E.; Smeets, N. M. B.; Dorrington, H.; Hoare, T. "Off-the-Shelf" Thermoresponsive Hydrogel Design: Tuning Hydrogel Properties by Mixing Precursor Polymers with Different Lower-Critical Solution Temperatures. *RSC Adv.* 2015, *5* (42), 33364–33376.

(49) Hu, Z.; Willsky, G. Utilization of Two Sample T-Test Statistics from Redundant Probe Sets to Evaluate Different Probe Set Algorithms in GeneChip Studies. *BMC Bioinformatics* 2006, *7* (1), 12.

(50) Sonawane, M. D.; Nimse, S. B. Surface Modification Chemistries of Materials Used in Diagnostic Platforms with Biomolecules. *Journal of Chemistry* 2016, *2016*, 1–19.

(51) Singh, A.; Lantigua, D.; Meka, A.; Taing, S.; Pandher, M.; Camci-Unal, G. Paper-Based Sensors: Emerging Themes and Applications. *Sensors* 2018, *18* (9), 2838.

(52) Liana, D. D.; Raguse, B.; Gooding, J. J.; Chow, E. Recent Advances in Paper-Based Sensors. *Sensors* 2012, *12* (9), 11505–11526.

(53) Smeets, N. M. B.; Bakaic, E.; Yavitt, F. M.; Yang, F.-C.; Rheinstädter, M. C.; Hoare, T. Probing the Internal Morphology of Injectable Poly(Oligoethylene Glycol Methacrylate) Hydrogels by Light and Small-Angle Neutron Scattering. *Macromolecules* 2014, *47* (17), 6017–6027.

(54) Clausson, C.-M.; Arngården, L.; Ishaq, O.; Klaesson, A.; Kühnemund, M.; Grannas, K.; Koos, B.; Qian, X.; Ranefall, P.; Krzywkowski, T.; Brismar, H.; Nilsson, M.; Wählby, C.; Söderberg, O. Compaction of Rolling Circle Amplification Products Increases Signal Integrity and Signal-to-Noise Ratio. *Sci Rep* 2015, *5* (1), 12317.

(55) Squires, T. M.; Messinger, R. J.; Manalis, S. R. Making It Stick: Convection, Reaction and Diffusion in Surface-Based Biosensors. *Nat Biotechnol* 2008, *26* (4), 417–426.

(56) Dorris, D. R.; Nguyen, A.; Gieser, L.; Lockner, R.; Lublinsky, A.; Patterson, M.; Touma, E.; Sendera, T. J.; Elghanian, R.; Mazumder, A. Oligodeoxyribonucleotide Probe Accessibility on a Three-Dimensional DNA Microarray Surface and the Effect of Hybridization Time on the Accuracy of Expression Ratios. *BMC Biotechnol.* 2003, *3* (6).

(57) Sobek, J.; Aquino, C.; Weigel, W.; Schlapbach, R. Drop Drying on Surfaces Determines Chemical Reactivity - the Specific Case of Immobilization of Oligonucleotides on Microarrays. *BMC Biophys* 2013, *6* (1), 8.

(58) Araque, J. C.; Robert, M. A. Lattice Model of Oligonucleotide Hybridization in Solution. II. Specificity and Cooperativity. *The Journal of Chemical Physics* 2016, *144* (12), 125101.

(59) Mardoum, W. M.; Gorczyca, S. M.; Regan, K. E.; Wu, T.-C.; Robertson-Anderson, R. M. Crowding Induces Entropically-Driven Changes to DNA Dynamics That Depend on Crowder Structure and Ionic Conditions. *Front. Phys.* 2018, *6*, 53.

(60) Nakano, S.; Miyoshi, D.; Sugimoto, N. Effects of Molecular Crowding on the Structures, Interactions, and Functions of Nucleic Acids. *Chem. Rev.* 2014, *114* (5), 2733–2758.

(61) Kunzelmann, S.; Morris, C.; Chavda, A. P.; Eccleston, J. F.; Webb, M. R. Mechanism of Interaction between Single-Stranded DNA Binding Protein and DNA. *Biochemistry* 2010, *49* (5), 843–852.

(62) Markarian, M. Z.; Schlenoff, J. B. Effect of Molecular Crowding and Ionic Strength on the Isothermal Hybridization of Oligonucleotides. *J. Phys. Chem. B* 2010, *114* (32), 10620–10627.

(63) Nakano, S.; Yamaguchi, D.; Sugimoto, N. Thermal Stability and Conformation of DNA and Proteins under the Confined Condition in the Matrix of Hydrogels. *Mol Biol Rep* 2018, *45* (4), 403–411.

2.6. Appendix – Supporting Information Chapter 2

2.6.1. DNA Sequences used in DNA Hybridization Assay

Table S2.1 DNA sequences, molecular weights, and melting points of oligonucleotide probes used for the multiplex hybridization assay (Signal = complementary probe to RCA sequence; Noise = non-complementary probe to RCA sequence)

DNA probe	Sequence (5'-3')	Molecular Weight (kDa)	Theoretical T_m (°C)[a]
Signal – 10 nt	/5Alex647N/ TGT CTT CGC C	3.99	51.7
Noise – 10 nt	/5Alex647N/TGC TTA GTC G	4.05	46.7
Signal – 20 nt	/5Alex647N/TGT CTT CGC CTT CTT GTT TC	7.03	66.5
Noise – 20 nt	/5Alex647N/TGC TTA GTC GAA AGA AAG AA	7.22	63.8
Signal – 27 nt	/5Alex647N/TGT CTT CGC CTT CTT GTT TCC TTT CCT	9.11	72.6
Noise – 27 nt	/5Alex647N/TGC TTA GTC GAA AGA AAG AAA GGA AGA	9.46	69.5
Signal – 40 nt	/5Alex647N/TGT CTT CGC CTT CTT GTT TCC TTT CCT TGA AAC TTC TTC C	13.06	75.7
Noise – 40 nt	/5Alex647N/TGC TTA GTC GAA AGA AAG AAA GGA AGA AGT TTC AAG GAA A	13.53	74.2
Signal – 61 nt	/5Alex647N/TGT CTT CGC CTT CTT GTT TCC TTT CCT TGA AAC TTC TTC CTT TCT TTC TTT CGA CTA AGC A	19.46	78.6
Noise – 61 nt	/5Alex647N/TGC TTA GTC GAA AGA AAG AAA GGA AGA AGT TTC AAG GAA AGG AAA CAA GAA GGC GAA GAC A	20.14	78.6

[a] Expressed for concentration of 2 μM DNA in 10mM $MgCl_2$.

2.6.2. Characterization of synthesized POA and POH polymers

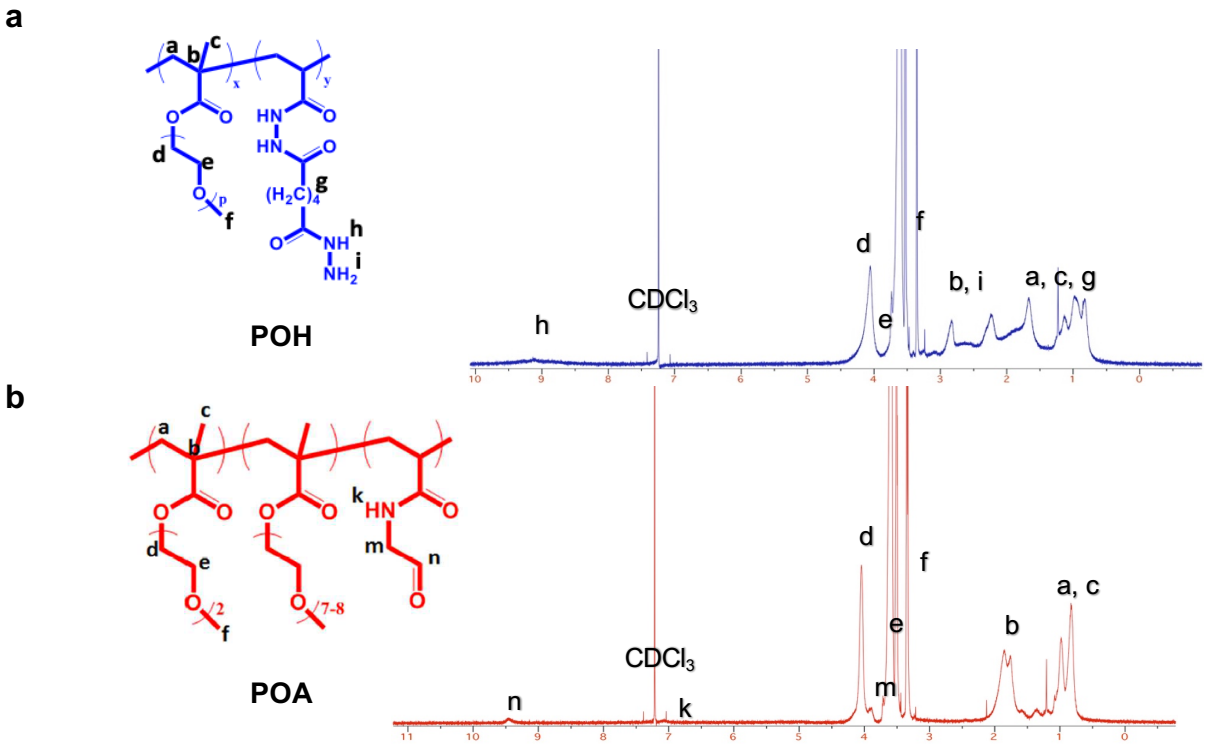

Figure S2.1 [1]H-NMR spectra of hydrazide-functionalized (POH) and aldehyde-functionalized (POA) poly (oligoethylene glycol methacrylate) (POEGMA) precursor polymers. (a) Hydrazide-functionalized poly (oligoethylene glycol methacrylate) (POH) (b) Aldehyde-functionalized poly(oligoethylene glycol methacrylate) (POA). Chemical shifts are reported relative to residual deuterated solvent peaks. Peak assignments are given on each spectrum based on the anticipated chemical structure of each polymer[1,2].

Table S2.2 Chemical properties of synthesized hydrazide-functionalized (POH) and aldehyde-functionalized (POA) poly (oligoethylene glycol methacrylate) (POEGMA) precursor polymers.

Polymer Precursor	**Functional Monomer**	**Functional Monomer, mol%**	**M_n, $\times 10^3$ g/mol**	***Đ***	**Viscosity, (25 °C, shear rate 10 s^{-1}), mPa s**
POH	$NHNH_2$	21.9 [a]	26.7 [c]	3.89	4.5 [d]
POA	CHO	9.1 [b]	17.9 [c]	2.52	1.5 [d]

[a] Determined by conductometric titration; [b] Determined by [1]H-NMR; [c] Determined by DMF-SEC; [d] Determined by viscosity vs. shear rate measurements using a DHR-2 rheometer

2.6.3. Qualitative analysis of microarray printing reproducibility and stability with 0.003 pmol/microzone of RCA product

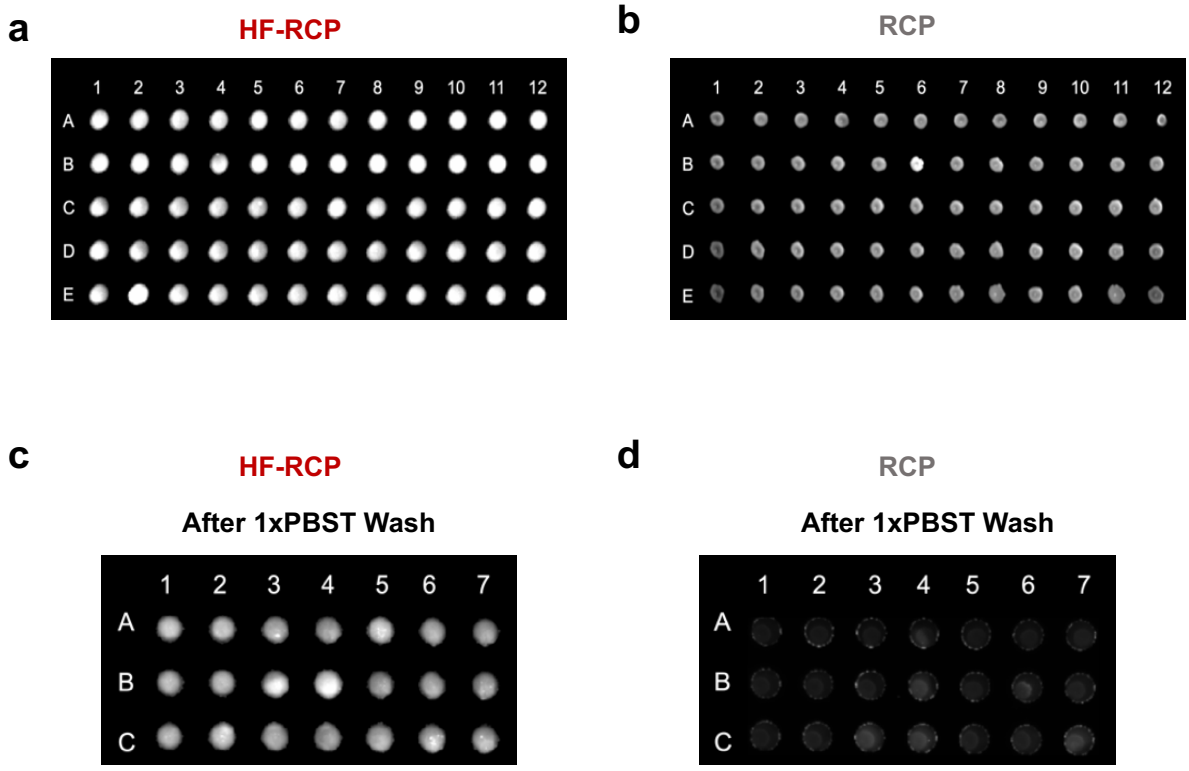

Figure S2.1 Qualitative analysis of printing reproducibility and stability of RCA product microarray with 0.003 pmol/microzone. The printing reproducibility images show the visual representation of the data from the 60 replicates or 5×12 (row × column) microarray, while stability of RCA product images show the visual representation of the fluorescence retention data from the 3×7 (row × column) microarray; (a) Printing reproducibility of RCA product in a hydrogel microarray (b) Printing reproducibility of RCA-only microarray; (c, d) Retention of fluorescence intensity (corresponding to retained RCA product concentration) in a hydrogel-printed RCA product microarray (c) compared to a RCA-only printed microarray (d) following washing in 1× PBST, pH=7.5 for 2 hours.

2.6.4. Reproducibility of microarray printing with 0.015 pmol/microzone of RCA product

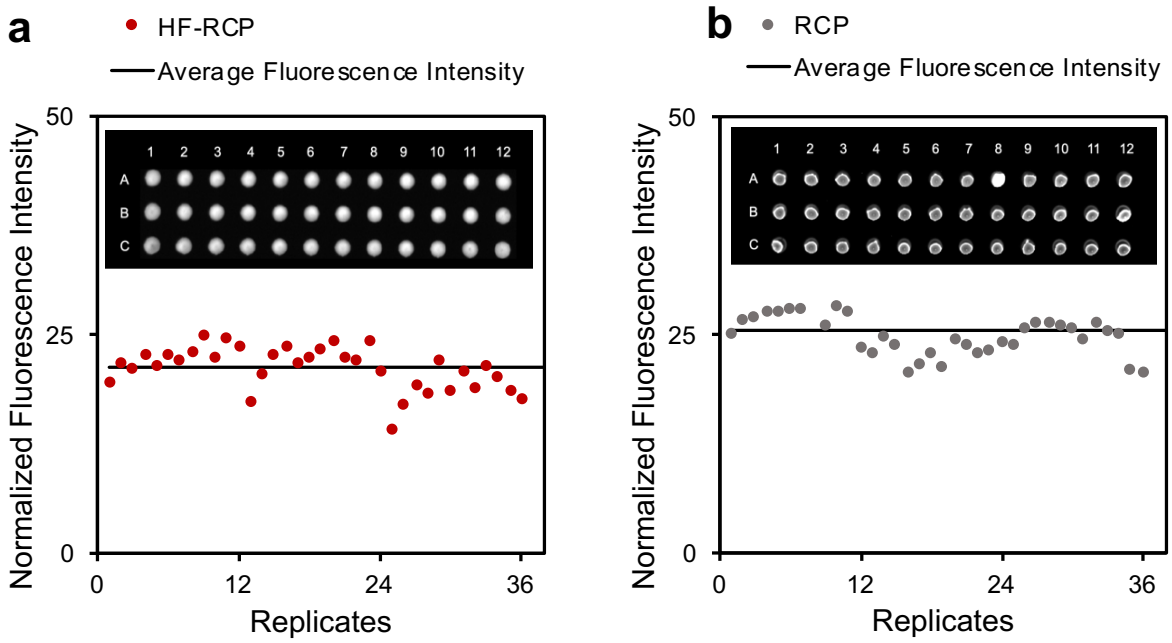

Figure S2.2 Reproducibility of RCA product microarray printing at higher DNA density. (a) Hydrogel-printed RCA product microarray (0.015 pmol/microzone, coefficient of variation = 11.4%); the inset image shows the visual representation of this data; (b) RCA product-only microarray (0.015 pmol/microzone, coefficient of variation = 19.0%); the inset image shows the visual representation of this data.

2.6.5. RCA product physisorption on nitrocellulose

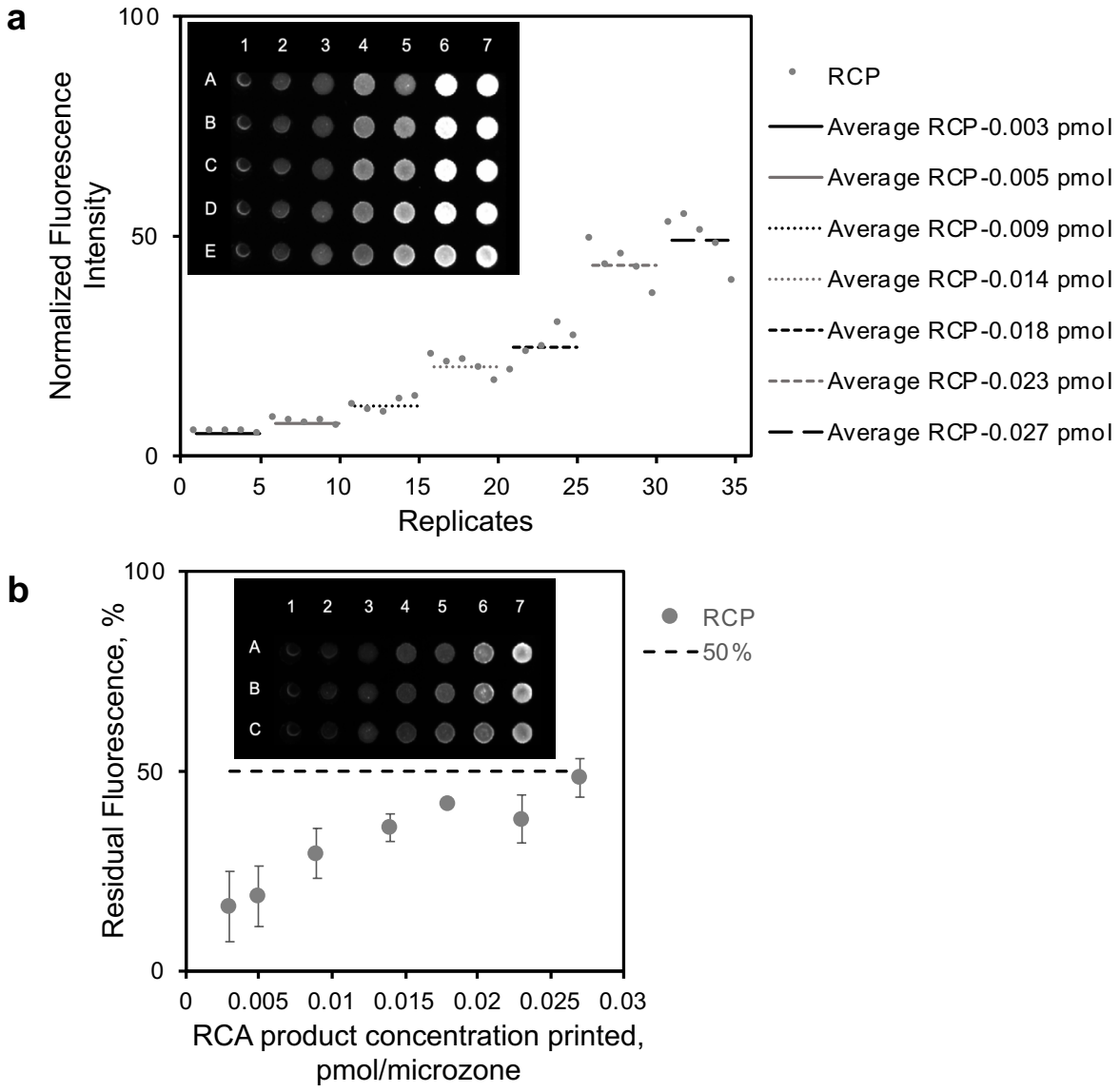

Figure S2.3 Printability and retention of RCA product-only microarray at different RCA product concentrations. RCA product was printed at a concentration of 0.0018 μM using printing volumes between 1.5 μL-15 μL, resulting in DNA surface densities between 0.003-0.027 pmol/microzone. (a) Average fluorescence intensities measured at different RCA product concentrations; the inset image visually represents the printed RCA product-only microarray. Each column shows a different RCA product concentration, with the rows (A-E) representing n=5 replicates; (b) Retention of fluorescence intensity in RCA product-only printed microarray with different RCA product concentrations following washing in 1× PBST, pH=7.5 for 2 hours; the inset image shows the visual representation of the quantified data while the dashed line shows 50% retention of the fluorescence signal for reference. Each column shows a different RCA product concentration, with the rows (A-C) representing n=3 replicates. The fluorescence intensity was normalized against the local background from hydrated nitrocellulose.

2.6.6. RCA product retention following washing from hydrogel-printed and RCA-only microarrays prepared at different RCA concentrations

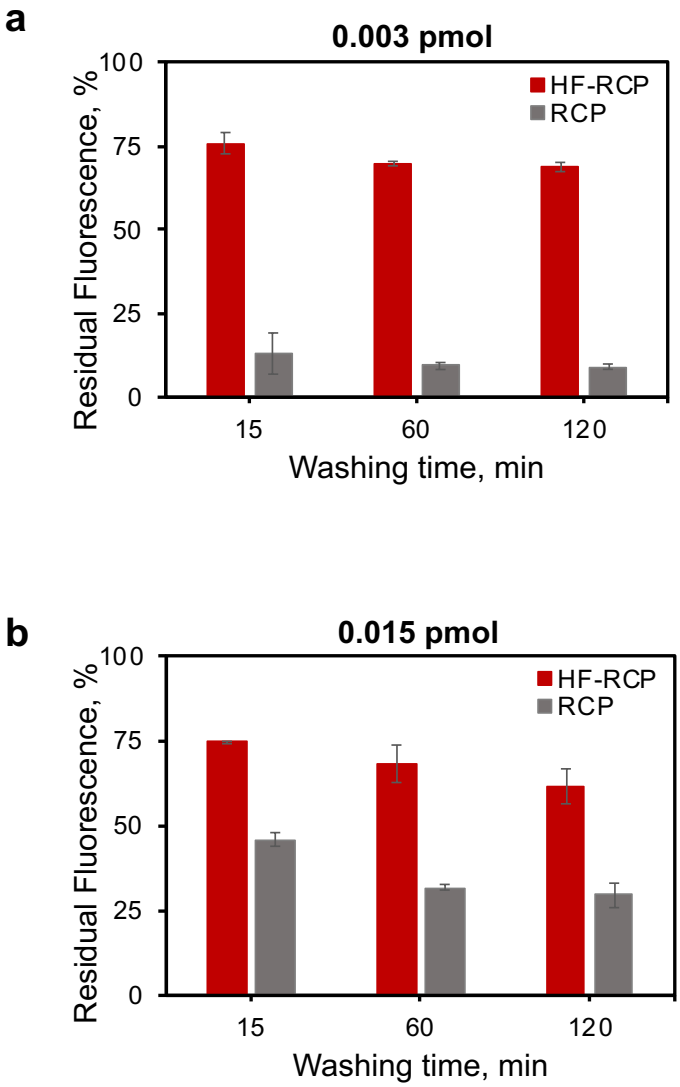

Figure S2.4 RCA product retention in printed hydrogel (HF-RCP) and control (RCP) microarrays after washing. The microarrays were printed and washed in 1× PBST (pH=7.5, 150 RPM). Residual fluorescence intensity (corresponding to the residual RCA product retention) was measured after washing for 15 min., 1 h, or 2 h. (a) 0.003 pmol/microzone RCA product – Hydrogel-printed microarrays (red column) provide stable retention of RCA product over the entire course of washing protocol, with ~ 7-fold higher retention capacity relative to the control RCA-only microarray (grey column) that showed almost complete RCA product loss after the first 15 min. of washing. (b) 0.015 pmol/microzone RCA product – Hydrogel-printed microarrays (red column) provide more stable retention of RCA product, with ~ 2-fold higher retention capacity relative to the control RCA-only microarray (grey column) at the end of the wash. Data presented represent the average of n=9 replicates.

2.6.7. RCA product retention determined based on the residual fluorescence in the wash buffer

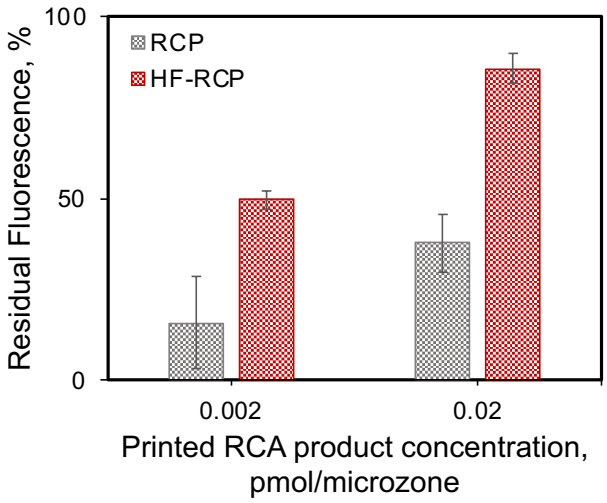

Figure S2.5 Immobilization of AlexaFluor 647-RCA product on a nitrocellulose substrate following printing as determined from the fluorescence intensity of the washing supernatant. The hydrogel and RCA-only microarrays were printed at 0.002 pmol RCA product/microzone (left) and 0.02 pmol/microzone (right), with the percentage retention of fluorescence intensity (i.e. the relative concentration of AlexaFluor 647-labeled RCA product) quantified after vigorous washing with 1× PBST over 2 hours. Data are normalized relative to a negative control sample (0% leaked product) and a positive control (with 100% leaked product) in duplicate. The hydrogel-printed RCA microarray at 0.002 pmol RCA/microzone shows 49 ± 8% retention of the original fluorescence signal after washing, while RCA-only printed microarrays enabled just 16 ± 13% retention. The hydrogel-printed RCA microarrays printed with a 10-fold higher RCA density exhibited 86 ± 4% retention while RCA-only printed microarrays enabled the retention of only 38 ± 3% of the originally printed RCA product following washing.

2.6.8. Three-dimensional confocal microscopy images of printed HF-RCP and RCP arrays

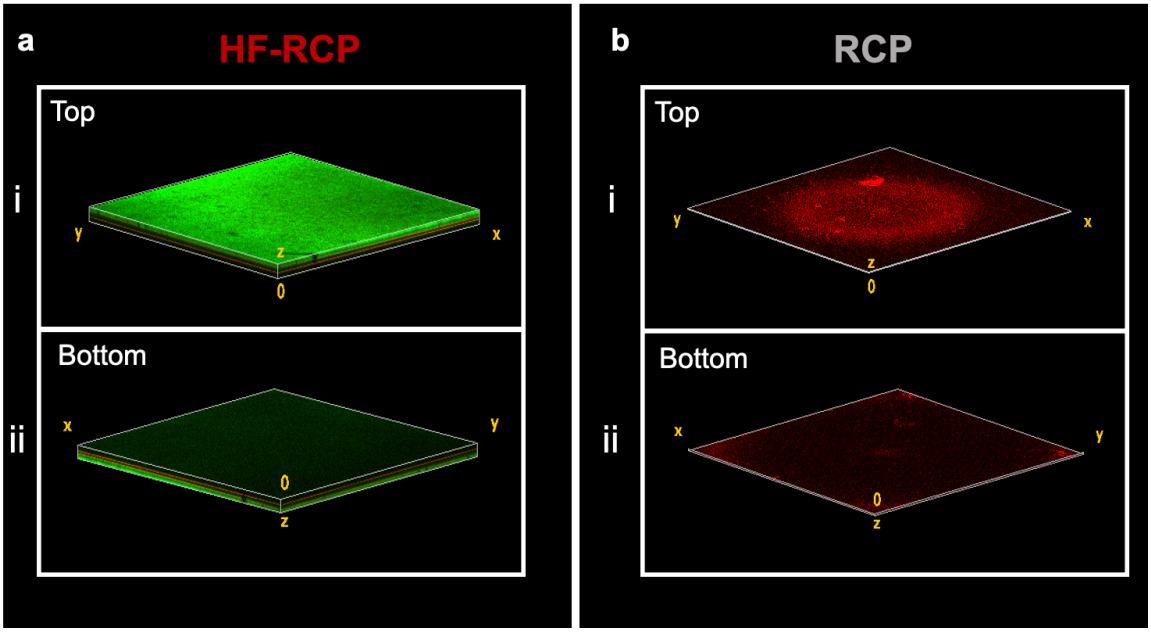

Figure S2.6 3D confocal microscopy images of a printed HF-RCP array (a) and a printed RCP array (b). 3D images were processed using ImageJ-Fiji software with the Volume Viewer analyzer using trilinear interpolation mode.

2.6.9. RCA product synthesis and solution-based confirmation of hybridization

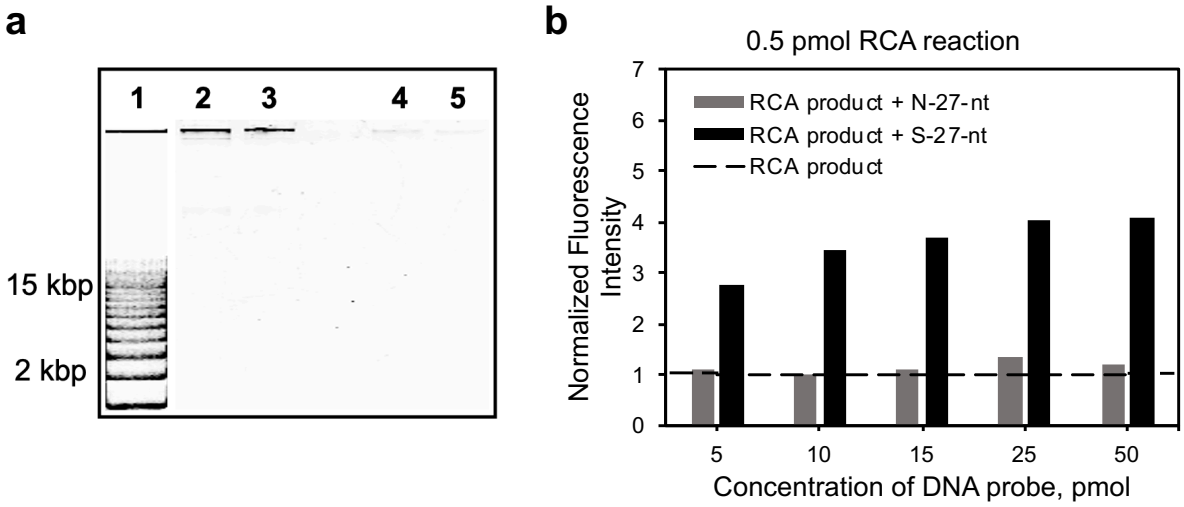

Figure S2.7 Confirmation of RCA product generation and solution-based hybridization efficiency. In order to confirm the hybridization efficiency of the synthesized RCA product and estimate the concentration of the DNA-probe that saturates the concatemeric RCA product, the RCA product was titrated with varying concentrations of a complementary (S) and non-complementary (N) 27-nt oligonucleotide. The RCA product was generated over a shorter reaction time (20 min. instead of 1 hour) and at a lower density (0.5 pmol instead of 10 pmol) in an effort to avoid RCA product aggregation and allow optimal conditions for hybridization. (a) RCA product detection via 0.6% agarose gel electrophoresis: The 0.5 pmol of RCA product was produced over a 20 min. reaction at 30°C in duplicate (Lane 2, Lane 3). A negative control RCA reaction was allowed to proceed without a priming ligation template. (Lane 4, Lane 5). A 10 µL aliquot of the reaction mixture was mixed with 2 µL of 6× Gel Loading Dye (Fisher Scientific) and run through the agarose gel stained with GelRed against 1KbpPlus ladder (Lane 1). The gel was scanned through the GelRed channel. Given the MDa molecular weight of the RCA product, it does not migrate through the gel and is visualized as a strong fluorescence signal retained inside the gel loading wells. The negative control does not generate a signal since the RCA reaction could not be initiated in the absence of the ligation template. (b) Solution-based hybridization of RCA product with complementary single-stranded DNA probe: Fifteen separate RCA reactions were initiated at a concentration of 0.5 pmol over 20 min at 30°C. The hybridization reaction was then tested with 27-nt complementary and non-complementary DNA-probe (RCP+S-27-nt and RCP+N-27-nt, respectively) relative to the blank comprised of RCA product alone. Ten minutes after the reaction initiation, different concentrations (5-50 pmol) of S-27-nt and N-27-nt were added in each reaction sample and allowed to in situ hybridize with the generating RCA product. The reaction was stopped by heating at 90°C for 10 min. After cooling back to room temperature, samples were stained with 2× QuantiFluor dsDNA dye (PROMEGA) over 10 min and their fluorescence was quantified using a NanoQuant spectrophotometer (504 nm excitation/531 nm emission wavelength). The fluorescence intensity data were normalized against the blank samples (dashed line). The result indicates successful hybridization of RCA product with complementary DNA sequences in solution, suggesting a saturation "duplex" concentration of 25 pmol of probe/0.5 pmol of RCA product generated over 20 min. of amplification.

2.6.10. Optimization of post-hybridization washing conditions

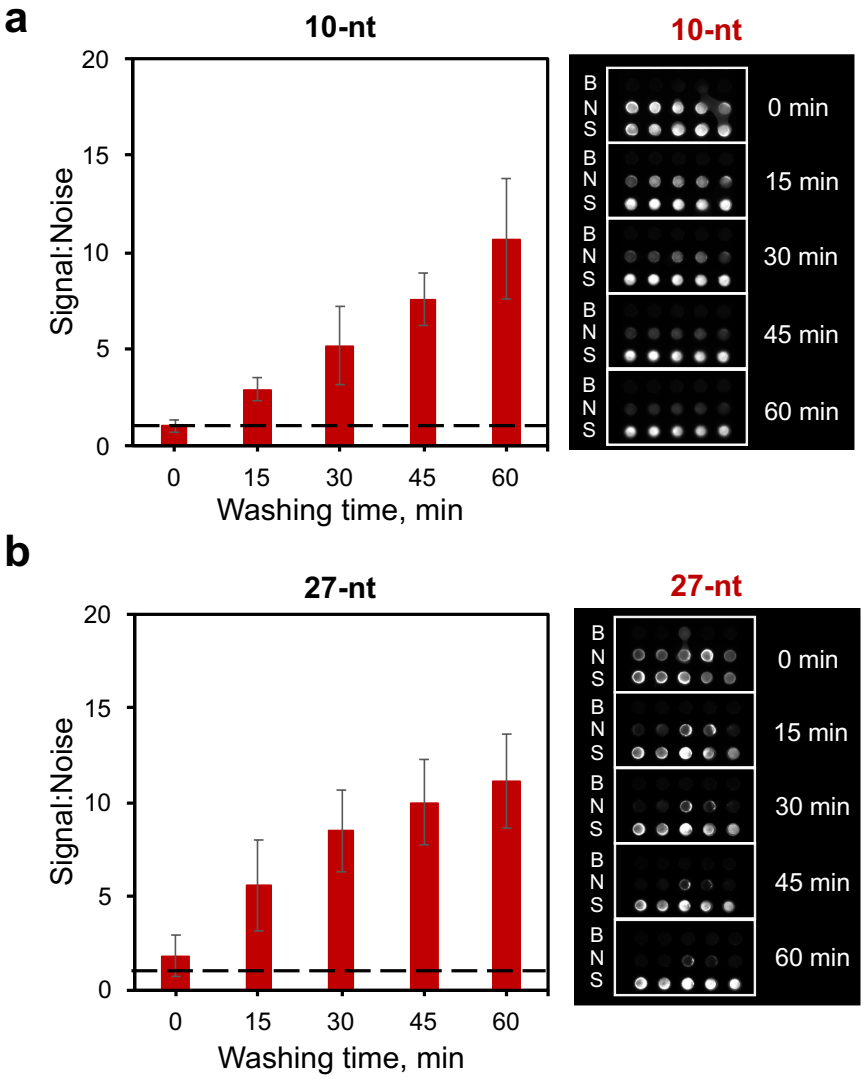

Figure S2.8 Optimization of post-hybridization removal of non-specifically bound probe over multiple washing cycles. Both complementary (S) and non-complementary (N) DNA probes of sizes 10-nt (a) and 27-nt (b) were hybridized with the entrapped RCA product in density of 0.01 pmol/microzone (n=5). Unbound DNA probe was then removed from the gel using 4×15 min washing cycles in 1× PBST under gentle shaking. The fluorescence intensity was measured by scanning the microarrays through the AlexaFluor 647 channel (650 excitation/670 nm emission) and calculating the ratio between the signals measured for the complementary and non-complementary DNA probes.

The shortest probe (10-nt, a) requires longer post-hybridization rinses in order to reach a plateau signal:noise ratio, suggesting that smaller nucleic acids are capable of diffusing into the gel matrix and are thus more challenging to remove after hybridization. Conversely, hybridization with the longer probe (27-nt, b) yields a plateau signal:noise ratio soon after the first 30 min of rinsing, consistent with slower and/or less effective probe diffusion into the gel. To ensure sufficient time for complete removal of any sized of unbound DNA probe, 1 hour was selected as the total washing time to be used throughout the comparative assay experiments.

2.6.11. Hybridization efficiency in hydrogel arrays as a function of RCA product density

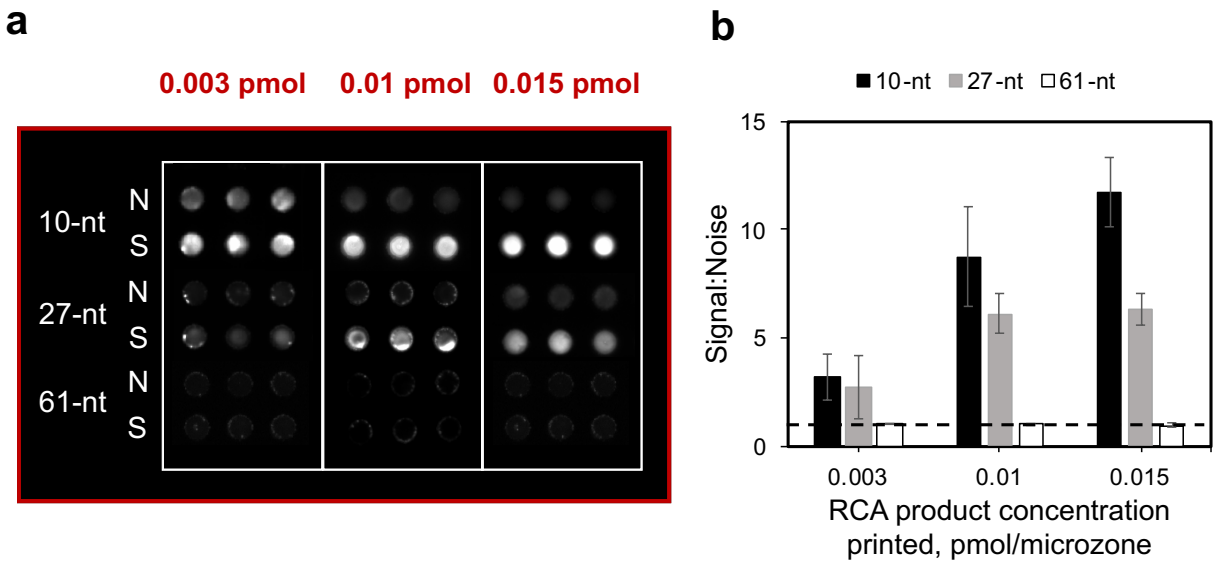

Figure S2.9 Hydrogel arrays with higher RCA product densities demonstrate better hybridization efficiency. The signal:noise ratio for three different DNA-probes (10-nt, 27-nt and 61-nt) was compared between hydrogel microarrays prepared with RCA product concentrations of 0.003, 0.01, or 0.015 pmol/microzone. (a) Qualitative and (b) quantitative signal:noise ratios associated with the hybridization between complementary (S) and non-complementary (N) AlexaFluor 647-labeled DNA probes of different lengths in DIW. The hydrogel-printed microarray prepared with 0.015 pmol RCA product/microzone gives a 3-fold higher signal:noise ratio for 10-nt and a 2-fold higher signal:noise ratio for 27-nt relative to the hydrogel-printed microarray containing 0.003 pmol RCA product/microzone; no signal was observed with the 61-nt probe given that it does not diffuse into the hydrogel coating to access the complementary RCA product.

Of note, the signal:noise ratio for 27-nt is ~2-fold lower to that of 10-nt at 0.015 pmol RCA product/microzone, consistent with the size-selective nature of hybridization profile of the printed hydrogel platform.

2.6.12. Hydrogel based microarrays sensing performance for short DNA-targets reported in previous publications

Table S2.3 Comparison of the sensing performance for the smallest reported oligonucleotide probe in previous publications involving hydrogel-based DNA microarrays.

Microarray composition	**Detection Limit (DNA length, minimum nt)**	**Reference**
1. UV-initiated polymerization of dextran methacrylate incorporating the sensing DNA via a **thiol-acrylate** reaction on polycarbonate and alkene-functionalized **glass slides**	0.1 nM (21-nt)	[3]
2. UV-initiated polymerization of acrylate phosphorylcholine incorporating the sensing DNA via a **thiol-acrylate** reaction on **blue-ray discs**	6 nM (21-nt)	[4]
3. Light-initiated polymerization of bis-acryl-amidopropyl-polyethylene glycol covalently linking amino- or thiol-modified DNA on **glass slides**	0.39 nM (24-nt)	[5]
4. Thermally-initiated polymerization of N,N methylene-bis-acrylamide **cross-linked** 6-acryloyl-b-O-methyl-galactopyranoside-co-aminopropyl-methacrylamide incorporating the sensing DNA by covalent linkage with **bis-sulfosuccinimidyl-suberate** on **aldehyde-functionalized glass slides**	0.19 µM (20-nt, 50-nt, 70-nt)	[6]
5. UV-initiated polymerization of dimethylacrylamide-co-vinylphosphonic acid-co- 4-methacryloyloxy-benzophenone covalently binding amine-terminated sensing DNA on a **shrinking polystyrene** surface	1 nM (20-nt)	[7]
6. Thermally-initiated polymerization of dimethylacrylamide-trimethoxysilyl)-propyl methacrylate-acryloyloxy-succinimide covalently binding amine-terminated sensing DNA on a **silicon oxide** surface	1 µM (23-nt)	[8]
7. Surface-initiated atom transfer radical polymerized poly(2-hydroxyethyl methacrylate) brush matrix post-oxidized to introduce aldehyde groups covalently binding amine-terminated sensing DNA on **silicon or quartz** substrates	1 µM (16-nt)	[9]
8. *In situ* **hydrazone cross-linked** poly(oligoethylene glycol) methacrylate based hydrogel array physically encapsulating **long chain DNA** sensing material on **nitrocellulose** substrate	1 µM (10-nt)	Present work

2.6.13. Supporting References

(1) Smeets, N. M. B.; Bakaic, E.; Patenaude, M.; Hoare, T. Injectable and Tunable Poly(Ethylene Glycol) Analogue Hydrogels Based on Poly(Oligoethylene Glycol Methacrylate). *Chem. Commun.* **2014**, *50* (25), 3306.

(2) Bakaic, E.; Smeets, N. M. B.; Dorrington, H.; Hoare, T. "Off-the-Shelf" Thermoresponsive Hydrogel Design: Tuning Hydrogel Properties by Mixing Precursor Polymers with Different Lower-Critical Solution Temperatures. *RSC Adv.* **2015**, *5* (42), 33364–33376.

(3) Díaz-Betancor, Z.; Bañuls, M.-J.; Maquieira, Á. Photoclick Chemistry to Create Dextran-Based Nucleic Acid Microarrays. *Anal Bioanal Chem* **2019**, *411* (25), 6745–6754.

(4) Díaz-Betancor, Z.; Bañuls, M.-J.; Sanza, F. J.; Casquel, R.; Laguna, M. F.; Holgado, M.; Puchades, R.; Maquieira, Á. Phosphorylcholine-Based Hydrogel for Immobilization of Biomolecules. Application to Fluorometric Microarrays for Use in Hybridization Assays and Immunoassays, and Nanophotonic Biosensing. *Microchim Acta* **2019**, *186* (8), 570.

(5) Beyer, A.; Pollok, S.; Berg, A.; Weber, K.; Popp, J. Easy Daylight Fabricated Hydrogel Array for Colorimetric DNA Analysis: Daylight Fabricated Hydrogel Array. *Macromol. Biosci.* **2014**, *14* (6), 889–898.

(6) Soto, C. M.; Patterson, C. H.; Charles, P. T.; Martin, B. D.; Spector, M. S. Immobilization and Hybridization of DNA in a Sugar Polyacrylate Hydrogel. *Biotechnol. Bioeng.* **2005**, *92* (7), 934–942.

(7) Le Goff, G. C.; Blum, L. J.; Marquette, C. A. Shrinking Hydrogel-DNA Spots Generates 3D Microdots Arrays: Shrinking Hydrogel-DNA Spots Generates 3D Microdots Arrays. *Macromol. Biosci.* **2013**, *13* (2), 227–233.

(8) Yalçın, A.; Damin, F.; Özkumur, E.; di Carlo, G.; Goldberg, B. B.; Chiari, M.; Ünlü, M. S. Direct Observation of Conformation of a Polymeric Coating with Implications in Microarray Applications. *Anal. Chem.* **2009**, *81* (2), 625–630.

(9) Bilgic, T.; Klok, H.-A. Oligonucleotide Immobilization and Hybridization on Aldehyde-Functionalized Poly(2-Hydroxyethyl Methacrylate) Brushes. *Biomacromolecules* **2015**, *16* (11), 3657–3665.

3. Chapter 3

An Aptamer-based Hydrogel Sensing Platform Enabling Low Micromolar Detection of Small Molecules Using Low Sample Volumes

Preface

This chapter and its supporting information-appendix are reproduced from the publication describing the integration and thermodynamic stabilization of FRET-based structure switching aptamer constructs of varying quencher stem lengths within hydrazone cross-linked hydrogels for improved sensing of small molecules. Encapsulated adenosine aptamer reporters were investigated on their stability against varying denaturing agents in addition to their sensing performance towards a cognate ligand. In particular, the ability of hydrogel to suppress the fluorescent background in more-responsive aptamer reporters assembled with short quencher stems, was investigated with the aim to lower the detection limit while maintaining solution-like ligand-induced kinetic response.

Milana Pikula,[1,2] Yingfu Li,[3] Carlos D. M. Filipe,[1,*] and Todd Hoare[1,*]

[1]Department of Chemical Engineering, McMaster University, Hamilton, ON L8S 4K1, Canada;

[2]Biointerfaces Institute, McMaster University, Hamilton, ON L8S 4L8, Canada;

[3]Department of Biochemistry and Biomedical Sciences, McMaster University, Hamilton, ON, L8S 4K1, Canada.

In *ACS Applied Materials and Interfaces* (2024): 10.1021/acsami.3c19203

Abstract

Poor fluorescence recovery at low analyte dosages and slow ligand binding kinetics are critical challenges currently limiting the use of aptamer-functionalized hydrogels for sensing small molecules. In this paper, we report an adenosine-responsive hydrogel sensor that integrates FRET-signaling aptamer switches into in situ-gelling thin-film hydrogels. The hydrogel sensor is able to entrap a high proportion of the sensing probes (>70% following vigorous washing), delay nucleolytic degradation, stabilize weak aptamer complexes to improve hybridization affinity and suppress fluorescence background, and provide high sensitivity in biological fluids (i.e., undiluted human serum). Furthermore, the developed hydrogel sensors were able to achieve low limits of detection (5.3 μM in buffer and 8.8 μM in serum) within 4 minutes of exposure to the sample, with signal generation requiring only 20 μL/well of analyte sample. The physical nature of the aptamer encapsulation allows this approach to accommodate virtually any small-molecule aptamer, avoiding the need for covalent anchoring and the complex modification of nucleic acid sequences typically required for effective aptamer-based molecular recognition.

3.1. Introduction

Aptamer-functionalized hydrogels represent an emerging class of biomaterials for small-molecule detection in biomedical and food-safety diagnostics[1–5] as they can facilitate the design of sensors with high immobilization ability,[6] good analyte enrichment capacity,[7] improved nucleolytic protection,[8] and lower background signals.[6,9] In particular, hydrogels that feature embedded structure-switching aptamers[10] offer numerous benefits over self-assembled pure DNA gels[11] and aptamer cross-linked/polymer hybrids,[12] including enabling the label-free detection of various analytes, the ability to achieve sensing capacity using up to 1000x less DNA,[9] and the lack of a need for expensive signaling agents,[13–15] or DNA modifications[16,17] for covalent anchoring of aptamer molecules. Structure-switching aptamer reporters are created by disrupting the binding domain in fluorophore-labelled aptamers (FA) via the introduction of a quencher-labelled oligonucleotide (Q), causing the aptamer to unfold and position the fluorophore and quencher molecules in close proximity to one another in the absence of a target.[18,19] Target binding triggers aptamer refolding and conformational transition from a DNA-duplex to a DNA-target complex through intramolecular (aptamer beacons) or intermolecular (duplexed aptamers) Q-DNA strand displacement, thus increasing the distance between the fluorophore and quencher and generating a fluorescence resonance energy transfer (FRET) read-out signal of a magnitude correlated to the target concentration.[18,20]

Multiple examples of physically encapsulated structure-switching aptamers have been reported, with the use of polyacrylamide (PAAm) nanoparticles[8] or arrayed sol-gel films[21,22] being most common. The embedded reporters are typically based on a well-studied adenosine triphosphate (ATP) aptamer[23] that undergoes FRET rearrangements upon exposure to a ligand. Although encapsulated aptamer reporters retain their signaling ability and provide higher resistance to nucleolytic attack, they face challenges in terms of their high limits of detection (LOD), slow binding kinetics, and poor fluorescence recovery (*i.e.* low signal-to-background (S:B) ratio). For example, PAAm-embedded aptamer beacons facilitated only a maximum 2.5-fold S:B ratio, resulting in an LOD of only 50 μM; such performance is a result of the lower hybridization energy designed into the intramolecular switching probes to enable rapid adenosine-induced activation at the cost of increased background fluorescence.[24] Regulating the aptamer beacons' thermodynamic stability and affinity towards a cognate ligand to address this challenge requires complex manipulations around the intramolecular linkers, the DNA stem length, and/or the placement of the aptamer sequence within the stem-loop architecture,[25,26] introducing a significant challenge for the practical adaption and sensing versatility of this technology.

Conversely, duplexed aptamers based on an intermolecular switching mechanism are more adaptable to different sensing formats.[20] Duplexed aptamers are comprised of a separate Q-DNA strand hybridized to an extended aptamer strand labelled by a covalently-bound fluorophore (bipartite) or via hybridization with fluorophore-labelled DNA (tripartite), with the latter exhibiting higher signaling ability due to the greater restriction of the motion of the fluorophore segment that enables more effective FRET.[18,27] Relative to the intramolecular aptamer beacon design, the hybridization dynamics of intermolecularly switchable duplexed aptamers are readily tunable based on the nucleic acid hybridization thermodynamics *via* adjusting the Q-DNA length/content/mismatch frequency (typically involving 9- and 15-bp-long quencher stems) and/or the salt content in the buffer.[20,28,29] As one example, a 12-nt-long Q-DNA tripartite reporter was embedded in an optimized sol-gel composition based on sodium silicate, enabling up to a 20-fold enhancement in fluorescence at saturating adenosine dosages and an LOD of 28 μM.[21] However, sample volumes in the hundreds of microliters are required to sufficiently hydrate the sol-gel, aptamer reporters encapsulation efficiencies were relatively low (<50%), and any signal enhancement was accompanied by a tradeoff in kinetic response of the sensor, necessitating at least 1 h to complete the detection. The slower binding kinetics were attributed to the high-level thermal stabilization of the quencher stem within the sol-gel matrix (with the melting temperature (T_m) observed

to increase by up to 8°C relative to the solution-based reporter) and the long diffusional path between the sensing probe and the target resulting from the high sample volumes required. Such problems are even more acute in hydrogel monoliths designed with larger dimensions, introducing more diffusional limitations to signal generation and thus requiring hours of incubation and/or mL-scale volumes of analyte to enable effective sensing.[30,31] Varying the length of the Q-DNA competitors improves their diffusibility within the hydrogel and enhances ligand-induced dehybridization to accelerate binding kinetics and improve signal resolution but (as with molecular beacons) at a cost of introducing higher levels of background due to less efficient hybridization; 10-bp stems in particular were noted to leave a substantial amount of dissociated Q-DNA in the absence of a target.[27] Thus, there is a critical need to improve the design of aptamer hydrogel-based sensors to enable efficient immobilization of small-molecule aptamers coupled with fast and specific detection at low analyte dosages.

To address the above-discussed challenges, it is necessary to engineer hydrogels with (1) minimal bulk dimensions to enable fast diffusion of the target to the aptamer probes, (2) optimized internal porosity that enables good analyte distribution while also preventing the leaching of the sensing probes[6,7], (3) optimized thermodynamic equilibrium with the embedded aptamer reporters to reduce nonspecific Q-DNA dissociation and thus enable more sensitive read-out with minimal background while avoiding excessive stabilization that makes aptamer-ligand complexation less favourable[10], and (4) mild synthetic conditions to protect more ligand-responsive aptamer reporters that are susceptible to denaturation due to various environmental triggers such as reduced metal ion content,[22] temperature variations,[19] the generation of alcohol byproducts and hydrophobic moieties,[21,27,32] and multi-step processing steps such as washing, hydration, or gel aging.[32]

In this work, we propose the integration of a tripartite structure-switching adenosine aptamer within *in situ* cross-linkable poly (oligoethylene glycol methacrylate) (POEGMA) hydrogels. We have previously reported the benefits of hydrazone-crosslinked POEGMA hydrogels formed by mixing hydrazide- and aldehyde-functionalized POEGMA precursor polymers in terms of their ability to encapsulate DNA and proteins without inducing denaturation,[33,34] exploiting the room temperature and bio-inert nature of hydrazone chemistry; POEGMA-based hydrogels have also been demonstrated to facilitate improved hybridization efficiency for shorter DNA strands.[34] Building on these findings, herein we hypothesize that thin film POEGMA hydrogels could not only facilitate effective immobilization of aptamers but also further reinforce aptamer duplexes to allow the use of shorter quencher strands in the aptamer reporter assembly. Such a property would leave more of the aptamer sequence free for ligand binding and thus facilitate higher sensitivity with a lower trade-off in background signal, all while exhibiting solution-like kinetics facilitated by the tunably swollen polymeric network. The simple mixing-based gelation mechanism also offers potential to fabricate hydrogel microarrays using scalable fabrication strategies (*i.e.*, sequential pipetting or printing low volumes of the polymer precursor solutions) that minimize the required volume of the hydrogel phase, thus minimizing the mass transport limitations associated with sensing while allowing the use of a lower volume of analyte. By physically encapsulating adenosine aptamer constructs with varying Q-DNA sizes (12- to 9-nt) into in-situ-gelling POEGMA hydrogels with varying hydrophilicities and crosslink densities, we demonstrate high retention of the sensing reporter (up to 73% retention following extensive washing), significantly delayed DNase degradation, reduced fluorescence background, and thermal stabilization of short Q-DNA duplexes by 2 to 5 °C relative to the same system in solution. The proposed approach is then applied to fabricate a hydrogel-based aptasensor capable of sensitive and fast signaling in both pure reaction buffer and undiluted serum, with limits of detection ranging from 5.3–8.8 μM (depending on the reaction media) achieved within minutes of target injection.

3.2. Experimental Section

3.2.1. Materials.

All DNA oligonucleotides were purchased from Integrated DNA Technologies. Acrylic acid (AA, Sigma-Aldrich, 99%), 2,2-azobisisobutryic acid dimethyl ester (AIBMe, Wako Chemicals, 98.5%), N′-ethyl-N-(3-dimethylaminopropyl)-carbodiimide (EDC, Carbosynth, Compton CA, commercial grade), thioglycolic acid (TGA, Sigma-Aldrich, 98%), adipic acid dihydrazide (ADH, Alfa Aesar, 98%), and human serum (normal, Sigma-Aldrich) were used as received, while N-(2,2-dimethoxyethyl) methacrylamide (DMEMAm) was synthesized in-house according to a previously reported method.[35,36] Diethylene glycol methyl ether methacrylate ($M(EO)_2MA$, Sigma-Aldrich, 98%) and oligo(ethylene glycol) methyl ether methacrylate ($OEGMA_{500}$, M_n = 500 g/mol, Sigma-Aldrich, 95%) were purified using a column of basic aluminum oxide (Sigma-Aldrich, type CG-20) to remove the inhibitors prior to use. Deoxyribonuclease I (DNase I, 2000 U/mL) was purchased from NEB, and the adenosine 5'-triphosphate (ATP), cytidine 5'-triphosphate (CTP), guanosine 5'-triphosphate (GTP), and uridine 5'-triphosphate (UTP) solutions (100 mM) were all purchased from Fisher Scientific. HEPES buffer (1 M, sterile solution), sodium chloride (NaCl, >99%) magnesium chloride ($MgCl_2$, >99%), Tris-HCl (99.5%), and sodium hydroxide (NaOH, >98%) were purchased from Bioshop Canada Inc. Milli-Q-grade distilled deionized water (DIW) was used for all experiments. Treated clear-bottom black 96-well plates were purchased from Corning (Polystyrene, Cat. No. #CLS3603), while the PCR tubes used for the FRET melting assay (0.2 mL 8-tube strips, Cat. No. #TLS0851EDU) were purchased from BioRad.

The 1xGelation buffer was prepared by co-dissolving 20 mM HEPES, 5 mM $MgCl_2$, and 300 mM NaCl at pH=7.5, with the resultant buffer being stored at 4°C until use. The 1xAssay buffer was prepared by co-dissolving 20 mM Tris-HCl, 5 mM $MgCl_2$, and 300 mM NaCl adjusted to pH=7.5 using 0.1 M NaOH followed by storage at 4°C until use.

3.2.2. POEGMA Polymer Synthesis and Characterization and Hydrogel Fabrication.

Hydrazide-functionalized (POH) and aldehyde-functionalized (POA) hydrogel precursors containing varying contents of $OEGMA_{500}$ were synthesized and characterized according to methods detailed elsewhere[34–36] (see Supporting Table S3.1 for full details). Two aldehyde-functionalized polymers ($PO_{10}A_{15}$ and $PO_{50}A_{15}$) were synthesized, with the PO subscript representing the mole fraction of $OEGMA_{500}$ relative to $M(EO)_2MA$ used to prepare the polymer and the A subscript representing the target mole fraction of the aldehyde-containing monomer in the polymer. Two hydrazide-functionalized polymers ($PO_{10}H_{30}$ and $PO_{100}H_{30}$) were also synthesized, with the PO subscript representing the mole fraction of $OEGMA_{500}$ relative to $M(EO)_2MA$ used to prepare the polymer and the H subscript representing the target mole fraction of hydrazide-functionalized monomer residues. Measured degrees of functionalization were 20-23 mol% of total monomer residues for the hydrazide-functionalized polymers and 9-11 mol% of total monomer residues for the aldehyde-functionalized polymers, with molecular weights for all synthesized polymers lying in the 13-20 kDa range (Table S3.2, Figures S3.1 and S3.2). The resultant polymers were subsequently mixed in different combinations to form the hydrogels summarized in Table 3.1. Polymers for hydrogel preparation were dissolved at a concentration of 20 wt% in the 1xGelation Buffer (20 mM HEPES, 5 mM $MgCl_2$, 300 mM NaCl, pH=7.5) and stored at 4°C until use.

Table 3. 1 Compositions of hydrogels used for sensor preparation.

Hydrogel	Aldehyde Polymer		Hydrazide Polymer	
	Polymer Code	Concentration (wt%)	Polymer Code	Concentration (wt%)
HG_{10}	$PO_{10}A_{15}$	6	$PO_{10}H_{30}$	6
HG_{100}	$PO_{50}A_{15}$		$PO_{100}H_{30}$	

3.2.3. Design of FRET Reporter Oligonucleotides.

Adenosine tripartite aptamer reporters (AFQ) were formed using three oligonucleotide sequences: (1) an aptamer sequence (A); (2) fluorescent DNA tagged by AlexaFluor 647 ($AlexaF_{647}$) at the 5'end (F); and (3) a quencher DNA tagged by Black Hole Quencher 3 (BHQ3) (Q) (See Figure 3.1). Following previous reports,[18,37] the aptamer was designed as a 63-nt sequence composed of a 27-nt ATP-aptamer binding motif[23] (bold blue) extended at the 5'-end with 5 non-essential oligonucleotides (italic black) and the F-DNA binding primer region (bold black). The 16-nt-long F-DNA binding motif was placed close to the Q-DNA complementary region within the aptamer sequence. Q-DNA sequences were designed to hybridize to 12 bases (Q_{12}), 11 bases (Q_{11}), 10 bases (Q_{10}), or 9 bases (Q_9) at the 5'-end of aptamer, beginning with five non-essential oligonucleotides outside the consensus aptamer sequence, by directly denaturing (Q_{12}, Q_{11}, Q_{10}) or interfacing (Q_9) target binding site II (bold blue underlined) within a cooperative two binding site pocket.[23]

3.2.4. Preparation of Solution-based Tripartite Aptamer Reporter (S:AFQ) and Solution FRET Assay.

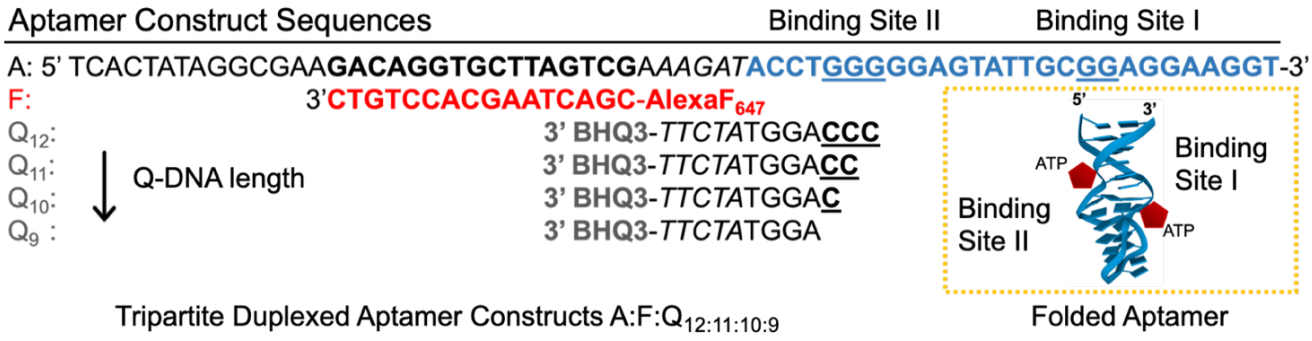

Figure 3.1 Compositions of adenosine tripartite aptamer reporter (AFQ). The AFQ complex was assembled by hybridizing aptamer sequence (A) with complementary fluorophore- (F) and quencher- (Q) labeled oligonucleotides, thus enabling FRET. Q-DNAs were employed with lengths of 12-, 11-, 10-, and 9-nt and are denoted as Q12, Q11, Q10 and Q9, respectively.

All purchased DNA sequences were reconstituted to a concentration of 100 µM in DIW and stored at -20°C. The concentration of the DNA stock solution was confirmed by measuring the absorbance at 260 nm using UV-vis spectrophotometry (Tecan, NanoQuant Infinite 200 Pro Microplate Reader). The tripartite assembly was prepared by mixing A:F:Q (Q_9, Q_{10}, Q_{11}, Q_{12}) at a molar ratio of 2:1:6 by mixing of 400 nM (A), 200 nM (F), and 1200 nM (Q) (each initially dissolved from a 10 µM master stock in DIW) followed by dilution with 2xAssay buffer at a ratio of 1:1 v/v. The mixture was then heated for 5 min at 90°C followed by cooling at 25°C for 1.5 h to allow the DNA strands to reanneal and reach

equilibrium prior fluorescence measurements. The prepared aptamer constructs were distributed as 50 µL samples in clear-bottom 96-well plates using a multi-channel pipette (8-channel mLINE Biohit, Sartorius). Fluorescence measurements were obtained with a Tecan M1000 microplate reader (Infinite Pro) operating in bottom fluorescence mode using 640/672 nm excitation/emission wavelengths (5 nm bandwidth) at an optimal gain maintained at 25°C. The emission intensities of solution (S)-based reporter (S:AFQ) and fluorescent aptamer constructs without the quencher strand (S:FA) were collected and corrected by subtracting the fluorescence intensity associated with undoped buffer samples (blank). The FRET efficiency (*i.e.,* fluorescence quenching) was calculated as the ratio between the normalized fluorescence intensity of the S:AFQ relative to S:FA, defined as: I_{AFQ}/I_{FA}. All data were reported as the average of at least n=3 replicates ± SD (standard deviation).

3.2.5. Preparation of Hydrogel-based Tripartite Aptamer Reporter (HG:AFQ) and Solid-Phase FRET Assay.

Aptamer reporters with varying Q-DNA stem lengths (Q_9, Q_{10}, Q_{11}, and Q_{12}) were physically entrapped in POEGMA hydrogels (HG_{10} or HG_{100}) to fabricate aptamer-functionalized hydrogels labeled as HG_x:AFQ_y, where x is the mole fraction of $OEGMA_{500}$ used to prepare the hydrogel precursor polymers and y is the quencher sequence stem length. The hydrogel samples were prepared as 50 µL monoliths in a 96-well plate by sequentially pipetting 25 µL of a 6 wt% POA solution in 1xGelation buffer and 25 µL of a 6 wt% POH solution co-dissolved with a 2x concentration of AFQ (POH:2xAFQ) in 1xGelation buffer. To make POH:2xAFQ, a 4xAFQ (400 nM F) mixture was dissolved in 1xGelation buffer, heated for 5 min at 90°C, cooled to 25°C over the following 30 min, and then mixed with a 12 wt% POH solution in 1xGelation Buffer at a ratio of 1:1 v/v. The resulting 6 wt% POH:2xAFQ construct was then allowed to incubate and equilibrate at room temperature for 60–90 min prior to hydrogel preparation. During the layer-by-layer dispensation of the hydrogel components, the samples were left to cross-link overnight at ambient temperature to ensure the full gelation of each hydrogel composition (gelation times = 10 min for HG_{10}:AFQ, and 19h for HG_{100}:AFQ). Fluorescence intensities were measured as described above using the Tecan M1000 microplate reader, with the FRET efficiency calculated as the ratio between the normalized fluorescence intensity of the HG:AFQ and the hydrogel-based fluorescent aptamer construct without the quencher strand (HG:FA), $I_{HG:AFQ}/I_{HG:FA}$. All data were reported as the average of at least n=3 replicates ± SD.

3.2.6. Hydrogel Encapsulation Efficiency.

Hydrogel-based fluorescent aptamer construct without the quencher strand (HG:FA, mixed in the ratio of 100 nM F: 200nM A) were prepared as described in Section 3.2.4. The resulting HG:FA samples were incubated with 50 µL/well of 1xAssay buffer (20 mM Tris-HCl, 300 mM NaCl, 5 mM MgCl2, pH=7.5) and then subjected to several washing cycles, with supernatant removal during each step, as follows: an initial 1-hour wash step, followed by 2 x 5 min rinses, and then a final 1-hour wash step under orbital shaking of 1 mm amplitude for 2 s between each measurement. The fluorescence emission was measured before and after each washing/rinsing step using the Tecan M1000 plate reader (bottom reading, 640/672 nm excitation/emission wavelengths, 25°C), with the resulting data being normalized based on the hydrogel/buffer autofluorescence values collected for samples prepared without FA (blanks). The aptamer content retained by the hydrogel was quantified by comparing the normalized fluorescence intensity of the hydrogel before and after each wash/rinse step. All data were reported as the average of at least n=3 replicates ± SD.

3.2.7. DNase I Degradation Assay.

Nucleolytic degradation assay was performed using tripartite aptamer reporters dissolved in solution (S:AFQ) and encapsulated in a hydrogel (HG_x:AFQ), with the latter condition tested following the 1 h washing/rinsing cycle described in Section 3.2.6. Deoxyribonuclease DNase I was added to each sample at a concentration of 20 U/well, and the fluorescence signal indicative of construct disassembly resulting from aptamer degradation and F-DNA release was measured every minute using the Tecan M1000 plate reader (bottom reading, 640/672 nm excitation/emission wavelengths, 25°C). The obtained values were then corrected against the solution-only or hydrogel-only fluorescence intensities and compared to the fluorescence intensity of S:FA or HG:FA at the same overall volumetric concentration prior DNase I digestion (corresponding to 100% DNA degradation).

3.2.8. Adenosine Binding Assay.

Adenosine triphosphate (ATP) binding assays were carried out using tripartite aptamer reporters dissolved in free solution (S:AFQ) and encapsulated in a hydrogel (HG_x:AFQ_y, where x = 10 or 100 and y = 9, 10, 11, or 12). To assess the target binding kinetics, 5 mM of ATP solution was added to the solution-based or hydrogel-encapsulated aptamer reporters, with the resultant samples mixed via orbital shaking of 1 mm amplitude for 2 s between each measurement over 1 hour at 25°C. Prior to adding the ATP, the baseline fluorescence was determined by employing a Tecan M1000 plate reader (bottom read, 640/672 nm excitation/emission wavelength, 5 nm bandpass) to acquire fluorescence measurements from samples incubated with 7 µL of 1xAssay buffer every 60 s for 10 min. After obtaining the baseline fluorescence, 3 µL of concentrated ATP solution was injected to achieve a final concentration of 5 mM ATP/well, with the fluorescence emission then measured every minute for an additional 50 min to track the release of the quencher sequence. The measured fluorescence values were corrected for undoped hydrogel/buffer autofluorescence. The ligand binding kinetics and ligand-induced aptamer activation were reported as the time-dependent fluorescence increase normalized against the fluorescence intensity of the FA constructs ($I_{AFQ + 5mM\ ATP}$ /$I_{FA+ Buffer}$), in free solution or encapsulated. The signal:background ratio (S:B) was estimated as the ratio between target-induced fluorescent intensity enhancement (Signal: $I_{AFQ + 5mM\ ATP}$) and the fluorescence intensity of the aptamer reporters incubated with 1xAssay buffer (Background: $I_{AFQ + Buffer}$) over a 60 min reaction time. The FRET efficiency (I_{AFQ}/I_{FA}) and FRET efficiency change ($I_{AFQ + Buffer}/I_{FA + Buffer}$) were quantified at the beginning (t = 0 min) and at the end (t = 60 min) of the target binding assay.

3.2.9. Adenosine Binding Affinity.

Aptamer reporters were dissolved in free solution (S:AFQ_y) or encapsulated in hydrogel (HG_x:AFQ_y, where x = 10 or 100 and y = 9, 10, 11, or 12) and incubated with serial dilutions of ATP at a volume of 20 µL/well volume for 1 h at 25°C over a concentration range of 0-10 mM in either 1xAssay buffer (for y = 9, 10, 11, or 12) or undiluted serum (for y = 10 and 12). Fluorescence emission values from the AFQ samples treated with ATP (signal, S) or buffer (background, B) were collected, corrected for undoped hydrogel/buffer autofluorescence (blanks), and presented as an S:B ratio. To account for spot-to-spot and batch-to-batch FRET variations, the fluorescence values for each ATP concentration (Signal, n=3 replicates) were normalized against the mean fluorescence from the 0 mM ATP background array (background, n=12 replicates). A four-parameter logistic regression (GraphPad Prism v9) was applied to fit the binding affinity data between the bottom plateau (minimal curve asymptote) and the top plateau

(maximum dose response curve asymptote) using the binding affinity dissociation constant (K_d) and the Hill slope (h, indicating the cooperativity of binding sites).

3.2.10. FRET Melting Assay and Thermodynamic Evaluation.

Aptamer reporters were dissolved in free solution (S:AFQ_y) or encapsulated in hydrogel (HG_x:AFQ_y, where x = 10 or 100 and y = 9, 10, 11, or 12) in a total volume of 50 µL. Thermal denaturation assays were performed in a PCR machine (BioRad, RT96), and fluorescence emissions related to Q-DNA dehybridization were acquired in the red channel (Cy5; 651 nm/670 nm excitation/emission) as a function of temperature using CFX Maestro 1.1 software. The PCR machine was programmed to hold each sample at 20°C for 2 min followed by heating to 80°C in 2°C increments, with equilibration performed at each increment for 2 min prior to measuring the fluorescence. The melting curves were constructed by plotting the measured fluorescence enhancement as a function of temperature. To determine the melting temperatures (T_m) of Q-DNAs and estimate the thermodynamic hybridization parameters, the melting curve values were corrected for the autofluorescence of undoped hydrogel/solution samples and normalized against the fluorescent signal from the same concentration of FA complex in hydrogel/solution (maximum fluorescence intensity) to account for the temperature-dependent decrease in the fluorescence of AlexaFlour647 fluorophores. The T_m values were extracted via 4-parameter Boltzmann (AFQ_{10}, AFQ_{11}, and AFQ_{12}) and asymmetrical 5-parameter sigmoidal fitting[38–40] (AFQ_9) of the melting curves using GraphPad Prism v9, with Tm corresponding to the midpoint of the normalized maximum fluorescence enhancement (i.e., the temperature point at which the complex is 50% dissociated) (n=3 replicates). The hybridization affinity of the Q-DNAs to the FA construct was evaluated based on the thermodynamic parameters from the FRET melting experiments using van't Hoff's analytical method.[41] The AFQ reporters were prepared in serial dilutions to form solutions with total strand contents (Ct) ranging from 315 nM to 3600 nM in 1xGelation buffer at 25°C. Dilutions with Ct values between 585 nM to 1350 nM were chosen for linear fitting of the van't Hoff plot. The reciprocal of the melting temperature values $1/T_m$ (K^{-1}) was then plotted against ln(Ct/4), and the van't Hoff equation was used to estimate the enthalpy change, ΔH (kJ/mol), and the entropy change, ΔS (J/mol K), as shown in Equation 1 (n=3 replicates):

$$T_m^{-1} = \frac{R}{\Delta H} \ln\frac{Ct}{4} + \frac{\Delta S}{\Delta H} \quad (1)$$

where R is the gas constant (8.3145 J/mol K). The Gibbs free energy change, ΔG (kJ/mol), associated with the DNA hybridization was then calculated using Equation 2:

$$\Delta G = \Delta H - T\Delta S \quad (2)$$

3.2.11. Predicted Melting Temperatures and Thermodynamic parameters.

The DNAmelt application, "Hybridization of Two Different Strands of DNA or RNA," powered by the UNAFold software package (http://www.unafold.org), was utilized to predict the melting temperatures for each Q-DNA stem (9, 10, 11, or 12 base nucleotides) used to fabricate the AFQ reporters.[42]

The following parameters were used for the Tm prediction: temperature range: 20–80°C in 2°C increments; nucleic acid (NA) type: DNA; initial concentration of hybridizing strands: modified aptamer [A_0]=0.2 µM and quencher DNA [B_0]= 0.6 µM; salts: [Na+]=300 mM, [Mg2+]=5 mM. The predicted T_m, "T_m (Conc)," corresponds to the temperature at which the concentration of A:Q duplexed strands is at half of its maximum value. The thermodynamic parameters (*i.e.* Gibbs free energy, enthalpy, and entropy change) were predicted utilizing the UNAFold "Two-state melting (hybridization)" application, assuming the same conditions at 25°C and a 0.8 µM total strand concentration. The obtained values were

confirmed using Integrated DNA Technology Server:Oligo Analyzer application (https://www.idtdna.com/calc/analyzer).

3.3. Results and Discussion

3.3.1. Preparation of Aptamer Reporter-Functionalized POEGMA Hydrogel.

The hydrogel-encapsulated aptamer sensors were prepared via the layer-by-layer deposition of aldehyde (POA)- and hydrazide (POH)-functionalized POEGMA (PO) precursors (Figures S3.1, S3.2 and S3.3; Tables S3.1 and S3.2) mixed with the DNA aptamer reporter (Figures 3.1 and 3.2a). The process of hydrazone cross-linking, which proceeds at room temperature without the need for any external gelation aids, allowed for the entrapment of the aptamer complexes within 50 μL hydrogel volumes arrayed in 96-well plates following simple sequential pipetting. A widely reported aptamer for binding adenosine and adenine nucleotides (ATP, ADP, AMP)[23] was used as the biosensing model in this study. The tripartite aptamer reporter (AFQ) sensing ATP, was assembled as a FRET-based duplexed construct and consisted of a fluorescent and quenching stem brought into apposition with one another via hybridization between the 5'-extended aptamer sequence (A), the fluorescent-DNA (F), and the quencher DNA (Q) strands[18,19,21], as illustrated in Figure 3.1. Target molecule binding transforms the aptamer duplex into the aptamer:target complex via the structure-switching mechanism, with the separation of the $AlexaF_{647}$ fluorophore from the BHQ3 quencher resulting in increased fluorescence (Figure 3.2a, inset).

Prior to being encapsulated in the hydrogel, the molar ratio of the DNA strand within the aptamer reporter assembly in solution was optimized using a 12-nt long Q-DNA ($S:AFQ_{12}$), as shown in Figure S3.4. When using 100 nM of F-DNA strand (previously reported to be the optimal signaling concentration[21]) it was necessary to utilize A-DNA and Q-DNA concentrations that were at least 2x and 3x higher, respectively, in order to achieve effective FRET efficiency (*i.e.*, fluorescence quenching, defined as fluorescence intensity (I) ratio between the tripartite aptamer reporter and the fluorescent aptamer construct without the quencher strand; I_{AFQ}/I_{FA}). In 1xAssay buffer, the FRET efficiency was assessed to be 0.017±0.004, corresponding to 98.3% fluorescence quenched (Figure S3.4a). Exposure to 5 mM of ATP resulted in high fluorescent recovery with rapid kinetics (<2 minutes following ATP addition) and an at least 50-fold S:B ratio (Figure S3.4b,c). Higher molar concentrations of both Q- and A- DNA enabled even greater background fluorescence reduction (>99%) along with significantly improved S:B ratios (≥80-fold; Figure S3.4a,c), allowing DNA complexes to be simply tuned based on their quencher stem content. Of note, the values for FRET efficacy and ligand-induced fluorescence are significantly higher than those reported for equivalent DNA complexes used in earlier sol-gel sensors.[21,27] We attribute this improved performance to the use of different fluorophore-quencher pairs (*i.e.,* $AlexaFluor_{647}$-BlackHole3 versus Fluorescein-DABCYL), with the black hole quencher showing a high propensity to bind to fluorophores and enhance quenching efficiency via contact quenching[43] while still facilitating fast switching between conformations to enable efficient FRET-based signaling ability.[44]

To provide a balance between sensing performance and DNA consumption, we identified the $A:F:Q_{12}$ construct with a 2:1:6 molar ratio as the optimal reporter for use in further assays. This reporter provides 27x and 2x lower background fluorescence, respectively, compared to the 1:1:6 and 2:1:3 reporters previously adapted in sol-gel assemblies[21,37] without any trade-off in signaling ability while also enabling 99% fluorescence quenching, a S:B of up to 70-fold minutes after the addition of 5 mM of ATP, and sufficient duplex stability for the introduction of truncated Q-DNA reporters (Figure S3.4). The optimized $A:F:Q_{12}$ construct was then encapsulated by sequentially pipetting a 6 wt% POA polymer solution in 1xGelation buffer followed by a 6 wt% POH polymer solution also containing the pre-formed aptamer reporter into a well of a 96-well plate and allowing the mixture to gel. The initial study was

performed on a single hydrogel (HG) configuration (HG_{100}; Table 3.1) utilizing PO_{100} polymer precursors. The fluorescence quenching of the hydrogel-embedded reporter (HG:AFQ) was even higher than that of the solution-based construct (S:AFQ), reaching a FRET efficiency of $I_{AFQ}/I_{AF} = 0.006 \pm 0.001$ (Figure 3.2b, table inset). We attribute this result to closer FRET pair positioning within the hydrogel due to confinement of the construct inside hydrogel pores. In addition, none of the reporter elements whether in free solution, in precursor polymer solution, or when encapsulated underwent FRET individually, thus providing a signaling mechanism for specific target recognition. Upon addition of 5 mM of ATP to hydrogel-embedded or polymer co-dissolved aptamer reporters, the fluorescence recovery triggered was almost on par with that of the solution-based reporters (Figure 3.2c-i); the thermal stability of the corresponding Q-DNA duplexes (Figure 3.2c-ii) exhibited only a minimal increase in the melting temperature ($\Delta T_m = 1°C$) , even in more concentrated hydrogels (i.e., 8 wt% or 10 wt%; Figure S3.5). Collectively, these results strongly suggest that the aptamer reporters remain fully hybridized and accessible to externally added ligands once encapsulated in arrayed POEGMA hydrogel films. Correspondingly, the pore size within the HG_{100} network allows for sufficient Q-DNA displacement from the fluorophore and thus large fluorescence onset in the presence of the ligand. As such, rapid detection was still achievable using the hydrogel-encapsulated reporters, with a signal resolution plateau being reached within 6 min of ligand addition compared to 2 minutes in either in free solution or precursor polymer solutions (Figure 3.2c-i). Furthermore, given that the physical entrapment mechanism allows all the DNA present to be exclusively dedicated to molecular recognition rather than forming the hydrogel scaffold, DNA concentrations in the nM scale (as desired for DNA diagnostic systems[9]) can be used for efficient detection; this result is in contrast to stimuli-responsive hydrogel sensors that utilize DNA as a hydrogel component and thus require mM-scale aptamer concentrations and expensive acrydite or amino modification of functional oligonucleotides to facilitate sensor fabrication.[5,11,45]

a.

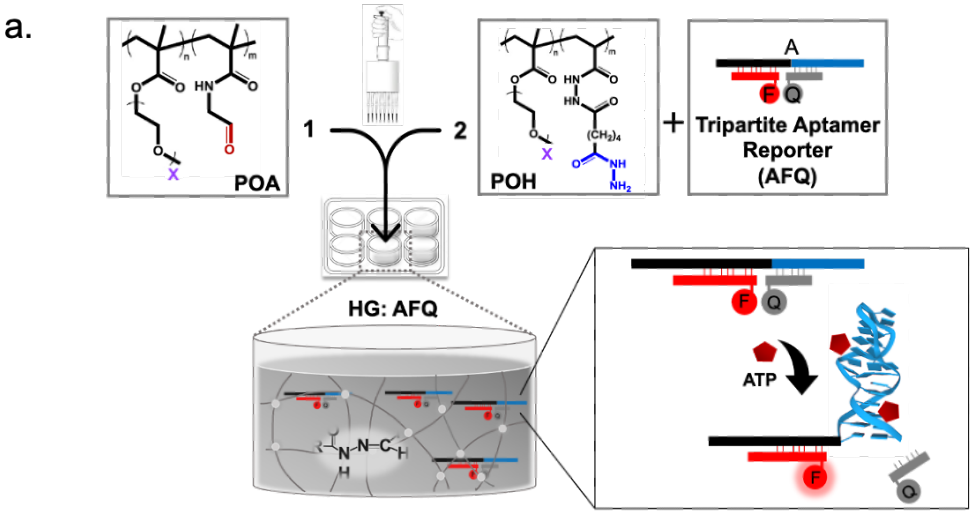

b.

	Solution, S	Polymer 1, POA	Polymer 2, POH	Hydrogel, HG
Sample	Normalized* Fluorescence Intensity	Normalized* Fluorescence Intensity	Normalized* Fluorescence Intensity	Normalized* Fluorescence Intensity
F	0.89 ± 0.06	1.14 ± 0.04	1.38 ± 0.02	1.16 ± 0.04
FQ	0.97 ± 0.08	0.92 ± 0.01	1.22 ± 0.05	1.01 ± 0.16
FA	1	1	1	1
AFQ	**0.009 ± 0.003**	**0.006 ± 0.003**	**0.008 ± 0.002**	**0.006 ± 0.001**

*All values are normalized against FA construct

c. i. ii.

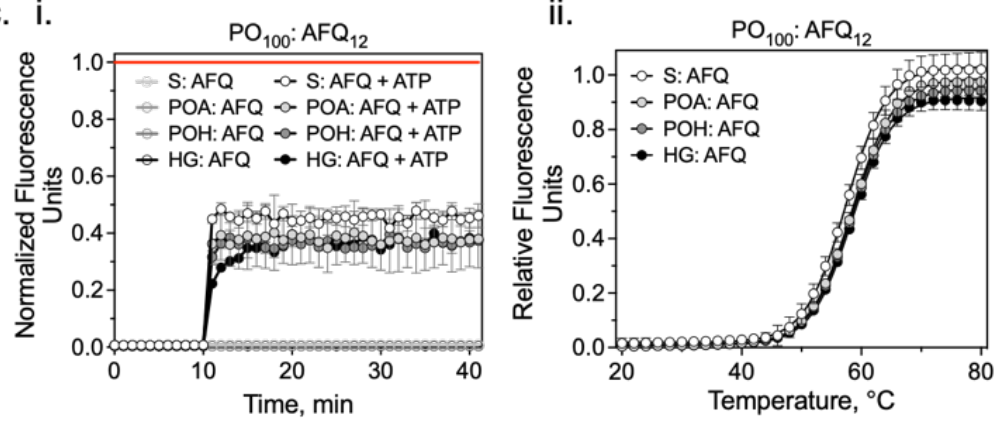

Figure 3.2 Fabrication of hydrogel-based ATP sensing platform. (a) A hydrazone cross-linked hydrogel was formed by mixing poly (oligoethylene glycol methacrylate) polymers functionalized with aldehyde (POA) or hydrazide (POH) functional groups. The tripartite aptamer reporter (AFQ) containing the adenosine binding sequence was assembled as a two-stem structure switching construct based on fluorescent DNA (F) and quencher DNA (Q) hybridized with complementary segments in a modified aptamer sequence (A) to enable FRET, based on the close proximity of the FRET pairs in the complex structure. Aptamer reporter (AFQ), co-dissolved with POH polymer, was co-deposited with a POA polymer solution in a 96-well plate to physically entrap the AFQ complex in the in situ-gelling covalently crosslinked hydrogel. The resulting aptamer-functionalized hydrogel (HG:AFQ) reports ATP concentration upon ligand-induced Q-DNA displacement and fluorescence recovery.[18] (b) Fluorescence quenching of individual aptamer reporter components and its entire assembly co-dissolved in free solution (S:), in hydrogel precursor polymers (POH: or POA:), or encapsulated inside a hydrogel (HG:). The aptamer reporter was prepared with a 12-bp quencher stem (AFQ_{12}). (c) Time-resolved fluorescence recovery in the presence of 5 mM of ATP injected in a volume of 2.5 µL/well (i) and the thermal melting profile (ii) of aptamer reporters prepared with 12-bp quencher stems (AFQ_{12}) co-dissolved in free solution (S:), in hydrogel precursor polymers (POH: or POA:) or encapsulated inside a hydrogel (HG:).

3.3.2. Hydrogel Stabilization of Adenosine Sensing Aptamer Reporters.

After confirming that FRET-based aptamer reporters retain their functionality inside POEGMA hydrogels, we assessed the stability of constructs inside the hydrogel when prepared with decreasing quencher stem lengths and/or in the presence of varying denaturing conditions to optimize the hydrogel properties in support of enhanced sensing performance. To better understand the effect that our hydrogel system exerts on duplexed DNA aptamers and the possibilities for optimizing and improving sensing performance, we designed a series of hydrogel-based aptamer reporters and challenged them against various denaturing conditions (thermal, vigorous washing, and nucleolytic attack). Two parameters associated with the hydrogel sensing system HG_x:AFQ_y were evaluated: (1) the hydrophilicity of the POEGMA hydrogels, modified by testing x = 10 or 100 molar percentages of the more hydrophilic $OEGMA_{500}$ relative to the less hydrophilic $M(EO)_2MA$ moiety to prepare the precursor polymers; and (2) the length of the Q-DNA strand, modified by testing y = 9, 10, 11, or 12 nucleotides long complementary sequences in the quenching strand. Reduced hydrogel hydrophilicity is hypothesized to decrease hydrogel swelling and thus stabilize hybridized strands in more confined and denaturation-protective environment, comparing to hydrogels of higher hydrophilicity expected to swell more and provide a more solution-like environment with somewhat lower stabilizing capacity. Reduced quencher strand lengths that create more ligand responsive but thermodynamically weaker aptamer complexes are anticipated to particularly benefit from the hydrogel's stabilizing potential and thus enable improved overall reporters' affinity and sensitivity, the latter assisted by a lower trade-off in background fluorescence relative to free in solution sensors (see Figure 3.3a). The change in Gibbs free energy of hybridization ($\Delta G^{\ominus}$) in each aptamer reporter following hydrogel encapsulation was assessed using van't Hoff analysis (Figure 3.3a, Table 3.2), which allows the direct extraction of thermodynamic values associated with FRET melting data (Figures S3.6 and S3.7) assuming a "two-state melting transition" from a double helix to a single stranded state;[38,46,47] the validity of this assumption is consistent with the use of short oligonucleotide duplexes[41] (*i.e.*, <15−20 bp, as is the case for all tested Q-DNA) and the black hole quencher FRET component known not to interfere with two-state DNA melting profiles.[38]

The experimentally obtained values for $\Delta G^{\ominus}$ under solution-only conditions (S:AFQ) were generally well-predicted by the UNAFold software system ($S:^{Sim}AFQ$), with the shorter Q-DNA constructs AFQ_9 and AFQ_{10} yielding values 1.2% and 5.3% lower than predicted while the longer Q-DNA constructs AFQ_{11} and AFQ_{12} yielded slightly higher $\Delta G^{\ominus}$ values than predicted (particularly for AFQ_{12}, which was 8.7% higher; see Table 3.2). The obtained results were consistent with previous findings showing that BHQ-labeled relative to BHQ-unlabeled duplexes tend to increase melting temperatures (T_m) due to contact-quenching stabilization, a mechanism that is likely to be more pronounced in FRET pairs with longer stems.[43,48] With respect to the impact of hydrogels on DNA hybridization, two key observations can be made: (1) the more hydrophilic hydrogel (HG_{100}) enabled better stabilization of the aptamer complex regardless of the Q-DNA length tested; and (2) thermodynamic stabilization of the duplex within the hydrogel was more significant with aptamer reporters assembled with shorter Q-DNAs regardless of the type of hydrogel used. For example, at a total strand concentration of Ct = 585 nM (corresponding to 65 nM F), the melting point of encapsulated AFQ_{10} reporter was 4.8°C higher in HG_{100} and 2.7°C higher in HG_{10} relative to that observed in free solution while encapsulated AFQ_{12} reporters showed only 1.2°C and 0.9°C increases in T_m in HG_{100} and HG_{10} respectively (Figure 3.3b). Correspondingly, $\Delta G^{\ominus}$ values for the shorter (*i.e.*, less inherently stable) AFQ_9 or AFQ_{10} duplexes

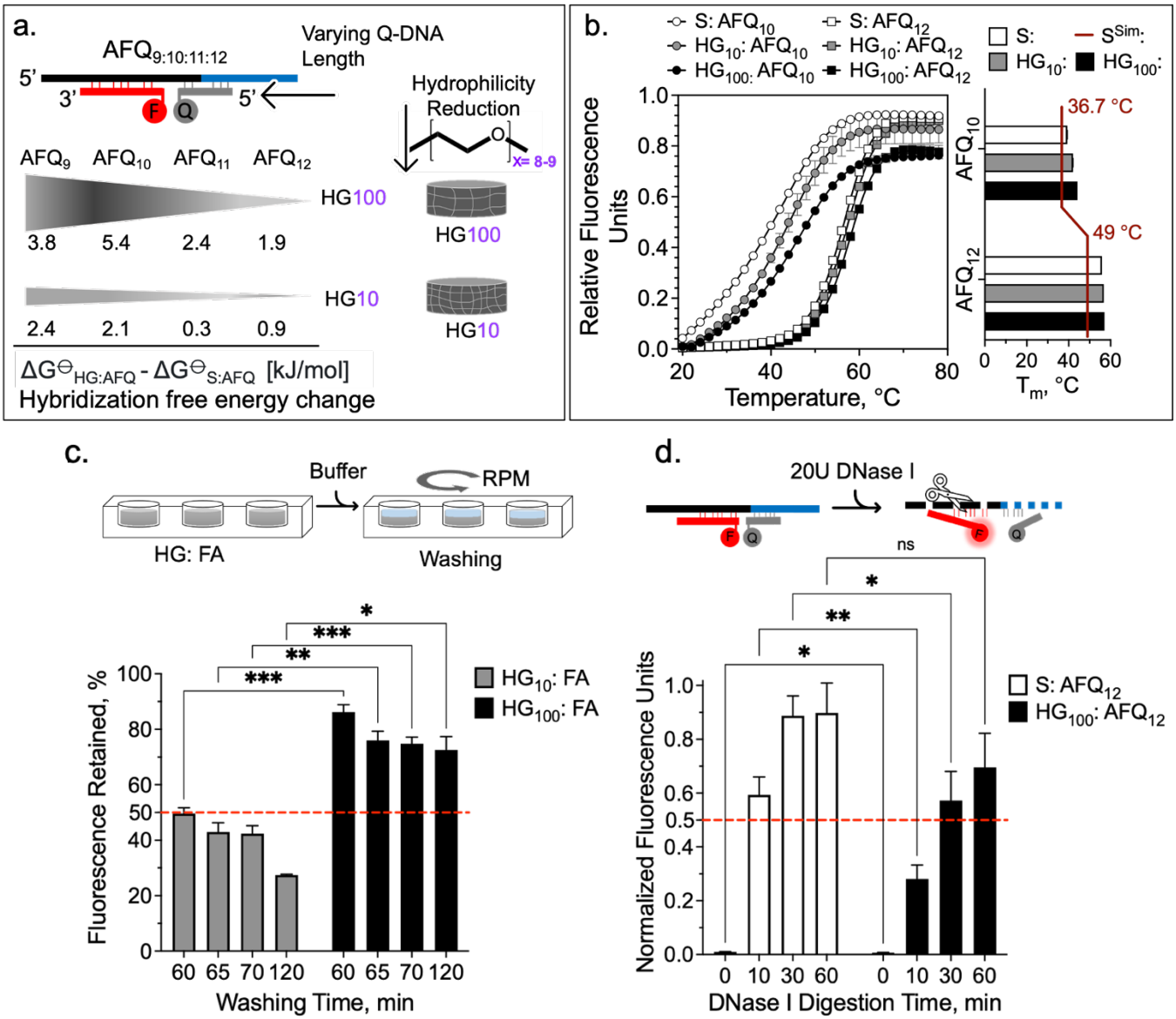

Figure 3.3 Effect of quencher stem length and hydrogel hydrophilicity on aptamer sensor stability. (a) Design scheme of a tripartite aptamer reporter exploiting quencher stem lengths of 9-, 10-, 11-, or 12-bp physically encapsulated in a hydrogel of higher (HG_{100}:AFQ) or lower (HG_{10}:AFQ) hydrophilicity; the Gibbs free energy changes of hybridization between hydrogel- and solution-based aptamer reporters are summarized with respect to these two variables to show the effect of hydrogel hydrophilicity and quencher stem length on aptamer reporter's thermodynamic stability; (b) Fluorescence recovery due to Q-DNA dehybridization as a function of temperature in AFQ_{10} and AFQ_{12} reporters assembled at 65 nM F-DNA content in solution (S), less hydrophilic (HG_{10}), or more hydrophilic (HG_{100}) hydrogel; obtained melting temperatures, T_m, corresponding to 50% signal enhancement are summarized relative to the simulated values for solution (S^{Sim}) (side bar graph inset). (c) Time-resolved fluorescent aptamer construct (FA) encapsulation efficiency in POEGMA hydrogels with higher (HG_{100}) and lower (HG_{10}) hydrophilicity; (d) Stability of AFQ_{12} reporter upon incubation with DNase I (20 U/well) over 60 min when encapsulated inside HG_{100} hydrogel relative to in free solution (S).

encapsulated in the more hydrophilic HG_{100} system were up to 5 kJ/mol higher than those in free solution while constructs prepared with longer Q-DNA stems or in less hydrophilic gel matrices showed lower changes in $\Delta G^{\ominus}$. This result is consistent with the higher inherent thermodynamic stability of the longer Q-DNA duplexes in free solution, such that the additional hydrogen bonding and/or

confinement/crowding offered by the hydrogel would provide less relative stabilization benefits to longer duplexes versus shorter duplexes.

The reason for the improved stabilization capacity of the HG_{100} hydrogel relative to the less hydrophilic HG_{10} hydrogel is less clear. We hypothesize that the temperature-responsive HG_{10} hydrogel (which has a volume phase transition temperature of ~ 36°C[36] versus >60°C in HG_{100}[36,49]) collapses prior to the melting point of the longer Q-DNA complexes, thereby increasing gel-gel interactions at the cost of gel-complex stabilizing interactions. However, the length of the PEG side chains in the POEGMA polymers may also be correlated with this result.[50,51] Prior findings have indicated that larger steric crowders (including longer-chain PEGs greater than or equal to the n=8-9 repeat unit in side chain length of $OEGMA_{500}$) can act as volume excluders that tend to thermodynamically stabilize DNA base pairs by favoring net volume reduction and thus the formation of more compact and ordered structures.[52] In contrast, smaller crowders (*i.e.*, the shorter n=2-3 repeat unit $M(EO)_2MA$ side chains) tend to interact more directly with the DNA double helix minor or major grooves to reduce complex stabilization, depending on the smaller crowder chemistry and concentration.[46,53] Importantly, hydrogel encapsulation did not appear to have a destabilizing effect in any condition in this work, meaning that that hydrogels can be leveraged to enhance sensitivity based on Q-DNA truncation. This result also represents a key benefit of our hydrogel approach relative to previously reported sol-gel compositions that could exert up to 20°C of thermal destabilization on AFQ_{12} reporters, a result of the hydrophobic moieties and residual methanol byproducts present in the encapsulating matrix that are fully avoided with the dynamic covalent chemistry used in our POEGMA-based system.[21,22]

Table 3.2 Changes in the Gibbs free energy during the hybridization of AFQ reporters in free solution or encapsulated in HG_{10} or HG_{100} hydrogel relative to predicted values.

Tripartite Aptamer Reporter	**$\Delta G^{\ominus}$ [kJ/mol]**			
	$S.^{Sim}$	S:	HG_{10}:	HG_{100}:
AFQ_{12}	-65.7	**-71.4**	**-72.3**	**-73.3**
AFQ_{11}	-57.3	**-59.8**	**-60.1**	**-62.2**
AFQ_{10}	-48.9	**-46.3**	**-48.4**	**-51.7**
AFQ_{9}	-41.4	**-40.9**	**-43.3**	**-44.7**

To assess the stability of the complexes against vigorous washing conditions, the immobilization efficiency (*i.e.,* percentage of the added aptamer construct that remains physically entrapped inside the hydrogel) of the fluorescent aptamer formed in the absence of Q-DNA (FA, 100nM F) and encapsulated within 6 wt% HG_{10} and HG_{100} hydrogels was investigated by quantifying the residual fluorescence in the hydrogel samples (Figure 3.3c) after multiple 2-hour washing and rinsing cycles in 1xAssay buffer. Each hydrogel can efficiently encapsulate FA, although the retention capacity depends on the hydrogel composition. Somewhat surprisingly, the most hydrophilic (i.e., highest porosity) hydrogel HG_{100} enabled the highest aptamer retention (73 ± 5%), while the less hydrophilic HG_{10} hydrogel retained only 28 ± 1% of the originally encapsulated aptamer. We attribute this result to the syneresis observed with the HG_{10} hydrogel, which de-swelled by up to 33% of its initial weight in the washing solution[54] and thus could convectively expel the complexes from the gel during the washing steps; in contrast, HG_{100} did not undergo any deswelling (indeed, it swells under the same conditions[35]) and did thus avoided such

convective removal of the construct to enable higher retained encapsulation despite its significantly higher pore size in the swollen state. Interestingly, higher concentrations of HG_{100} (8 wt% and 10 wt%) did not promote higher encapsulation efficacy for the FA complexes, ultimately yielding retained fluorescence values comparable to those observed at 6 wt% HG_{100} (Table S3.3). This result suggests that the strong interactions between HG_{100} and the aptamers (consistent with the enhancement in the complexes' thermal stability upon HG_{100} encapsulation, Figs. 3.3a and 3.3b) can effectively compete with diffusion to retain the aptamers inside the gel network even when hydrogels with larger pore sizes are used. Notably, similar retention values were observed for a single-stranded and less bulky fluorescent aptamer (Fa) in the HG_{100} hydrogel (Table S3.4), further suggesting that the more hydrophilic hydrogel configuration is still capable of effectively immobilizing various sizes of DNA molecules and that the fluorescent aptamer construct likely remains in a duplex form upon encapsulation; as such, any fluorescence leakage does not derive primarily from the melting of the fluorescently-labelled DNA strand from the aptamer. It should be emphasized that HG_{100} hydrogels significantly outperformed previously reported hydrogels in which aptamers were either physically entrapped in a sol-gel matrix or modified with acrydite and then immobilized in polyacrylamide microparticles (both of which yielded <50% complex retention[17,21]) without requiring the modification of the gel via the inclusion of cationic groups,[55] the PEGylation of the loaded sensing and chromogenic molecules,[56] or more complex polymerization methods that are both more expensive and significantly more likely to negatively impact structure-switching ability and/or double helix stability.[57]

Encapsulating the aptamer in a hydrogel also offers the potential to reduce nucleolytic degradation kinetics based on steric exclusion by limiting DNase diffusion into the hydrogel and the accessibility of DNase substrate sites within the aptamer construct to the enzyme (Figure 3.3d). While DNase I (31 kDa molecular weight and of 2.5 nm hydrodynamic radius[58]) can diffuse into HG_{100} hydrogel mesh (estimated porosity: 5-10 nm[34,35]), the rate of denaturation is significantly slowed; specifically, ~30 min was required for the nuclease to digest ∽50% of the encapsulated aptamer reporter while almost complete digestion occurred over the same time in free solution. A similar trend was observed at lower DNase I concentrations (1U/well) and within HG_{100} hydrogels prepared with higher precursor polymer concentrations of 8 wt% and 10 wt% (Figure S3.8a). Interestingly, despite having lower porosity than HG_{100}, HG_{10} was comparatively less efficient with respect to protecting the encapsulated aptamer (Figure S3.8b). We hypothesize this result is related to the higher density of long-chain $OEGMA_{500}$ at the interface in HG_{100} that can more strongly sterically inhibit DNase access to the nucleolytic cleavage sites compared to less hydrophilic hydrogels. Notably, the aptamers' sensing ability was preserved even within a nucleolytic environment (Figure S3.8c), suggesting that the quantification of ATP would be possible even after extended exposure to a real biological sample. As such, the hydrogel can not only stabilize a broader range of potential aptamer reporter designs (enabling more options to tune reporter affinity for optimizing signal:background ratio) but also protect the constructs against degradation or denaturation commonly observed in solution.

3.3.3. Signal Generation and Sensing Kinetics in Buffer.

The potential of the encapsulated AFQs to detect the target ligand (ATP) was assessed as a function of both the quencher's stem length (y = 9, 10, 11, or 12 bp) and the hydrogel's hydrophilicity (HG_{10} and HG_{100}). Note that sensing assays were pursued with both HG_{10} and the best-performing HG_{100}, as HG_{10}'s capacity to retain >50% of the encapsulated aptamer after 1 hour of washing is still competitive with the performance of previously reported physically encapsulated hydrogel sensors as described in Section 3.3.2. Performance was assessed relative to solution-based constructs with regards to fluorescence quenching efficiency (FRET), changes in fluorescence quenching upon exposure to ligand-free buffer

(FRET change), and the signal enhancement upon exposure to a saturating concentration of the target ligand ATP (S:B ratio). The results of these experiments are summarized in Figures 3.4a and 3.4b. As indicated by darker landscapes in the heat maps in Figure 3.4a-i, the use of longer quencher stems enabled higher FRET efficiency in both the encapsulated (HG:AFQ) and in-solution (S:AFQ) reporters. However, hydrogel encapsulation significantly improved the FRET efficiency in the aptamer reporters hybridized with shorter quencher stems, consistent with the higher melting temperatures observed for those complexes within the hydrogel (Fig. 3.3b). For example, HG_{100} enabled FRET efficiencies up to 50% higher in the AFQ_{10} reporters and 30-40% higher in the AFQ_9 reporters relative to the solution-based control experiments (Figure 3.4a-i). Thus, the proposed hydrogel system can facilitate shorter nucleotides to yield measurable and relevant signal outputs.

1xAssay buffer with and without ATP ligand was then directly deposited onto arrayed hydrogels to assess the potential for spontaneous de-quenching in the absence of the target molecule (Figure 3.4a-ii) and signal recovery in the presence of ATP (Figure 3.4b) within different sensor constructions. Upon exposure to buffer only for 1 hour, the highest spontaneous de-quenching (*i.e.*, the lightest signal on the heat map in Fig. 3.4a-ii) was observed with the $S:AFQ_9$ system, with longer quenchers (particularly >10 bp) yielding more stable reporters in free solution. While the encapsulated aptamers also experienced some spontaneous de-quenching, this phenomenon occurred at a significantly lower rate within the hydrogels, having 20% (longer quencher stems) to 50% (shorter quencher stems) lower background fluorescence signals relative to solution-based constructs. Interestingly, while the HG_{100} hydrogel offered clear advantages in complex stabilization and retention, a similar FRET change was observed with all the tested hydrogels. Thus, even lower degree of complex stabilization provided by the HG_{10} hydrogels can still significantly reduce spontaneous de-quenching and background signals in the encapsulated aptamer sensors.

The sensing response after exposing the aptamer sensors to 5 mM of ATP was quantified as the ratio between the on-target (signal) and off-target (background) fluorescence signals (*i.e.*, S:B ratio), with the results of these tests shown in Figure 4b in which lighter landscapes indicate higher S:B ratios. Hydrogel encapsulation yielded S:B ratios that were at least as high as those recorded in free solution, suggesting that the capacity for effective Q-DNA strand release and switching between conformations was preserved under a confined environment. This retained signal generation potential combined with the lower background fluorescence achieved (Fig. 3.4a-i,ii) resulted in S:B ratio enhancements between 25-50% depending on the quencher size and hydrogel hydrophilicity. Interestingly, while HG_{10} was particularly effective at enhancing the fluorescence signal generated in reporters hybridized with longer quencher stems (S:B ~ 100 for HG_{10}:AFQ_{12}), no improvement was observed with shorter quencher stems; in contrast, more hydrophilic gels

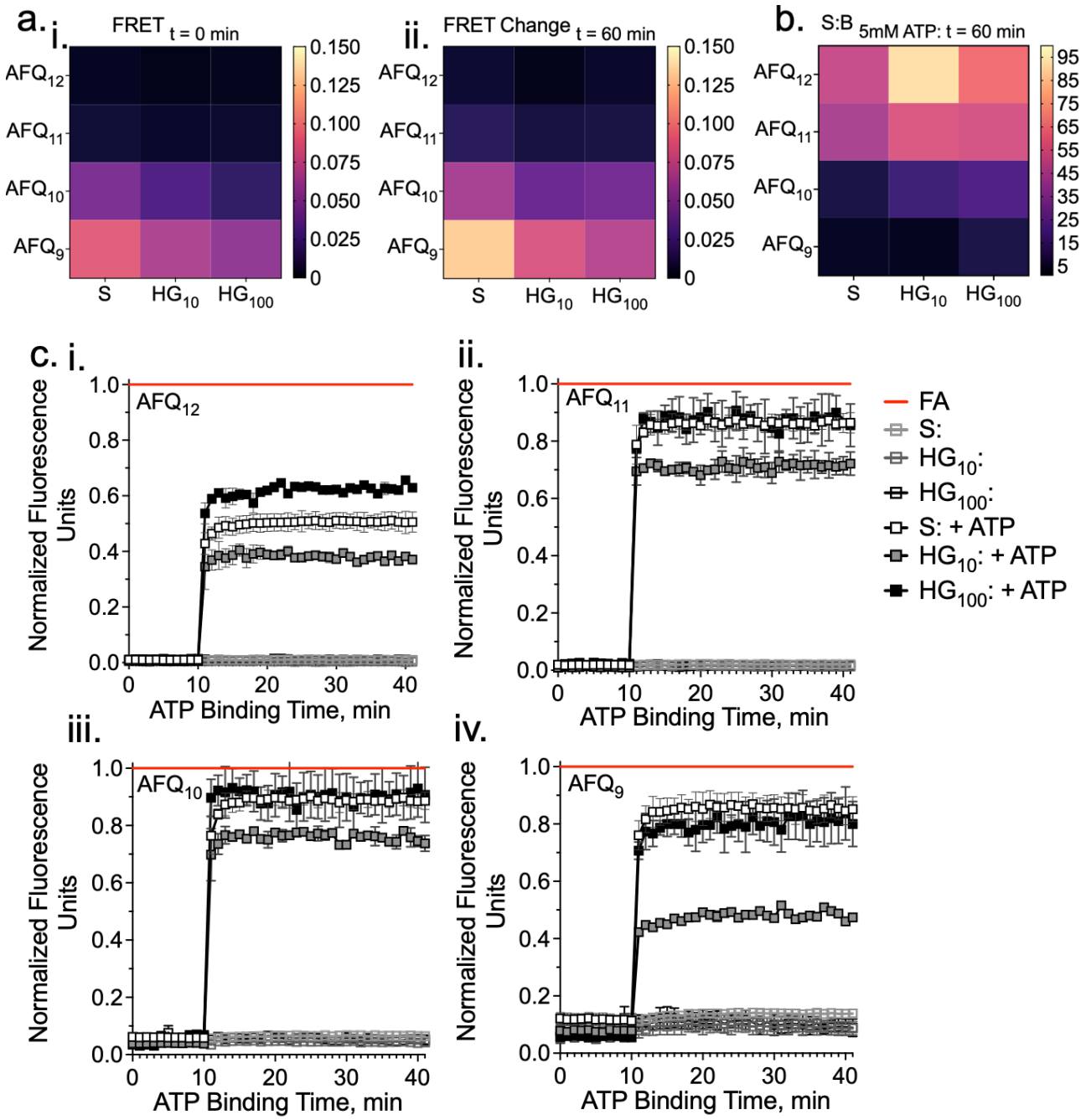

Figure 3.4 Fluorescence quenching and ligand-induced signaling enhancement of hydrogel-encapsulated aptamer sensors prepared with varying quencher stem lengths (9-, 10-, 11-, and 12-bp) and hydrogels with different hydrophilicities (HG10 or HG100) relative to the same constructs in free solution. (a) FRET of aptamer reporters (i) prior to target addition (t = 0 min, with darker landscapes corresponding to reduced background fluorescence) and (ii) following exposure to ligand-free 1xAssay buffer (t = 60 min; lighter landscapes correspond to increasing fluorescence background levels due to spontaneous de-quenching). (b) Signal:background (S:B) ratios measured 1 h after the addition of 5 mM of ATP to the aptamer constructs (t = 60 min; lighter landscapes indicate higher S:B ratios and thus enhanced signal generation capacity). (c) Ligand-binding kinetics of each aptamer reporter with quencher stem lengths of (i) 12 bp, (ii) 11 bp, (iii) 10 bp, or (iv) 9 bp in HG100 (black markers), HG10 (grey markers), and in free solution (white markers).

improved the signal across all tested reporters, with HG_{100} enabling 2x better fluorescence recovery for shorter quencher stems (S:B~22 for HG_{100}:AFQ_{10} and S:B~11 for HG_{100}:AFQ_9) relative to corresponding

solution-based constructs; enhanced performance is also noted relative to that reported in similar designs documented in the literature.[20,28] We hypothesize that the ability of HG_{100} to provide improved aptamer complex stabilization (Fig. 3.3a), reduced backgrounds (Fig. 3.4a), and higher internal network flexibility[6,12] makes this system better able to accommodate effective aptamer renaturation (and thus signal generation) across a broad range of potential quencher compositions.

The response kinetics and extent of aptamer activation upon exposure to the ATP target were then monitored via time-resolved fluorescence recovery using a saturating concentration of ATP ligand to compare the response times of the hydrogel-encapsulated relative to solution-based aptamer reporters; the extent of aptamer activation (i.e., % of Q-DNA replaced from the original aptamer complex) was used as an indication of the accessibility of encapsulated ATP reporter inside the hydrogel relative to in free solution (Figure 3.4c). All aptamer reporters showed rapid responses to the introduction of ATP, with fluorescence onset observed within seconds and equilibrium signal being reached within five to ten minutes following ligand addition depending on the size and location of the Q-DNA. In free solution (S:AFQ), the rate of response followed the trend $AFQ_{10} \simeq AFQ_{11} > AFQ_9 \simeq AFQ_{12}$, with the generally faster response of the shorter quencher stems being consistent with the weaker hybridization between the Q-DNA and the aptamer in those cases. Q_9 was an exception to this trend because it does not directly hybridize with the aptamer binding site (Fig. 3.1) and thus does not promote cooperativity between two ligand binding sites as is typically required for enhanced signaling ability.[28,29] The degree of aptamer activation in free solution upon ATP exposure followed the trend $AFQ_{10}>AFQ_{11}>AFQ_9>AFQ_{12}$, with the Q_{10} and Q_{11} quencher stems facilitating a ≥86% fluorescence recovery and the Q_9 quencher stem exhibiting only slightly lower fluorescence recovery (85±4%) at equilibrium relative to the same concentration of quencher-free complex. In contrast, Q_{12} showed a significantly lower equilibrium fluorescence recovery value of 50±4% consistent with its high thermodynamic stability as a result of its size, the high occupancy of the native aptamer binding sites, and enhanced FRET pair contact quenching that can be tuned based on the Q-DNA molar concentration (Figure S3.4).

The hydrogel-based reporters (HG:AFQ) showed similar responses to the free solution constructs for the adenine nucleotides, with equilibrium being reached within four to eleven minutes suggesting minimal resistance to ligand diffusion into the hydrogel. The extent of aptamer activation in the hydrogel-based constructs also followed the general trend observed in free solution; however, the magnitude of the response was additionally influenced by the hydrophilicity of the hydrogel used. The more hydrophilic hydrogel (HG_{100}) enabled very high equilibrium fluorescence recoveries of ≃ 90% of the maximum signal for the AFQ_{10} and AFQ_{11} reporters but just ≃ 80% for AFQ_9 and only 65±1% for AFQ_{12}. In contrast, hydrogel HG_{10} facilitated significantly lower fluorescence recoveries, with AFQ_{11} and AFQ_{10} achieving ≃71% and ≃75% activation, respectively, while AFQ_{12} activated to only 39±1% of the maximum value. As such, the AFQ_{10} reporter demonstrates superior performance in ligand response given its consistently shorter ligand binding rate and higher fluorescence recoveries in all tested hydrogels (Table S3.5).

This result is consistent with the deswelling observed with HG_{10} under the assay conditions that restricts both the mobility of the aptamer as well as the diffusibility of ATP to the binding site, confirming the preferential use of HG_{100} for fabricating the hydrogel-based constructs. Of note, this general performance can be maintained upon the addition of various volumes of the added ligand and the nature of the hydrogel pre-treatment employed prior to the binding assay (Figures S3.9 and S3.10), with effective fluorescence recoveries observed even with very small working volumes (10 μL) in contrast to ≥100 μL analyte volumes reported in previously published systems; such performance is also achievable without the need for hydrogel washing or pre-hydration prior to analysis as has been required in previous hydrogel designs.[1,9,45] As such, the proposed hydrogel system can enable fast and cost-efficient target detection. Finally, the potential of hydrogel to preserve fluorescence quenching and ligand binding activity within

encapsulated aptamer constructs was assessed following 1 day and 7 days of storage at ambient temperature (Figure S3.11). The hydrogel can maintain >90% activity after 1 day of storage relative to fresh samples prepared with either AFQ_{12} and AFQ_{10} constructs; in contrast, the same constructs in solution show lower residual activity ranging between 82±4% for AFQ_{12} and 86±1% in AFQ_{10}. Hydrogel-encapsulated AFQ_{12} also retains 93±4% of activity even after 7 days of ambient storage, ~14% higher than in same construct in solution. In contrast, encapsulated AFQ_{10} samples maintain only 56±2%, a result we attribute to greater stabilizing effect the hydrogel exerts on shorter quencher stems that, upon hydrogel aging, improves FRET efficiency and thus reduces ligand-induced fluorescence recovery. Overall, the obtained results show that the optimal hydrogel configuration HG_{100} promoted lower background fluorescence and higher ligand-induced signaling gain within aptamer reporters of shorter quencher stems while introducing minimal diffusional barriers that would negatively impact sensing kinetics.

3.3.4. Sensing Performance in Buffer.

To assess the hydrogel-based sensors' practical applicability, the binding affinity of aptamer reporters prepared with varying quencher stem lengths (9 bp, 10 bp, 11 bp, and 12 bp) encapsulated in the optimal HG_{100} hydrogel was assessed. Figures 3.5a-c compare the binding affinities and limits of detection achieved for each tested quencher stem in free solution or encapsulated, including the corresponding dissociation constants (K_d), limits of detection for the ATP ligand, and Hill coefficients that indicate the cooperativity between two ligand binding sites (h>1 indicates positive cooperation) (Table 3.3). The measured K_d values (120-1400 μM) in free solution significantly differed from those of the native aptamer (K_d = 6-40 μM[23]) consistent with the applied signal-transducing post-modifications (Fig. 3.1); however, the obtained K_d values were still within the range reported for other functional aptamers with similar designs.[18,28,29] Consistent with the FRET response kinetics data (Figure 3.4c), shorter Q-DNA aptamer reporters generally exhibited higher binding affinities (lower K_d values) due to the weaker hybridization of shorter Q-DNA strands to the aptamer needing to be displaced in order to enable signal generation; however, despite being the weakest thermodynamically, the binding affinity of AFQ_9 was 7-fold lower than that of AFQ_{10} consistent with the different active site interaction of the Q_9 quencher stem.[28] The hybridization of Q-DNAs to guanosine bases within binding site II (Q_{10}, Q_{11}, and Q_{12}; Figure 3.1a) promotes an induced-fit ligand-binding mechanism that enables increasingly faster binding kinetics, higher signal recovery, and affinity enhancement consistent with Hill coefficients indicating positive cooperativity (h>1); conversely, Q-DNAs that leave site II G-bases unhybridized (i.e., Q_9) promote conformational selection ligand binding pathways and an altered sensing profile that is non-cooperative (h~1). These results generally agree with those documented in previous reports,[20,28,29] although slight allostery differences can be observed depending on the selected fluorophore-quencher pair.[8]

The K_d values for the hydrogel-encapsulated aptamer complexes were similar to those measured in free solution with the exception of the shortest complex (AFQ_9), which exhibited up to 33% higher K_d values consistent with the enhanced $\Delta G^{\ominus}$ values of the Q_9-DNA hybridization occurring in this hydrogel (Fig. 3.3a). Additionally, broader sensing dynamic ranges could be achieved relative to solution-based results with hydrogel sensors incorporating quencher stems <12 bp; of particular note, the dynamic range of the HG_{100}:AFQ_9 sensor covers almost three orders of magnitude while providing at least 2x higher signal enhancement at higher ATP concentrations compared to the equivalent free solution constructs or similar sensors reported in the literature.[28,29]

Importantly, the encapsulation process does not interfere with the selectivity of the aptamer reporter (Figure S3.12).

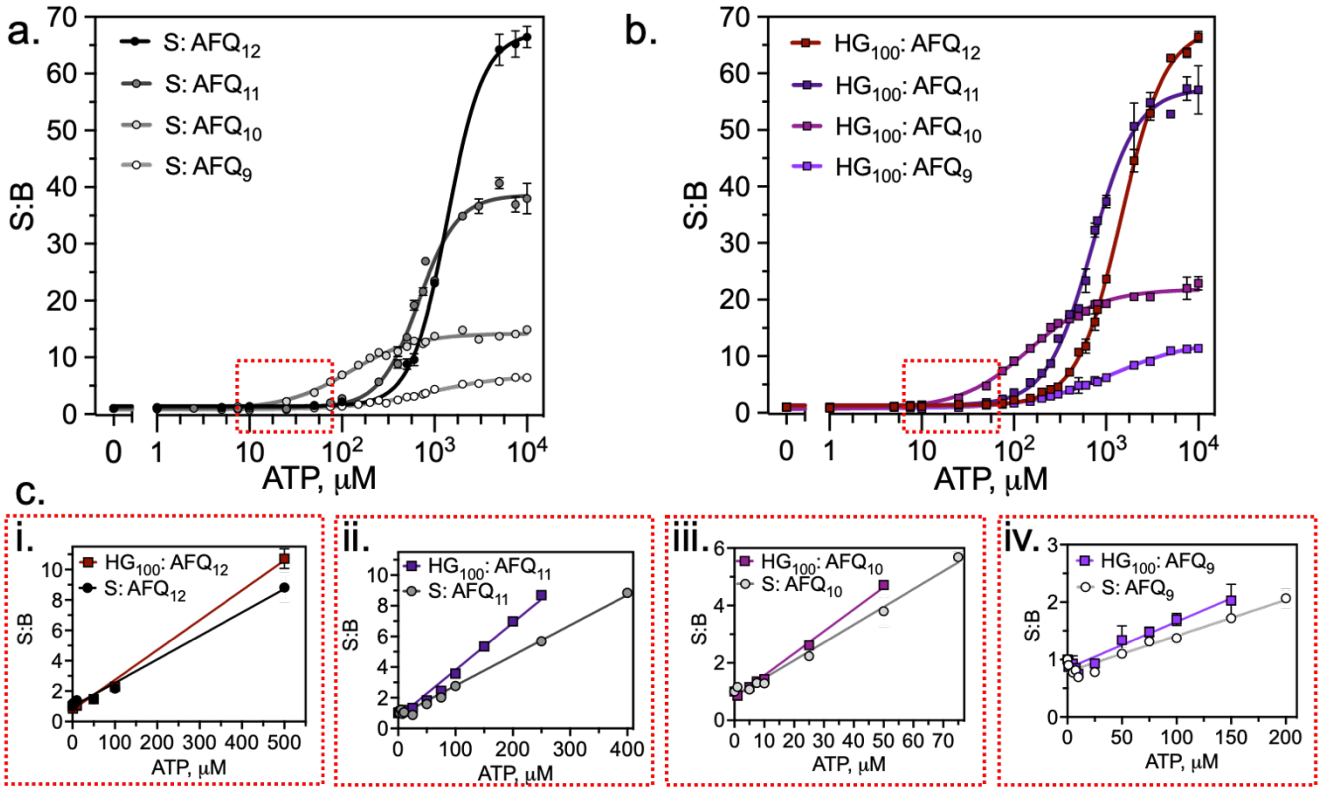

Figure 3.5 Binding affinity and sensitivity of ATP aptamer reporters in 1xAssay buffer. Concentration response of adenosine reporters (a) in free solution or (b) encapsulated in HG_{100} titrated with 0-10 mM ATP at 20 µL/well volume (25°C, 1 hour incubation time) and prepared with quencher stem lengths of 12 bp, 11 bp, 10 bp, and 9 bp. (c) Linear detection range response for each aptamer reporter in free solution or encapsulated in HG_{100} hydrogel with quencher stem lengths of (i) 12 bp, (ii) 11 bp, (iii) 10 bp, and (iv) 9 bp.

Table 3.3 Summary of the various aptamer reporters' affinity, cooperativity, and sensitivity data relating to ATP binding in pure buffer.

Tripartite Aptamer Reporter	In Solution, S:			Hydrogel Encapsulated, HG_{100}:		
	K_d (µM)	h	LOD (µM)	K_d (µM)	h	LOD (µM)
AFQ_{12}	1374	2.0	56.4	1461	1.8	48.4
AFQ_{11}	674	2.0	38	701	1.8	33.1
AFQ_{10}	123	1.2	10	148	1.1	5.3
AFQ_9	865	1.0	56	1158	1.0	41.6

The limits of detection (LODs) for the hydrogel-based sensors were assessed based on 3σ/initial slope, wherein σ represents a standard deviation within the linear range of binding curve (see Figure 3.5c). The obtained values ranged from 5.3 µM (for HQ_{100}:AFQ_{10}) to 48.3 µM (for HQ_{100}:AFQ_{12}), with the linear regime enabling quantitative adenosine detection between 50 µM and 500 µM depending on Q-DNA size. The LODs measured for the hydrogel-based sensors were 1.5-2x lower than those observed in free solution (Table 3.3), ~5-fold lower than that those measured for the AFQ_{12} FRET tripartite construct embedded in an optimal sol-gel composition (LOD = 28 µM),[21] and ~10-fold lower than other hydrogel-

based designs that apply colorimetric and fluorescent visualization of ATP molecules.[1,5] Since our thin layer hydrogels enable the efficient detection of ligands in small sample volumes, the LODs achieved under our experimental conditions represent as little as 54 ng of ATP, again significantly lower than the values achievable with other reported hydrogels.[14,16,17,56]

3.3.5. Stability and Sensing Performance in Serum.

To demonstrate the potential application of the hydrogel-based sensors for operation in real biological samples, AFQ_{12} (highest S:B ratio in 1xAssay buffer, Figure 3.5b) and AFQ_{10} (lowest K_d value in 1xAssay buffer, Table 3.3) were encapsulated in the optimal HG_{100} hydrogel system (highest S:B ratios among hydrogels, Figure 3.4a) and titrated with 0-10 mM of ATP dissolved in undiluted human serum. Figures 3.6a and b compare the solution-based and HG_{100} hydrogel-encapsulated binding affinities for the two tested quencher stem lengths, with the corresponding dissociation constants (K_d) and LODs, summarized in Table 3.4. As in the buffer, similar S:B ratios and LODs were achieved in serum with the strongly hybridized AFQ_{12} reporters whether in free solution or encapsulated in HG_{100} hydrogel, with both exhibiting 1.5-2x lower sensitivity for ATP (Figure 3.5c) and moderately lower K_d values (Table 3.3) compared to ATP dissolved in Tris-buffer. It is noteworthy that the use of serum introduces an altered salt concentration profile (*i.e.,* reduced Mg^{2+} and Na^{+} ion concentrations[59]) in addition to various DNA-binding species (e.g., single-stranded DNA binding proteins[60]) that can disrupt aptamer assemblies.[8] Furthermore, the aptamer reporters' relatively poor ability to discriminate between adenine-based nucleotides (ATP, ADP, and AMP)[62,63] typically present in biological samples may also influence the sensor responses given that ATP molecules are regularly converted to ADP during various metabolic reactions.[8]

Solution-based AFQ_{10} reporters also showed reduced sensing performance in serum relative to that achieved in 1xAssay buffer, with a significantly narrowed dynamic range and a LOD >20 μM. However, the hydrogel encapsulated AFQ_{10} reporters exhibited a dynamic range and sensitivity almost 3x higher compared to the in free solution constructs and could achieve an LOD of 8.8 mM; of note, this LOD result is on the same order of magnitude as that observed in buffer (5.3 mM) and can be achieved with only 20 μL/well of analyte. Increasing the sample volume to 50 μL/well (still well below that required for most previous sensors) maintains a rapid signal response (10 minutes to equilibrium signal generation) while further lowering the detection limit to 3-4 μM (Figure S3.13). The lower K_d value observed for HG_{100}:AFQ_{10} suggests that the potential concentration of ionic gradients associated with serum within the hydrogel may perturb the stability of the duplex structure and drive the reporter into a more open conformation that would enable more effective liberation of aptamer assemblies in the presence of ligands.[61]

The low LOD values achieved with our hydrogel-based sensors demonstrate the benefits of utilizing a stabilizing gel phase for the analysis of real biological samples, particularly given the strong interference that biological fluids exert on weaker aptamer complexes.[3] The aptamer-complex stabilization and solution filtering effects afforded by the hydrogel facilitate improved signal enhancement and sensitivity among the aptamer reporters, with significantly lower LODs consequently achievable relative to those previously reported in undiluted serum for solution-based tripartite reporters using luminescent resonance energy transfer ATP detection (LOD = 60 μM in 100% serum)[64] or bipartite FRET aptamer reporters immobilized on magnetic beads for flow cytometry- assisted ATP detection (LOD = 167 μM and 200 μM in 30% and 90% serum, respectively).[65] Moreover, the developed hydrogel sensors are able to achieve these results while requiring in many cases order-of-magnitude lower sample volumes. Furthermore, while previous work has detailed the challenges associated with improving sensitivity based on high background fluorescence values (e.g., sol-gel materials[27,21,55,66]), sensor leaching, and/or

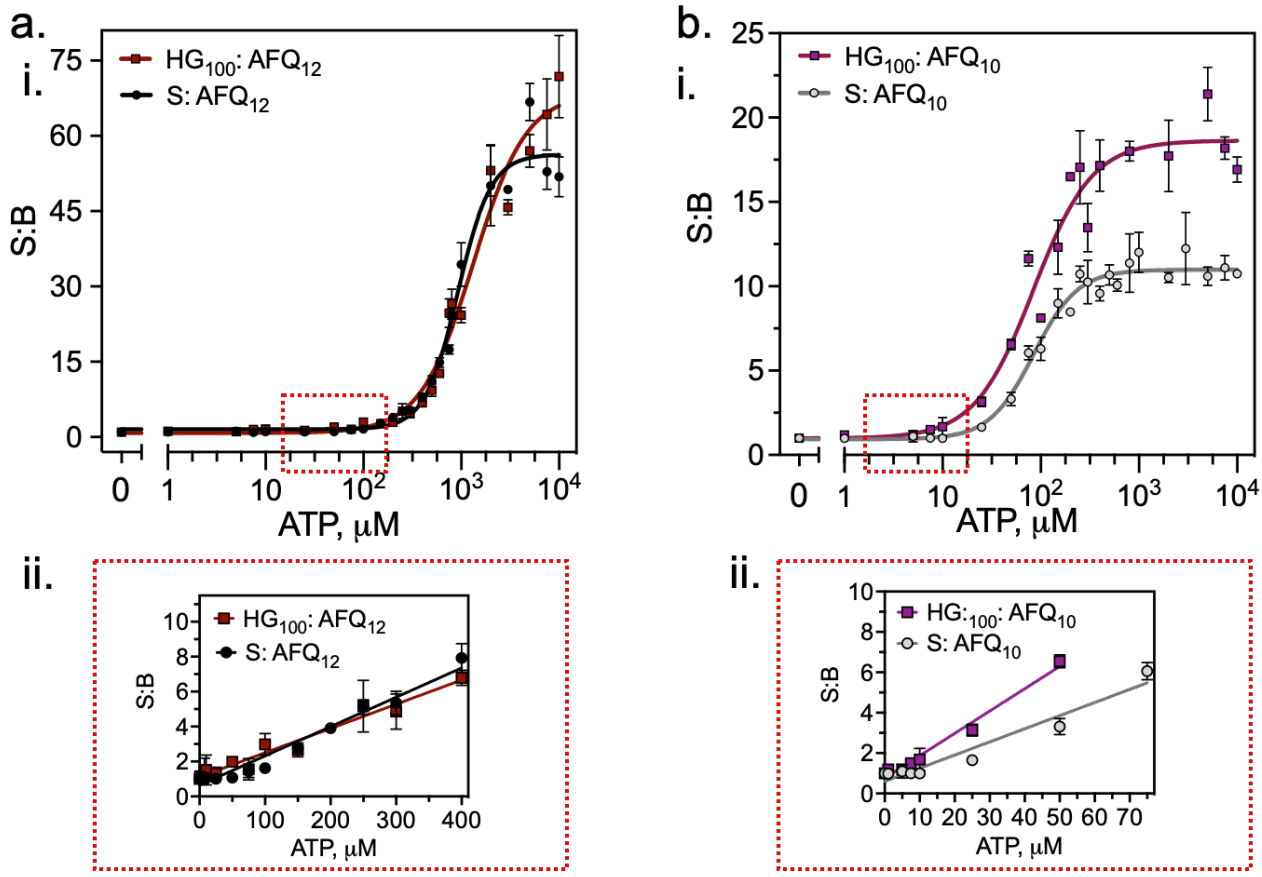

Figure 3.6 Binding affinity and sensitivity of adenosine aptamer reporters in undiluted human serum. Concentration response of adenosine reporters prepared with (a) quencher stem lengths of 12 bp encapsulated in HG_{100} hydrogel (red markers) or in free solution (black markers) and (b) quencher stem lengths of 10 bp encapsulated in HG_{100} hydrogel (purple markers) or in free solution (grey markers) titrated with 0-10 mM ATP in undiluted human serum (25°C, 1 hour incubation time). Insets represent the linear detection range response for encapsulated or free solution (i) AFQ_{12} or (ii) AFQ_{10} aptamer reporters.

Table 3.4 Summary of the aptamer reporters' affinity, cooperativity, and sensitivity data relating to ATP binding in undiluted serum.

Tripartite Aptamer Reporter	In Solution, S:			Hydrogel Encapsulated, HG_{100}:		
	K_d (μM)	h	LOD (μM)	K_d (μM)	h	LOD (μM)
AFQ_{12}	926	2.0	82	1331	1.6	92
AFQ_{10}	84.3	2.0	23.9	84.5	1.3	8.8

the need for large concentrations of DNA,[56] the design proposed in this work facilitates high detection limits in a cost-effective and amplification/enzyme-free manner based on strand-displacement that does not require sequence engineering[5] or truncated aptamers.[67] Our method instead increases quencher stem stability (and thus reduces non-specific background signal generation in the absence of the target analyte) by combining truncated Q-DNAs with hydrogels, facilitating improved reporter stability together with solution-like affinity recognition to enable significant improvements in sensor performance.

3.4. Conclusions

Physical encapsulation of adenine-responsive FRET-signaling DNA aptamers inside *in situ*-crosslinkable thin-film POEGMA-based hydrogels can enable high immobilization capacity, improved thermal stabilization of the reporting nucleic acid duplexes, delayed nucleolytic degradation, and signaling responses with similar or better magnitudes and kinetics to those observed in free solution. Furthermore, the affinity of the embedded aptamer constructs can be tuned by regulating the content and location of quencher stem, allowing convenient and amplification-free sensitivity enhancement in both pure and complex reaction media that addresses a pervasive challenge limiting the use of nucleic aptamer technology for small molecule sensing. Additionally, the proposed sensors enabled LODs in the low μM range (even in undiluted human serum) within minutes following ATP exposure while using low sample volumes of 20 μL/well. These sensitivities were at least 5-fold higher compared to previously reported FRET-based sensors that typically require much larger sample volumes (Table S3.6). The sensor design is also directly adaptable to aptamers for any small molecule of interest due to the physical nature of the reporter encapsulation (avoiding the need for complex aptamer functionalization for immobilization) and the presence of a solution-like immobilizing environment that unlocks the potential for high-affinity interactions while supporting a diversity of ligand binding pathways.

3.5. References

(1) Abune, L.; Davis, B.; Wang, Y. Aptamer-functionalized Hydrogels: An Emerging Class of Biomaterials for Protein Delivery, Cell Capture, Regenerative Medicine, and Molecular Biosensing. *WIREs Nanomed Nanobiotechnol* **2021**, *13* (6). https://doi.org/10.1002/wnan.1731.

(2) Murtaza, G.; Rizvi, A. S.; Qiu, L.; Xue, M.; Meng, Z. Aptamer Empowered Hydrogels: Fabrication and Bio-sensing Applications. *J of Applied Polymer Sci* **2022**, *139* (26). https://doi.org/10.1002/app.52441.

(3) Yoo, H.; Jo, H.; Oh, S. S. Detection and beyond: Challenges and Advances in Aptamer-Based Biosensors. *Mater. Adv.* **2020**, *1* (8), 2663–2687. https://doi.org/10.1039/D0MA00639D.

(4) Ruscito, A.; DeRosa, M. C. Small-Molecule Binding Aptamers: Selection Strategies, Characterization, and Applications. *Front. Chem.* **2016**, *4*. https://doi.org/10.3389/fchem.2016.00014.

(5) Yu, H.; Alkhamis, O.; Canoura, J.; Liu, Y.; Xiao, Y. Advances and Challenges in Small-Molecule DNA Aptamer Isolation, Characterization, and Sensor Development. *Angew. Chem. Int. Ed.* **2021**, *60* (31), 16800–16823. https://doi.org/10.1002/anie.202008663.

(6) Herrmann, A.; Haag, R.; Schedler, U. Hydrogels and Their Role in Biosensing Applications. *Adv. Healthcare Mater.* **2021**, *10* (11), 2100062. https://doi.org/10.1002/adhm.202100062.

(7) Jung, I. Y.; Kim, J. S.; Choi, B. R.; Lee, K.; Lee, H. Hydrogel Based Biosensors for In Vitro Diagnostics of Biochemicals, Proteins, and Genes. *Adv. Healthcare Mater.* **2017**, *6* (12), 1601475. https://doi.org/10.1002/adhm.201601475.

(8) Nielsen, L. J.; Olsen, L. F.; Ozalp, V. C. Aptamers Embedded in Polyacrylamide Nanoparticles: A Tool for *in Vivo* Metabolite Sensing. *ACS Nano* **2010**, *4* (8), 4361–4370. https://doi.org/10.1021/nn100635j.

(9) Liu, J. Oligonucleotide-Functionalized Hydrogels as Stimuli Responsive Materials and Biosensors. *Soft Matter* **2011**, *7* (15), 6757. https://doi.org/10.1039/c1sm05284e.

(10) Feagin, T. A.; Maganzini, N.; Soh, H. T. Strategies for Creating Structure-Switching Aptamers. *ACS Sens.* **2018**, *3* (9), 1611–1615. https://doi.org/10.1021/acssensors.8b00516.

(11) Li, J.; Mo, L.; Lu, C.-H.; Fu, T.; Yang, H.-H.; Tan, W. Functional Nucleic Acid-Based Hydrogels for Bioanalytical and Biomedical Applications. *Chem. Soc. Rev.* **2016**, *45* (5), 1410–1431. https://doi.org/10.1039/C5CS00586H.

(12) Kwak, M.; Herrmann, A. Nucleic Acid/Organic Polymer Hybrid Materials: Synthesis, Superstructures, and Applications. *Angewandte Chemie International Edition* **2010**, *49* (46), 8574–8587. https://doi.org/10.1002/anie.200906820.

(13) Liu, M.; Zhang, J.; Liu, S.; Li, B. A Label-Free Visual Aptasensor for Zearalenone Detection Based on Target-Responsive Aptamer-Cross-Linked Hydrogel and Color Change of Gold Nanoparticles. *Food Chemistry* **2022**, *389*, 133078. https://doi.org/10.1016/j.foodchem.2022.133078.

(14) Yang, H.; Liu, H.; Kang, H.; Tan, W. Engineering Target-Responsive Hydrogels Based on Aptamer−Target Interactions. *J. Am. Chem. Soc.* **2008**, *130* (20), 6320–6321. https://doi.org/10.1021/ja801339w.

(15) Zhu, Z.; Wu, C.; Liu, H.; Zou, Y.; Zhang, X.; Kang, H.; Yang, C. J.; Tan, W. An Aptamer Cross-Linked Hydrogel as a Colorimetric Platform for Visual Detection. *Angew. Chem. Int. Ed.* **2010**, *49* (6), 1052–1056. https://doi.org/10.1002/anie.200905570.

(16) Dave, N.; Chan, M. Y.; Huang, P.-J. J.; Smith, B. D.; Liu, J. Regenerable DNA-Functionalized Hydrogels for Ultrasensitive, Instrument-Free Mercury(II) Detection and Removal in Water. *J. Am. Chem. Soc.* **2010**, *132* (36), 12668–12673. https://doi.org/10.1021/ja106098j.

(17) Helwa, Y.; Dave, N.; Froidevaux, R.; Samadi, A.; Liu, J. Aptamer-Functionalized Hydrogel Microparticles for Fast Visual Detection of Mercury(II) and Adenosine. *ACS Appl. Mater. Interfaces* **2012**, *4* (4), 2228–2233. https://doi.org/10.1021/am300241j.

(18) Nutiu, R.; Li, Y. Structure-Switching Signaling Aptamers. *J. Am. Chem. Soc.* **2003**, *125* (16), 4771–4778. https://doi.org/10.1021/ja028962o.

(19) Nutiu, R.; Li, Y. Structure-Switching Signaling Aptamers: Transducing Molecular Recognition into Fluorescence Signaling. *Chem. Eur. J.* **2004**, *10* (8), 1868–1876. https://doi.org/10.1002/chem.200305470.

(20) Munzar, J. D.; Ng, A.; Juncker, D. Duplexed Aptamers: History, Design, Theory, and Application to Biosensing. *Chem. Soc. Rev.* **2019**, *48* (5), 1390–1419. https://doi.org/10.1039/C8CS00880A.

(21) Hui, C. Y.; Li, Y.; Brennan, J. D. Fluorescence Analysis of the Properties of Structure-Switching DNA Aptamers Entrapped in Sol–Gel-Derived Silica Materials. *Chem. Mater.* **2014**, *26* (5), 1896–1904. https://doi.org/10.1021/cm404114g.

(22) Hui, C. Y.; Lau, P. S.; Li, Y.; Brennan, J. D. Investigation of RNA Structure-Switching Aptamers in Tunable Sol–Gel-Derived Materials. *J Sol-Gel Sci Technol* **2019**, *89* (1), 234–243. https://doi.org/10.1007/s10971-018-4588-z.

(23) Huizenga, D. E.; Szostak, J. W. A DNA Aptamer That Binds Adenosine and ATP. *Biochemistry* **1995**, *34* (2), 656–665. https://doi.org/10.1021/bi00002a033.

(24) Wang, K.; Tang, Z.; Yang, C. J.; Kim, Y.; Fang, X.; Li, W.; Wu, Y.; Medley, C. D.; Cao, Z.; Li, J.; Colon, P.; Lin, H.; Tan, W. Molecular Engineering of DNA: Molecular Beacons. *Angew. Chem. Int. Ed.* **2009**, *48* (5), 856–870. https://doi.org/10.1002/anie.200800370.

(25) Armstrong, R. E.; Strouse, G. F. Rationally Manipulating Aptamer Binding Affinities in a Stem-Loop Molecular Beacon. *Bioconjugate Chem.* **2014**, *25* (10), 1769–1776. https://doi.org/10.1021/bc500286r.

(26) Wilson, B. D.; Hariri, A. A.; Thompson, I. A. P.; Eisenstein, M.; Soh, H. T. Independent Control of the Thermodynamic and Kinetic Properties of Aptamer Switches. *Nat Commun* **2019**, *10* (1), 5079. https://doi.org/10.1038/s41467-019-13137-x.

(27) Rupcich, N.; Nutiu, R.; Li, Y.; Brennan, J. D. Entrapment of Fluorescent Signaling DNA Aptamers in Sol−Gel-Derived Silica. *Anal. Chem.* **2005**, *77* (14), 4300–4307. https://doi.org/10.1021/ac0506480.

(28) Munzar, J. D.; Ng, A.; Corrado, M.; Juncker, D. Complementary Oligonucleotides Regulate Induced Fit Ligand Binding in Duplexed Aptamers. *Chem. Sci.* **2017**, *8* (3), 2251–2256. https://doi.org/10.1039/C6SC03993F.

(29) Munzar, J. D.; Ng, A.; Juncker, D. Comprehensive Profiling of the Ligand Binding Landscapes of Duplexed Aptamer Families Reveals Widespread Induced Fit. *Nat Commun* **2018**, *9* (1), 343. https://doi.org/10.1038/s41467-017-02556-3.

(30) Xu, Y.; Wu, Q.; Sun, Y.; Bai, H.; Shi, G. Three-Dimensional Self-Assembly of Graphene Oxide and DNA into Multifunctional Hydrogels. *ACS Nano* **2010**, *4* (12), 7358–7362. https://doi.org/10.1021/nn1027104.

(31) Tan, B.; Zhao, H.; Du, L.; Gan, X.; Quan, X. A Versatile Fluorescent Biosensor Based on Target-Responsive Graphene Oxide Hydrogel for Antibiotic Detection. *Biosensors and Bioelectronics* **2016**, *83*, 267–273. https://doi.org/10.1016/j.bios.2016.04.065.

(32) Monton, M. R. N.; Forsberg, E. M.; Brennan, J. D. Tailoring Sol–Gel-Derived Silica Materials for Optical Biosensing. *Chem. Mater.* **2012**, *24* (5), 796–811. https://doi.org/10.1021/cm202798e.

(33) Mateen, R.; Ali, M. M.; Hoare, T. A Printable Hydrogel Microarray for Drug Screening Avoids False Positives Associated with Promiscuous Aggregating Inhibitors. *Nat Commun* **2018**, *9* (1), 602. https://doi.org/10.1038/s41467-018-02956-z.

(34) Pikula, M.; Ali, M. M.; Filipe, C.; Hoare, T. Single-Step Printable Hydrogel Microarray Integrating Long-Chain DNA for the Discriminative and Size-Specific Sensing of Nucleic Acids. *ACS Appl. Mater. Interfaces* **2021**, *13* (2), 2360–2370. https://doi.org/10.1021/acsami.0c21061.

(35) Smeets, N. M. B.; Bakaic, E.; Patenaude, M.; Hoare, T. Injectable and Tunable Poly(Ethylene Glycol) Analogue Hydrogels Based on Poly(Oligoethylene Glycol Methacrylate). *Chem. Commun.* **2014**, *50* (25), 3306. https://doi.org/10.1039/c3cc48514e.

(36) Smeets, N. M. B.; Bakaic, E.; Patenaude, M.; Hoare, T. Injectable Poly(Oligoethylene Glycol Methacrylate)-Based Hydrogels with Tunable Phase Transition Behaviours: Physicochemical and Biological Responses. *Acta Biomaterialia* **2014**, *10* (10), 4143–4155. https://doi.org/10.1016/j.actbio.2014.05.035.

(37) Carrasquilla, C.; Kapteyn, E.; Li, Y.; Brennan, J. D. Sol-Gel-Derived Biohybrid Materials Incorporating Long-Chain DNA Aptamers. *Angew. Chem. Int. Ed.* **2017**, *56* (36), 10686–10690. https://doi.org/10.1002/anie.201702859.

(38) You, Y.; Tataurov, A. V.; Owczarzy, R. Measuring Thermodynamic Details of DNA Hybridization Using Fluorescence. *Biopolymers* **2011**, *95* (7), 472–486. https://doi.org/10.1002/bip.21615.

(39) Spiess, A.-N.; Feig, C.; Ritz, C. Highly Accurate Sigmoidal Fitting of Real-Time PCR Data by Introducing a Parameter for Asymmetry. *BMC Bioinformatics* **2008**, *9* (1), 221. https://doi.org/10.1186/1471-2105-9-221.

(40) Schroeder, S. J.; Turner, D. H. Optical Melting Measurements of Nucleic Acid Thermodynamics. In *Methods in Enzymology*; Elsevier, 2009; Vol. 468, pp 371–387. https://doi.org/10.1016/S0076-6879(09)68017-4.

(41) Wu, P.; Nakano, S.; Sugimoto, N. Temperature Dependence of Thermodynamic Properties for DNA/DNA and RNA/DNA Duplex Formation: Temperature Dependence of Thermodynamic Properties. *European Journal of Biochemistry* **2002**, *269* (12), 2821–2830. https://doi.org/10.1046/j.1432-1033.2002.02970.x.

(42) Markham, N. R.; Zuker, M. DINAMelt Web Server for Nucleic Acid Melting Prediction. *Nucleic Acids Research* **2005**, *33* (Web Server), W577–W581. https://doi.org/10.1093/nar/gki591.

(43) Marras, S. A. E.; Kramer, F. R.; Tyagi, S. Efficiencies of Fluorescence Resonance Energy Transfer and Contact-Mediated Quenching in Oligonucleotide Probes. *Nucleic Acids Research* **2002**, *30* (21), 8.

(44) Hall, B.; Cater, S.; Levy, M.; Ellington, A. D. Kinetic Optimization of a Protein-Responsive Aptamer Beacon. *Biotechnol. Bioeng.* **2009**, *103* (6), 1049–1059. https://doi.org/10.1002/bit.22355.

(45) Chen, M.; Wang, Y.; Zhang, J.; Peng, Y.; Li, S.; Han, D.; Ren, S.; Qin, K.; Li, S.; Gao, Z. Stimuli-Responsive DNA-Based Hydrogels for Biosensing Applications. *J Nanobiotechnol* **2022**, *20* (1), 40. https://doi.org/10.1186/s12951-022-01242-x.

(46) Miyoshi, D.; Nakamura, K.; Tateishi-Karimata, H.; Ohmichi, T.; Sugimoto, N. Hydration of Watson−Crick Base Pairs and Dehydration of Hoogsteen Base Pairs Inducing Structural Polymorphism under Molecular Crowding Conditions. *J. Am. Chem. Soc.* **2009**, *131* (10), 3522–3531. https://doi.org/10.1021/ja805972a.

(47) Sugimoto, N.; Nakano, S.; Katoh, M.; Matsumura, A.; Nakamuta, H.; Ohmichi, T.; Yoneyama, M.; Sasaki, M. Thermodynamic Parameters To Predict Stability of RNA/DNA Hybrid Duplexes. *Biochemistry* **1995**, *34* (35), 11211–11216. https://doi.org/10.1021/bi00035a029.

(48) Moreira, B. G.; You, Y.; Behlke, M. A.; Owczarzy, R. Effects of Fluorescent Dyes, Quenchers, and Dangling Ends on DNA Duplex Stability. *Biochemical and Biophysical Research Communications* **2005**, *327* (2), 473–484. https://doi.org/10.1016/j.bbrc.2004.12.035.

(49) Bakaic, E.; Smeets, N. M. B.; Dorrington, H.; Hoare, T. "Off-the-Shelf" Thermoresponsive Hydrogel Design: Tuning Hydrogel Properties by Mixing Precursor Polymers with Different Lower-Critical Solution Temperatures. *RSC Adv.* **2015**, *5* (42), 33364–33376. https://doi.org/10.1039/C5RA00920K.

(50) Nakano, S.; Yamaguchi, D.; Sugimoto, N. Thermal Stability and Conformation of DNA and Proteins under the Confined Condition in the Matrix of Hydrogels. *Mol Biol Rep* **2018**, *45* (4), 403–411. https://doi.org/10.1007/s11033-018-4174-z.

(51) Nakano, S.; Miyoshi, D.; Sugimoto, N. Effects of Molecular Crowding on the Structures, Interactions, and Functions of Nucleic Acids. *Chem. Rev.* **2014**, *114* (5), 2733–2758. https://doi.org/10.1021/cr400113m.

(52) Knowles, D. B.; LaCroix, A. S.; Deines, N. F.; Shkel, I.; Record, M. T. Separation of Preferential Interaction and Excluded Volume Effects on DNA Duplex and Hairpin Stability. *Proceedings of the National Academy of Sciences* **2011**, *108* (31), 12699–12704. https://doi.org/10.1073/pnas.1103382108.

(53) Spink, C. H.; Chaires, J. B. Effects of Hydration, Ion Release, and Excluded Volume on the Melting of Triplex and Duplex DNA. *Biochemistry* **1999**, *38* (1), 496–508. https://doi.org/10.1021/bi9820154.

(54) Bakaic, E.; Smeets, N. M. B.; Hoare, T. Injectable Hydrogels Based on Poly(Ethylene Glycol) and Derivatives as Functional Biomaterials. *RSC Adv.* **2015**, *5* (45), 35469–35486. https://doi.org/10.1039/C4RA13581D.

(55) Carrasquilla, C.; Lau, P. S.; Li, Y.; Brennan, J. D. Stabilizing Structure-Switching Signaling RNA Aptamers by Entrapment in Sol–Gel Derived Materials for Solid-Phase Assays. *J. Am. Chem. Soc.* **2012**, *134* (26), 10998–11005. https://doi.org/10.1021/ja304064a.

(56) Oishi, M.; Nakatani, K. Dynamically Programmed Switchable DNA Hydrogels Based on a DNA Circuit Mechanism. *Small* **2019**, *15* (15), 1900490. https://doi.org/10.1002/smll.201900490.

(57) Li, Y.; Gao, H.; Qi, Z.; Huang, Z.; Ma, L.; Liu, J. Freezing-Assisted Conjugation of Unmodified Diblock DNA to Hydrogel Nanoparticles and Monoliths for DNA and Hg^{2+} Sensing. *Angew. Chem. Int. Ed.* **2021**, *60* (23), 12985–12991. https://doi.org/10.1002/anie.202102330.

(58) Lizárraga, B.; Sánchez-Romero, D.; Gil, A.; Melgar, E. The Role of Ca2+ on pH-Induced Hydrodynamic Changes of Bovine Pancreatic Deoxyribonuclease A. *Journal of Biological Chemistry* **1978**, *253* (9), 3191–3195. https://doi.org/10.1016/S0021-9258(17)40822-2.

(59) Psychogios, N.; Hau, D. D.; Peng, J.; Guo, A. C.; Mandal, R.; Bouatra, S.; Sinelnikov, I.; Krishnamurthy, R.; Eisner, R.; Gautam, B.; Young, N.; Xia, J.; Knox, C.; Dong, E.; Huang, P.; Hollander, Z.; Pedersen, T. L.; Smith, S. R.; Bamforth, F.; Greiner, R.; McManus, B.; Newman, J. W.; Goodfriend, T.; Wishart, D. S. The Human Serum Metabolome. *PLoS ONE* **2011**, *6* (2), e16957. https://doi.org/10.1371/journal.pone.0016957.

(60) Sylvia, P.; Brehm, S. O.; Hoch, H. J. A. DNA-Binding Proteins in Human Serum. *Biochemical and Biophysical Research Communications* **1975**, *63* (1), 24–31. https://doi.org/10.1016/S0006-291X(75)80005-2.

(61) Xia, T.; Yuan, J.; Fang, X. Conformational Dynamics of an ATP-Binding DNA Aptamer: A Single-Molecule Study. *J. Phys. Chem. B* **2013**, *117* (48), 14994–15003. https://doi.org/10.1021/jp4099667.

(62) Hermann, T.; Patel, D. J. Adaptive Recognition by Nucleic Acid Aptamers. *Science* **2000**, *287* (5454), 820–825. https://doi.org/10.1126/science.287.5454.820.

(63) Lin, C. H.; Patei, D. J. Structural Basis of DNA Folding and Recognition in an AMP-DNA Aptamer Complex: Distinct Architectures but Common Recognition Motifs for DNA and RNA Aptamers Complexed to AMP. *Chemistry & Biology* **1997**, *4* (11), 817–832. https://doi.org/10.1016/S1074-5521(97)90115-0.

(64) Li, L.-L.; Ge, P.; Selvin, P. R.; Lu, Y. Direct Detection of Adenosine in Undiluted Serum Using a Luminescent Aptamer Sensor Attached to a Terbium Complex. *Anal. Chem.* **2012**, *84* (18), 7852–7856. https://doi.org/10.1021/ac302167d.

(65) Huang, P.-J. J.; Liu, J. Flow Cytometry-Assisted Detection of Adenosine in Serum with an Immobilized Aptamer Sensor. *Anal. Chem.* **2010**, *82* (10), 4020–4026. https://doi.org/10.1021/ac9028505.

(66) Carrasquilla, C.; Li, Y.; Brennan, J. D. Surface Immobilization of Structure-Switching DNA Aptamers on Macroporous Sol−Gel-Derived Films for Solid-Phase Biosensing Applications. *Anal. Chem.* **2011**, *83* (3), 957–965. https://doi.org/10.1021/ac102679r.

(67) Zhang, Z.; Oni, O.; Liu, J. New Insights into a Classic Aptamer: Binding Sites, Cooperativity and More Sensitive Adenosine Detection. *Nucleic Acids Research* **2017**, *45* (13), 7593–7601. https://doi.org/10.1093/nar/gkx517.

3.6. Appendix – Supporting Information Chapter 3

3.6.1. POEGMA Polymer Synthesis and Characterization

Table S3.1 Recipes for the synthesis of hydrazide (H) and aldehyde (A)-functionalized poly(oligoethylene glycol methacrylate) (POEGMA) polymers (PO).

Polymer Precursor	Functional Group	$M(EO)_2MA$ (g)	$OEGMA_{500}$ (g)	AA (g)	DMEMAm (g)	TGA, (µL)	AIBMe (mg)
$PO_{10}H_{30}$	$NHNH_2$	3.10	0.90	0.55	-	7.5	37
$PO_{100}H_{30}$	$NHNH_2$	0	4.0	0.30	-	1.0	37
$PO_{10}A_{15}$	CHO	3.10	0.90	-	0.63	7.5	50
$PO_{50}A_{15}$	CHO	1.15	2.85	-	0.36	4	50

Table S3.2 Physicochemical properties of synthesized hydrazide-functionalized (POH) and aldehyde-functionalized (POA) poly(oligoethylene glycol methacrylate) (POEGMA) polymers.

Polymer Precursor	Functional Monomer	Functional Monomer, mol%	M_n, $\times 10^3$ g/mol	$Đ$
$PO_{10}H_{30}$	$NHNH_2$	20.0 [a]	14.6	2.8
$PO_{100}H_{30}$	$NHNH_2$	21.3 [a]	19.3	2.7
$PO_{10}A_{15}$	CHO	11.1 [b]	12.5	2.5
$PO_{50}A_{15}$	CHO	8.7 [b]	15.9	2.7

[a] Determined by conductometric titration. [b] Determined by ^{1}H-NMR.

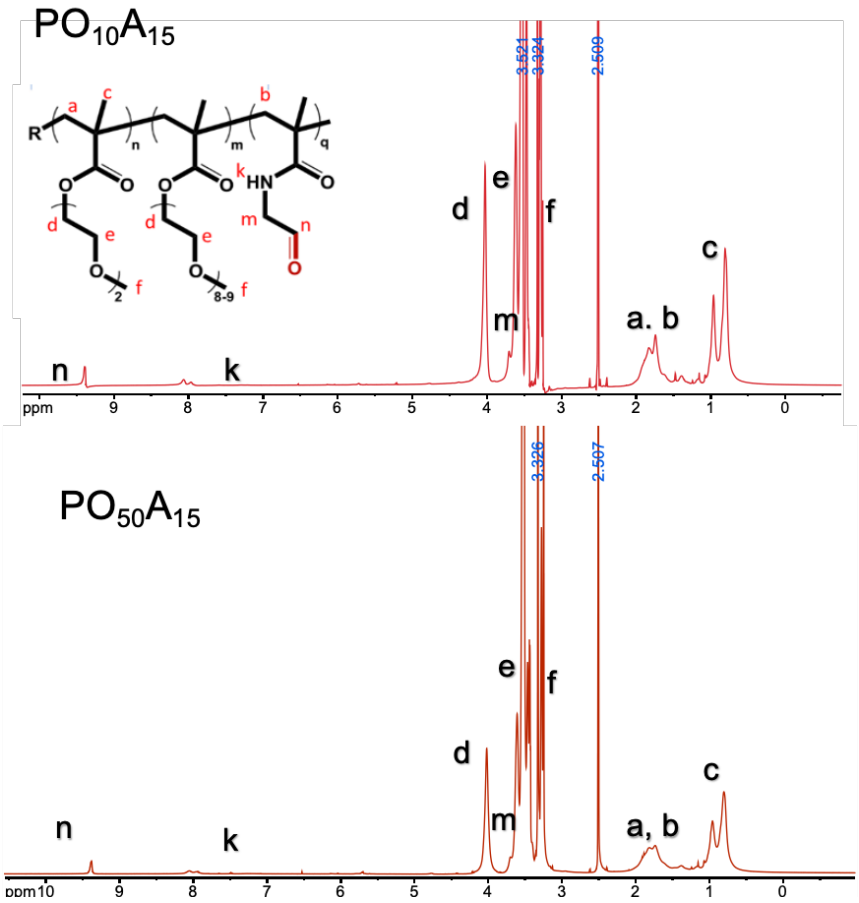

Figure S3.1 ^{1}H NMR spectra *(DMSO*-d_6*)* of aldehyde-functionalized (POA) poly(oligoethylene glycol methacrylate) (POEGMA) precursor polymers. Chemical shifts are reported relative to the residual deuterated solvent peaks. Peak assignments given for each spectrum are based on the anticipated chemical structure of each polymer.[1–3]

a. i. $PO_{10}H_{30}$

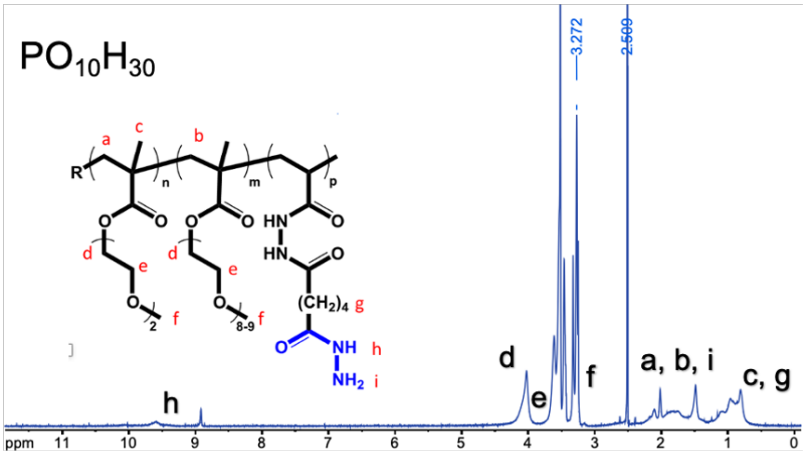

ii. $PO_{100}H_{30}$

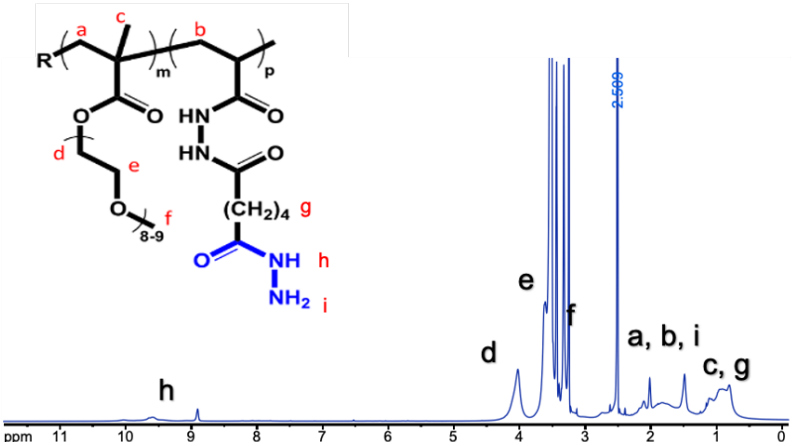

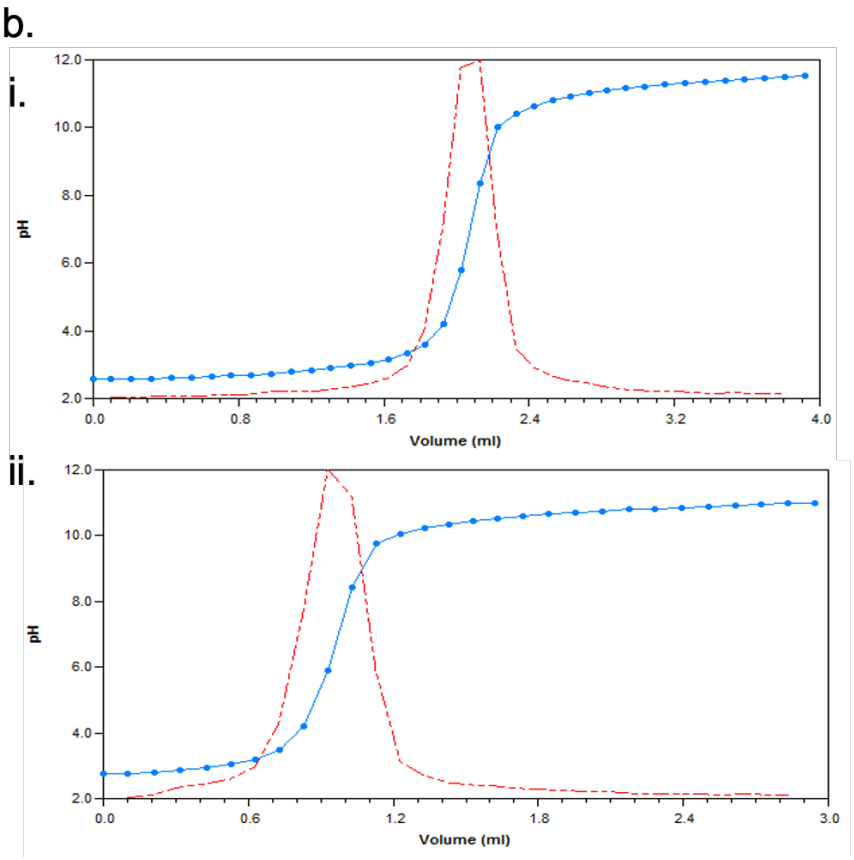

Figure S3.2 ^{1}H-NMR spectra *(DMSO*-d_6*)* (a) and conductometric pH-Volume titration curve (b) of hydrazide-functionalized (POH) poly(oligoethylene glycol methacrylate) (POEGMA) precursor polymers: $PO_{10}H_{30}$ (i) and $PO_{100}H_{30}$ (ii). Chemical shifts are reported relative to the residual deuterated solvent peaks. Peak assignments given for each spectrum are based on the anticipated chemical structure of each polymer.

3.6.2. Rheological Characterization of POEGMA Hydrogels

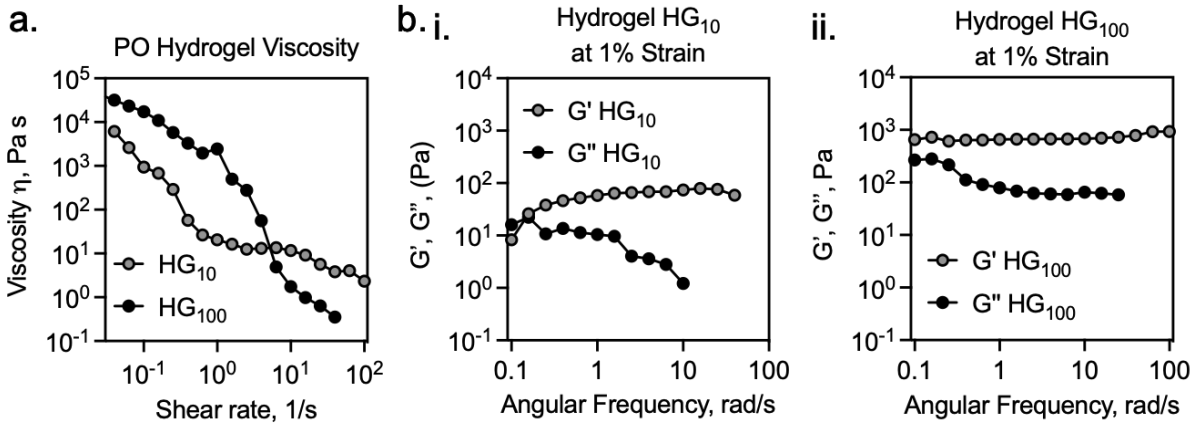

Figure S3.3 Mechanical properties of HG_{10} and HG_{100} hydrogels assessed through (a) viscosity versus shear rate flow sweep experiments and (b) frequency sweep rheology experiments at 1% strain for (i) HG_{10} and (ii) HG_{100}. The tests were performed using Discovery hybrid rheometer (DHR-2) TA instrument equipped with stainless steel Peltier plate using the 8 mm parallel plate geometry, using a gap size of 1000 µm for HG_{10} and 700 µm for HG_{100}. Flow sweep tests (viscosity vs. shear rate) were run at shear rates between 0.01 to 100 1/s, while oscillation frequency sweep tests (storage (G') and loss (G'') moduli vs. angular frequency) were run at angular frequencies between 0.1 to 100 rad/s at a 1.0% strain confirmed to lie within the linear viscoelastic range. The obtained results suggest that both hydrogels are shear thinning and are primarily elastic in their response (G'>G") over a large frequency range, both typical of hydrogel formulations.

3.6.3. Tripartite Aptamer Construct Design - Optimization

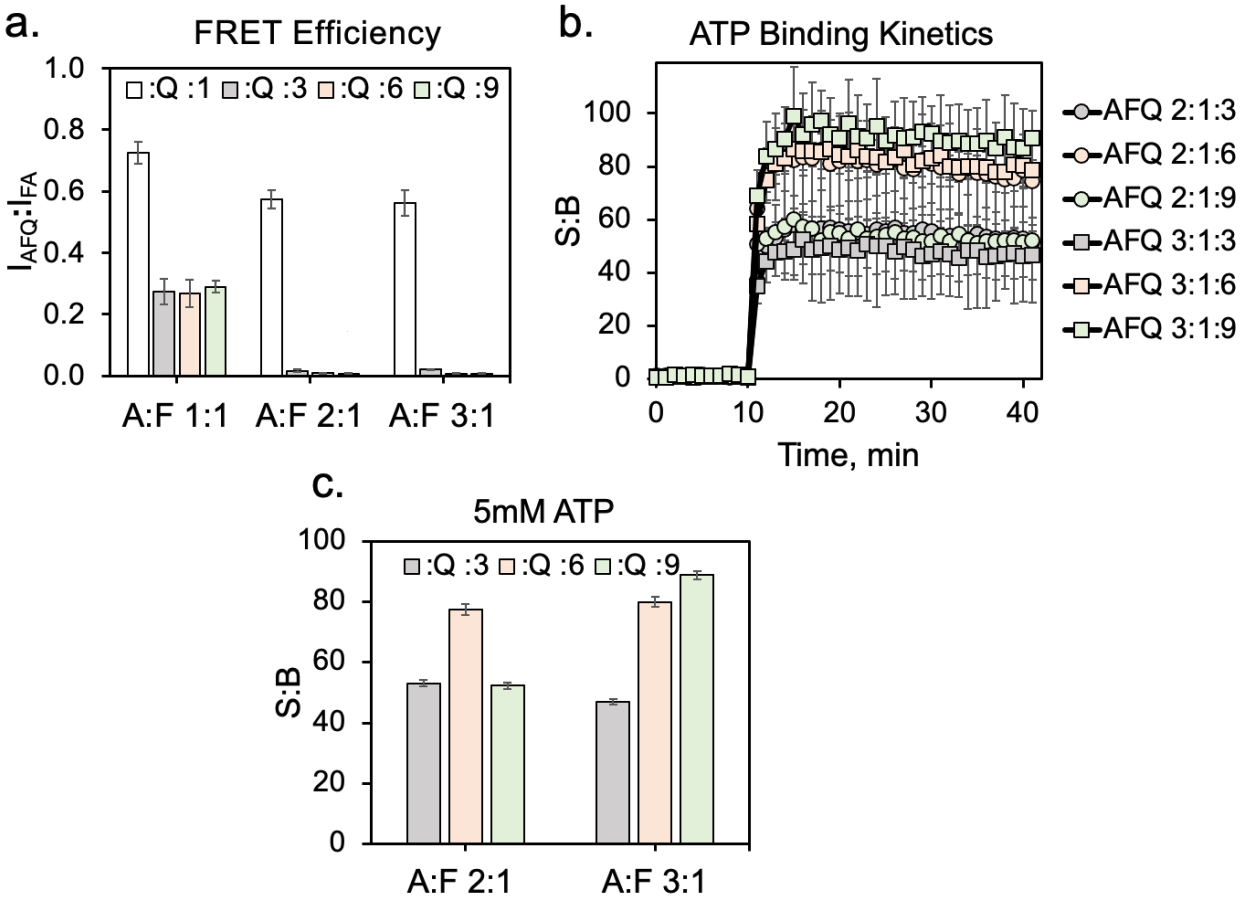

Figure S3.4 Optimization of fluorescence quenching in solution-based tripartite aptamer reporters. The A:F:Q molar ratio was optimized using the Q_{12} (12 bp stem length) Q-DNA. (a) Fluorescence quenching (FRET) of AFQ constructs prepared at a constant F-DNA (F) concentration of 100 nM and increasing molar equivalents of both the modified aptamer (A) and Q-DNA (Q); (b) Ligand binding kinetics assessed as a time-resolved signal enhancement relative to background fluorescence (S:B ratio) in selected AFQ reporters upon incubation with 5 mM ATP over 30 min at 25°C; The baseline florescence was collected every 60 s for 10 min prior to ligand addition; (c) Signal response at the end of the binding cycle in selected AFQ reporters at 5 mM ATP concentration. Error bars represent the standard deviation (SD) relative to three independent replicate experiments.

The optimal constructs were selected to be A:F:Q 2:1:3 (grey circles) and 2:1:6 (orange circles). Construct A:F:Q 2:1:6 was ultimately selected for use in subsequent experiments, as it allowed for higher quenching efficiency (a) without a trade-off in signaling (c).

3.6.4. Melting Curves of Tripartite Aptamer Encapsulated in Varying Concentrations of HG_{100}

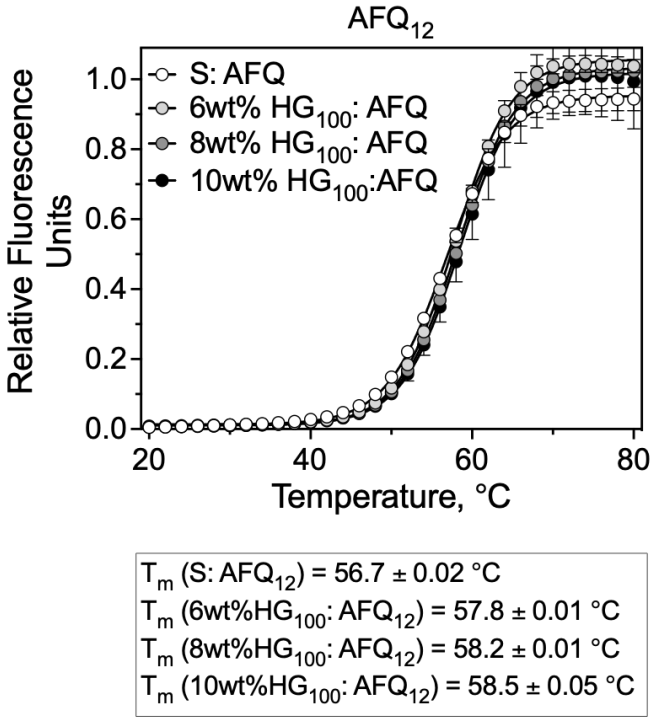

Figure S3.5 Melting profile of optimal tripartite aptamer reporter AFQ encapsulated in HG_{100} hydrogel prepared at varying precursor polymer concentrations. Fluorescence enhancement as a function of temperature for the 2:1:6 A:F:Q aptamer construct encapsulated in HG_{100} hydrogel prepared at precursor polymer concentrations of 6 wt%, 8 wt%, and 10 wt% relative to free solutions. Error bars represent the standard deviation (SD) based on three replicates.

Higher hydrogel concentrations do not provide significant improvement in thermal stability.

3.6.5. Evaluating Fluorometric Thermodynamic Parameters of Q-DNA Hybridization within Aptamer Reporters

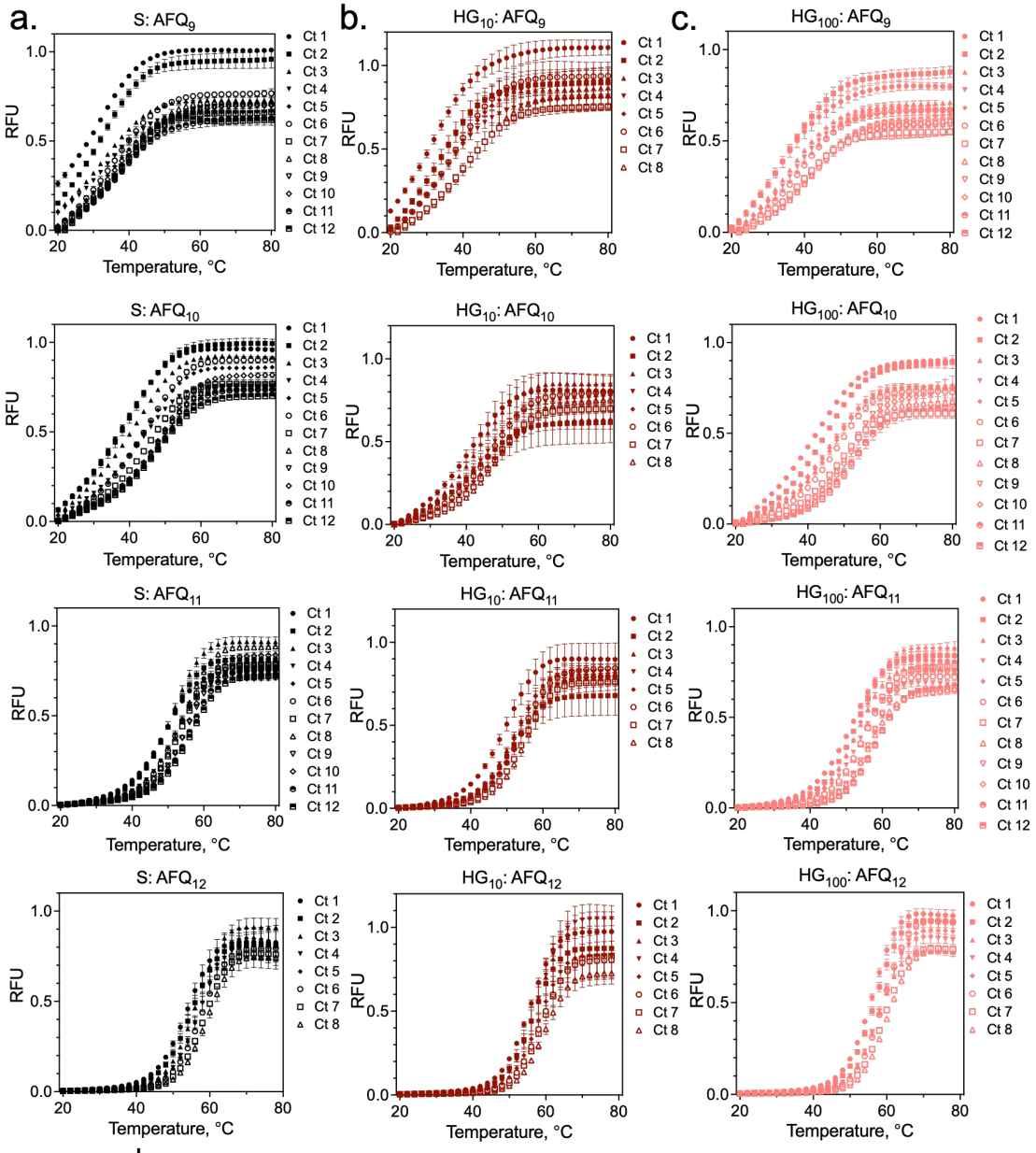

d.

Ct, μM	Ct 1	Ct 2	Ct 3	Ct 4	Ct 5	Ct 6	Ct 7	Ct 8	Ct 9	Ct 10	Ct 11	Ct 12
	315	450	585	720	900	1125	1350	1800	2250	2700	3150	3600
F, μM	35	50	65	80	100	125	150	200	250	300	350	400

Figure S3.6 Melting profiles of tripartite aptamer reporters (A:F:Q 2:1:6) in free solution (S:AFQ, column 1, a) and encapsulated in HG_{10} (column 2, b) or HG_{100} (column 3, c) hydrogels with quencher stem lengths of 9 bp (first row), 10 bp (second row), 11 bp (third row), and 12 bp (fourth row). The total strand concertation, C_t, was varied from 315 nM to 3600 nM (d). Thermal melting disrupts Watson-Crick base pairs in a highly cooperative manner and causes an increase in fluorescence as a function of temperature due to the melting of the Q-DNA strand.

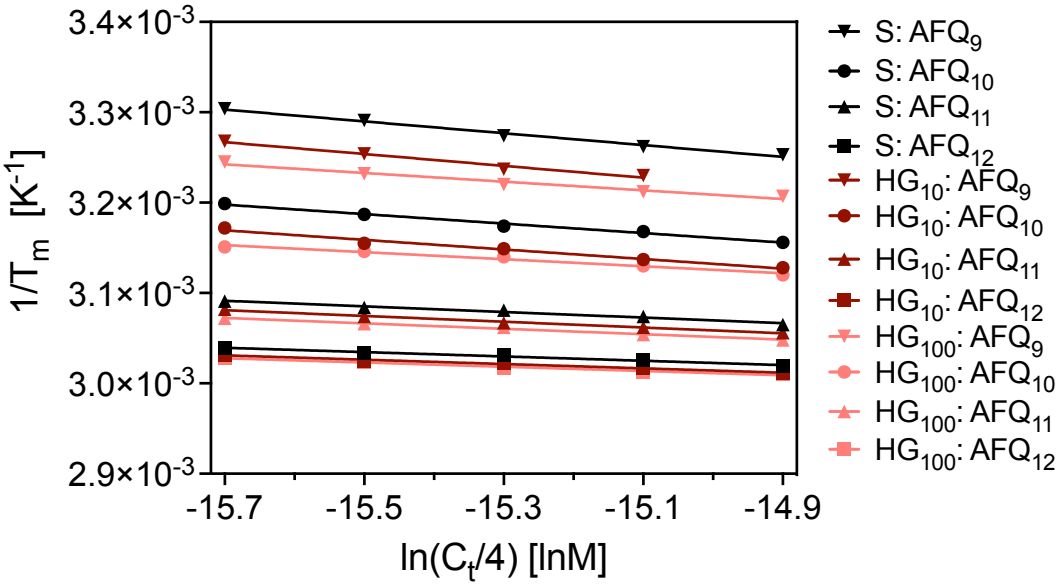

Figure S3.7 Van't Hoff plot for tripartite aptamer reporters (A:F:Q 2:1:6) prepared with quencher stem lengths of 9 bp, 10 bp, 11 bp, or 12 bp in either free solution (S:AFQ) or encapsulated in HG_{10} or HG_{100} hydrogel over five serial dilutions (C_t: 585 nM to 1350 nM). Each data point represents the mean value obtained from fitting triplicate FRET melting curves.

3.6.6. Encapsulation Efficiency of Tripartite Aptamer Constructs in POEGMA Hydrogels

Table S3.3 Residual fluorescence of F:A (100 nM F, no quencher strand) encapsulated in HG_{100} hydrogels prepared with different precursor polymer concentrations as a function of washing time.

HG_{100}: FA	**Fluorescence Retained, %**	
Washing Time	**8wt% HG_{100}**	**10wt% HG_{100}**
60 min	81 ± 1.2	79 ± 6.5
65 min	75 ± 2.8	77 ± 5.6
70 min	75 ± 3.3	74 ± 6.5

Table S3.4 Comparison between residual fluorescence of fluorophore-labeled single-stranded DNA containing aptamer sequence, Fa (100 nM Fa, without a quencher strand) and double-stranded fluorescent aptamer construct, F:A (100nM F: 200 nM A, without a quencher strand, designed as shown in Figure 3.1 of Main Text) encapsulated in 6 wt% HG_{100} hydrogel as a function of washing time.

HG_{100}: Fa* (Single-stranded DNA)	**Fluorescence Retained, %**	**HG_{100}: FA** (Double-stranded DNA)	**Fluorescence Retained, %**
Washing/Rinsing Time	**6wt% HG_{100}**	Washing/Rinsing Time	**6wt% HG_{100}**
Wash 1 (60 min)	87 ± 4.7	Wash 1 (60 min)	86 ± 2.6
Rinse (1x5 min)	75 ± 3.7	Rinse (2x5 min)	75 ± 2.4
Wash 2 (60 min)	71 ± 3.1	Wash 2 (60 min)	73 ± 4.9

*The sequence Fa is designed as follows:

Fa: 5'-TTTTTTTTTTTTTTTTTTTTTTTTTTTTTTTT**F(T)***AAGAT***ACCTGGGGGAGTATTGCGGAGGAAGGT**-3'

3.6.7. Nuclease Activity (DNase I)

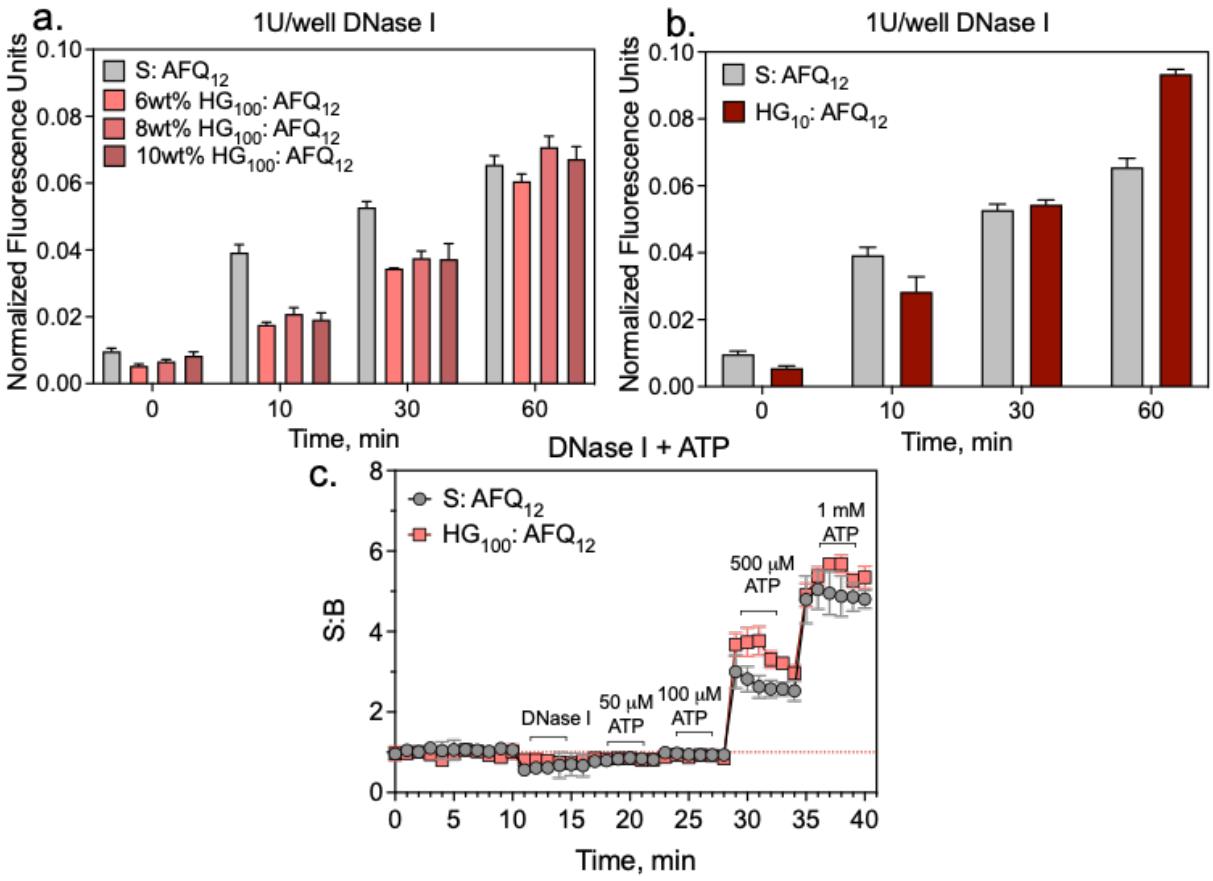

Figure S3.8 Nucleolytic degradation upon exposure to 1 U/well of DNase I of aptamer reporter AFQ_{12} in free solution ($S:AFQ_{12}$) or encapsulated in: (a) HG_{100} of varying concentrations (6 wt%; 8 wt%; 10 wt% precursor polymer concentrations used) or (b) 6 wt% HG_{10}. (c) Signaling ability (i.e., signal-to-baseline fluorescence ratio) of tripartite aptamer reporter AFQ_{12} in free solution or encapsulated in 6w*t* % HG_{100} during exposure to 1 U/well of DNase I. Baseline fluorescence was collected over an initial 10 min interval followed by DNAse I injection, after which the S:B ratio was tracked for an additional 5 min. After DNase I injection, ATP was injected at increasing concentrations at 5-minute intervals. The sensors retained their sensing ability (i.e., maintaining a S:B above the red dotted line equivalent to S:B = 1) even in the presence of nuclease at only slightly lower S:B ratios, suggesting the stability of the sensor performance even in the presence of a nucleolytic environment. Error bars represent the standard deviation (SD) based on three replicates.

3.6.8. Ligand Binding Kinetic Assay

Table S3.5 Summary of Figure 3.4c data on ligand binding kinetics showing the optimal performance of the AFQ_{10} reporter.

Parameter	**Tripartite Aptamer Reporter**	**AFQ_{12}**	**AFQ_{11}**	**AFQ_{10}**	**AFQ_{9}**
Ligand Binding Rate, min	**S:**	10-11	6	5	8-9
AFQ Activation, %		50 ± 4.0	86 ± 2.2	89 ± 2.4	85 ± 4.4
Ligand Binding Rate, min	**HG_{10}:**	10 – 11	7-8	5-6	12
AFQ Activation, %		39 ± 1.1	71 ± 3.1	75 ± 0.9	48 ± 1.2
Ligand Binding Rate, min	**HG_{100}:**	11-12	5-6	4	10-11
AFQ Activation, %		65 ± 1.1	89 ± 5.7	93 ± 6.8	80 ± 6.1

3.6.9. Optimizing the Target Binding Assay in Hydrogel Materials (1)

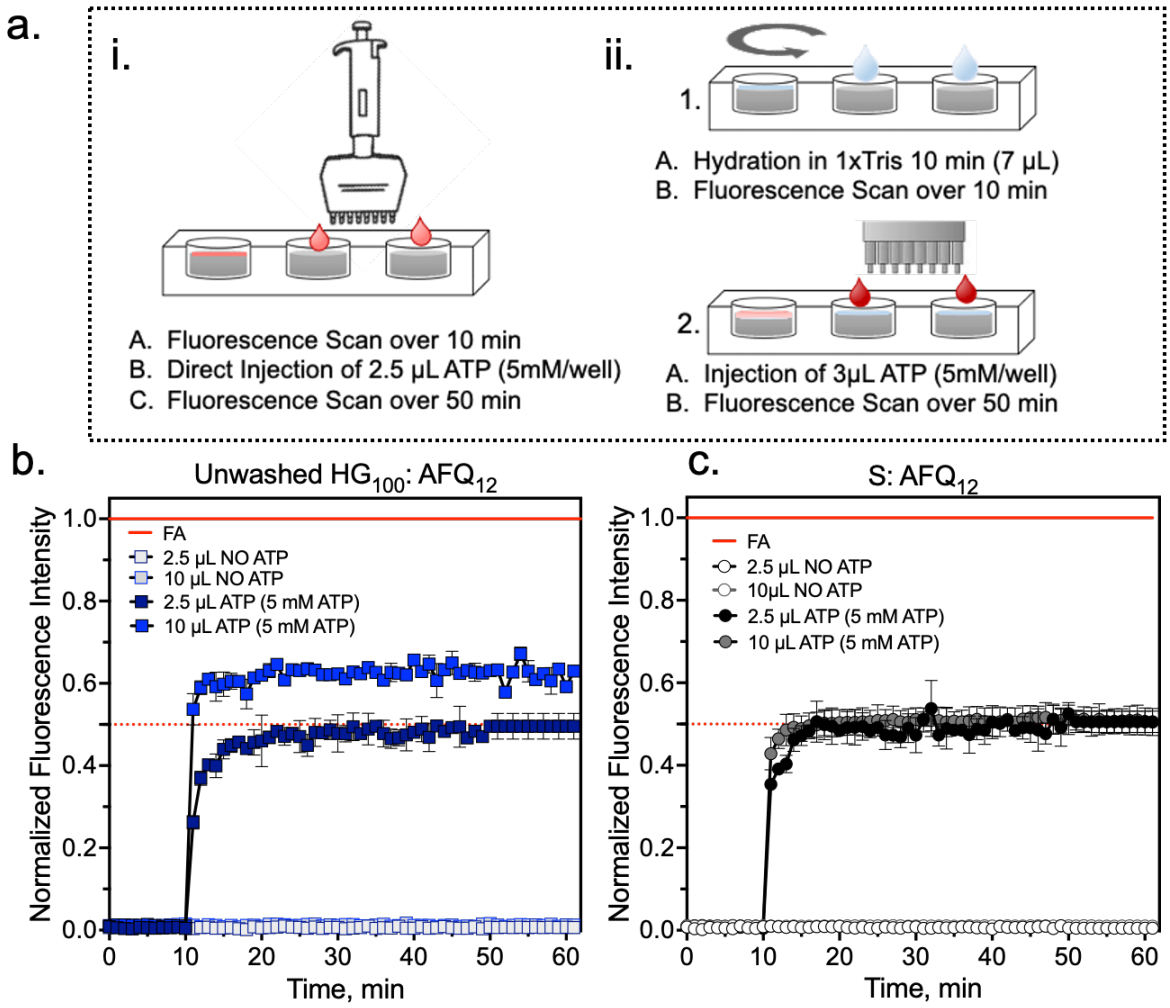

Figure S3.9 Signal response and binding kinetics of AFQ_{12} reporters exposed to 5 mM ATP injected at varying volumes. (a) Schematic of ligand binding with ATP added either (i) directly or (ii) into pre-hydrated hydrogel samples in 1xAssay buffer (1xTris Selection Buffer) as a concentrated solution to achieve a final concentration of 5 mM/well; (b) 6wt% HG_{100}: AFQ_{12} was used directly following the gelation step (unwashed HG). Baseline fluorescence was monitored over an intial 10 min interval followed by an additional 50 min after the injection of various volumes of ATP solution to obtain 5 mM ATP concentration/well at 25°C. Controls were conducted by adding the same volume of buffer without the ATP. (c) Signal response in the free solution construct S: AFQ_{12} in response to adding varying volumes of ATP solution to obtain 5 mM ATP concentration/well, over 60 min at 25°C. The solid red line represents fluorescent aptamer F:A in the absence of quencher (normalized as 1 Unit), while the red dotted line represents 50% of fluorescence recovery. Filled markers represent the samples treated with ATP while unfilled markers represent samples treated with buffer only. Error bars represent standard deviation (SD) based on three replicates.

3.6.10. Optimizing the Target Binding Assay in Hydrogel Materials (2)

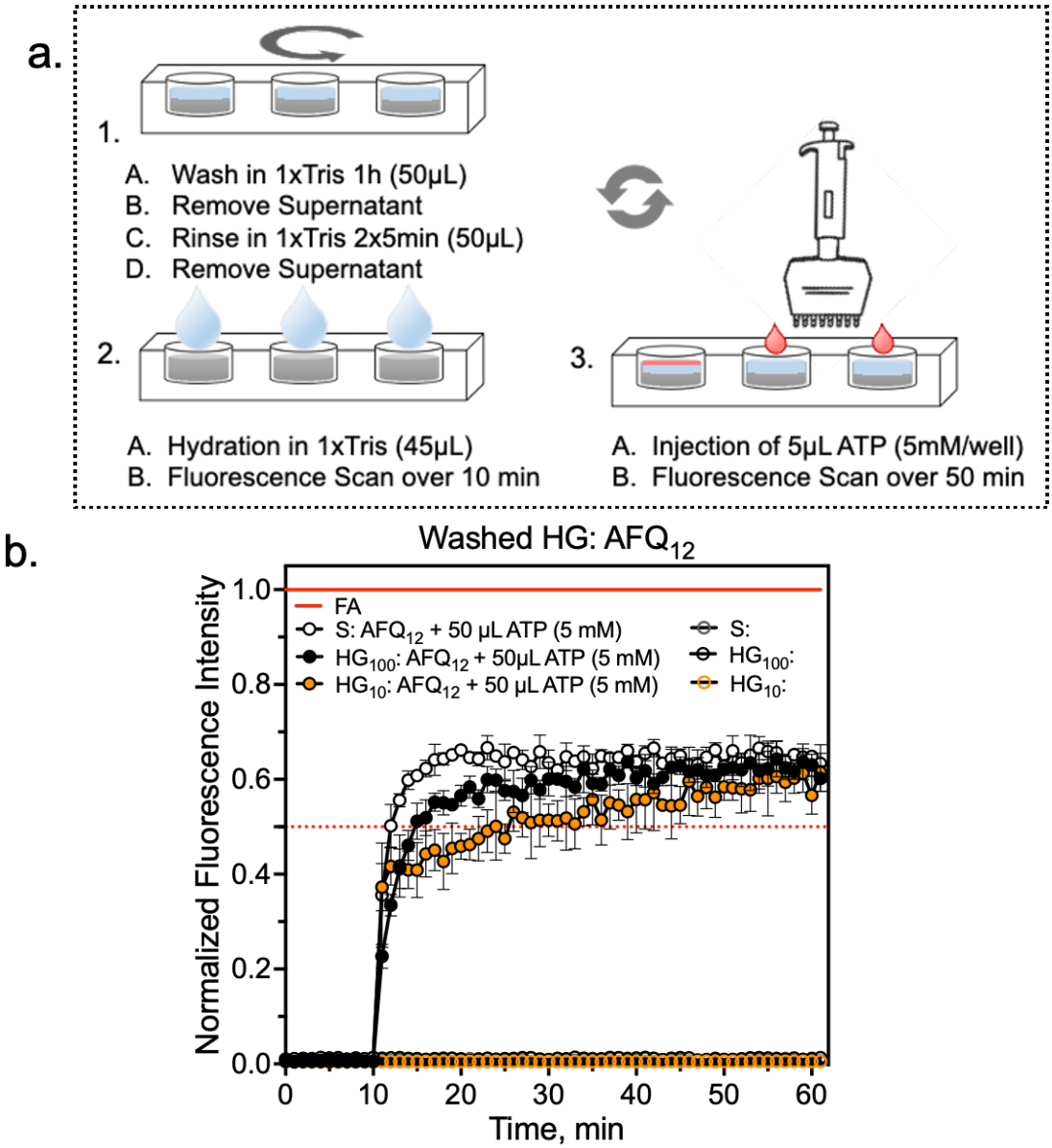

Figure S3.10 Signal response and binding kinetics of AFQ_{12} reporters with 5 mM of ATP in washed HG_{10} and HG_{100} relative to solution-based reporters over 60 min at 25°C. (a) Schematic of ligand binding with ATP added to pre-treated hydrogel samples. (b) 6 wt% HG:AFQ_{12} hydrogels were washed and pre-hydrated (washed HG) in 1xAssay buffer (1xTris). Baseline fluorescence was monitored over an intial 10 min interval, followed by additional 50 min after the injection of 50 µL of ATP solution to obtain 5 mM ATP concentration/well at 25°C. The solid red line represents fluorescent aptamer F:A in the absence of quencher, defined as 1 Unit, while the red dotted line represents 50% fluorescence recovery, defined as 0.5 Units. Filled markers represent the samples treated with ATP while unfilled markers represent samples treated with buffer only. Error bars represent the standard deviation (SD) based on three replicates.

3.6.11. Long Term Stability of Aptamer Constructs AFQ_{12} and AFQ_{10} encapsulated in HG_{100} or free-in-solution

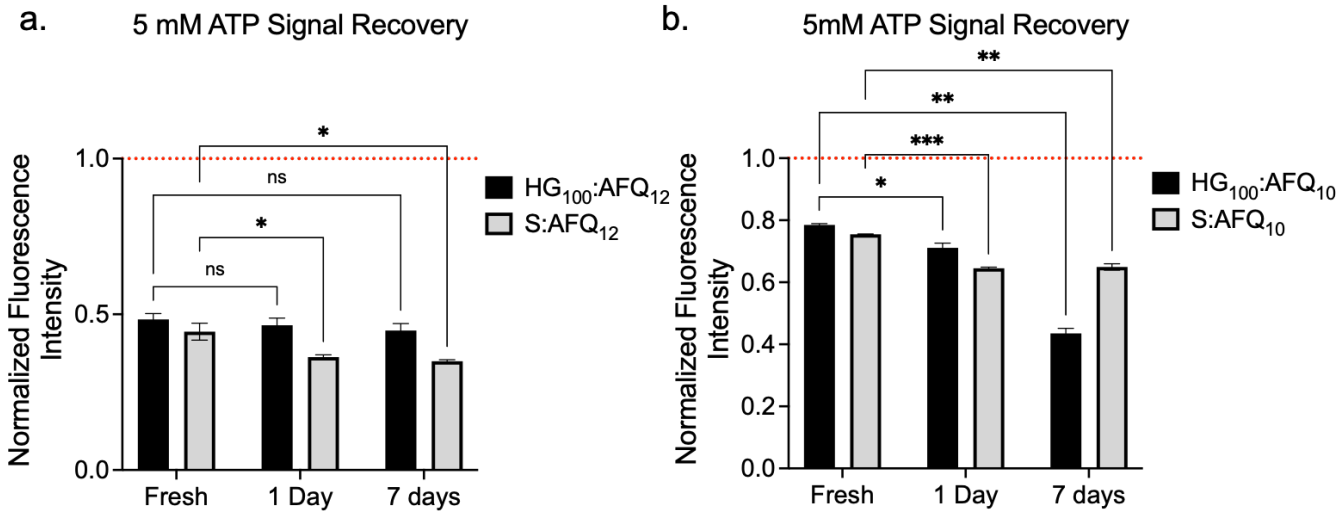

Figure S3.11 Signal recovery of aptamer constructs (a) AFQ_{12} and (b) AFQ_{10} encapsulated in hydrogel (HG_{100}) or free-in-solution (S) following 7-day storage at ambient conditions.

Assembled aptamer constructs were tested for fluorescence recovery following 60 min exposure to a saturating ATP concentration of 5 mM/well and analyzed fresh or after 1 or 7 days of storage at room temperature. Hydrogel-based samples prepared fresh or tested after 1 day of storage were used as is, while 7-day-old samples were re-hydrated with 50 µL/well in 1xAssay buffer over 30 min prior to the ligand-binding assay. (a) After one or seven days of storage, the solution-based AFQ_{12} aptamer construct retained 81.8 ± 4.1% and 78.8 ± 4.1% of their activity relative to the fresh samples respectively; in contrast, hydrogel-encapsulated AFQ_{12} sensors preserved 96.1 ± 3.2% and 92.7 ± 4.4% of their activity after 1 day or 7 days of ambient storage respectively relative to the fresh samples. (b) Solution-based aptamer construct assembled with shorter quencher strand AFQ_{10} preserved 85.6 ± 0.3% and 86.1 ± 1.2% of their activity relative to fresh samples, following 1 day and 7 days of ambient storage respectively while hydrogel encapsulation maintains 90.6 ± 1.5% of activity after 1 day of ambient storage and 55.5% ± 2.4% activity after 7 days of ambient storage. The lower fluorescence recovery observed after 7 days of storage of the HG_{100}:AFQ_{10} construct was attributed to the higher stabilizing potential that hydrogel exerts on shorter quencher strands; upon aging, this construct generates even higher FRET efficiency and thus lower ligand-induced recovery. Error bars represent the standard deviation (SD) based on three replicates.

3.6.12. Aptamer Reporter Binding Selectivity

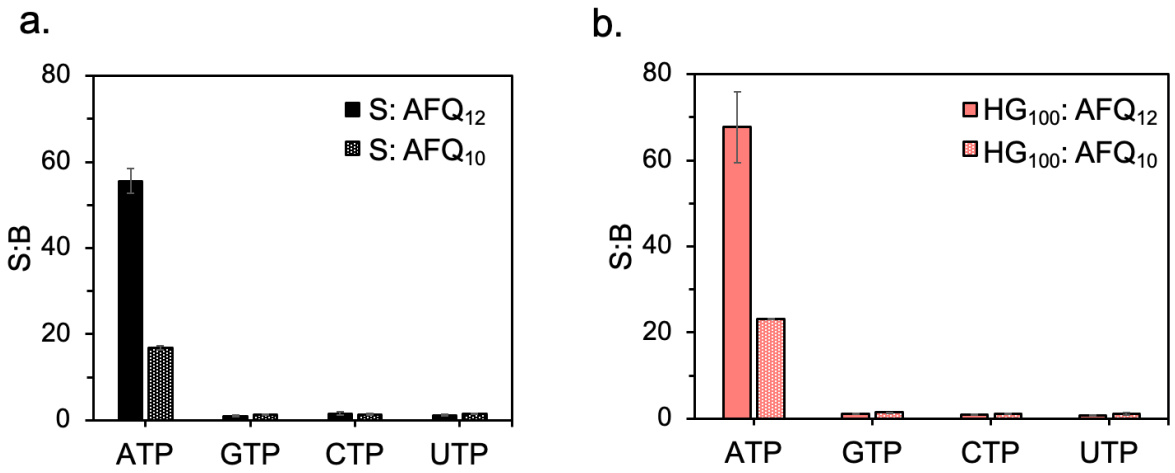

Figure S3.12 Selecitivty of AFQ_{12} and AFQ_{10} tripartite aptamer reporters as: (a) constructs in free solution or (b) physically encapsulated in HG_{100} hydrogel. Nucleoside triphosphates (ATP, GTP, CTP or UTP) were added at a volume of 10 µL/well at a concetration of 5 mM/well at 25 °C, with the fluorescence tracked over 60 min. The encapsulated aptamer reporter retains high selectivity towards adenine-based nucleotides similar to that observed in free solution. Error bars represent the standard deviation (SD) based on three replicates.

3.6.13. Binding Kinetics at Larger Sample Volumes: HG_{100}:AFQ_{10}

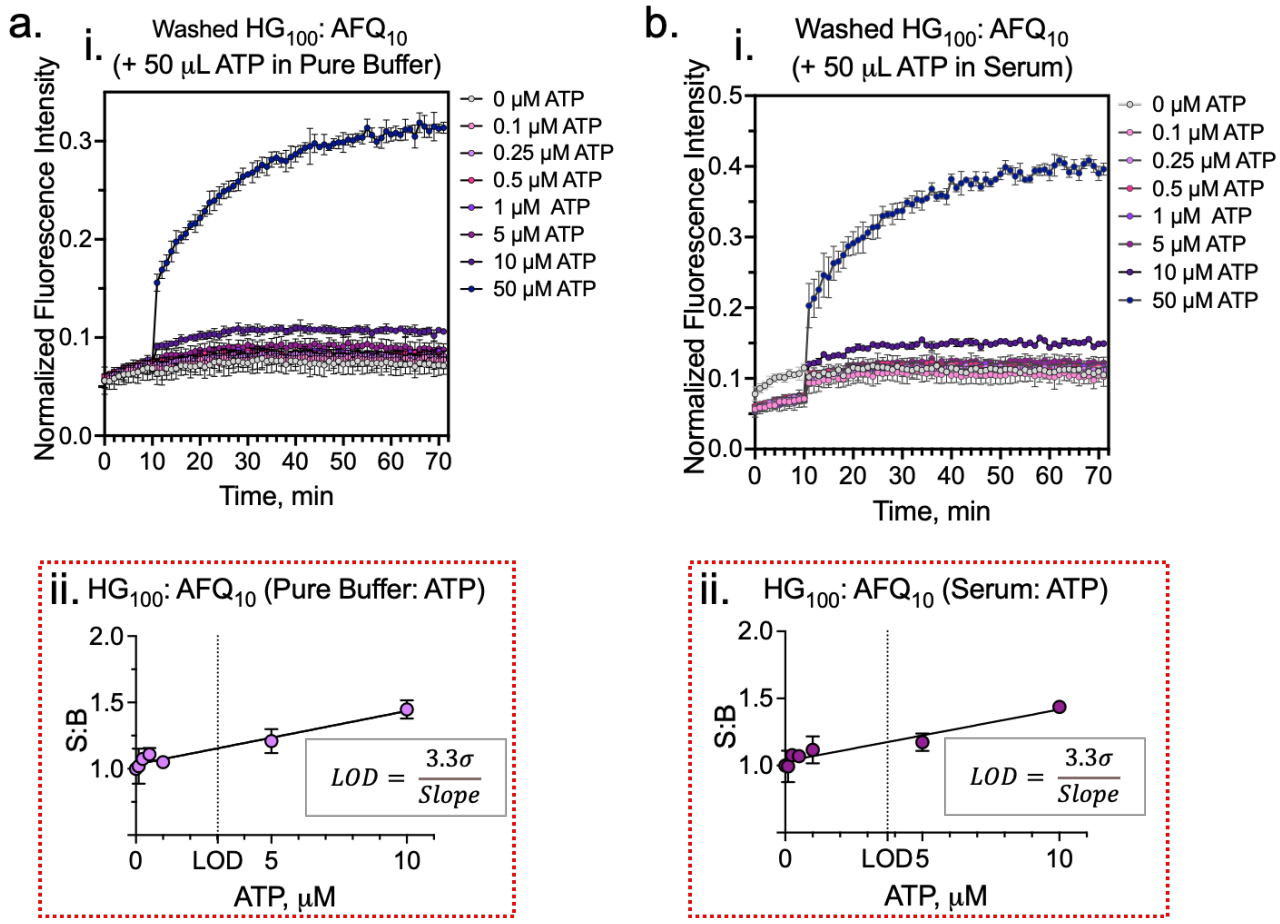

Figure S3.13 Binding kinetics of tripartite aptamer reporter AFQ_{10} physically encapsulated in HG_{100} hydrogel using 50 µL/well volumes of analyte with ATP concentrations ranging from 0.1-50 µM/well in: (a) pure 1xAssay buffer (Tris-ATP), and (b) undiluted serum (Serum-ATP) over 1 hour. Estimated LODs correspond to exposure to (i) Tris-ATP or (ii) Serum-ATP. Error bars represent the standard deviation (SD) based on three replicates.

3.6.14. Comparative study

Table S3.6 Comparison between the analytical performance of different hydrogel-based aptamer sensors in sensing small molecules.

Design strategy	Aptamer content	Aptamer attachment method	Detection method	Target	LOD/K_d	Response time / Through put	Detection range / Saturating S:B ratio	Sensor volume/ Analyte volume	Reference*
PAAm Nanogel Particles	100 nM	Entrapment	FRET (Structure Switching)	ATP	50 µM/ 273 µM	2 s/ Low	50 – 5000 µM/ 2.2-fold	1 mg/mL gel beads/ 2 mL	Nielsen *et al.* (2010) [8]
PAAm - PDDA Monoliths	5 µM	Electrostatic	Colorimetric (Hydrogel collapse)	ZEN (Toxin)	0.98 ng/mL/ N/A	2.5 h/ Low	2.5 – 100 ng/mL/8-fold	1 mL/ 500 µL	Liu *et al.* (2022) [13]
PAAm Microgel Particles	2 µM	Covalent	Fluorescence (Visual) (Dye Insertion)	ATP	45 µM/ N/A	2 min/ Low	20 – 2000 µM/ N/A	10 mg/mL gel beads/ 1 mL	Helwa *et al.* (2012) [17]
Sodium silicate Sol-Gel Array	200 nM	Entrapment	FRET (Structure Switching)	ATP	28 µM/ N/A	60 min/ High	28-3000 µM / 20-fold	50 µL / 100 µL	Hui *et al.* (2014) [21]
Sodium silicate Sol-Gel Array	1.1 µM	Entrapment	FRET (Structure Switching)	ATP	N/A	60 min/ High	100-3000 µM/ 12-fold	40 µL / 100 µL	Rupcich *et al.* (2005) [27]
Graphene-Oxide Monolith	5 µM	π-π Stacking	FRET	OTC (Anti-biotic)	25 µg/L/ N/A	2 h/ Low	25–1000 µg/L/2-fold	600 µL / 2 mL	Tan *et al.* (2016) [31]
DNA hydrogel	100 µM	Hybridiza-tion	Colorimetric (Visual)	ATP	5.6 µM/ N/A	30 min/ Low	5 - 500 µM/3-fold	5 µL / 35 µL	Oishi *et al.* (2019) [56]
Sodium silicate Sol-Gel Array	200 nM	Affinity	FRET (Structure Switching)	ATP	400 µM/ N/A	60 min/ High	400 - 1500 µM/ 8-fold	50 µL / 100 µL	Carrasquilla *et al.* (2011) [66]
POEGMA Hydrogel Array	200 nM	Entrapment	FRET (Structure Switching)	ATP	5.3 µM/ 123 µM	3 min/ High	5-3000 µM/ 20 fold	50 µL / 20 µL	**Our work (2023)**

*References cited in the order cited in the main text.

3.6.15. Supporting References

(1) Smeets, N. M. B.; Bakaic, E.; Patenaude, M.; Hoare, T. Injectable and Tunable Poly(Ethylene Glycol) Analogue Hydrogels Based on Poly(Oligoethylene Glycol Methacrylate). *Chem. Commun.* **2014**, *50* (25), 3306. https://doi.org/10.1039/c3cc48514e.

(2) Smeets, N. M. B.; Bakaic, E.; Patenaude, M.; Hoare, T. Injectable Poly(Oligoethylene Glycol Methacrylate)-Based Hydrogels with Tunable Phase Transition Behaviours: Physicochemical and Biological Responses. *Acta Biomaterialia* **2014**, *10* (10), 4143–4155. https://doi.org/10.1016/j.actbio.2014.05.035.

(3) Pikula, M.; Ali, M. M.; Filipe, C.; Hoare, T. Single-Step Printable Hydrogel Microarray Integrating Long-Chain DNA for the Discriminative and Size-Specific Sensing of Nucleic Acids. *ACS Appl. Mater. Interfaces* **2021**, *13* (2), 2360–2370. https://doi.org/10.1021/acsami.0c21061.

4. Chapter 4.

A hydrogel film microarray stabilizes very short structure switching aptamer duplexes to achieve enhanced sensing of small molecules

Preface

This chapter and its supporting information-appendix are submitted for the publication describing the translation of aptamer-functionalized hydrogel system developed in Chapter 3 to a printable nitrocellulose-supported microarray sensor. The adenosine sensing hydrogel-microarray was additionally optimized based on hydrogel concentration, DNA aptamer surface density and structure switching construct design to support higher affinity and sensitivity towards a cognate ligand. In particular, ultrashort quencher stems rationally positioned to promote optimal ligand-binding pathway within FRET-aptamer constructs were employed that enabled minimal reduction of native ligand-binding affinity, provided by hydrogel stabilizing effect and ability to allow for solution-like, unrestricted affinity interactions.

Milana Pikula,[1,2] Yingfu Li,[3] Todd Hoare[1,*] and Carlos D. M. Filipe,[1,*]

[1]Department of Chemical Engineering, McMaster University, Hamilton, ON L8S 4K1, Canada;

[2]Biointerfaces Institute, McMaster University, Hamilton, ON L8S 4L8, Canada;

[3]Department of Biochemistry and Biomedical Sciences, McMaster University, Hamilton, ON, L8S 4K1, Canada.

The manuscript submitted to *Chemical Engineering Journal*.

Abstract

The reduction of affinity associated with the modifications required to create FRET- aptamer constructs represents a key challenge hindering the practical adaptation of such systems for small molecule detection. While the use of shorter and rationally positioned quencher stems is desirable to enhance target-induced fluorescence recovery, the weak hybridization potential of such stems results in high levels of background fluorescence and poor sensitivity. Herein, we introduce a hydrogel microarray sensor able to thermally stabilize very short aptamer duplexes (*i.e.*, quencher stems ≤ 10-bp), resulting in improved FRET efficiency and reduced background levels across a broad range of conditions. The hydrogel microarray can physically entrap >75% of loaded aptamer reporters while maintaining high accessibility to the target molecules, enabling accurate quantification of dose-responsive affinity interactions. Using an ATP aptamer reporter, the hydrogel sensor can achieve a binding affinity as low as 14.7 μM - comparable to the native aptamer – and very low limits of detection (LOD) of 1.2 μM in a pure buffer and 4.6 μM in 50% serum. Moreover, the developed hydrogel microarray is reusable, amenable to printing fabrication, and provides protection against nuclease-based degradation. This simple approach thus holds promise for advancing microarray aptamer technology in critical biosensing applications.

4.1. Introduction

While antibodies are widely used for detecting a wide variety of protein targets of interest,[1] their application in designing diagnostics for small molecules such as drugs, toxins, antibiotics, and metabolites is challenging.[2] Accurate detection of small molecules instead usually requires time-consuming and labor-intensive techniques such as high-performance liquid chromatography and mass spectrometry.[3] Aptamer microarrays,[4,5] produced by immobilizing aptamer reporters on a solid surface (typically based on glass,[6] gold,[7] or silicone[8]), represent an emerging alternative to these conventional methods. Structure-switching aptamer constructs (SSACs) have attracted particular interest as fluorescence-based reporters given their advantages over other methods (e.g. organic dye displacement[9] or nanoparticle reporters[10]) in achieving fast kinetics and stable signal generation over wider dynamic ranges. The SSAC approach relies on the aptamer's ability to undergo a target-dependent conformational transition that results in the competitive displacement of one or more complementary oligonucleotides upon target binding.[11] In a typical SSAC design based on fluorescence resonance energy transfer (FRET), ligand-competing oligonucleotides are tagged with a quencher (Q-DNA) and hybridized to a fluorophore-labelled DNA molecule containing the aptamer sequence (*i.e.*, duplexed aptamer).[12] In the absence of the ligand, the FRET pair molecules are in apposition and fluorescence is quenched; in the presence of the ligand, a structural switch is triggered that results in the release of the Q-DNA strand and a rapid increase in the fluorescence signal.

The main challenge with the practical implementation of such FRET-based systems is that the required modification of aptamers to achieve signaling leads to a significant reduction in the aptamer's binding affinity due to the denaturation of the native aptamer conformation upon Q-DNA hybridization.[11,13,14] While affinity reduction is a general feature of SSACs, it particularly affects the small molecule binders since those aptamers have inherently lower affinities, with native constants of dissociation (K_d) typically in the μM range.[14] For example, the well-studied adenosine triphosphate (ATP) binding DNA aptamer has a native K_d of 6-10 μM[15]; however, once translated into a FRET-based SSAC with 12-bp long quencher stem, a >100-fold reduction in affinity (*i.e.*, $K_d \sim 600$ μM to 1 mM) is observed depending on the FRET pair used.[12,16] The loss in affinity is linked to the thermodynamic stability of duplexes formed to make the construct, which typically utilize 10- to 15-nt long Q-DNAs in order to provide sufficient hybridization strength to minimize background fluorescence levels for high signal-on sensing.[17]

Strategies utilized to overcome this issue are typically based on the reduction of quencher stem length and/or the rational localization of Q-DNA oligonucleotides relative to the ligand binding pocket within the aptamer sequence. Reducing the quencher stem involved in signaling lowers the energy barrier necessary for Q-DNA removal, while rational positioning of Q-DNA molecules enhances the ligand binding pocket structure to improve aptamer affinity to ligand binding. For example, by utilizing 10-nt instead of 12-nt long quencher stems positioned to interface with a DNA aptamer binding site, the binding affinity of adenosine aptamer reporter can be enhanced by almost one order of magnitude (*i.e.*, $K_d \sim 100$ μM).[16] However, this strategy faces limitations when translated into microarray formats, particularly in terms of the extent of Q-DNA truncation due to the altered hybridization efficiency of short oligonucleotides on surfaces,[18] and the increased tendency for incorrect orientations and/or limited accessibilities of immobilized aptamer molecules.[4,19] Indeed, the DNA hybridization potential can be suppressed up to 20-40-fold[18] on 2D surfaces, attributed to the steric blocking imparted by the surface coupled with the restricted translational and rotational freedom of the immobilized aptamers[20]. As an example, Munzar *et al*. showed that the assembly of 9-bp DNA adenosine aptamer duplexes on glass microarray slides exhibited an almost 3-fold lower affinity compared to the 10-bp aptamer reporters despite the reduced length and optimal location within a binding pocket[16]. Shorter complementary oligonucleotides (down to 7-bp aptamer duplexes) further reduce the effective formation of DNA aptamer reporters, leading to high dissociation rates even in the absence of the target and thus both high

background levels and weak ligand-induced signaling.[21] Increasing the density of the spotted aptamer (*i.e.*, number of aptamers present per surface area) often further reduces the aptamer's activity, a result attributed to a combination of steric hindrance and electrostatic repulsion[22] interfering with proper aptamer orientation and 3D folding. For example, 30-40% lower signal generation was achieved for sensing ethanolamine on planar glass slides when the spotted aptamer density was increased by a factor of 5[6] while the immobilization of a SSAC for ATP onto a sol-gel film *via a* streptavidin-avidin linkage showed an ~8-fold lower LOD relative to the solution result (~ 400 μM[23] compared to 25 μM[12]) despite a 6-fold higher loading efficiency compared to that achieved on planar glass. As such, changing either the aptamer length or density cannot fully address the sensitivity challenges with aptamer-based microarrays.

Beyond these aptamer-specific challenges, additional drawbacks associated with the immobilization of SSACs on surfaces include: (1) the need for chemical modifications of both the surface and the aptamers[4,23] to enable covalent/affinity coupling; (2) the absence of protection against nucleases or other harsh components in the samples that can affect the stability of the construct;[24] (3) the slow kinetics of hybridization associated with surface-immobilized ligands, often requiring DNA overnight incubation for complete hybridization;[21] (4) the need to include blocking buffers to suppress non-specific binding that can lead to interfering signals and/or suppressed target signals;[16,21] and (5) the need to incorporate DNA anchoring spacers[4,6] for effective hybridization. Immobilizing SSACs in 3D porous polymeric hydrogels offers a potential solution to these challenges. By designing the pore size of the hydrogel to enable effective entrapment of the aptamer reporters but facile diffusion of the small molecule targets, the SSAC can be effectively protected from nucleolytic degradation[25] and immobilized while avoiding the need for covalent anchoring and thus the introduction of other functional entities on the SSAC that can reduce its affinity for the target molecule.[26,27] The highly swollen hydrogel network in aqueous media provides efficient diffusional transport of the analytes from the bulk solution and increased accessibility of the entrapped sensing probes without the steric restrictions associated with making typical high-density 2D microarrays.[27] The composition of the hydrogel could also be tuned to control the degree of interaction between DNA molecules and other analytes, offering the potential to enhance the thermal stability of short DNA hybridization via a combination of enthalpic[28] and entropic[29] contributions. This effect allows the minimum required length of complementary DNA necessary for effective fluorophore quenching to be decreased, resulting in an improvement of the reporters' overall affinity and responsiveness towards the ligand while avoiding increases in the background signal associated with the premature release of the shorter Q-DNA strand.

Although the potential of hydrogels in biosensing is immense, their application in aptamer-based diagnostics has rarely been extended beyond simple immobilization[30,31] or the assembly of aptamer crosslinked stimuli-responsive[32] and conductive materials.[33,34] Moreover, there is a lack of simple and scalable hydrogel fabrication techniques that can be easily adapted to produce miniaturized hydrogel-SSACs microarrays. In this context, herein we propose the physical entrapment of SSAC within *in situ*-crosslinkable poly(oligoethylene glycol methacrylate) (POEGMA) hydrogel film microarrays co-printed on a nitrocellulose substrate via the sequential casting of aldehyde and hydrazide-functionalized precursor polymers (POA and POH, respectively) co-dissolved with the DNA aptamer assembly. We have previously applied similar hydrogel systems to create DNA-based hybridization sensors based on encapsulated rolling circle amplification (RCA) product that enabled improved annealing efficiency and detection potential for small DNA oligonucleotides relative to hydrogel-free microarrays[35]; in follow-up work, we demonstrated that hydrogel arrays assembled in a 96-well microtiter plate could stabilize FRET SSAC adenosine reporters to enable effective detection in complex biological samples[36], with the affinity of aptamer reporters tuned based on the length of the quencher stems to improve the sensitivity of weakly hybridized aptamer duplexes and thus enable improved sensor performance. In the current study, we expand on this strategy by translating the system onto a portable nitrocellulose-supported microarray

while additionally modulating the SSAC configuration using shorter quencher stems (7-bp, 9-bp and 10-bp) specifically positioned to occupy only one essential oligonucleotide within the ligand binding site, freeing most of the aptamer sequence for optimal ligand binding while also reducing the energy barrier for Q-DNA removal.[16,17] By regulating the ligand binding conditions by optimizing the hydrogel concentration and surface density of DNA aptamer assemblies, improved SSAC affinity towards the cognate ligand can be achieved (similar to those of the native aptamer in solution) with reduced backgrounds relative to previously reported approaches. The sensors are reusable, printable and can be stored for at least 7 days at room temperature with <20% loss of signal generation ability. We also demonstrate that the Q-DNA strand can be added to a previously assembled POEGMA hydrogel film containing the fluorophore-tagged sensing DNA (but not the Q-DNA) to allow for the *in situ* formation of a fully functional SSAC. Collectively, the benefits of the hydrogel-based system can address the key challenges associated with small molecule sensing using SSACs at surfaces.

4.2. Experimental Section

4.2.1. Materials

All DNA oligonucleotides were purchased from Integrated DNA Technologies. Acrylic acid (AA, Sigma-Aldrich, 99%), 2,2-azobisisobutryic acid dimethyl ester (AIBMe, Wako Chemicals, 98.5%), N′-ethyl-N-(3-dimethylaminopropyl)-carbodiimide (EDC, Carbosynth, Compton CA, commercial grade), thioglycolic acid (TGA, Sigma-Aldrich, 98%), adipic acid dihydrazide (ADH, Alfa Aesar, 98%), glycerol (Sigma-Aldrich, ≥99%), nitrocellulose plastic-backed membrane (Cytiva Whatman Membrane, FF120HP DIN A4), and human serum (normal, Sigma-Aldrich, 20 mL) were used as received. N-(2,2-dimethoxyethyl) methacrylamide (DMEMAm) was synthesized in-house according to a previously reported method.[37,38] Diethylene glycol methyl ether methacrylate ($M(EO)_2MA$, Sigma-Aldrich, 98%) and oligo(ethylene glycol) methyl ether methacrylate ($OEGMA_{500}$, M_n = 500 g/mol, Sigma-Aldrich, 95%) were purified on a column of basic aluminum oxide (Sigma-Aldrich, type CG-20) to remove the inhibitors prior to use. Deoxyribonuclease I (DNase I, 2000 UmL^{-1}) was purchased from NEB, while adenosine 5'-triphosphate (ATP), cytidine 5'-triphosphate (CTP), guanosine 5'-triphosphate (GTP), and uridine 5'-triphosphate (UTP) solutions (100 mM) were all purchased from Fisher Scientific. Urea (99.5%), HEPES buffer (1 M, sterile solution), sodium chloride (>99%) magnesium chloride (>99%), Tris-HCl (99.5%), and sodium hydroxide (>98%) were all purchased from Bioshop Canada Inc. Milli-Q-grade distilled deionized water (DIW) was used for all experiments. Treated clear-bottom black 96-well plates were purchased from Corning (polystyrene, Cat. No. #CLS3603), while the PCR tubes used for the FRET melting assay were purchased from BioRad (0.2 mL 8-tube strips, Cat. No. #TLS0851EDU).
The 1xGelation buffer was prepared by co-dissolving 20 mM HEPES, 5 mM $MgCl_2$, and 300 mM NaCl at pH=7.5. The 1xAssay buffer used for the solution-phase assay was prepared by co-dissolving 20 mM Tris-HCl, 5 mM $MgCl_2$, and 300 mM NaCl. Both buffers were adjusted to pH=7.5 using 0.1M NaOH and were stored at ambient conditions until use.

4.2.2. POEGMA Polymer Synthesis and Characterization:

Hydrazide-functionalized (POH) and aldehyde-functionalized (POA) hydrogel precursors containing varying contents of $OEGMA_{500}$ monomer (medium: POA with 50% $OEGMA_{500}$ and 50% $M(EO)_2MA$; high: POH with 100% $OEGMA_{500}$) were synthesized and characterized according to methods detailed elsewhere[35,37,38] (see Supporting Information and Table S1 for full details). Polymers for hydrogel preparation were dissolved to form a master stock of 20 wt% solutions in 1xGelation buffer (20 mM

HEPES, 5 mM $MgCl_2$, 300 mM NaCl, pH=7.5) and stored at 4°C until use. Prior to their use to form hydrogel films, the master stock solutions were diluted to 6 wt%, 8 wt%, or 10 wt% in 1xGelation buffer containing 5 vol% glycerol.

4.2.3. Preparation of Solution Phase Aptamer Reporter (S: AFQ) and Solution-Based FRET Assays

All purchased DNA sequences were reconstituted to a concentration of 100 μM in DIW and stored at -20°C. The concentration of the DNA stock solution was confirmed by measuring the absorbance at 260 nm using UV-vis spectrophotometry (Tecan, NanoQuant Infinite 200 Pro Microplate Reader). The aptamer reporter was prepared by assembling A_x:F:Q_y, at a molar ratio of 2:1:6, where *x* is the number of non-essential oligonucleotides within the aptamer-containing-DNA strand 5'extension and *y* is the quencher-DNA-strand length, to build A_2:F:Q_7, A_4:F:Q_9, and A_5:F:Q_{10} using the preparation procedure previously reported[36]. Seven serial dilutions of aptamer assembly were prepared corresponding to F-DNA contents of 10 nM, 25 nM, 50 nM, 75 nM, 100 nM, 125 nM, and 150 nM; for example, an aptamer reporter corresponding to 100 nM F-DNA was prepared by mixing 400 nM (A), 200 nM (F), and 1200 nM (Q) (each dissolved from 10 μM master stocks in DIW) followed by dilution with 2xAssay buffer at a ratio of 1:1 v/v. The mixture was then heated for 5 min at 90°C followed by cooling at 25°C for 1.5 h to allow the DNA strands to reanneal and reach equilibrium before fluorescence measurements. The prepared aptamer constructs were deposited as 50 μL samples in clear-bottom 96-well plates using a multi-channel pipette. Fluorescence measurements were obtained using a Tecan M1000 microplate reader (Infinite Pro) operating in bottom fluorescence mode using 640/672 nm excitation/emission wavelengths (5 nm bandwidth) at an optimal gain maintained at 25°C. The emission intensities of solution (S)-based quenched aptamer constructs (S:AFQ) and fluorescent aptamer constructs without the quencher strand (S:FA) were collected and corrected by subtracting the fluorescence intensity associated with the buffer samples (blank). The FRET efficiency (*i.e.,* fluorescence quenching) was calculated as the ratio between the normalized fluorescence intensity of the quenched construct (S:AFQ) relative to the non-quenched aptamer duplex (S:FA). All data were reported as the average of at least *n*=3 replicates ± SD (standard deviation).

4.2.4. Manual Preparation of Solid-Phase Hydrogel Film Aptamer Reporter Microarrays (HF:AFQ)

Hydrogel film microarrays encapsulating DNA aptamer reporters (HF:AFQ) were fabricated using a multi-channel pipette on a plastic-backed nitrocellulose membrane (Cytiva FF-120) pre-modified by printing hydrophobic wax barriers using a Xerox ColorQube 8570N solid wax printer to form a 96-well-plate template (4 mm diameter wells with a 9 mm inter-well distance, 8 row x 12 column pattern). The wax-printed nitrocellulose sheet was cured in the oven for 2 min at 110 °C to melt the wax through the membrane and form defined microzone spots. Aptamer reporters with varying Q-DNA stem lengths (Q_7, Q_9, and Q_{10}) were physically entrapped in 6 wt%, 8 wt% and 10 wt% POEGMA hydrogel films (6HF, 8HF and 10HF) by sequentially pipetting 2.5 μL of a POA solution prepared at a concentration of 6 wt%, 8 wt% or 10 wt% in 1xGelation buffer containing 5 vol% glycerol followed by 2.5 μL of a POH solution prepared at the same concentration co-dissolved with a 2x concentration of AFQ (POH:2xAFQ) in 1xGelation buffer containing 5 vol% glycerol. To make POH:2xAFQ, a 4xAFQ mixture was dissolved in 1xGelation buffer, heated for 5 min at 90°C, cooled to 25°C over 30 min, mixed with a 2xPOH solution containing 10 vol% glycerol at a 1:1 v/v ratio, and equilibrated at room temperature for 60–90 min before hydrogel film preparation. Prepared microarrays were left to cross-link overnight at 4 °C to ensure the completion of the gelation process and then dried for 4-5 h at ambient temperature prior to their use for

analysis. Seven serial dilutions of aptamer assembly were prepared corresponding to F-DNA contents of 10 nM, 25 nM, 50 nM, 75 nM, 100 nM, 125 nM, and 150 nM; for example, the hydrogel microarray that containing an aptamer reporter corresponding to 100 nM F-DNA was assembled using POH co-dissolved with aptamer construct in a molar ratio of 400 nM A: 200 nM F: 1200 nM Q. The resulting aptamer-functionalized hydrogel microarrays were labeled as zHF:A_xFQ_y in which *z* is the hydrogel concentration, *x* is the number of non-essential oligonucleotides within the 5'extension of the aptamer-containing DNA strand, and *y* is quencher DNA strand length.

4.2.5. Printable Fabrication of Hydrogel Film Aptamer Reporter Microarrays (HF:AFQ)

Printed hydrogel film microarrays were fabricated using the same hydrogel precursor solutions used for manual arraying. A BioJet HR™ non-contact solenoid dispenser was used to print the polymer inks on the wax-modified paper microzones of the 96-well plate template in an 8 row x 12 column pattern. To print 8HF:A_5FQ_{10}, one line was charged with POA-ink and the other line was charged with POH:2xA_5FQ_{10} ink corresponding to a 100 nM F-DNA concentration, with both inks containing 5 vol% glycerol as a humectant and viscosity modifier to facilitate printing. The printer was programmed to stay open for 6 ms, with the frequency set to 100 Hz as per previous reports[35,39]. Microarrays were fabricated by dispensing 2.5 µL of POA ink onto each microzone followed by 2.5 µL of POH:2xA_5FQ_{10} ink. Microarrays containing unquenched fluorescent construct (8HF:FA_5) and control hydrogel-only (8HF) microarrays (blank) were fabricated using the same method but altering the top layer with POH/2xFA_5 or POH only respectively (maintaining the same polymer concentration in each control). Printed microarrays were left to cross-link overnight at 4 °C to ensure the completion of the gelation process and then dried for 4-5 h at ambient temperature prior to their use for analysis.
Printing reproducibility was determined on a hydrogel film microarray encapsulating fluorescent aptamer construct 8HF:FA_5 (100 nM F-DNA concentration), with the spot-to-spot fluorescent intensity quantified using the Chemidoc MP System (BioRad) operating at 650 nm excitation/665 nm emission. The resulting image was processed using the round-based volume tool in Image Lab software (BioRad) to enable quantitative detection of the fluorescence signals.

4.2.6. Solid Phase FRET Assay

FRET assays were conducted on both manual (section 4.2.4) and printed (section 4.2.5) microarrays. FRET assays in manual microarrays were performed using 8HF:A_xFQ_y assemblies prepared with varying concentrations of assembled A:F:Q aptamer reporter (*i.e.*, DNA surface densities) corresponding to F-DNA contents of 10 nM, 25 nM, 50 nM, 75 nM, 100 nM, 125 nM and 150 nM per microzone. The FRET assay for printed microarray was performed for the 8HF:A_5FQ_{10} assembly corresponding to the 100 nM F-DNA concentration. The resulting fluorescence intensities were measured using a Chemidoc MP System (BioRad) operating at 650 nm excitation/665 nm emission, with the image acquired subsequently processed using the round-based volume tool in Image Lab software (BioRad) to enable quantitative determination of the fluorescence signals. Values of fluorescent intensities were collected for hydrogel microarray samples of quencher sequence-containing constructs (HF:AFQ) and the non-quenched fluorescent aptamer duplex (HF:FA) and corrected by subtracting fluorescence intensity associated with hydrogel-only (HF) control microarray (blank). FRET efficiency was calculated as the ratio between the normalized fluorescence intensity of the quencher sequence-containing constructs (HF:AFQ) and the non-quenched fluorescent aptamer duplex (HF:FA). The data reported represent the average of at least n=3 replicates ± SD.

4.2.7. Hydrogel Film Microarray Encapsulation Efficiency

Hydrogel film microarrays containing the fluorescent aptamer construct F:A_5 (HF:FA, prepared with 100 nM F:200 nM A_5) were prepared as described in sections 4.2.4 and 4.2.5. The resulting HF:FA_5 microarrays were incubated with 10 µL/microzone of 1xAssay buffer (20 mM Tris-HCl, 300 mM NaCl, 5 mM $MgCl_2$, pH=7.5) and then subjected to two rounds of 30 min washes followed by 1 min rinses with 20 mL of fresh 1xAssay buffer and a final 1 hour washing step with an additional 1 min rinse with 20 mL of fresh 1xAssay buffer; the wash supernatant was fully removed after each step. The fluorescence emission was measured before and after each wash/rinse step using the Chemidoc MP System (BioRad) operating at 650 nm excitation/665 nm emission, with the resulting image processed as described in section 4.2.6. The collected fluorescence data were normalized by subtracting the fluorescence intensity obtained in the assay from the hydrogel-only control samples prepared without FA_5 (blank). The aptamer content retained by the hydrogel film was quantified by comparing the normalized fluorescence intensity of the hydrogel film microarrays before and after each wash/rinse step. All data were reported as the average of at least n=3 replicates ± SD for manually pipetted samples and the average of n=5 replicates per each column ± SD (total n=60 replicates) for printed microarray samples.

4.2.8. DNase I Degradation Assay

Nucleolytic degradation assays were performed using aptamer reporter complexes dissolved free-in-solution (S:A_5FQ_{10}) or encapsulated in hydrogel microarrays (HF:A_5FQ_{10}) prepared with 6 wt%, 8 wt%, or 10 wt% precursor polymer concentrations. Hydrogel-based microarrays were washed and rinsed over 30 min prior to testing to remove loosely bound aptamer constructs as described in section 4.2.7. For solution-based constructs, 5 µL aliquots of deoxyribonuclease DNase I in 1xAssay buffer was pipetted into each well to achieve a concentration of 5 U/well. For hydrogel-based constructs, washed hydrogel microarrays were dried at ambient temperature for 10 min followed by incubation in 5 µL/well of 1xAssay buffer containing 10 vol% glycerol for 10 min and subsequent incubation in 5 µL/well DNase I in 1xAssay buffer containing 10 vol% glycerol (5 U/well total concentration). Fluorescence signal increases indicative of construct disassembly resulting from aptamer degradation and F-DNA release were measured over 60 min following DNase I addition, with the obtained values corrected against the solution-only or hydrogel-only fluorescence (blank) intensities and compared to the fluorescence of a solution or hydrogel containing only the fluorescent aptamer duplex (FA_5) at the same overall volumetric concentration prior to the DNase I digestion (corresponding to 100% DNA degradation). All data were reported as the average of n=3 replicates ± SD.

4.2.9. Adenosine Binding Assay

The adenosine triphosphate (ATP) binding assays were carried out using aptamer reporter complexes dissolved free-in-solution (S:A_5FQ_{10}) or encapsulated in a hydrogel film microarray (HF:A_5FQ_{10}) prepared with 6 wt%, 8 wt%, or 10 wt% precursor polymer concentrations and F-DNA contents of 100 nM within a A:F:Q construct prepared at a 2:1:6 molar ratio. To assess the target binding kinetics in solution, 50 µL/well of 5 mM ATP was pipetted in 1xAssay buffer into a solution-assembled aptamer reporter. To assess the target binding in a hydrogel, 5 µL/well of 5 mM ATP was pipetted in 1xAssay buffer containing 5 vol% glycerol as a humectant on to a hydrogel film-encapsulated aptamer reporter microarray. The fluorescence intensity enhancement was tracked over 1 hour at 25°C as described in sections 4.2.3 and 4.2.6. The measured fluorescence values were corrected by subtracting the autofluorescence measured from the buffer or hydrogel (blanks) from the solution-based or hydrogel-based samples respectively. The ligand binding kinetics are reported as the time-dependent normalized

fluorescence increases of samples treated with ATP (signal) relative to the fluorescence intensity of samples treated with the 1xAssay buffer (background), representing the signal:background ratio (S:B).
To assess fluorescence quenching during the target binding assay, the FRET efficiency (0 min) and FRET efficiency change over 60 min of target binding (1 min, 5 min, 15 min, 30 min and 60 min) were assessed in both solution-based or hydrogel-based aptamer construct samples treated with 1xAssay buffer; the data are reported as the ratio between the normalized fluorescence intensity of the quenched construct (AFQ) relative to the non-quenched aptamer duplex (FA). Target binding assays were conducted at both 50 μM and 5 mM ATP concentrations for both S:A_xFQ_y and 8HF:A_xFQ_y (where x = 2, 4 and 5 and y = 7, 9 and 10) at varying concentrations of assembled A:F:Q aptamer reporter (*i.e.*, DNA surface densities) corresponding to increasing F-DNA contents of 10 nM, 25 nM, 50 nM, 75 nM, 100 nM, 125 nM and 150 nM per well. All data were reported as the average of n=3 replicates ± SD.
The target binding kinetics and S:B assessment were repeated on printed hydrogel microarray samples (8HF:A_5FQ_{10}) encapsulating A:F:Q constructs with 100 nM F-DNA contents using a 5 mM ATP concentration over a 60 min assay time. The FRET efficiency was assessed based on the normalized fluorescence intensity of ATP-treated or buffer-treated printed samples (8HF:A_5FQ_{10}) relative to the normalized fluorescent intensity of hydrogel samples encapsulating unquenched fluorescent construct (8HF:FA_5) as measured 60 min after ligand addition. The fluorescence values were normalized by subtracting the fluorescence intensity of hydrogel-only (8HF) microarray samples (blank). All data were reported as the average of n=24 replicates ± SD.

4.2.10. Adenosine Binding Affinity

Aptamer reporter complexes were dissolved free-in-solution (S:A_xFQ_y) or encapsulated in a hydrogel film (8HF:A_xFQ_y, where x = 2, 4 and 5, and y = 7, 9 and 10, respectively) containing F-DNA at concentration of 25 nM or 150 nM prepared into A:F:Q reporters with a molar ratio of 2:1:6. Samples were incubated with serial dilutions of ATP over a concentration range of 0-10 mM in either pure buffer (for x = 2, 4 and 5 and y = 7, 9 and 10, respectively) at 25 nM and 150 nM F-DNA density or 50% serum (for x = 4 and 5 and y = 9 and 10) at 25 nM F-DNA density, each for 1 h at 25°C. ATP addition for each sensor was performed as described in section 4.2.9. Fluorescence emission values from the AFQ samples treated with ATP in 1xAssay buffer or in 50% serum (signal, S) and from the AFQ samples treated with 1xAssay buffer or 50% serum only (background, B) were collected, corrected by subtracting the measured hydrogel-only microarray or solution-only autofluorescence values measured in 1xAssay buffer or 50% serum (blanks), and presented as a S:B ratio. To account for spot-to-spot and batch-to-batch FRET variations in the hydrogel microarray samples, the fluorescence values for each ATP concentration (signal, n=3 replicates) were normalized against the mean fluorescence from the 0 mM ATP samples (background array, n=24 replicates). A four-parameter logistic regression (GraphPad Prism v9) was applied to fit the binding affinity data between the bottom plateau (minimal curve asymptote) and the top plateau (maximum dose-response curve asymptote) using the binding affinity dissociation constant (K_d) and the Hill slope (indicative of binding sites cooperativity) as the fitting parameters. All data were reported as the average of n=3 replicates ± SD.

4.2.11. FRET Melting Assay

Aptamer reporter complexes were dissolved free-in-solution (S:A_xFQ_y) or encapsulated in hydrogel films containing 5 vol% glycerol (8HF:A_xFQ_y, where x = 2, 4 and 5, and y = 7, 9 and 10, respectively), both prepared at a total volume of 50 μL in PCR tubes. Thermal denaturation was performed using a PCR machine (BioRad, RT96), with fluorescence emissions related to Q-DNA de-hybridization acquired in the red channel (Cy5; 651 nm/670 nm excitation/emission) as a function of temperature using the CFX

Maestro 1.1 software. The PCR machine was programmed to hold each sample at 20°C for 2 min followed by heating to 80°C in 2°C increments, with equilibration at each step for 2 min before measuring the fluorescence. The melting curves were constructed by plotting the fluorescence enhancement as a function of temperature. To determine the melting temperatures (T_m) of Q-DNAs, the melting curve values were corrected for the autofluorescence of undoped hydrogel or solution samples and normalized against the fluorescent signal from the same concentration of FA complex in hydrogel or solution (maximum fluorescence intensity) to account for the temperature-dependent decrease in the fluorescence of AlexaFlour$_{647}$ fluorophores. The T_m values were extracted using a 5-parameter sigmoidal fitting[40–42] of the melting curves using GraphPad Prism v9, with T_m corresponding to the midpoint of the normalized maximum fluorescence enhancement (*i.e.* the temperature at which the complex is 50% dissociated). All data were reported as the average of n=3 replicates per sample ± SD.

4.2.12. Hydrogel film Aptamer Reporter Microarray Assembly via Q-DNA Hybridization (HF:AF+Q)

Hydrogel film microarrays encapsulating the fluorescent aptamer constructs 8HF:FA$_4$ and 8HF:FA$_5$, each containing 100 nM F-DNA, were fabricated as described in section 4.2.4. Quencher-labeled oligonucleotides Q_9 and Q_{10} were hybridized to 8HF:FA$_4$ and 8HF:FA$_5$ microarrays respectively in concentrations of 1x (1x 600 nM), 5x (5x 600 nM = 3 μM) and 10x (10x 600 nM = 6 μM) by pipetting 5 μL/well of Q-DNA solution in 1xAssay buffer containing 5 vol% glycerol. The hybridization reaction was allowed to proceed over 90 min at ambient conditions. Following hybridization, the hydrogel microarrays containing quenched fluorescent constructs were washed via two 30 min cycles of hydration in 10 μL/well 1xAssay buffer followed by a 1 min gentle rinse in 20 mL 1xAssay buffer. The FRET efficiency was assessed as described in section 4.2.6 before the Q-DNA hybridization and 30 min, 60 min and 90 min after the initiation of the hybridization reaction, including after each wash step. The FRET efficiency was compared to the hydrogel microarray samples fabricated with the pre-formed AFQ constructs 8HF:A$_4$FQ$_9$ and 8HF:A$_5$FQ$_{10}$. All data were reported as the average of at least n=3 replicates ± SD.

4.2.13. Regeneration of Hydrogel Film Immobilized Aptamer Sensors

Aliquots of 5 mM ATP (5 μL/well) were added to 8HF:A$_4$FQ$_9$ or 8HF:A$_5$FQ$_{10}$ microarrays prepared with 100 nM F-DNA content to induce signaling as described in section 4.2.9. Following, samples were rinsed with 20 mL of 1xAssay buffer over 1 min of gentle shaking followed by 10 min of drying at ambient conditions to ensure the recovery of the hydrophobic barriers around the printed microzones. Two recovery methods were probed. (1) In recovery by washing, 1xAssay buffer was pipetted on to dried hydrogel microarrays at a volume of 10 μL/well and allowed to hydrate the microarray for 30 min followed by 1 min gentle rinsing in 20 mL of 1xAssay buffer. The procedure was repeated with an additional 30 min hydration/wash step. Following 10 min of drying at ambient conditions, regenerated hydrogel microarrays were probed for their capacity to conduct a second cycle of 5 mM ATP sensing over a 30 min analysis time. The regeneration effectiveness was assessed by comparing the S:B ratio achieved following the first cycle of ATP binding with those measured in the intermediate washing steps and the second cycle of ATP binding, with the fluorescence quantified as described in section 4.2.9 for both aptamer constructs tested. (2) In recovery by denaturation, 10 μL/well of 8 M urea was pipetted onto rinsed/dried hydrogel microarrays and allowed to incubate for 15 min followed by gentle rinsing in 20 mL of 1xAssay buffer. Rinsed samples were hydrated in 10 μL/well of 1xAssay buffer for an additional 15 min to refold the denatured aptamer followed by an additional 1 min of gentle rinsing in 20 mL of 1xAssay buffer to remove the excess buffer. Following 10 min of drying at ambient conditions, 10x

concentrated Q-DNA solution (6 μM) was pipetted at a volume of 5 μL/well in 1xAssay buffer containing 5 vol% glycerol. The hybridization reaction was allowed to proceed for 30 min at ambient conditions in the closed container followed by washing via one rinse/hydration/rinse cycle. Regenerated samples were dried over 10 min and probed for their activity toward a second cycle of 5 mM ATP sensing, using a 30 min assay time. The regeneration effectiveness was assessed by comparing the S:B ratio measured following the first cycle of ATP binding, denaturation/refolding, and 10xQ hybridization/washing to the same ratio measured for the second ATP binding cycle, with the data acquisition and analysis conducted as described in section 4.2.9 for both aptamer constructs. All data were reported as the average of at least n=4 replicates ± SD.

4.2.14. Statistics

Statistical analysis was performed using GraphPad-Prism software v9. Statistical significance of construct encapsulation and FRET efficiencies before and after nucleolytic conditions in both sample groups (solution-based and hydrogel-based) and for the hybridization and regeneration assays in hydrogel-based microarrays were assessed using a 2-way ANOVA model, using the adjusted threshold for multiple comparison $p \leq 0.05$ to test statistical significance. The statistical analysis of FRET efficiency at varying concentrations of aptamer construct for both sample groups (solution-based and hydrogel-based) was performed the Multiple Unpaired Welch t-test model, using the adjusted threshold for multiple comparison $p \leq 0.05$ to test significance.

4.3. Results and Discussion

4.3.1. Fabrication, stability and sensing of POEGMA hydrogel film microarray encapsulating ATP aptamer reporter

A hydrogel film (HF) microarray containing DNA aptamer was fabricated via the layer-by-layer deposition of aldehyde- (POA) and hydrazide- (POH)- functionalized POEGMA (PO) hydrogel precursors (Table S4.1) co-dissolved with the SSAC (*i.e.,* AFQ duplexed aptamer) (Figure S4.1). The precursor polymers had degrees of functionalization of 22 mol% for the hydrazide-functionalized polymer and 9 mol% for the aldehyde-functionalized polymer and molecular weights in the 16-20 kDa range (Table S4.2, Figure S4.2), enabling both *in situ* gelation without the need for external crosslinking chemicals/stimuli as well as facile processibility due to the low viscosity of the low molecular weight precursor polymers. Based on the equal weight fractions of both precursor polymers used to form all hydrogels and the roughly double hydrazide precursor polymer degree of functionalization relative to that of the aldehyde precursor polymer, the resulting gel was designed to have a significant excess of hydrazide groups to ensure full aldehyde crosslinking and minimize the potential of non-specific protein interactions with the hydrogel; coupled with the ether groups present on the POEGMA side chains, the hydrogel thus has high hydrogen bonding capacity to stabilize encapsulated aptamer complex.

For this study, a widely investigated aptamer for sensing adenosine and adenine nucleotides (ATP, ADP, AMP)[15,43] was utilized in the form of a tripartite FRET-based SSAC (Figure S4.1). Three oligonucleotide sequences involving (1) a long DNA strand containing the aptamer sequence (A), (2) fluorescently labelled DNA (F) at the 5' end and (3) a quencher labeled DNA (Q) at 3' end, were assembled via base-pairing into a FRET-signaling SSAC, provided by the proximity of F-DNA binding motif and Q-DNA complementary region within A-sequence. In the original design[12,44], the SSAC was assembled from a 63-nt long A-sequence composed of a 27-nt ATP-aptamer binding motif[15] extended at the 5'-end with 5 bases (A_5) of non-essential oligonucleotides to accommodate effective hybridization of signaling Q-DNAs.

The signaling oligonucleotides were associated with FRET-pair based on Alexa647 fluorophore and Black Hole Quencher 3 (BHQ3) and utilized to assemble a tripartite reporter in a A:F:Q molar ratio of 2:1:6 with 100 nM of F-DNA, previously established as an optimal configuration for signaling[36]. In the presence of ATP, the duplexed aptamer construct transforms into an aptamer-target complex, resulting in a fluorescence increase due to the displacement of the Q-DNA strand and the separation of the BHQ3 quencher away from the Alexa647 fluorophore (Figure 4.1a-inset). To ensure optimal viscosity for polymer deposition and to prevent premature drying over the cross-linking reaction, the hydrogel precursors were dissolved in 1xAssay buffer containing 5 vol% of glycerol as a humectant. Sequentially pipetting 2.5 μL of each polymer solution on to a 96-well plate wax-modified nitrocellulose membrane resulted in the formation of a hydrazone-crosslinked hydrogel that enables physical entrapment of adenosine aptamer reporters within the hydrogel matrix. The hydrogel configuration for microarray fabrication was optimized by changing the concentration of both polymer precursors between 6 wt% (6HF hydrogel), 8 wt% (8HF hydrogel), and 10 wt% (10HF hydrogel), with more concentrated hydrogels anticipated to promote higher cross-linking density and thus better aptamer immobilization efficiency and protection against denaturing agents without significantly affecting the diffusion of small molecular weight targets.

The hydrogel film immobilization capacity was quantified as the retained fluorescence content in hydrogel microarrays encapsulating the unquenched-aptamer construct (FA_5) following extended washing conditions (Figure S4.3 and Figure 4.1b). While all hydrogels tested facilitated high aptamer retention after two hours of washing (65-90%), more concentrated hydrogel configurations enabled higher aptamer retention following the trend 10HF>8HF>6HF. The effective physical entrapment efficiency provided by *in situ* hydrazone crosslinking is both higher and simpler to achieve compared to previously reported designs exploiting aptamer physisorption,[45–47] covalent conjugation to microgels onto nitrocellulose substrates[48], or polymerization within molecularly imprinted hydrogels,[49–51] techniques that typically result in 25%-55% aptamer retention while also requiring the modification of the aptamers to include covalent, affinity or polymerizable alkene or acryidite groups and/or isothermal amplification processes to achieve the desired aptamer structure and density for sensor fabrication. POEGMA hydrogel encapsulation also protects against DNase I degradation, one of the critical concerns in the practical adaption of aptamer sensing technology (Figure S4.4, Figure 4.1c)[2,11]. Upon exposure to 5U/well of DNase I, complete digestion of free-in-solution aptamer reporters was observed over the 1-hour incubation time while hydrogel film encapsulation maintained between 67-87% of aptamers intact; hydrogels prepared with higher concentrations of polymer precursors enabled improved protection due to the reduced diffusibility of DNase I as the polymer concentration was increased. Furthermore, following the washing and renaturation of retained aptamer reporters, all hydrogel assemblies treated with DNase I retained their responsiveness to ATP, enabling the hydrogel microarray to remain functional after being exposed to DNase I for subsequent sensing processes (Figure S4.4).

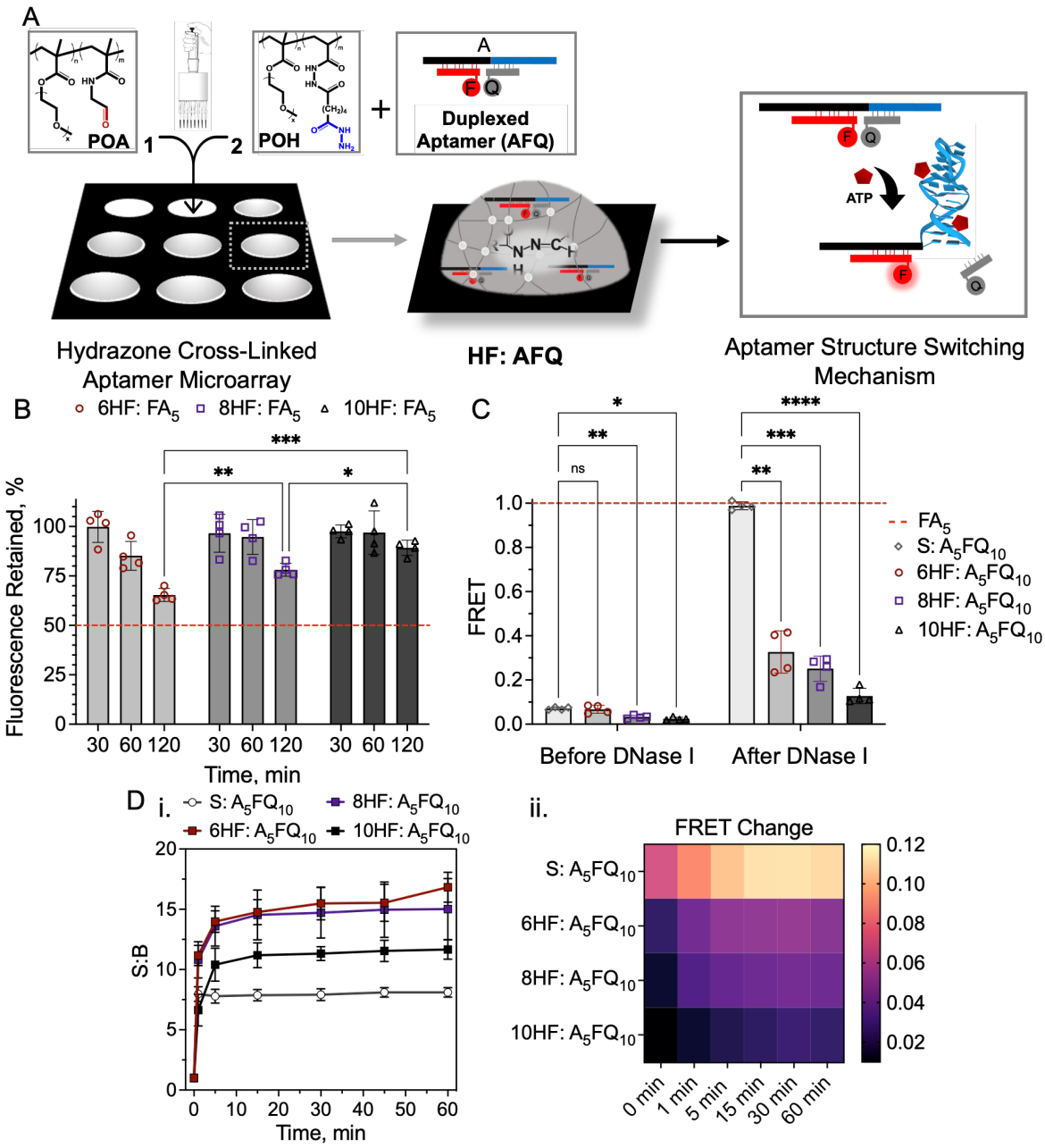

Figure 4.1 Fabrication, stability, and sensing capacity of the ATP-reporting hydrogel film microarray platform. (a) Schematic illustration of FRET-based adenosine structure switching aptamer construct (AFQ) encapsulation within the hydrazone cross-linked hydrogel film (HF) microarray assembled on a wax-modified nitrocellulose substrate. (b) Time-resolved fluorescent aptamer construct (FA_5) encapsulation efficiency in microarrays prepared with increasing hydrogel precursor polymer concentrations of 6 wt% (6HF), 8 wt% (8HF) or 10 wt% (10HF). (c) Stability of A_5FQ_{10} construct upon 60 min exposure to 5 U/well of DNase I when encapsulated in a hydrogel film (6HF, 8HF and 10HF) or free-in-solution (S). (d) Time-resolved (i) signaling enhancement (*i.e.,* S:B ratio) and (ii) fluorescence quenching efficiency (*i.e.,* FRET change) upon the exposure of A_5FQ_{10} constructs to saturating 5 mM ATP concentrations or ligand-free buffer, respectively, when free-in-solution (S) or encapsulated in a hydrogel microarray (6HF, 8HF, 10 HF) over 60 min. Data are presented as means ± SDs (*n*= at least 3 replicates).

To compare the ATP-induced sensing response rate at a saturating ATP concentration of 5 mM/well using hydrogel film-encapsulated (Figure S4.5) or free-in-solution constructs, the aptamer construct was assembled from 10-nt Q-DNA, A_5FQ_{10}, (Figure S4.1) previously identified to facilitate the highest

potential for sensitive and rapid response to cognate ligands[36] based on its reduced length and location relative to the aptamer binding site (*i.e.,* the construct was designed to occupy only one essential nucleotide within the aptamer binding pocket and thus promote a ligand-binding pathway associated with the enhanced signaling ability[12,13,16]). The effectiveness of sensing was determined by tracking the time-resolved ratio between the on-target (signal) and off-target (background) fluorescence signals (*i.e.*, S:B ratio, Figure 4.1d-i) and the corresponding changes in the fluorescence quenching efficiency upon exposure to ligand-free buffer (*i.e.*, FRET changes) indicative of the spontaneous dequenching and rise in the background fluorescence during the ligand binding period (Figure 4.1d-ii). The solution-based construct ($S:A_5FQ_{10}$) showed an instantaneous response to the addition of ATP, resulting in an 8-fold signal enhancement within the first minute after the addition; this result was expected based on the unrestricted ligand diffusion achievable in solution coupled with the low hybridization energy of the 10-nt long Q-DNA strands. Hydrogel encapsulated aptamers show a somewhat slower ligand response rate, with equilibrium being reached 15-30 min after the addition of ATP consistent with some reduction in the diffusional mobility of the ATP and/or the displaced Q-DNA molecules within the hydrogel network. However, the signaling enhancement achieved within the hydrogel films is significantly higher than achieved in solution, reaching S:B values between 12- and 16-fold (*i.e.*, up to 50% higher than the free-in-solution construct) depending on the hydrogel concentration following the trend 6HF>8HF>10HF. This result suggests that effective Q-DNA displacement can take place even within a confined environment. Furthermore, while high background levels and spontaneous fluorescence de-quenching (as indicated by lighter landscapes in FRET-change heat map, Figure 4.1d-ii) were observed over a one hour incubation time with the solution-based construct due to the relatively low stability of the shorter Q-DNA assembly, hydrogel encapsulation of the aptamer reporters resulted in significantly reduced background (as indicated by the darker landscape in Figure 4.1d-ii); the FRET efficiency improved by 2-fold in 6HF, 3-fold in 8HF and 4-fold in 10 HF relative to the solution-based construct. This result confirms the capacity of the hydrogel to stabilize the more labile 10-nt long Q-DNA complex while still providing effective signal-on sensing.

Several other assay conditions were iterated to optimize the preparation and performance of the sensing hydrogel microarrays. First, aiming to increase the rate and extent of fluorescence recovery, the concentration of the humectant within the assay buffer was increased from 5 vol% to 10 vol% or 20 vol%, motivated by our previous report[35] that indicated higher swelling ability under more humid conditions and thus faster diffusion of molecules in/out of the hydrogel network (Figure S4.6). Although the rate of fluorescence recovery could be increased by almost two-fold for the 10HF-based assemblies when using 20 vol% glycerol, the encapsulated adenosine reporters also demonstrated lower FRET efficiencies and up to 20-40% lower S:B ratios relative to assays conducted with 5 vol% of humectant. These effects may be caused by glycerol interfering with the duplex stability at higher concentrations,[52,53] thus reducing the hydrogel's overall stabilizing effect on DNA base pairing. Second, to improve the hydrogel immobilization and stabilizing capacity of the DNA sensors, the cross-linking/drying conditions were switched from 4°C/ambient to ambient temperature only, a condition expected to provide stronger polymer anchoring to the nitrocellulose membrane and a more tightly crosslinked polymer network upon exposure to washing/denaturing agents. The immobilization capacity reached 95±2% in 8HF and even 99±1% in 10HF assemblies (Figure S4.7a) when encapsulation was conducted under ambient conditions while the protection against DNase I remained relatively constant (Figure S4.7-b); however, a significant trade-off in sensing ability was observed, with lower signaling enhancement and S:B ratios of ≤ 10-fold observed particularly at higher humectant concentrations (Figure S4.8). These findings suggest that hydrogel fabrication using 5 vol% glycerol and using the 4°C/ambient temperature profile is optimal for sensor fabrication, consistent with our previous work on DNA microarrays[35].

The ability of the hydrogels to preserve the activity of immobilized aptamers upon storage for 1 month at ambient conditions was next assessed. Hydrogels prepared with higher precursor polymer

concentrations (8HF, 10HF) effectively retained the activity of the aptamer reporters within dehydrated films for 1 month after fabrication, maintaining S:B ratios at least as high as those observed in solution (Figure S4.9, Figure 4.1d). The long-term stability of DNA aptamers, even at elevated temperatures, is one of the key benefits over antibodies or RNA molecules;[4,14] as such, the development of immobilizing matrices that do not interfere with native DNA aptamer structural integrity over time is particularly important when designing novel diagnostic tools. Moreover, the selected microarray was effective in suppressing DNase I nucleolytic attack even under extended reaction times and increased enzyme concentrations (Figure S4.10), confirming the successful prevention of denaturing agent diffusion within the hydrogel network and the effective protection of the entrapped aptamer complex sensors through size-exclusion.

Based on these results, we selected the 8HF platform as the optimal system since it provides an effective balance between encapsulation efficiency (78±3% aptamer loading, Fig. 1b), signaling ability (S:B of 15±2, Fig. 4.1d-i), reduced fluorescent background (>60% reduction compared to the solution-only system throughout the entire assay, Fig. 4.1d-ii), high protection against nucleolytic degradation (70% aptamer activity retention upon exposure to 5 U DNase I, Fig. S4.4), and high storage stability (83% of the maximum signal generation preserved after 7 days of storage at ambient conditions, Fig. S4.9).

4.3.2. Designing a hydrogel microarray encapsulating ATP aptamer reporter for optimal sensing

Following the optimization of the hydrogel configuration, the DNA aptamer surface density[4,19,54] and the structure of the ligand-competing quencher stem[6,17] were optimized. Optimization of the spotted DNA density is required to minimize steric hindrance and incorrect aptamer folding[4,55] that can lead to limited dynamic ranges or poor signaling capacity when too high or too low an aptamer concentration is applied.[22,55,56] The DNA aptamer surface density was tuned by varying the concentration of the fluorophore-tagged complementary oligonucleotide F-DNA between 10 nM to 150 nM within the A:F:Q aptamer construct assembled in a molar ratio of 2:1:6 (Figure 4.2). The quencher stem was varied between 10-nt, 9-nt, and 7-nt within A_5FQ_{10}, A_4FQ_9 and A_2FQ_7 constructs, respectively, to vary the energy barrier for facile Q-DNA removal while following the ‘‘Rule of 7 of Watson–Crick base pairing’’ specifying the necessity of at least 7 consecutive base pairs for the formation of stable hybridization duplexes.[57] In order to leave most of the aptamer sequence available for ligand binding, all three quencher stems were positioned to interface with only one essential G-base inside the ligand binding pocket (Figure S4.1), thus facilitating aptamer’s ligand-induced renaturation. We hypothesize that the stabilizing effects of POEGMA hydrogel on DNA duplexes identified in our previous work[36] would enhance the responsiveness of shorter quencher stems by minimizing the fluorescent background and spontaneous dequenching (typically observed in designs with quencher stems ≤ 10-bp[17]) while maintaining high affinity interactions due to the hydrated solution-like hydrogel environment. Furthermore, the “2.5D” geometry of the hydrogels allows for the distribution of the constructs throughout a volume instead of only at an interface, expected to enable the use of lower DNA densities (i.e. reducing costs) while increasing the detection sensitivity for charged targets (e.g., ATP) whose distribution at the interface can be challenged by electrostatic repulsion[32].

Figure 4.2 shows the sensing responses of hydrogel microarrays prepared with varying F-DNA densities and Q-DNA lengths via FRET-based fluorescence quenching (see Figure S4.11 for qualitative data) and signal enhancement (S:B ratio) at both a low 50 μM ATP concentration (a typically reported LOD within most of the hydrogel-based aptamer switches[30]) and a high 5 mM ATP concentration (a saturating ligand condition) relative to the solution-based constructs.

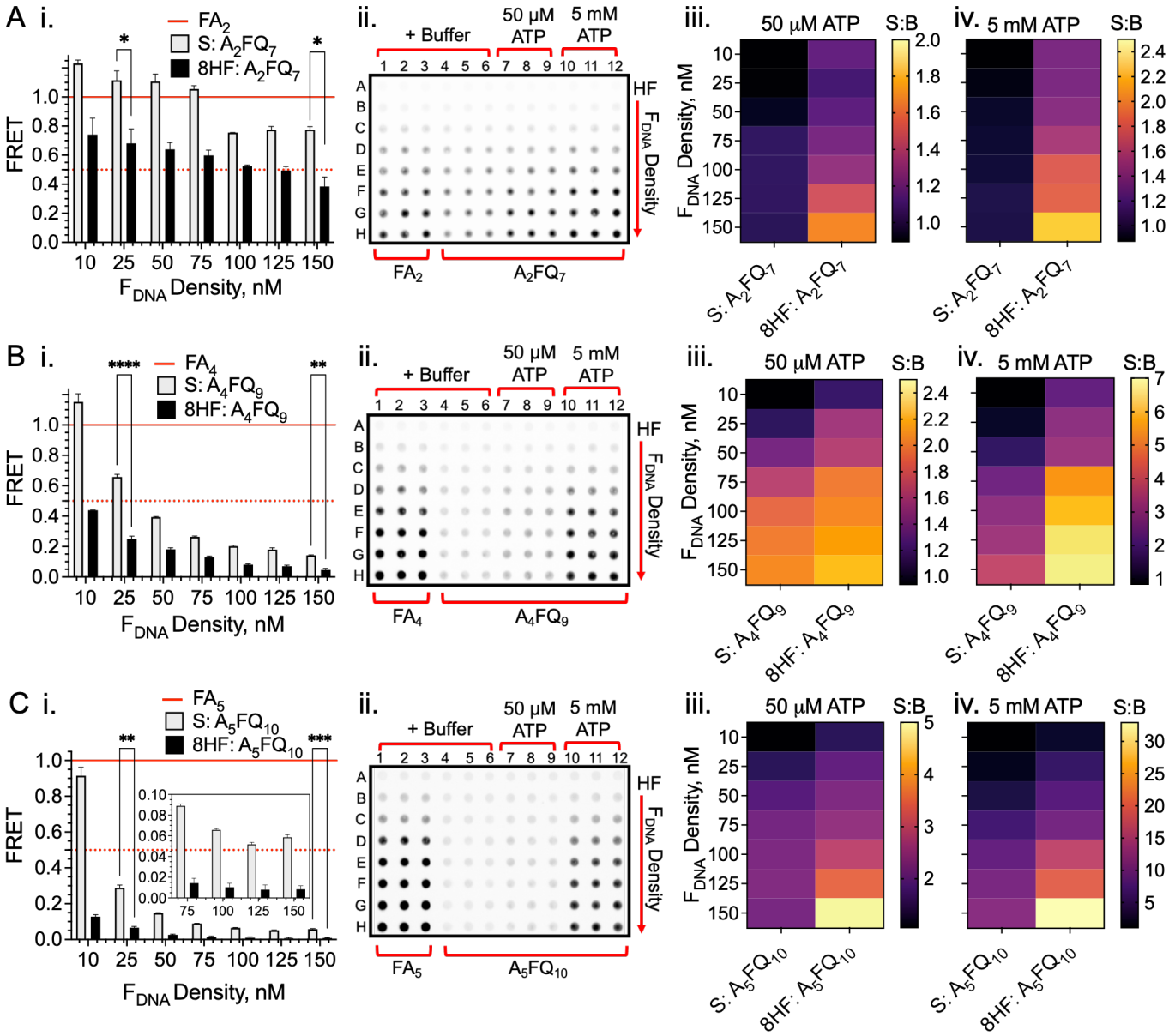

Figure 4.2 FRET and ATP sensing responses of structure-switching aptamer constructs (AFQ) assembled with varying Q-DNA lengths in a hydrogel film (8HF) or free-in-solution (S) at varying DNA aptamer densities corresponding F-DNA contents of 10 nM to 150 nM and construct molar ratios (A:F:Q) of 2:1:6. Sensing capacity of aptamer constructs prepared using a (a) 7 bp quencher stem, A_2FQ_7; (b) 9 bp quencher stem, A_4FQ_9; and (c) 10 bp quencher stem, A_5FQ_{10} as reported by (i) fluorescence quenching (FRET efficiency), (ii) response to ATP (qualitative image), and (iii, iv) signal: background ratio (S:B) at (iii) 50 μM and (iv) 5 mM ATP concentration. Data are presented as means ± SDs (n=3).

Significantly higher FRET efficiencies are observed in hydrogel film arrayed samples relative to solution-based constructs assembled with each quencher stem length at both the low and high DNA aptamer surface densities tested (Figure 4.2 a,b,c-i). Interestingly, at the lowest DNA aptamer density tested (corresponding to 10 nM F-DNA), no fluorescence quenching was observed in any of the solution-based constructs while hydrogel encapsulation enabled a ~90% fluorescence reduction in A_5FQ_{10}, a ~60% fluorescence reduction in A_4FQ_9, and a ~30% fluorescence reduction in A_2FQ_7. By increasing the DNA aptamer density, the FRET efficiency increased for all constructs; however, significantly higher increases were observed in the hydrogel-arrayed systems, particularly for constructs assembled using 9-bp and 10-bp quencher stems. For example, at least a 60% lower background fluorescence was achieved in 8HF:A_4FQ_9 at an aptamer reporter density of 25 nM F-DNA (a 4x lower aptamer concentration than

previously established as optimal for signaling[36,58]), while a 3-fold higher fluorescence quenching relative to the corresponding solution-based assemblies was observed using dense aptamer arrays containing 150 nM F-DNA. With A_5FQ_{10}, the benefit of the hydrogel in reducing background signal becomes even more pronounced, enabling 4- and 7-fold higher FRET efficiency with the 25 nM and 150 nM F-DNA-based aptamer hydrogels, respectively relative to the corresponding free-in-solution constructs. With the shorter quencher stems (A_2FQ_7), the hydrogel array facilitates a 32% fluorescence reduction with 25 nM F-DNA and a 62% fluorescence reduction with 150 nM F-DNA; in contrast, the solution-based constructs require ≥100 nM F-DNA to reach a maximum of ∼24% fluorescence quenching. As such, the hydrogel can significantly reduce both the total amount of reporter as well as the length of the Q-DNA required to facilitate effective, specific, and sensitive ATP sensing.

To assess the potential for ligand-induced signal recovery over a range of ATP concentrations, the sensing response to ATP was quantified as a S:B ratio (Figure 4.2 a,b,c-ii), with the results summarized in the heat maps shown in Figure 4.2 a,b,c-iii,iv; lighter landscapes indicate higher S:B ratios. More stable aptamer reporters enable greater fluorescence recovery in the solution system, consistent with previous literature reports[12,21,36]; fluorescence recovery can be further increased with increasing aptamer density (Figure 4.2 b,c-iii,iv), with S:B ratios reaching 2- to 2.2-fold for a solution containing 50 μM ATP and 3.8- to 11.3-fold for a solution containing 5 mM ATP using S:A_4FQ_9 and S:A_5FQ_{10}, respectively (detection time = 30 min). In contrast, aptamer reporters assembled with the shortest quencher stems in solution exhibit either low or a total lack of fluorescence signaling at any density of DNA aptamer, as indicated by the dark landscapes in Figure 4.2 a-iii,iv. Hydrogel encapsulation, however, can enable even the shortest quencher stems to yield measurable signal outputs, achieving S:B ratios > 2-fold at saturating ATP concentrations (detection time = 5 min). Hydrogel-encapsulated reporters with longer quencher stems can also facilitate 2- to 3-fold higher S:B ratios relative to the free-in-solution assemblies at higher aptamer densities (≥ 100 nM F-DNA), with 8HF:A_5FQ_{10} leading to the highest signaling improvements consistent with its most effective background reduction (Figure 4.2 c-i) across both ATP concentrations tested. Collectively, these results show that the proposed hydrogel system facilitates strong signal generation across a broad range of very short quencher stems, consistent with the hydrogel promoting stronger background fluorescence suppression and preserving "solution-like" aptamer renaturation within the confined environment.

4.3.3. Binding Affinity in Pure Buffer

To assess how varying quencher stem lengths and DNA surface densities affect the ligand binding affinity, aptamer reporters quenched with 7-bp (A_2FQ_7), 9-bp (A_4FQ_9) and 10-bp (A_5FQ_{10}) duplexes were assembled at high and low aptamer densities corresponding to 150 nM F-DNA and 25 nM F-DNA respectively in hydrogel films (8HF, selected as the lead composition based in the results in section 4.3.1) or free-in-solution (S). Fluorescence recovery increases as the ATP concentration increases (see Figure S4.12 for full qualitative data), with the linear response observed at lower ATP concentrations for each sensor assembly reported in Figure 4.3. The corresponding dissociation constants (K_d), limits of detection (LOD) for the ATP ligand, and the thermal stability estimated for each quencher stem are summarized in Table 4.1. At higher aptamer concentrations, the K_d values obtained with the hydrogel arrays encapsulating A_5FQ_{10} and A_4FQ_9 (plotted after 60 min) correlate with the results obtained with the free-in-solution constructs (assessed using a conventional microplate assay) and are comparable to literature affinity values for 9- to 12-bp duplexed ATP-binding aptamers.[16,21] These results indicate that the dose-response relationship between DNA aptamers and adenosine-based ligand is preserved in the hydrogel and that affinity interactions across different quencher compositions are not restricted by the confined environment. Owing to the thermal stabilization (Figure S4.13, Table 4.1) and the fluorescence background reduction provided by the hydrogel (Figure 4.2a,b,c-i), significantly higher signal

enhancement is observed with the hydrogel array relative to the solution-based sensor, particularly for more concentrated ATP samples; the gel-based assay provided 2- to 3- fold greater S:B ratios and at least 1-order of magnitude wider dynamic range with the A_5FQ_{10} and A_4FQ_9 constructs relative to the same constructs in free solution. The potential of hydrogels to stabilize very short duplexes further enables 7-bp long quencher stems to produce fluorescence increases 4.9-fold higher than the same assemblies in solution, in which the constructs are practically non-responsive to ligand addition (maximum signaling enhancement factor 1.1 ± 0.04). It is noteworthy that the K_d value obtained with 8HF:A_2FQ_7 (as low as 14 μM) is only slightly larger than that of the native adenosine-binding aptamer prior to assembly into the signaling construct (6-10 μM)[15], confirming our hypothesis that the hydrogel array is able to facilitate the use of very short ligand-competing oligonucleotides in aptamer reporter assemblies with substantially lower reduction in ligand-binding affinity.

The truncation of quencher stems within the DNA-stabilizing hydrogel arrays further enables improved sensitivity of surface-based sensors relative to the free-in-solution assay. Limits of detection (LOD), determined based on the 3σ/initial slope in which σ represents one standard deviation within the linear range of the binding curve (Figure 4.3-insets), were as low as 1.2 μM to 2 μM when using hydrogel-based assemblies with quencher stems <10-bp. These LOD values are at least 2x lower than the best-performing reporter in solution, 7x lower than a similar strand-displacement design involving aptamer molecules cross-linked within photonic crystal hydrogel array[34], and at least 10x lower than the originally developed aptamer reporters in solution (25 μM)[12] or other comparable hydrogel-based aptamer switch designs.[25,30,58] The obtained sensitivity is also on par with recently reported nanomolar affinity adenosine aptamer selected using more stringent ligand conditions, which achieved a LOD of 1.1 μM in solution upon duplex formation.[59] The encapsulation of lower aptamer concentrations (corresponding to 25 nM F-DNA) in hydrogel microarrays maintains low LOD values, with LODs of 1.8 μM and 3.5 μM observed for 8HF:A_4FQ_9 and 8HF:A_5FQ_{10}, respectively. Solution-based constructs, however, exhibit significantly higher increases in LODs, with values for S:A_5FQ_{10} and S:A_4FQ_9 constructs measured to be in the 10-20 μM range while S:A_2FQ_7 constructs are fully non-responsive. Interestingly, K_d value of 14.7 μM achieved using the A_2FQ_7 construct encapsulated in the 8HF hydrogel is comparable to that achieved at higher aptamer density (despite a lower saturating fluorescence recovery of 2 ± 0.2 as measured 15 min from ligand addition) in addition to the value in the originally selected native adenosine aptamer[15,43]. This result is also within the range of K_d values observed for the aforementioned nanomolar affinity adenosine binder upon assembly into a signaling reporter[60,61] (K_d = 19 μM after FRET construct assembly) and similar to or better than the K_d values achieved with polyacrylamide-based molecularly imprinted polymers co-polymerized with fluorophore and quencher-labeled split aptamers[51] or aptamer cross-linked stimuli-responsive hydrogels[34] (K_d = 68-400 μM). Overall, by truncating and rationally positioning the Q-DNA oligonucleotides, decreasing the surface density of the spotted aptamer, and leveraging the stabilizing properties of the hydrogel on the duplexes, a 17.5-fold higher affinity to adenosine binding can be achieved that is at least competitive with or better than other reported aptamer signaling approaches.

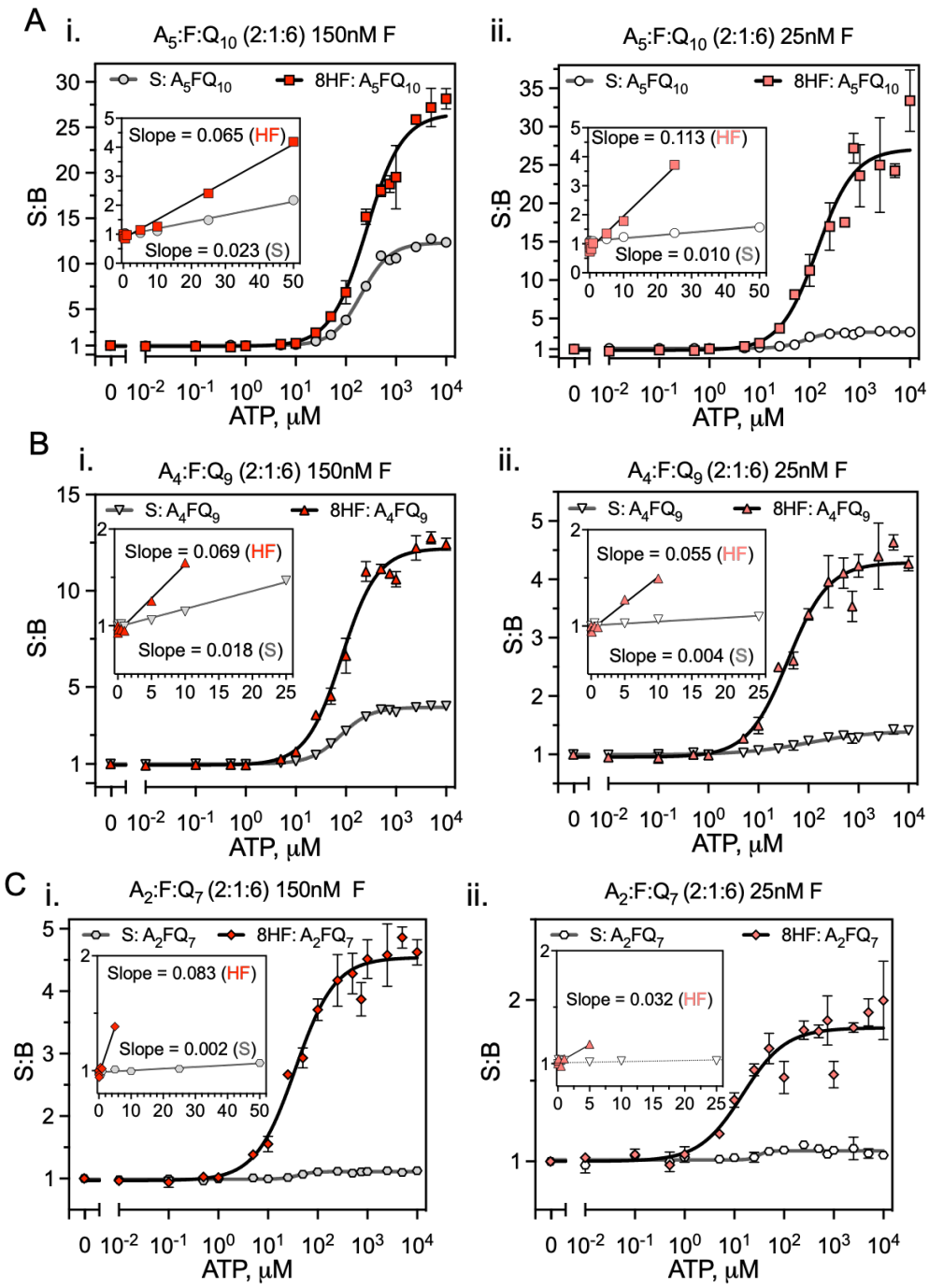

Figure 4.3 Binding affinity and sensitivity of ATP aptamer reporters assembled with varying Q-DNA lengths in hydrogel microarrays (8HF) or free-in-solution (S) at aptamer concentrations corresponding to F-DNA densities of 25 nm and 150 nm (A:F:Q molar ratio 2:1:6) and ATP concentrations ranging from 0-10 mM in pure buffer (25°C, incubation time 15 min – 60 min). Aptamer constructs (a) A5FQ10; (b) A4FQ9 and (c) A2FQ7 are tested at (i) 150 nm and (ii) 25 nm F-DNA aptamer surface densities. Inset figures represent the linear detection range response for each aptamer sensor at low ATP dosages. Data are presented as means ± SDs (n=3).

Table 4.1 Dissociation constant (K_d), limit of detection (LOD) and melting temperature (T_m) of aptamer reporters assembled with varying Q-DNA lengths in a hydrogel microarray (8HF) or free-in-solution (S) at aptamer concentrations corresponding to F-DNA densities of 25 nM and 150nM (A:F:Q molar ratio 2:1:6); see raw data for parameter fitting in Figure 4.3.

A:F:Q 2:1:6 (150 nM F-DNA)					A:F:Q 2:1:6 (25 nM F-DNA)		
Sensing ATP in Pure Buffer		**K_d, [μM]**	**LOD, [μM]**	**T_m, [°C]**	**K_d, [μM]**	**LOD, [μM]**	**T_m, [°C]**
Q_{10}	8HF	**257**	**6.1**	**45.2**	**142**	**3.5**	**37.3**
	S	204	7.7	42.0	80	13.4	34.9
Q_9	8HF	**82.9**	**2.0**	**38.1**	**39.3**	**1.8**	**31.8**
	S	77.8	4.0	31.5	~ 100	18.6	29.6
Q_7	8HF	**35.5**	**1.2**	**32.4**	**14.7**	**3.0**	**28.1**
	S	/	~ 30	28.5	/	~ 50	26.4

4.3.4. Binding Affinity in Serum

To demonstrate the practical application of the hydrogel microarray sensor in complex biological samples, A_5FQ_{10} and A_4FQ_9 constructs were assembled at a single aptamer concentration corresponding to 25 nM F-DNA and tested both encapsulated in 8HF and free-in-solution against 0-10 mM ATP spiked in 50% human serum. The binding affinities and sensitivities obtained from the resulting dose-response curves are summarized in Figure 4.4 and Table 4.2. Sensing in serum can be challenging due to the reduced metal ion content[62], aggregation with serum proteins, and/or the presence of various contaminants that interfere with aptamer proper folding and/or increase background fluorescence[11,24,60]. Such challenges were observed with the free-in-solution constructs; while the affinity constants were not significantly affected, the LOD values increase up to 27 μM and saturating S:B ratios of only 2.8 ± 0.4 for $S:A_5FQ_{10}$ and 1.4 ± 0.04 in $S:A_4FQ_9$ were observed over 60 min and 30 min incubation times respectively with ATP in 50% serum. In contrast, the hydrogel-based constructs, maintained LOD values of 4.6 μM and 14.4 μM for A_4FQ_9 and A_5FQ_{10}. These hydrogel-based construct LOD values represent up to a 5-fold lower detection limit relative to the free-in-solution constructs or reported hydrogel-based aptamer cross-linked designs that require extensive aptamer modification chemistry[34] and up to 10-fold lower LODs relative to previously reported solution-based[63] or magnetic bead-immobilized[64] FRET aptamer reporters in diluted human serum samples (60-200 μM). The effective maintenance of the LOD values in the hydrogel array sensors in serum suggests that aptamer duplex stabilization and solution filtering effects afforded by the cross-linked hydrophilic network can further expand the scope for encapsulated aptamer reporters to analyze real biological samples.

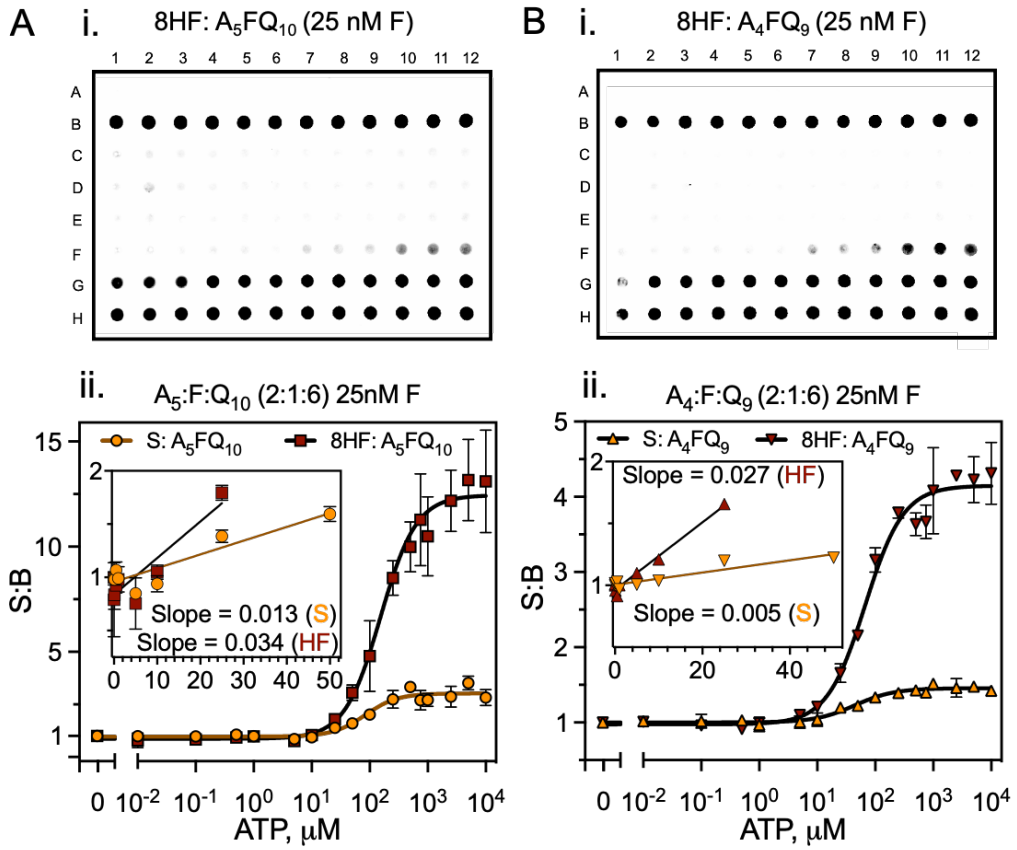

Figure 4.4 Binding affinity and sensitivity of ATP aptamer reporters assembled with varying Q-DNA lengths in a hydrogel microarray (8HF) or free-in-solution (S) at an aptamer concentration corresponding to a F-DNA density of 25 nM (A:F:Q molar ratio 2:1:6) and ATP concentrations ranging from 0-10 mM spiked in 50% serum (25°C, incubation time 30-60 min). Aptamer constructs (a) A_5FQ_{10} and (b) A_4FQ_9 were tested, with performance represented by (i) qualitative data presented as a fluorescent scan of paper-based sensor following incubation with ATP and (ii) the dose-response curves obtained from (i). Inset figures represent the linear detection range response for each aptamer sensor at low ATP concentrations. Data are presented as means ± SDs (n=3).

Table 4.2 Dissociation constant (K_d), and limit of detection (LOD) of aptamer reporters assembled with varying Q-DNA lengths in a hydrogel microarray (8HF) or free-in-solution (S) at an aptamer concentration corresponding to a F-DNA density of 25 nM (A:F:Q molar ratio 2:1:6); see raw data for parameter fitting in Figure 4.4.

A:F:Q 2:1:6 (25 nM F-DNA)							
Sensing ATP in 50% Serum		**K_d, [μM]**	**LOD, [μM]**			**K_d, [μM]**	**LOD, [μM]**
Q_{10}	8HF	**153**	**14.4**	**Q_9**	8HF	**67**	**4.6**
	S	84	26.9		S	~ 50	~ 27

4.3.5. Reusability of hydrogel-based aptamer reporters and microarray assembly via Q-DNA Hybridization

Next, the potential of hydrogel-based aptamer microarray to be regenerated and reused for subsequent ligand-binding assays was investigated. The reusability of duplexed aptamer reporters is typically assessed either by simple washing in ligand-binding buffer[23] or by using harsher procedures involving chemical denaturation of the aptamer complexes (*e.g.*, with 8 M urea, 10% SDS or 1 M NaCl)[19,23] that

completely strip the affinity-bound analytes and then re-fold the complexes into their active conformation after incubation in renaturing assay buffers. Following an initial ATP exposure, the microarray samples were rinsed and subjected to different regeneration procedures, with the results summarized in Figure 4.5.

Simple washing results in a moderate regeneration capacity, leading to 57% and 47% signaling recovery in 8HF:A_4FQ_9 and 8HF:A_5FQ_{10} respectively (Figure 4.5a). Thus, more severe treatment involving concentrated urea, known to effectively denature nucleic acid complexes,[18] was used. To obtain effective aptamer reporter re-assembly following urea denaturation, the hybridization conditions of quencher-labeled oligonucleotides (Q-DNA) with hydrogel-arrayed fluorescent aptamer constructs were first optimized (Figure 4.5b, c). In general, more concentrated Q-DNA solutions are necessary to achieve a FRET efficiency comparable to the aptamer reporters pre-formed and encapsulated within hydrogel film; the assembly of 8HF:A_4F + Q_9 and 8HF:A_5F + Q_{10} with an equivalent fluorescence quenching capacity relative to encapsulated pre-assembled 8HF:A_4FQ_9 and 8HF:A_5FQ_{10} microarrays requires a 10x Q-DNA concentration and a 90 min hybridization time. The process is also minimally affected by post-hybridization washing, suggesting that the hydrogel can successfully accommodate hybridization of signaling oligonucleotides and subsequently stabilize in-gel formed duplexes.

Based on this result, microarray samples were urea-denatured following an initial ATP exposure and re-assembled using a 10xQ-DNA concentration, with the S:B results summarized in Figure 4.5-d. No improvement in the sensor re-usability was observed in 8HF:A_4FQ_9 (*i.e.*, 56% signal recovery), while 8HF:A_5FQ_{10} enabled a ~20 % higher re-usability (*i.e.*, 72% signal recovery). The signal recovery of HF:A_5FQ_{10} can be further improved in hydrogels prepared with lower precursor polymer concentrations (6HF) that enable enhanced hybridization efficiency (Figure S4.14), with up to 98.6% of the signal recovered following urea denaturation; this result is consistent with previous results showing that 6 wt% precursor polymer hydrogels can provide optimal hybridization efficiency for short DNA duplexes at interfaces.[35] Of interest, successful annealing of Q-DNAs to the hydrogel-immobilized fluorescent aptamer constructs can be achieved even with the shortest (*i.e.*, 7-nt long) oligonucleotides (Figure S4.15), with 3x higher fluorescence quenching achievable following in-hydrogel hybridization of Q_7-DNA to FA_2 constructs encapsulated in both 6HF and 8HF relative to pre-assembled arrayed samples. This result opens the possibility of fabricating even more stable aptamer duplexes assembled with very short quencher stems and/or high throughput screening of optimal signaling oligonucleotides for designing more responsive SSACs.

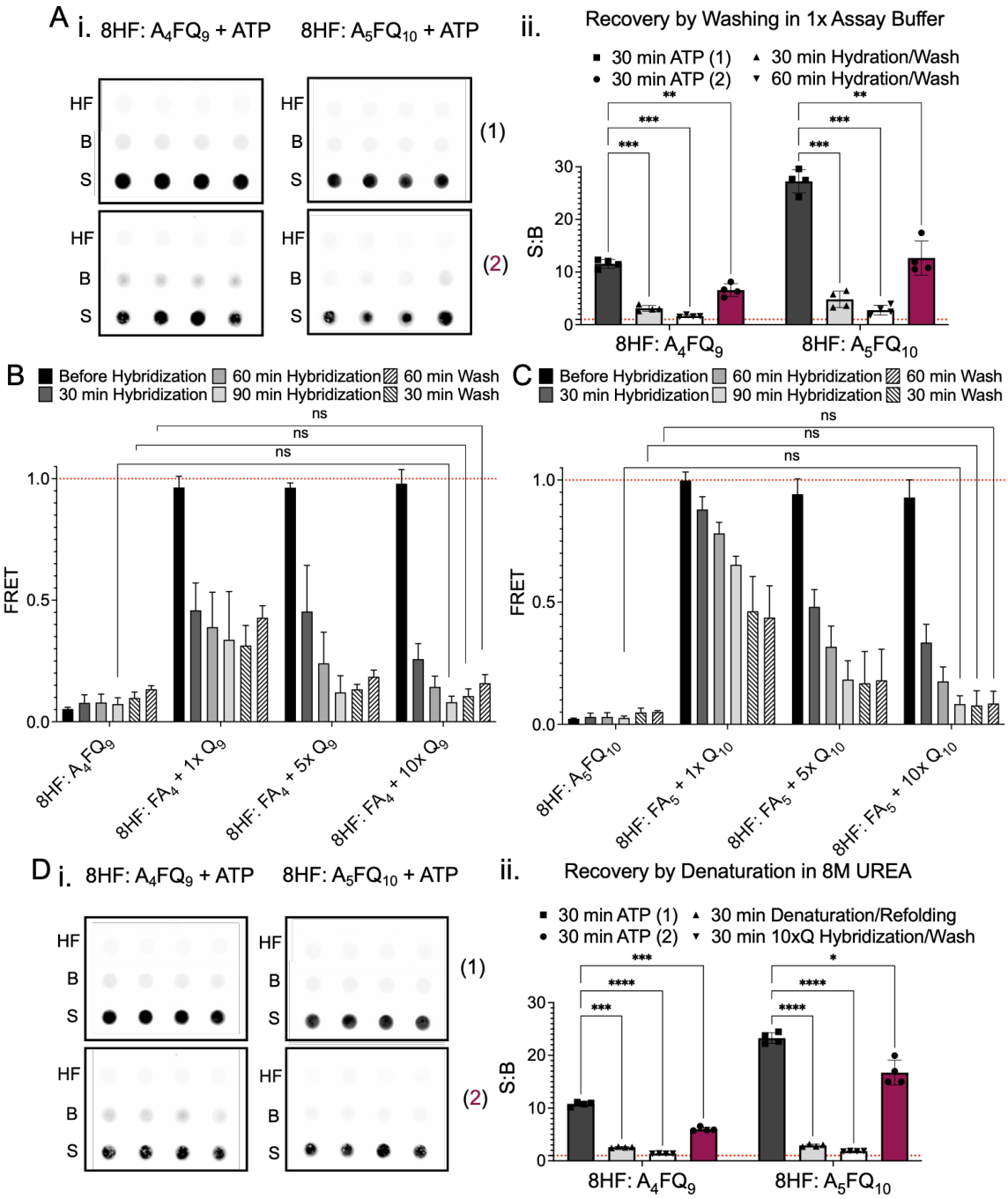

Figure 4.5 Reusability of hydrogel-based aptamer microarrays assembled with 9- and 10-bp quencher stems. (a) Following initial ATP incubation (1), the sensor was regenerated by (i) washing in 1xAssay buffer followed by another exposure to ATP (2), with the efficacy of sensor regeneration represented by (ii) the S:B ratio. (b,c) Optimization of Q-DNA hybridization to hydrogel-encapsulated fluorescent aptamer and *in situ* assembly and stability of (b) 9-bp and (c) 10-bp duplexed aptamers relative to encapsulated aptamer constructs. (d) Following initial ATP incubation (1), the sensor was regenerated by (i) urea denaturation and Q-DNA hybridization, followed by another exposure to ATP (2), with the efficacy of sensor regeneration represented by (ii) the S:B ratio.

4.3.6. Printing Fabrication of Hydrogel-Immobilized Aptamer Microarrays

To investigate the potential for automated fabrication of the hydrogel-based aptamer microarrays that would increase the commercialization potential of the developed platform,[19] hydrogel microarrays were prepared by sequential dispensing of hydrogel precursor "inks" in which POA and POH co-dissolved with duplex aptamer construct assembled with a 10-bp quencher stem (POH/A_5FQ_{10}) on to a wax-modified nitrocellulose substrates using a drop-on-demand syringe solenoid printer (Figure 4.6a). Both precursor polymer inks were dissolved as 8 wt% solutions containing 5 vol% glycerol as a humectant and viscosity modifier to obtain a printing-appropriate shear viscosity profile[35,39] and avoid nozzle clogging due to premature small droplet evaporation[65], both significant issues that have limited the printability of other biosensing materials (*e.g.,* sol-gel materials[66]). To assess the spot-to-spot uniformity of the printing process, fluorescent aptamer constructs (FA_5) were co-printed in the hydrogel (see Figure S4.16 for qualitative microarray pictures) and the fluorescent intensity was quantified across each microzone (Figure 4.6b). Consistent fluorescence signals were observed both spot-to-spot and within each spot area, with a coefficient of variation of just 5% observed over 84 replicate prints. Following vigorous washing for 2 hours under shaking, a high retention capacity of 92 ± 4% was observed for the printed hydrogel array; this degree of retention is ~14% higher than that achieved with manual deposition, likely due to the more consistent polymer deposition enabled by the automated printing equipment. Time-resolved fluorescence recovery (*i.e.,* S:B ratio) following exposure to saturating ATP concentrations (Figure 4.6d-i, ii) indicated that at least a 10-fold S:B ratio can be achieved 15 minutes following ligand addition, performance consistent with that observed with the manually prepared samples (Figure 4.1d). The results suggest that printing-based fabrication is a scalable approach to scale-up the manufacturing of hydrogel-array aptamer sensors and thus leverage the beneficial properties of the hydrogel in practical contexts.

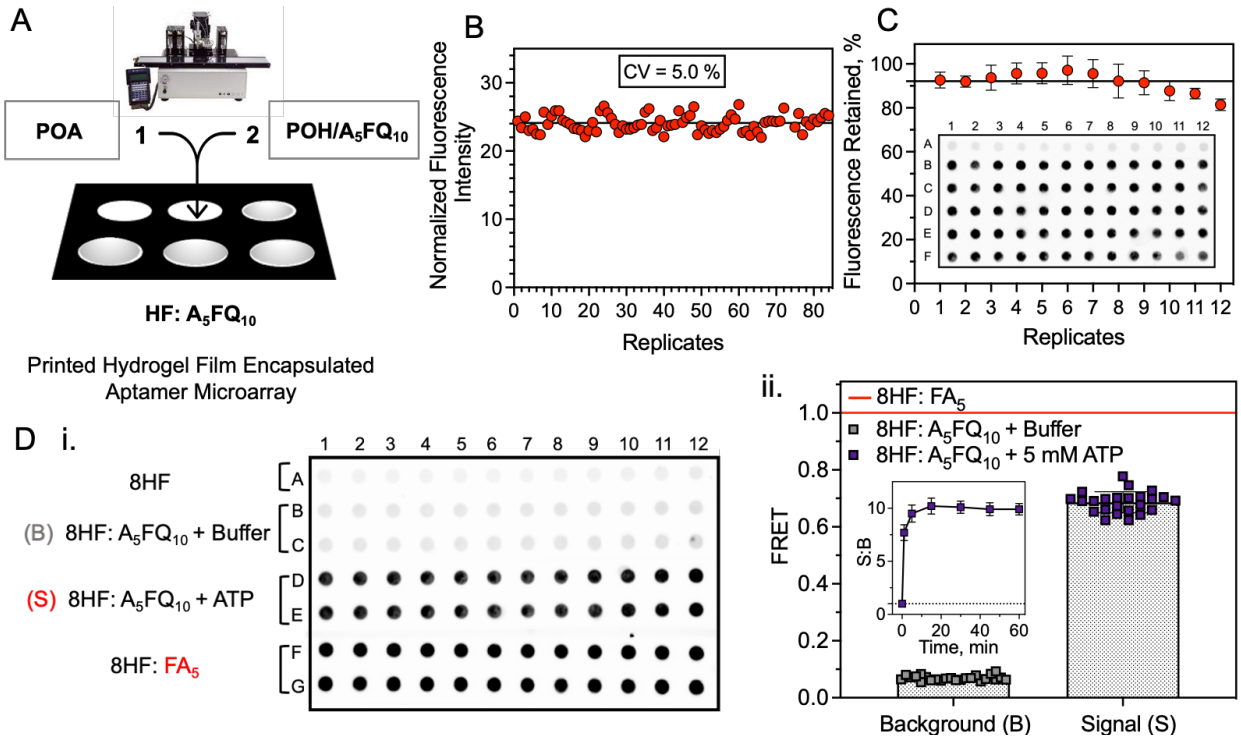

Figure 4.6 Fabrication and sensing performance of a hydrogel printed aptamer microarray sensor for ATP detection. (a) Layer-by-layer printing of an ATP-sensing hydrazone cross-linked hydrogel film (HF:AFQ, top) using a BioJet non-contact solenoid printer. (b) Spot-to-spot uniformity of a hydrogel printed microarray. (c) Encapsulation efficiency of the hydrogel printed microarray. Data are presented as means ± SDs (n=5). (d) Fluorescence recovery in a printed 8HF:AF_5Q_{10} array: (i) Row A = blank; rows B, C = background treated with ligand-free buffer (N); rows D,E = signal following exposure to 5 mM ATP over 60 min; rows F,G = positive controls of (F) the hydrogel only (8HF) and (G) a hydrogel-containing fluorescent aptamer construct (8HF:FA_5). (ii) Quantitative data on 8HF:AF_5Q_{10} microarray time-resolved S:B ratio and FRET-based fluorescence recovery following 60 min of exposure to 5 mM ATP. Data are presented as means ± SDs (n=24).

4.4. Conclusion

Transitioning from a solution-based assay to a surface-immobilized sensing platform is known to be a non-trivial and challenging task.[5,21] The hydrogel film microarray described herein enables the physical encapsulation of adenosine-responsive FRET-signaling DNA aptamers assembled with very short quencher stems for improved affinity. The developed hydrogel platform features a high immobilization capacity, protection against nucleolytic degradation, and enhanced thermal stabilization of the aptamer structure-switching duplexes, properties that result in a significant reduction in the fluorescent background signal and off-target fluorescence recovery coupled with an improvement in the signaling response compared with the same constructs used free-in-solution. By truncating and rationally positioning quencher stems from 10-bp to 7-bp and by modulating the DNA aptamer surface density, it is possible to increase the binding affinity by up to 17.5-fold, resulting in affinity constants comparable to the native adenosine aptamer and detection limits between 1.2-2 μM that are at least one order of magnitude better than that of the original solution-phase construct. The hydrogel sensors demonstrate fast kinetics (<30 min to signal), are applicable in complex biological fluid (50% human serum), are inexpensive to produce, and use at least 10x less sample compared to conventional solution assays. The microarrays are printable, reusable, and can be assembled even via the in-gel hybridization of signaling oligonucleotides, expanding the potential practical adaptation of aptamer sensing technology (including

the potential to re-use the sensor). The sensor design developed should also be directly translatable to any small molecule aptamer of interest, achieving effective aptamer immobilization without sacrificing (or even enhancing) aptamer binding selectivity and sensitivity for target ligands.

4.5. References

(1) Al-Qaoud, K. M.; Obeidat, Y. M.; Al-Omari, T.; Okour, M.; Al-Omari, M. M.; Ahmad, M. I.; Alshadfan, R.; Rawashdeh, A. M. The Development of an Electrochemical Immunosensor Utilizing Chicken IgY Anti-Spike Antibody for the Detection of SARS-CoV-2. *Sci Rep* **2024**, *14* (1), 748. https://doi.org/10.1038/s41598-023-50501-w.

(2) Yu, H.; Alkhamis, O.; Canoura, J.; Liu, Y.; Xiao, Y. Advances and Challenges in Small-Molecule DNA Aptamer Isolation, Characterization, and Sensor Development. *Angew. Chem. Int. Ed.* **2021**, *60* (31), 16800–16823. https://doi.org/10.1002/anie.202008663.

(3) Ruscito, A.; DeRosa, M. C. Small-Molecule Binding Aptamers: Selection Strategies, Characterization, and Applications. *Front. Chem.* **2016**, *4*. https://doi.org/10.3389/fchem.2016.00014.

(4) Witt, M.; Walter, J.-G.; Stahl, F. Aptamer Microarrays—Current Status and Future Prospects. *Microarrays* **2015**, *4* (2), 115–132. https://doi.org/10.3390/microarrays4020115.

(5) Walter, J.-G.; Heilkenbrinker, A.; Austerjost, J.; Timur, S.; Stahl, F.; Schepe, T. Aptasensors for Small Molecule Detection. *Zeitschrift für Naturforschung B* **2012**, *67* (10), 976–986. https://doi.org/10.5560/znb.2012-0147.

(6) Heilkenbrinker, A.; Reinemann, C.; Stoltenburg, R.; Walter, J.-G.; Jochums, A.; Stahl, F.; Zimmermann, S.; Strehlitz, B.; Scheper, T. Identification of the Target Binding Site of Ethanolamine-Binding Aptamers and Its Exploitation for Ethanolamine Detection. *Anal. Chem.* **2015**, *87* (1), 677–685. https://doi.org/10.1021/ac5034819.

(7) Zhang, F.; Huang, P.-J. J.; Liu, J. Sensing Adenosine and ATP by Aptamers and Gold Nanoparticles: Opposite Trends of Color Change from Domination of Target Adsorption Instead of Aptamer Binding. *ACS Sens.* **2020**, *5* (9), 2885–2893. https://doi.org/10.1021/acssensors.0c01169.

(8) Brittain, W. J.; Brandsetter, T.; Prucker, O.; Rühe, J. The Surface Science of Microarray Generation–A Critical Inventory. *ACS Appl. Mater. Interfaces* **2019**, *11* (43), 39397–39409. https://doi.org/10.1021/acsami.9b06838.

(9) Wang, X.; Yang, Y.; Yin, Y.; Zeng, N.; Dong, Y.; Liu, J.; Wang, L.; Yang, Z.; Yang, C. High-Throughput Aptamer Microarrays for Fluorescent Detection of Multiple Organophosphorus Pesticides in Food. *Anal. Chem.* **2022**, *94* (7), 3173–3179. https://doi.org/10.1021/acs.analchem.1c04650.

(10) Zhang, H.; Li, A. Z.; Liu, J. Surfactant-Assisted Label-Free Fluorescent Aptamer Biosensors and Binding Assays. *Biosensors* **2023**, *13* (4), 434. https://doi.org/10.3390/bios13040434.

(11) Nutiu, R.; Li, Y. Structure-Switching Signaling Aptamers: Transducing Molecular Recognition into Fluorescence Signaling. *Chem. Eur. J.* **2004**, *10* (8), 1868–1876. https://doi.org/10.1002/chem.200305470.

(12) Nutiu, R.; Li, Y. Structure-Switching Signaling Aptamers. *J. Am. Chem. Soc.* **2003**, *125* (16), 4771–4778. https://doi.org/10.1021/ja028962o.

(13) Feagin, T. A.; Maganzini, N.; Soh, H. T. Strategies for Creating Structure-Switching Aptamers. *ACS Sens.* **2018**, *3* (9), 1611–1615. https://doi.org/10.1021/acssensors.8b00516.

(14) Cho, E. J.; Lee, J.-W.; Ellington, A. D. Applications of Aptamers as Sensors. *Annual Rev. Anal. Chem.* **2009**, *2* (1), 241–264. https://doi.org/10.1146/annurev.anchem.1.031207.112851.

(15) Huizenga, D. E.; Szostak, J. W. A DNA Aptamer That Binds Adenosine and ATP. *Biochemistry* **1995**, *34* (2), 656–665. https://doi.org/10.1021/bi00002a033.

(16) Munzar, J. D.; Ng, A.; Corrado, M.; Juncker, D. Complementary Oligonucleotides Regulate Induced Fit Ligand Binding in Duplexed Aptamers. *Chem. Sci.* **2017**, *8* (3), 2251–2256. https://doi.org/10.1039/C6SC03993F.

(17) Munzar, J. D.; Ng, A.; Juncker, D. Duplexed Aptamers: History, Design, Theory, and Application to Biosensing. *Chem. Soc. Rev.* **2019**, *48* (5), 1390–1419. https://doi.org/10.1039/C8CS00880A.

(18) Gao, Y. Secondary Structure Effects on DNA Hybridization Kinetics: A Solution versus Surface Comparison. *Nucleic Acids Research* **2006**, *34* (11), 3370–3377. https://doi.org/10.1093/nar/gkl422.

(19) Collett, J. R.; Cho, E. J.; Ellington, A. D. Production and Processing of Aptamer Microarrays. *Methods* **2005**, *37* (1), 4–15. https://doi.org/10.1016/j.ymeth.2005.05.009.

(20) Peterson, A. W. The Effect of Surface Probe Density on DNA Hybridization. *Nucleic Acids Research* **2001**, *29* (24), 5163–5168. https://doi.org/10.1093/nar/29.24.5163.

(21) Munzar, J. D.; Ng, A.; Juncker, D. Comprehensive Profiling of the Ligand Binding Landscapes of Duplexed Aptamer Families Reveals Widespread Induced Fit. *Nat Commun* **2018**, *9* (1), 343. https://doi.org/10.1038/s41467-017-02556-3.

(22) Watkins, H. M.; Vallée-Bélisle, A.; Ricci, F.; Makarov, D. E.; Plaxco, K. W. Entropic and Electrostatic Effects on the Folding Free Energy of a Surface-Attached Biomolecule: An Experimental and Theoretical Study. *J. Am. Chem. Soc.* **2012**, *134* (4), 2120–2126. https://doi.org/10.1021/ja208436p.

(23) Carrasquilla, C.; Li, Y.; Brennan, J. D. Surface Immobilization of Structure-Switching DNA Aptamers on Macroporous Sol−Gel-Derived Films for Solid-Phase Biosensing Applications. *Anal. Chem.* **2011**, *83* (3), 957–965. https://doi.org/10.1021/ac102679r.

(24) Yoo, H.; Jo, H.; Oh, S. S. Detection and beyond: Challenges and Advances in Aptamer-Based Biosensors. *Mater. Adv.* **2020**, *1* (8), 2663–2687. https://doi.org/10.1039/D0MA00639D.
(25) Nielsen, L. J.; Olsen, L. F.; Ozalp, V. C. Aptamers Embedded in Polyacrylamide Nanoparticles: A Tool for *in Vivo* Metabolite Sensing. *ACS Nano* **2010**, *4* (8), 4361–4370. https://doi.org/10.1021/nn100635j.
(26) Jung, I. Y.; Kim, J. S.; Choi, B. R.; Lee, K.; Lee, H. Hydrogel Based Biosensors for In Vitro Diagnostics of Biochemicals, Proteins, and Genes. *Adv. Healthcare Mater.* **2017**, *6* (12), 1601475. https://doi.org/10.1002/adhm.201601475.
(27) Herrmann, A.; Haag, R.; Schedler, U. Hydrogels and Their Role in Biosensing Applications. *Adv. Healthcare Mater.* **2021**, *10* (11), 2100062. https://doi.org/10.1002/adhm.202100062.
(28) Tang, Z.; Mallikaratchy, P.; Yang, R.; Kim, Y.; Zhu, Z.; Wang, H.; Tan, W. Aptamer Switch Probe Based on Intramolecular Displacement. *J. Am. Chem. Soc.* **2008**, *130* (34), 11268–11269. https://doi.org/10.1021/ja804119s.
(29) Mariottini, D.; Idili, A.; Nijenhuis, M. A. D.; de Greef, T. F. A.; Ricci, F. DNA-Based Nanodevices Controlled by Purely Entropic Linker Domains. *J. Am. Chem. Soc.* **2018**, *140* (44), 14725–14734. https://doi.org/10.1021/jacs.8b07640.
(30) Abune, L.; Davis, B.; Wang, Y. Aptamer-functionalized Hydrogels: An Emerging Class of Biomaterials for Protein Delivery, Cell Capture, Regenerative Medicine, and Molecular Biosensing. *WIREs Nanomed Nanobiotechnol* **2021**, *13* (6). https://doi.org/10.1002/wnan.1731.
(31) Murtaza, G.; Rizvi, A. S.; Qiu, L.; Xue, M.; Meng, Z. Aptamer Empowered Hydrogels: Fabrication and Bio-sensing Applications. *J of Applied Polymer Sci* **2022**, *139* (26). https://doi.org/10.1002/app.52441.
(32) Liu, J. Oligonucleotide-Functionalized Hydrogels as Stimuli Responsive Materials and Biosensors. *Soft Matter* **2011**, *7* (15), 6757. https://doi.org/10.1039/c1sm05284e.
(33) Kassahun, G. S.; Griveau, S.; Juillard, S.; Champavert, J.; Ringuedé, A.; Bresson, B.; Tran, Y.; Bedioui, F.; Slim, C. Hydrogel Matrix-Grafted Impedimetric Aptasensors for the Detection of Diclofenac. *Langmuir* **2020**, *36* (4), 827–836. https://doi.org/10.1021/acs.langmuir.9b02031.
(34) Jang, K.; Westbay, J. H.; Asher, S. A. DNA-Crosslinked 2D Photonic Crystal Hydrogels for Detection of Adenosine Actuated by an Adenosine-Binding Aptamer. *ACS Sens.* **2022**, *7* (6), 1648–1656. https://doi.org/10.1021/acssensors.1c02424.
(35) Pikula, M.; Ali, M. M.; Filipe, C.; Hoare, T. Single-Step Printable Hydrogel Microarray Integrating Long-Chain DNA for the Discriminative and Size-Specific Sensing of Nucleic Acids. *ACS Appl. Mater. Interfaces* **2021**, *13* (2), 2360–2370. https://doi.org/10.1021/acsami.0c21061.
(36) Pikula M.;Li, Y.;Filipe, C.D.M.; Hoare, T. An Aptamer-Based Hydrogel Sensing Platform Enabling Low Micromolar Detection of Small Molecules Using Low Sample Volumes.. *ACS Appl. Mater. Interfaces* **2024**, 10.1021/acsami.3c19203
(37) Smeets, N. M. B.; Bakaic, E.; Patenaude, M.; Hoare, T. Injectable and Tunable Poly(Ethylene Glycol) Analogue Hydrogels Based on Poly(Oligoethylene Glycol Methacrylate). *Chem. Commun.* **2014**, *50* (25), 3306. https://doi.org/10.1039/c3cc48514e.
(38) Smeets, N. M. B.; Bakaic, E.; Patenaude, M.; Hoare, T. Injectable Poly(Oligoethylene Glycol Methacrylate)-Based Hydrogels with Tunable Phase Transition Behaviours: Physicochemical and Biological Responses. *Acta Biomaterialia* **2014**, *10* (10), 4143–4155. https://doi.org/10.1016/j.actbio.2014.05.035.
(39) Mateen, R.; Ali, M. M.; Hoare, T. A Printable Hydrogel Microarray for Drug Screening Avoids False Positives Associated with Promiscuous Aggregating Inhibitors. *Nat Commun* **2018**, *9* (1), 602. https://doi.org/10.1038/s41467-018-02956-z.
(40) You, Y.; Tataurov, A. V.; Owczarzy, R. Measuring Thermodynamic Details of DNA Hybridization Using Fluorescence. *Biopolymers* **2011**, *95* (7), 472–486. https://doi.org/10.1002/bip.21615.
(41) Spiess, A.-N.; Feig, C.; Ritz, C. Highly Accurate Sigmoidal Fitting of Real-Time PCR Data by Introducing a Parameter for Asymmetry. *BMC Bioinformatics* **2008**, *9* (1), 221. https://doi.org/10.1186/1471-2105-9-221.
(42) Schroeder, S. J.; Turner, D. H. Optical Melting Measurements of Nucleic Acid Thermodynamics. In *Methods in Enzymology*; Elsevier, 2009; Vol. 468, pp 371–387. https://doi.org/10.1016/S0076-6879(09)68017-4.
(43) Li, Y.; Liu, J. Aptamer-Based Strategies for Recognizing Adenine, Adenosine, ATP and Related Compounds. *Analyst* **2020**, *145* (21), 6753–6768. https://doi.org/10.1039/D0AN00886A.
(44) Carrasquilla, C.; Kapteyn, E.; Li, Y.; Brennan, J. D. Sol-Gel-Derived Biohybrid Materials Incorporating Long-Chain DNA Aptamers. *Angew. Chem. Int. Ed.* **2017**, *56* (36), 10686–10690. https://doi.org/10.1002/anie.201702859.
(45) Carrasquilla, C.; Little, J. R. L.; Li, Y.; Brennan, J. D. Patterned Paper Sensors Printed with Long-Chain DNA Aptamers. *Chem. Eur. J.* **2015**, *21* (20), 7369–7373. https://doi.org/10.1002/chem.201500949.
(46) Su, S.; Nutiu, R.; Filipe, C. D. M.; Li, Y.; Pelton, R. Adsorption and Covalent Coupling of ATP-Binding DNA Aptamers onto Cellulose. *Langmuir* **2007**, *23* (3), 1300–1302. https://doi.org/10.1021/la060961c.

(47) Liu, M.; Zhang, Q.; Kannan, B.; Botton, G. A.; Yang, J.; Soleymani, L.; Brennan, J. D.; Li, Y. Self-Assembled Functional DNA Superstructures as High-Density and Versatile Recognition Elements for Printed Paper Sensors. *Angew. Chem.* **2018**, *130* (38), 12620–12623. https://doi.org/10.1002/ange.201806489.
(48) Su, S.; Ali, Md. M.; Filipe, C. D. M.; Li, Y.; Pelton, R. Microgel-Based Inks for Paper-Supported Biosensing Applications. *Biomacromolecules* **2008**, *9* (3), 935–941. https://doi.org/10.1021/bm7013608.
(49) Zhang, Z.; Liu, J. Molecular Imprinting with Functional DNA. *Small* **2019**, *15* (26), 1805246. https://doi.org/10.1002/smll.201805246.
(50) Poma, A.; Brahmbhatt, H.; Pendergraff, H. M.; Watts, J. K.; Turner, N. W. Generation of Novel Hybrid Aptamer-Molecularly Imprinted Polymeric Nanoparticles. *Adv. Mater.* **2015**, *27* (4), 750–758. https://doi.org/10.1002/adma.201404235.
(51) Zhang, Z.; Liu, J. Molecularly Imprinted Polymers with DNA Aptamer Fragments as Macromonomers. *ACS Appl. Mater. Interfaces* **2016**, *8* (10), 6371–6378. https://doi.org/10.1021/acsami.6b00461.
(52) Nakano, S.; Miyoshi, D.; Sugimoto, N. Effects of Molecular Crowding on the Structures, Interactions, and Functions of Nucleic Acids. *Chem. Rev.* **2014**, *114* (5), 2733–2758. https://doi.org/10.1021/cr400113m.
(53) Markarian, M. Z.; Schlenoff, J. B. Effect of Molecular Crowding and Ionic Strength on the Isothermal Hybridization of Oligonucleotides. *J. Phys. Chem. B* **2010**, *114* (32), 10620–10627. https://doi.org/10.1021/jp103213w.
(54) Cho, E. J.; Collett, J. R.; Szafranska, A. E.; Ellington, A. D. Optimization of Aptamer Microarray Technology for Multiple Protein Targets. *Analytica Chimica Acta* **2006**, *564* (1), 82–90. https://doi.org/10.1016/j.aca.2005.12.038.
(55) Esteban Fernández de Ávila, B.; Watkins, H. M.; Pingarrón, J. M.; Plaxco, K. W.; Palleschi, G.; Ricci, F. Determinants of the Detection Limit and Specificity of Surface-Based Biosensors. *Anal. Chem.* **2013**, *85* (14), 6593–6597. https://doi.org/10.1021/ac4012123.
(56) Watkins, H. M.; Simon, A. J.; Ricci, F.; Plaxco, K. W. Effects of Crowding on the Stability of a Surface-Tethered Biopolymer: An Experimental Study of Folding in a Highly Crowded Regime. *J. Am. Chem. Soc.* **2014**, *136* (25), 8923–8927. https://doi.org/10.1021/ja411486g.
(57) Cisse, I. I.; Kim, H.; Ha, T. A Rule of Seven in Watson-Crick Base-Pairing of Mismatched Sequences. *Nat Struct Mol Biol* **2012**, *19* (6), 623–627. https://doi.org/10.1038/nsmb.2294.
(58) Hui, C. Y.; Li, Y.; Brennan, J. D. Fluorescence Analysis of the Properties of Structure-Switching DNA Aptamers Entrapped in Sol–Gel-Derived Silica Materials. *Chem. Mater.* **2014**, *26* (5), 1896–1904. https://doi.org/10.1021/cm404114g.
(59) Alkhamis, O.; Xiao, Y. Systematic Study of *in Vitro* Selection Stringency Reveals How To Enrich High-Affinity Aptamers. *J. Am. Chem. Soc.* **2023**, *145* (1), 194–206. https://doi.org/10.1021/jacs.2c09522.
(60) Ding, Y.; Liu, J. Pushing Adenosine and ATP SELEX for DNA Aptamers with Nanomolar Affinity. *J. Am. Chem. Soc.* **2023**, *145* (13), 7540–7547. https://doi.org/10.1021/jacs.3c00848.
(61) Ding, Y.; Xie, Y.; Li, A. Z.; Huang, P.-J. J.; Liu, J. Cross-Binding of Four Adenosine/ATP Aptamers to Caffeine, Theophylline, and Other Methylxanthines. *Biochemistry* **2023**, *62* (15), 2280–2288. https://doi.org/10.1021/acs.biochem.3c00260.
(62) Psychogios, N.; Hau, D. D.; Peng, J.; Guo, A. C.; Mandal, R.; Bouatra, S.; Sinelnikov, I.; Krishnamurthy, R.; Eisner, R.; Gautam, B.; Young, N.; Xia, J.; Knox, C.; Dong, E.; Huang, P.; Hollander, Z.; Pedersen, T. L.; Smith, S. R.; Bamforth, F.; Greiner, R.; McManus, B.; Newman, J. W.; Goodfriend, T.; Wishart, D. S. The Human Serum Metabolome. *PLoS ONE* **2011**, *6* (2), e16957. https://doi.org/10.1371/journal.pone.0016957.
(63) Li, L.-L.; Ge, P.; Selvin, P. R.; Lu, Y. Direct Detection of Adenosine in Undiluted Serum Using a Luminescent Aptamer Sensor Attached to a Terbium Complex. *Anal. Chem.* **2012**, *84* (18), 7852–7856. https://doi.org/10.1021/ac302167d.
(64) Huang, P.-J. J.; Liu, J. Flow Cytometry-Assisted Detection of Adenosine in Serum with an Immobilized Aptamer Sensor. *Anal. Chem.* **2010**, *82* (10), 4020–4026. https://doi.org/10.1021/ac9028505.
(65) Lee, S. C.; Gillispie, G.; Prim, P.; Lee, S. J. Physical and Chemical Factors Influencing the Printability of Hydrogel-Based Extrusion Bioinks. *Chem. Rev.* **2020**, *120* (19), 10834–10886. https://doi.org/10.1021/acs.chemrev.0c00015.
(66) Li, Y.; Dahhan, O.; Filipe, C. D. M.; Brennan, J. D.; Pelton, R. H. Optimizing Piezoelectric Inkjet Printing of Silica Sols for Biosensor Production. *J Sol-Gel Sci Technol* **2018**, *87* (3), 657–664. https://doi.org/10.1007/s10971-018-4762-3.

4.6. Appendix – Supporting Information Chapter 4

4.6.1. Design of FRET Reporter Oligonucleotides

Adenosine aptamer reporters were formed using three oligonucleotide sequences: (1) a long DNA strand containing the aptamer sequence (A); (2) fluorescently labelled DNA (F) tagged with AlexaFluor 647 ($AlexaF_{647}$) at the 5' end; and (3) a quencher labeled DNA (Q) tagged by Black Hole Quencher 3 (BHQ3) (Figure S4.1). Three different sizes of Q-DNA were utilized in assembling aptamer construct: 10-nt long (Q_{10}), 9-nt long (Q_9), and 7-nt long (Q_7) Q-DNA. Based on previous reports,[1,2] the SSAC utilizing 10-bp quencher stem was designed as a 63-nt sequence composed of a 27-nt ATP-aptamer binding motif [3] (bold blue) extended at the 5'-end with 5 bases (A_5) of non-essential oligonucleotides (italic black) and the F-DNA binding primer region (bold black). The 16-nt-long F-DNA binding motif was placed close to the Q_{10} complementary region within the A_5 sequence, enabling the assembly of the A_5FQ_{10} ATP-binding construct.

Truncation of Q-DNA, introduced in this work, was followed by the truncation of the 5' extension inside the original aptamer construct design to ensure an equivalent distance and thus FRET efficiency between the fluorophore and quencher pair using a single-size F-DNA strand. As such, aptamer reporters utilizing Q_9 and Q_7 were hybridized to truncated 5' extension of 4-bases and 2-bases long, respectively to assemble the A_4FQ_9 and A_2FQ_7 ATP-binding constructs. All three Q-DNA sequences were designed to directly denature the target binding site II (bold blue underlined) within a cooperative two binding site pocket by hybridizing with only one essential oligonucleotide (G-base) involved in ligand binding[3].

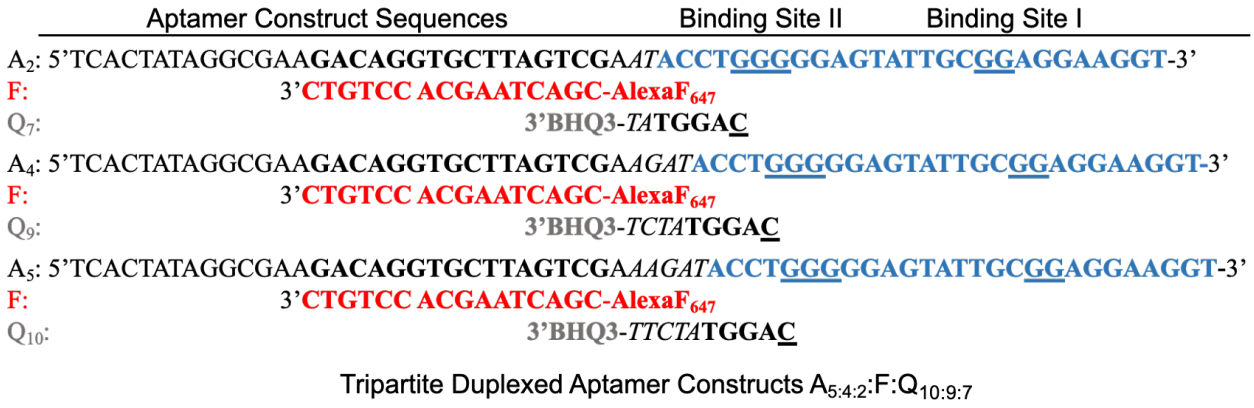

Figure S4.1 Components used for assembling the adenosine aptamer reporter. The SSACs (i.e., duplexed aptamer constructs) were assembled by hybridizing aptamer-containing sequence (A) having a 5' extensions of 5-nt (A_5), 4-nt (A_4) or 2-nt (A_2) long with complementary fluorophore- (F) and quencher-labeled (Q) oligonucleotides to enable FRET. Q-DNAs were employed with lengths of 10-, 9-, and 7-nt and are denoted as Q_{10}, Q_9, and Q_7, respectively.

4.6.1. POEGMA Polymer Synthesis and Characterization

Table S4.1 Recipes for the synthesis of hydrazide (H) and aldehyde (A)-functionalized poly(oligoethylene glycol methacrylate) (POEGMA) polymers (PO).

Polymer Precursor	Functional Group	$M(EO)_2MA$ (g)	$OEGMA_{500}$ (g)	AA (g)	DMEMAm (g)	TGA, (µL)	AIBMe (mg)
POH	$NHNH_2$	0	4.0	0.30	-	1.0	37
POA	CHO	1.15	2.85	-	0.36	4	50

Table S4.2 Physicochemical properties of synthesized hydrazide-functionalized (POH) and aldehyde-functionalized (POA) poly (oligoethylene glycol methacrylate) (POEGMA) polymers.

Polymer Precursor	Functional Monomer	Functional Monomer, mol%	M_n, $\times 10^3$ g/mol	$Đ$
POH	$NHNH_2$	21.3 [a]	19.3	2.7
POA	CHO	8.7 [b]	15.9	2.7

[a] Determined by potentiometric titration. [b] Determined by ^{1}H-NMR (600 MHz, $CDCl_3$).

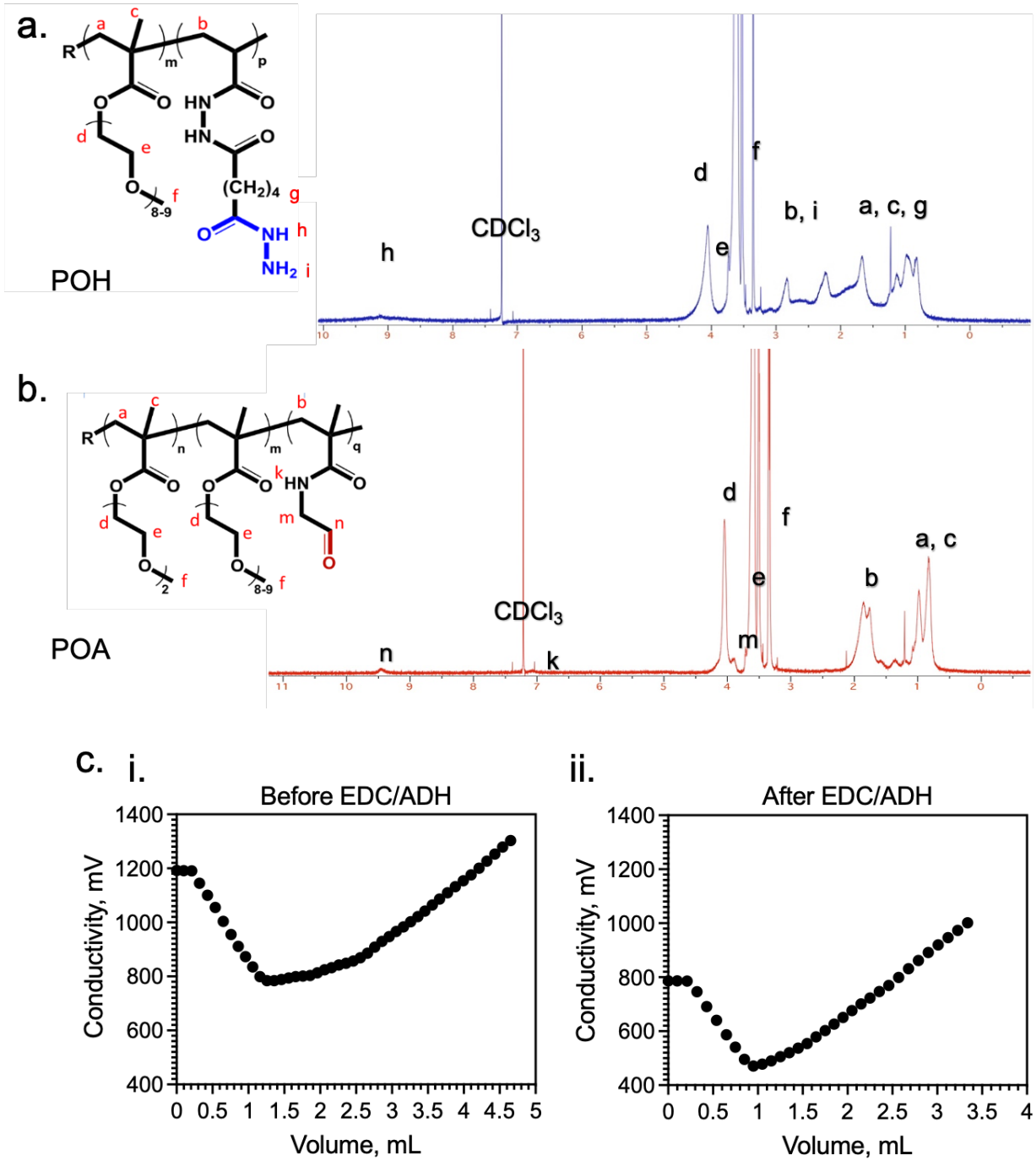

Figure S4.2 ^{1}H NMR *(*600 MHz, $CDCl_3$) spectra of poly(oligoethylene glycol methacrylate) (POEGMA) precursor polymer (a) hydrazide-functionalized (POH) and (b) aldehyde-functionalized (POA) and (c) potentiometric titration curves before (i) and after (ii) EDC/ADH functionalization to synthesize POH polymer. Chemical shifts are reported relative to the residual deuterated solvent peaks. (a,b) Peak assignments given for each spectrum are based on the anticipated chemical structure of each polymer; (c) the difference in -COOH content before and after EDC/ADH functionalization directly correlates to the efficiency of ADH conjugation.[4–6]

4.6.2. Encapsulation Efficiency of Hydrogel Film Microarrays Containing Fluorescent Aptamer Constructs

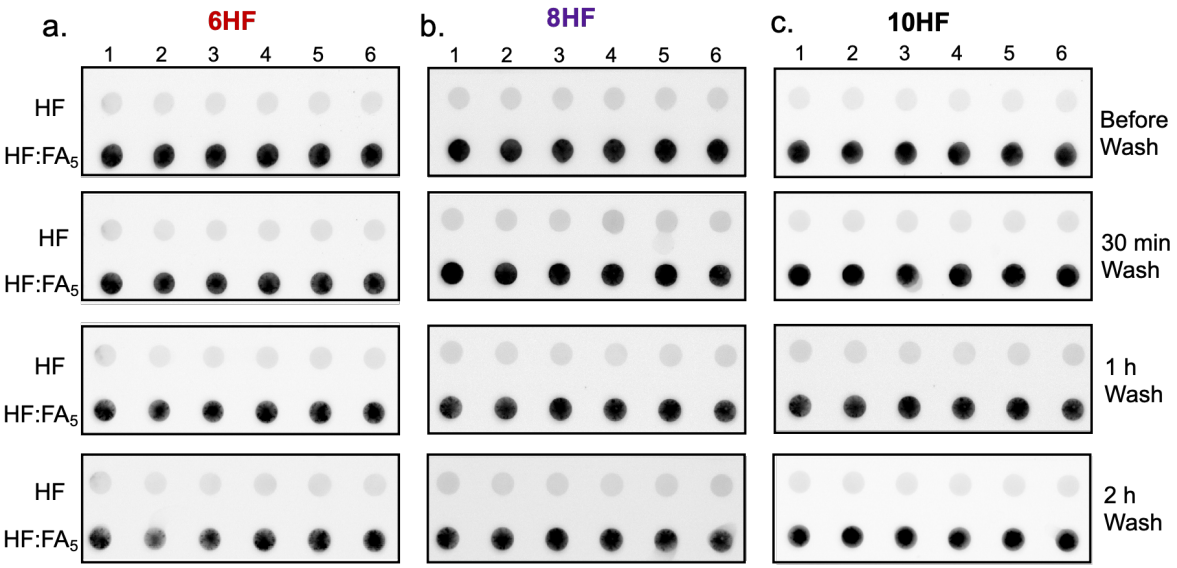

Figure S4.3 Fluorescent images of fluorescent aptamer construct (FA_5) encapsulated in a hydrogel film (HF) microarray scanned before washing (row 1) and after each step of a 2-hour washing cycle (row 2 – 30 minutes, row 3 – 1 hour, and row 4 – 2 hours). Encapsulation was performed (a) 6HF; (b) 8HF and (c) 10HF hydrogels, corresponding to hydrogel precursor polymer concentrations of 6 wt%, 8 wt% and 10 wt%, respectively. The strong retained fluorescence confirms the efficacy of the hydrogel in enabling aptamer construct retention inside the gel.

4.6.3. Nucleolytic Protection of Hydrogel Film Microarray Encapsulating Adenosine Aptamer Reporter

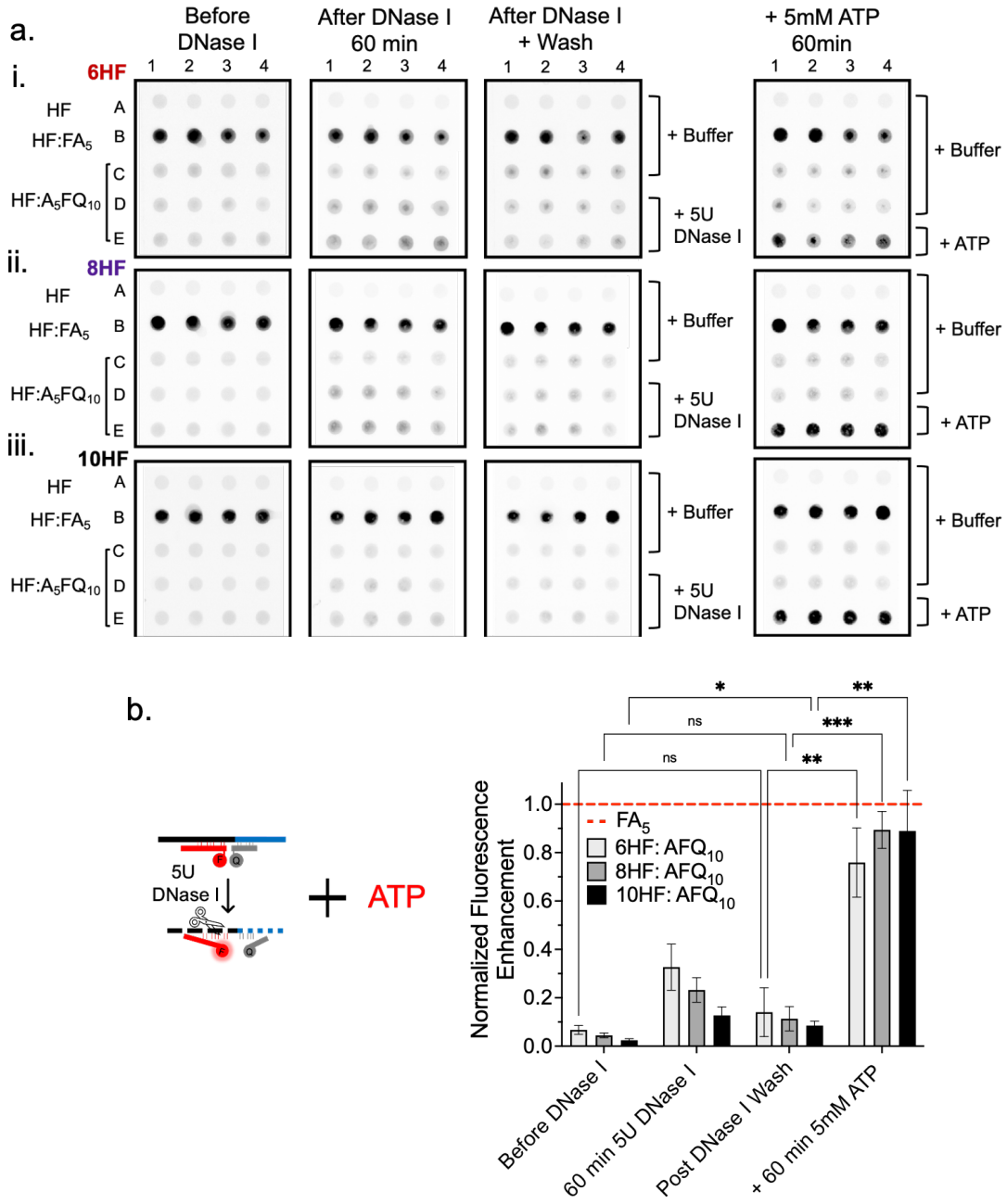

Figure S4.4 Hydrogel film microarrays protect encapsulated aptamer reporters from nucleolytic denaturation and preserves adenosine sensing functionality. (a) Qualitative fluorescence images of a hydrogel-encapsulated HF:A_5FQ_{10} microarray scanned prior DNase I denaturation (column 1), upon exposure to 5 U/well DNase I over 60 min (column 2), following a washing/renaturation step (column 3), and following a 5 mM ATP sensing assay over 60 min (column 4) in hydrogels prepared with precursor polymer concentrations of (i) 6 wt% (6HF), (ii) 8 wt% (8HF), and (iii) 10 wt% (10HF); (b) Quantitative intensity of fluorescent quenching (before DNase I exposure) and fluorescent enhacement (after DNase I denaturation, post-DNase I wash, and following ATP sensing) of HF:A_5FQ_{10} microarrays prepared in 6HF (6 wt%), 8HF (8 wt%), and 10HF (10 wt%) hydrogels relative to the unquenched construct FA_5 corresponding to 100% fluorescence recovery within the FRET structure switching construct.

4.6.4. ATP Binding Kinetics of Hydrogel Film Microarray Encapsulating Adenosine Aptamer Reporter

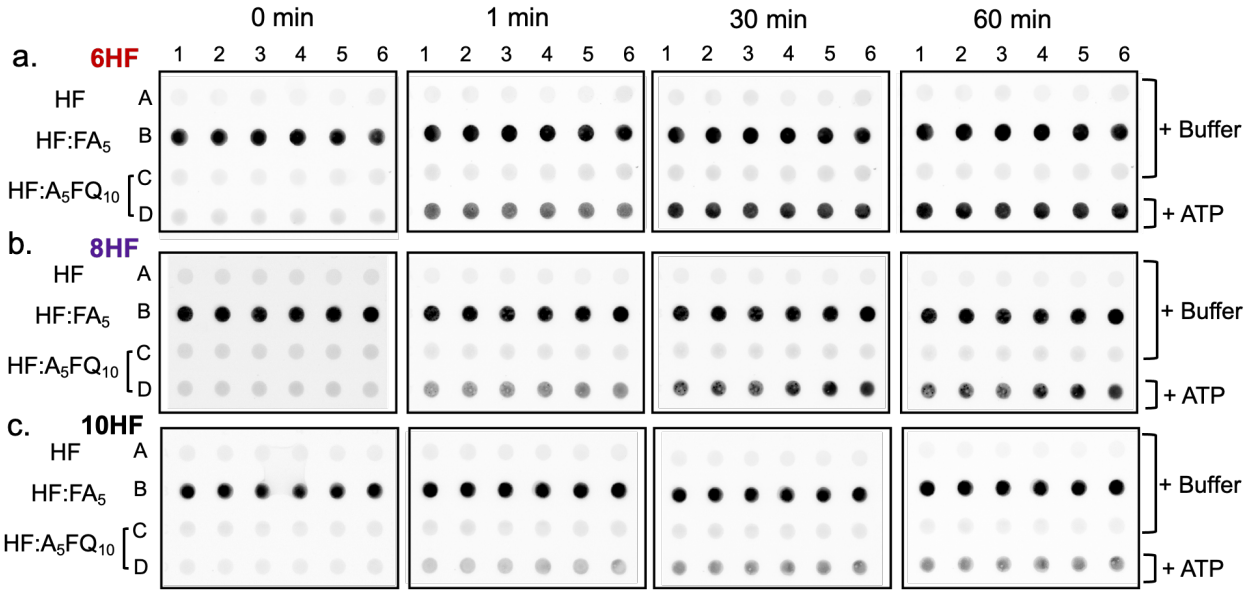

Figure S4.5 Fluorescent images of hydrogel film microarrays encapsulating the adenosine aptamer reporter HF:A_5FQ_{10} encapsulated in hydrogels prepared with precursor polymer solutions of varying concentrations of (a) 6 wt% (6HF); (b) 8 wt% (8HF), and (c) 10 wt% (10HF). Microarrays were scanned prior to ligand addition (0 min, column 1) and upon exposure to 5 mM ATP in 1x Assay buffer containing 5 vol% glycerol over 1 min (column 2), 30 min (column 3), or 60 min (column 4).

4.6.5. Optimization of Ligand Binding Assay: Varying the Humectant Content in the Ligand Binding Buffer

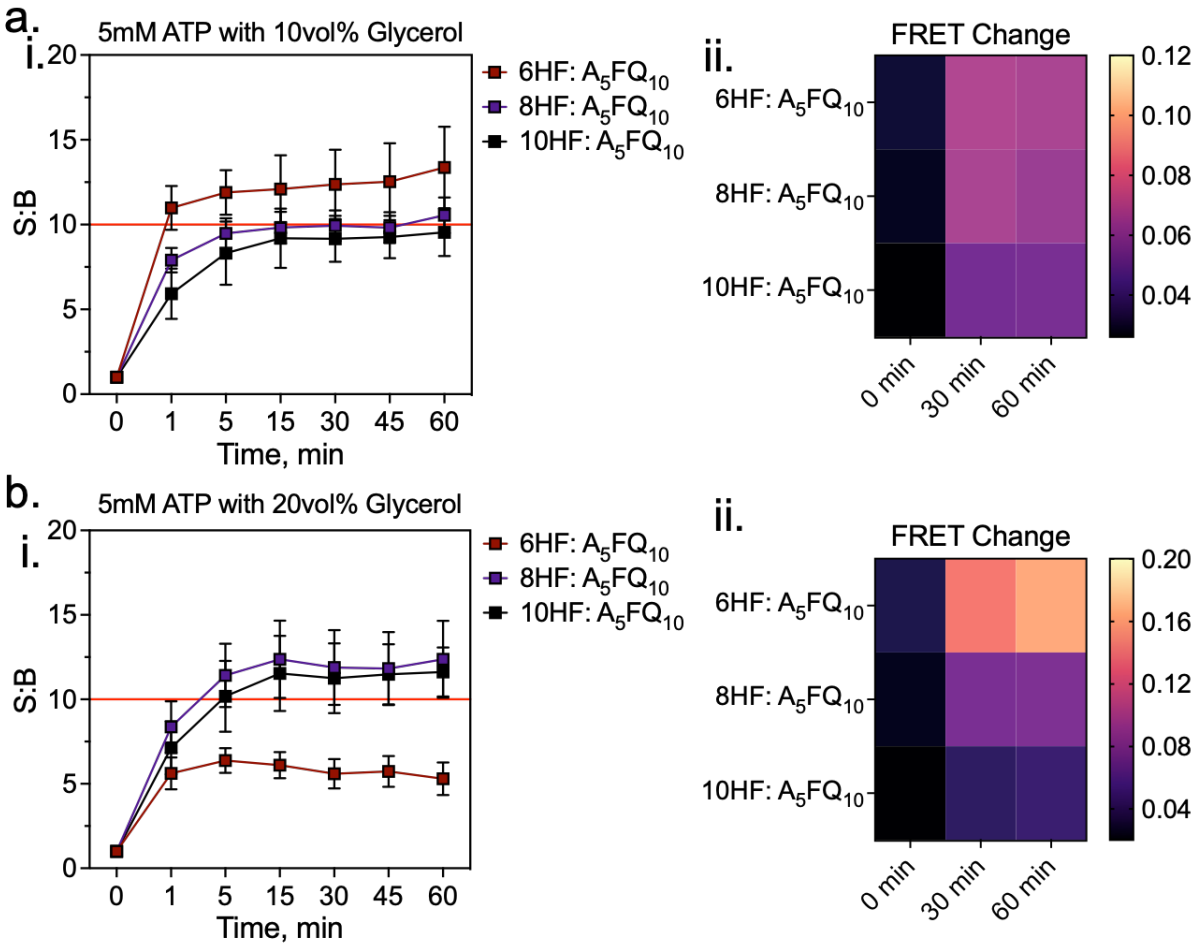

Figure S4.6 Ligand-induced signal enhancement and fluorescence quenching stability of adenosine aptamer reporter encapsulated in hydrogels prepared with precursor polymer solutions of varying concentrations of 6 wt% (6HF), 8 wt% (8HF), and 10 wt% (10HF) upon exposure to 1xAssay buffer containing (a) 10 vol% glycerol or (b) 20 vol% of glycerol; as quantified by (i) the time-resolved signal:background ratio (S:B) at a 5 mM ATP concetration and (ii) the change in the fluorescence quenching efficiency (FRET Change) at 1xAssay buffer over a 60 min reaction time at ambient conditions.

4.6.6. Stability of Adenosine Reporting Hydrogel Film Microarrays Prepared via Cross-linking and Drying at Ambient Conditions

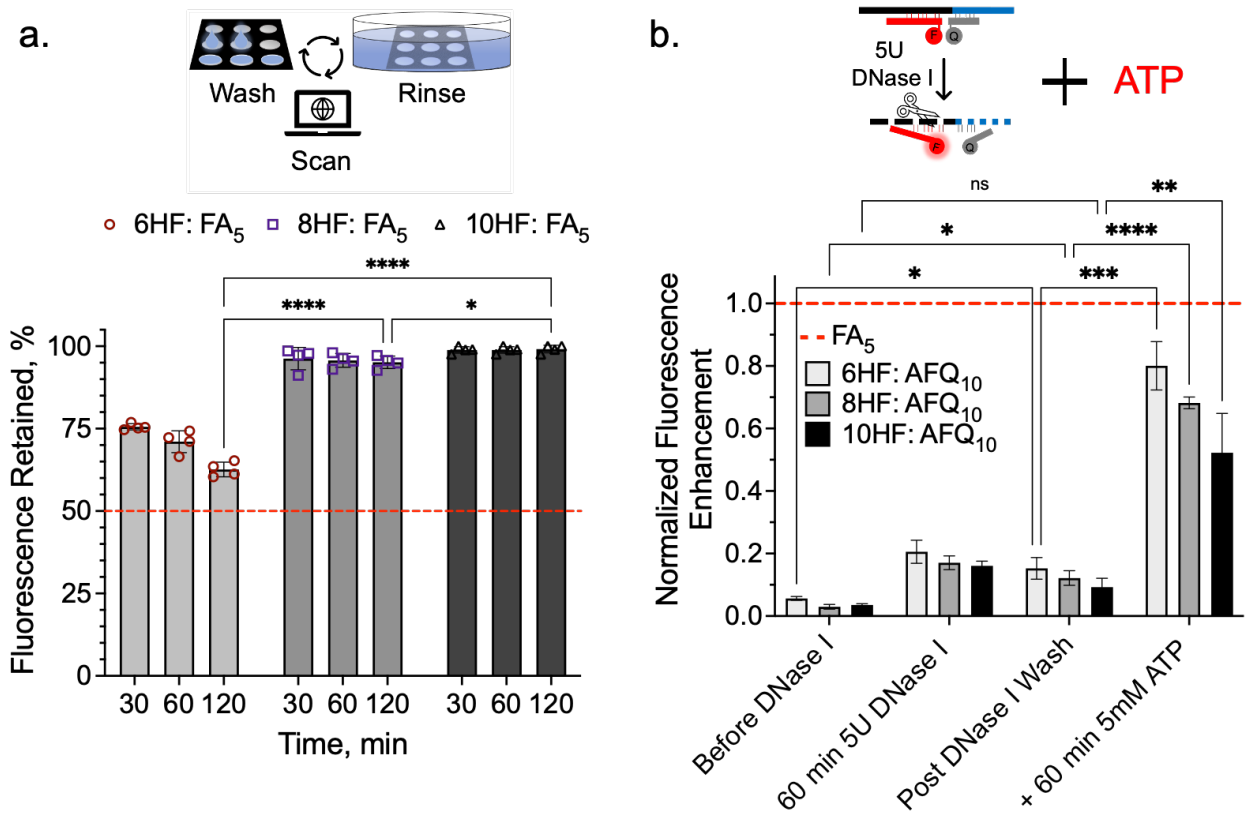

Figure S4.7 Stability of hydrogel film microarrays encapsulating adenosine aptamer reporter against (a) vigorous washing and (b) nucleolytic conditions. (a) Time-resolved fluorescent aptamer construct (FA_5) encapsulation efficiency in hydrogel film microarrays prepared with precursor polymer solutions of varying concentrations of (a) 6 wt% (6HF); (b) 8 wt% (8HF), and (c) 10 wt% (10HF). (b) Fluorescent quenching intensity (before DNase I exposure) and fluorescent enhancement intensity (after DNase I denaturation, post-DNase I wash, and following an ATP sensing assay) of a HF:A_5FQ_{10} microarray encapsulated in 6HF, 8HF, and 10HF hydrogels relative to the unquenched construct FA_5, which corresponds to 100% fluorescence recovered within the FRET structure switching construct.

4.6.7. Ligand Binding Assay in Hydrogel Film Microarrays Prepared via Cross-linking and Drying at Ambient Conditions

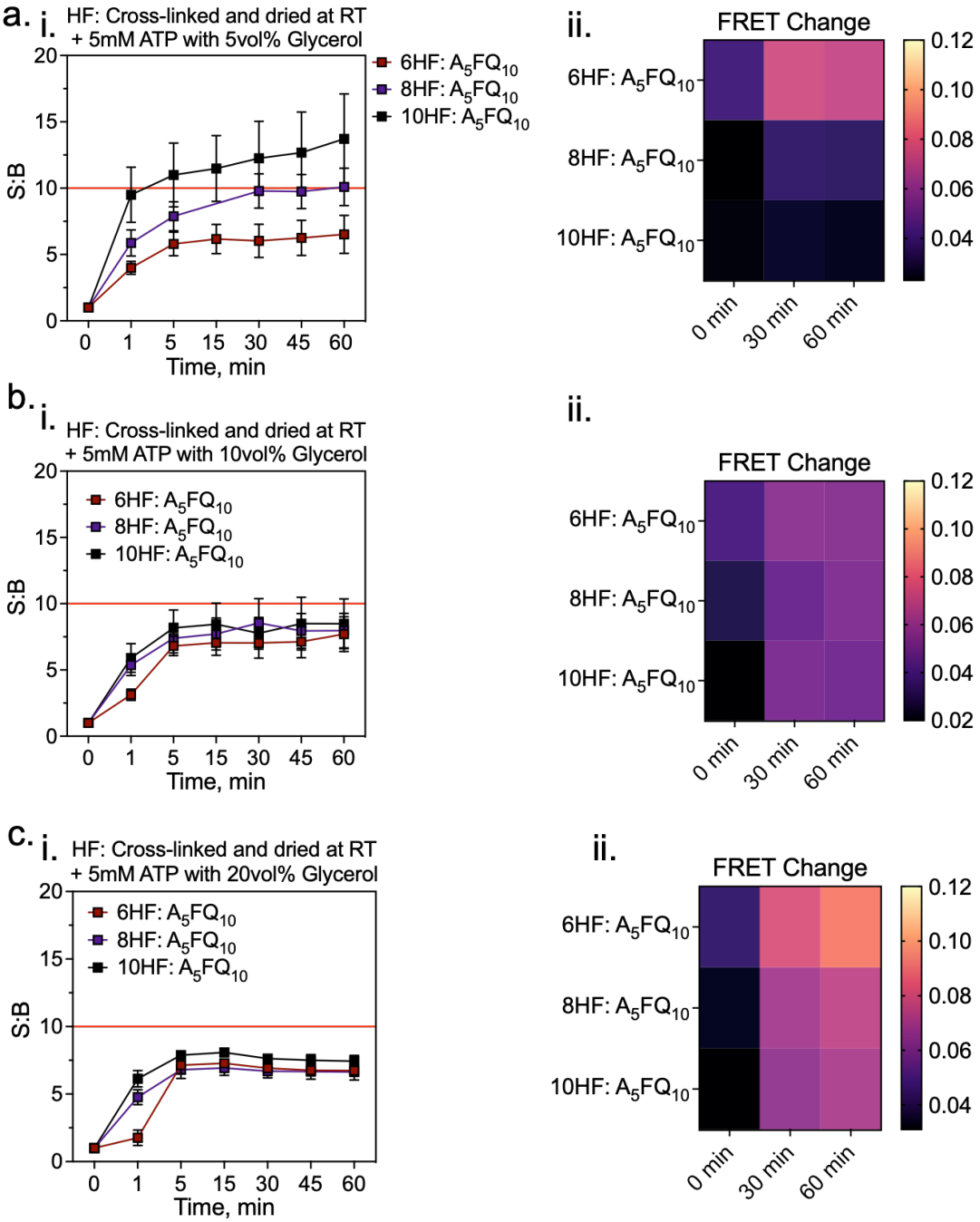

Figure S4.8 Ligand-induced signal enhancement and fluorescence quenching stability of adenosine aptamer reporter encapsulated in hydrogel film microarrays prepared with precursor polymer solutions of varying concentrations (6-10 wt%) upon exposure to 1xAssay buffer containing (a) 5 vol%, (b) 10 vol%, or (c) 20 vol% glycerol; as quantified by (i) the time-resolved signal:background ratio (S:B) at a 5 mM ATP concentration and (ii) the change in the fluorescence quenching efficiency (FRET Change) at 1xAssay buffer over a 60 min reaction time at ambient conditions.

4.6.8. Long-Term Stability of Adenosine Reporting in Hydrogel Film Microarrays

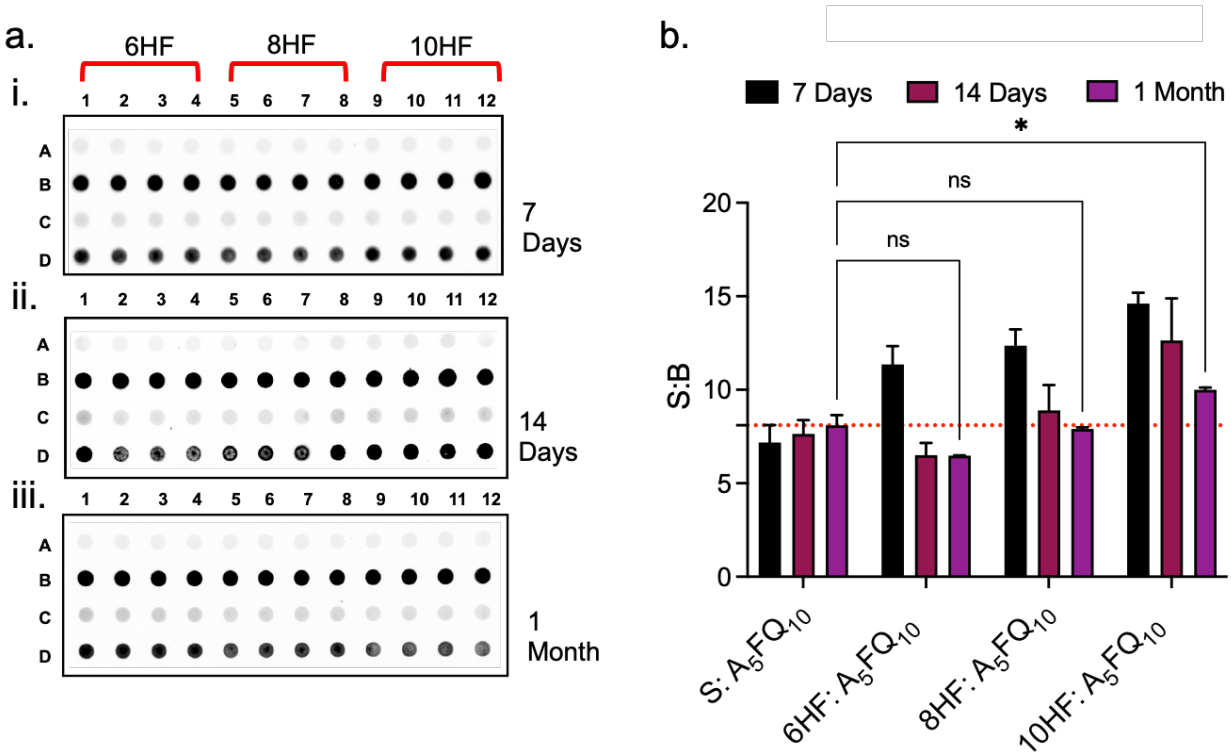

Figure S4.9 Long-term stability of the aptamer reporter A_5FQ_{10} assembled in solution (S) or in hydrogel film microarrays prepared with precursor polymer solutions of varying concentrations of 6 wt% (6HF), 8 wt% (8HF), or 10 wt% (10HF). (a) Qualitative fluorescent images of 5 mM ATP sensing activity of HF:A_5FQ_{10} microarrays stored at ambient conditions for (i) 7 days; (ii) 14 days and (iii) 1 month of fabrication. Row A represents blank HF subarrays, Row B represents the positive control H:FA subarrays, Row C represents the HF:AFQ background subarray treated with ligand-free buffer, and Row D represents the signal HF:AFQ subarray treated with 5 mM ATP. (b) Quantitative measurement of the signal-to-background (S:B) ratio of stored HF:A_5FQ_{10} microarrays upon 5 mM ATP exposure (F-DNA density = 100 nM, 2:1:6 A:F:Q ratio).

4.6.9. Nucelase Activity at Increasing DNase I Concentrations

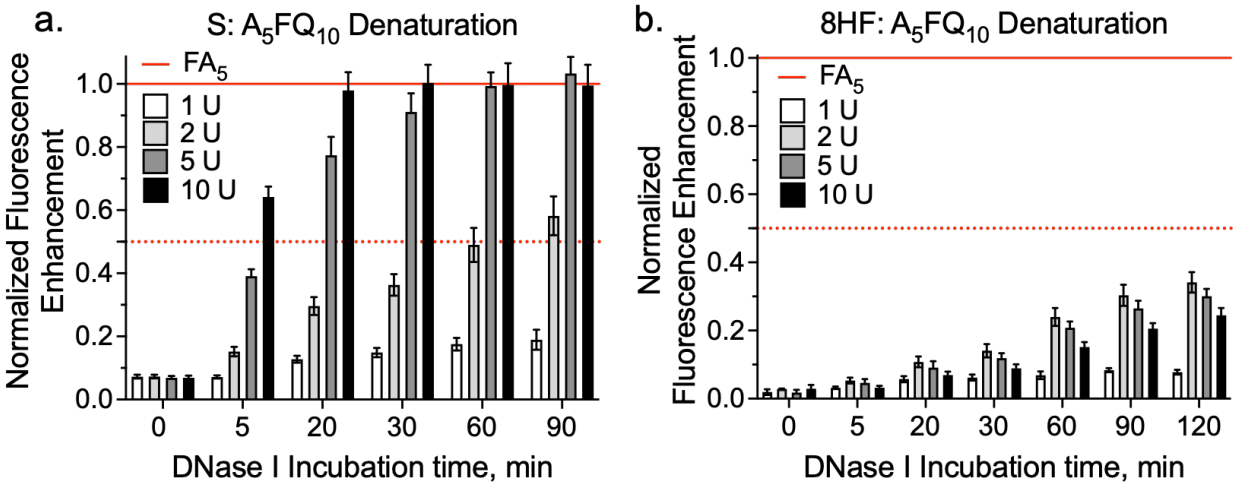

Figure S4.10 Nucleolytic denaturation of the adenosine aptamer reporter A_5FQ_{10} assembled in (a) solution (S); or (b) a hydrogel film microarray prepared with precursor polymer concentrations of 8 wt% (8HF) as quantified by the fluorescent enhancement of quenched aptamer reporters exposed to 1 U, 2 U, 5 U and 10 U of DNase I, relative to the unquenched fluorescent aptamer construct (FA_5) corresponding to 100% aptamer disassembly.

4.6.10. Qualitative Data on FRET Efficiency of Hydrogel-Based Aptamer Microarrays of Varying DNA Surface Densities

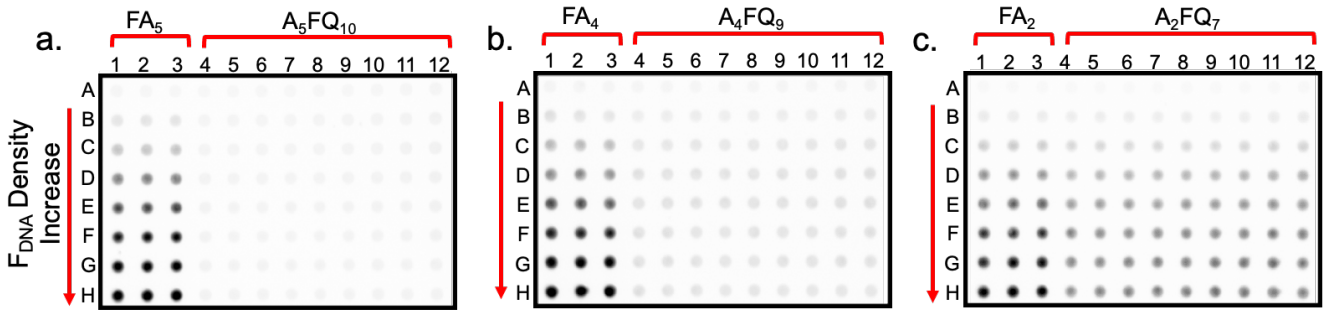

Figure S4.11 Qualitative data on FRET efficiency of structure-switching aptamer constructs assembled with varying Q-DNA lengths encapsulated in hydrogel films prepared with DNA densities ranging from 10 nM to 150 nM F-DNA (A:F:Q ratio 2:1:6): (a) A_5FQ_{10}; (b) A_4FQ_9; and (c) A_2FQ_7.

4.6.11. Qualitative Data on Binding Affinity in Pure Buffer

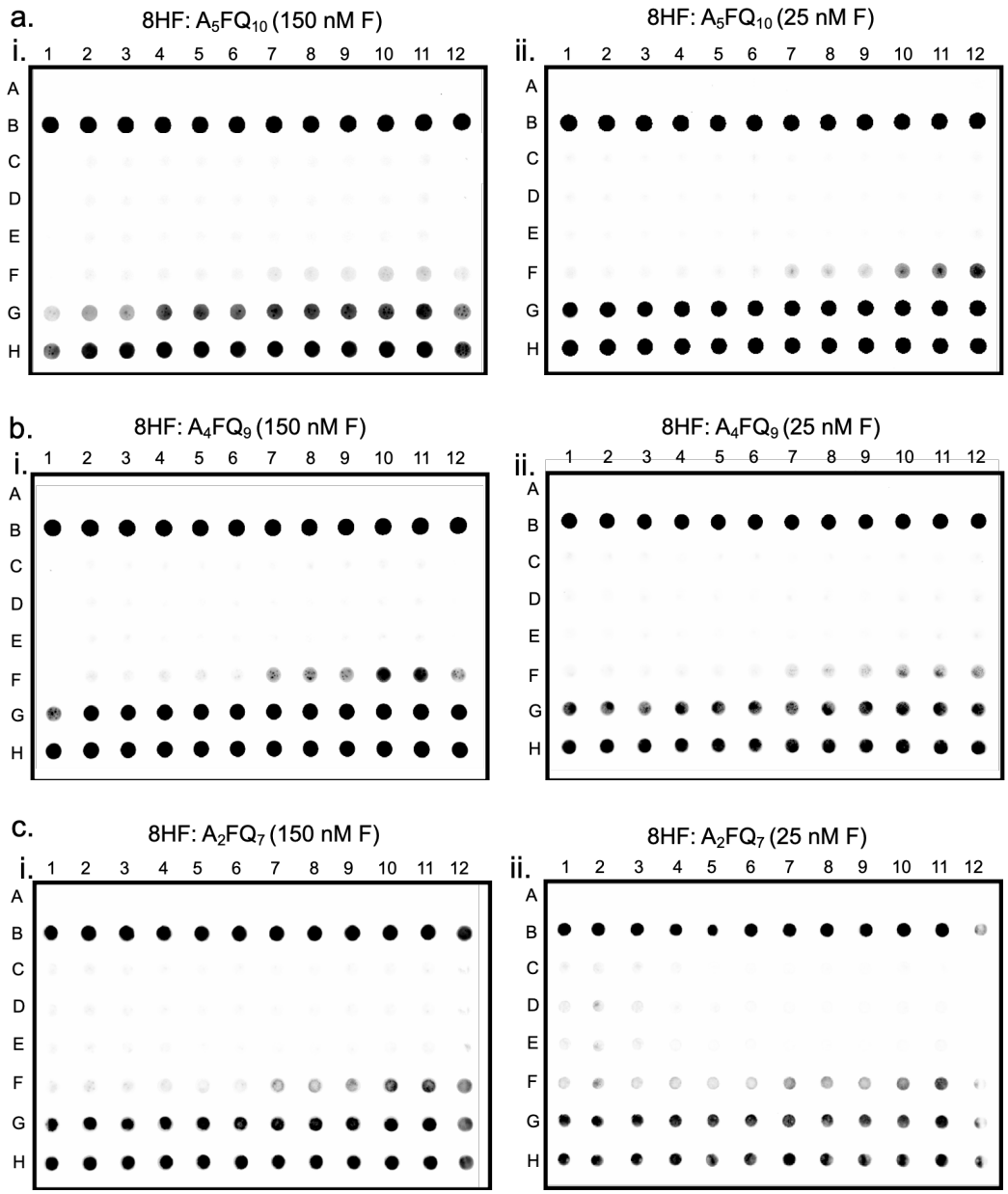

Figure S4.12 Qualitative data on the binding affinity of hydrogel microarray 8HF:AFQ reporters assembled using (a) Q_{10}, (b) Q_9, and (c) Q_7 quencher stems at aptamer densities corresponding to F-DNA contents of (i) 150 nM and (ii) 25 nM (A:F:Q molar ratio 2:1:6); corresponding quantitative data are presented in Figure 4.3 and Table 4.1 in the main text. Row A = HF (blank); Row B = HF:FA (positive control); Rows C and D = HF:AFQ + Buffer (0 mM ATP) (Background); Rows E,F,G,H = HF:AFQ + ATP (Signal) with 16 serial dilutions of ATP ranging from 100 nM to 10 mM (n = 3 replicates).

4.6.12. Melting Curves

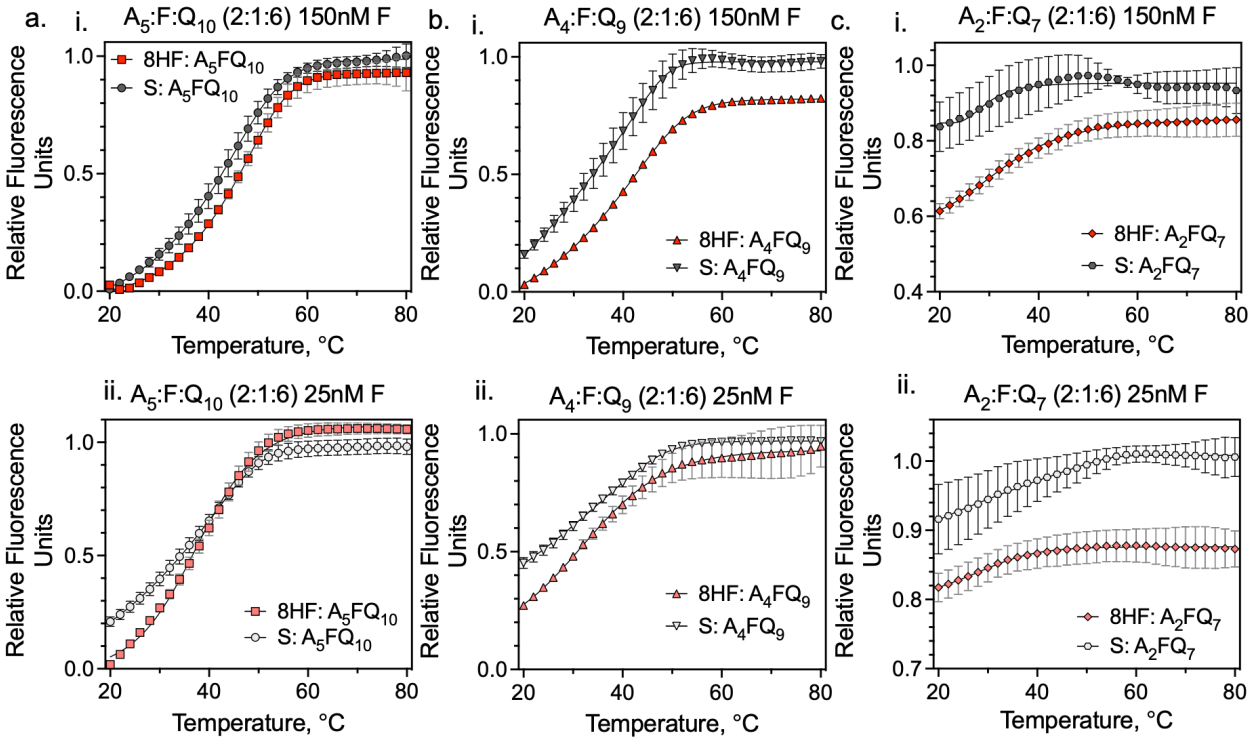

Figure S4.13 Thermal melting curves of (a) A_5FQ_{10}, (b) A_4FQ_9 and (c) A_2FQ_7 aptamer constructs encapsulated in a hydrogel array (8HF) or free-in-solution (S) at an aptamer density corresponding to a F-DNA content of (i) 150 nM and (ii) 25 nM (A:F:Q molar ratio 2:1:6); see summary data in Figure 4.4 and Table 4.1 in the main text.

4.6.13. Q-DNA Hybridization Optimization and Aptamer Microarray Reusability in Hydrogel Prepared with 6 wt% Precursor Polymer Concentrations

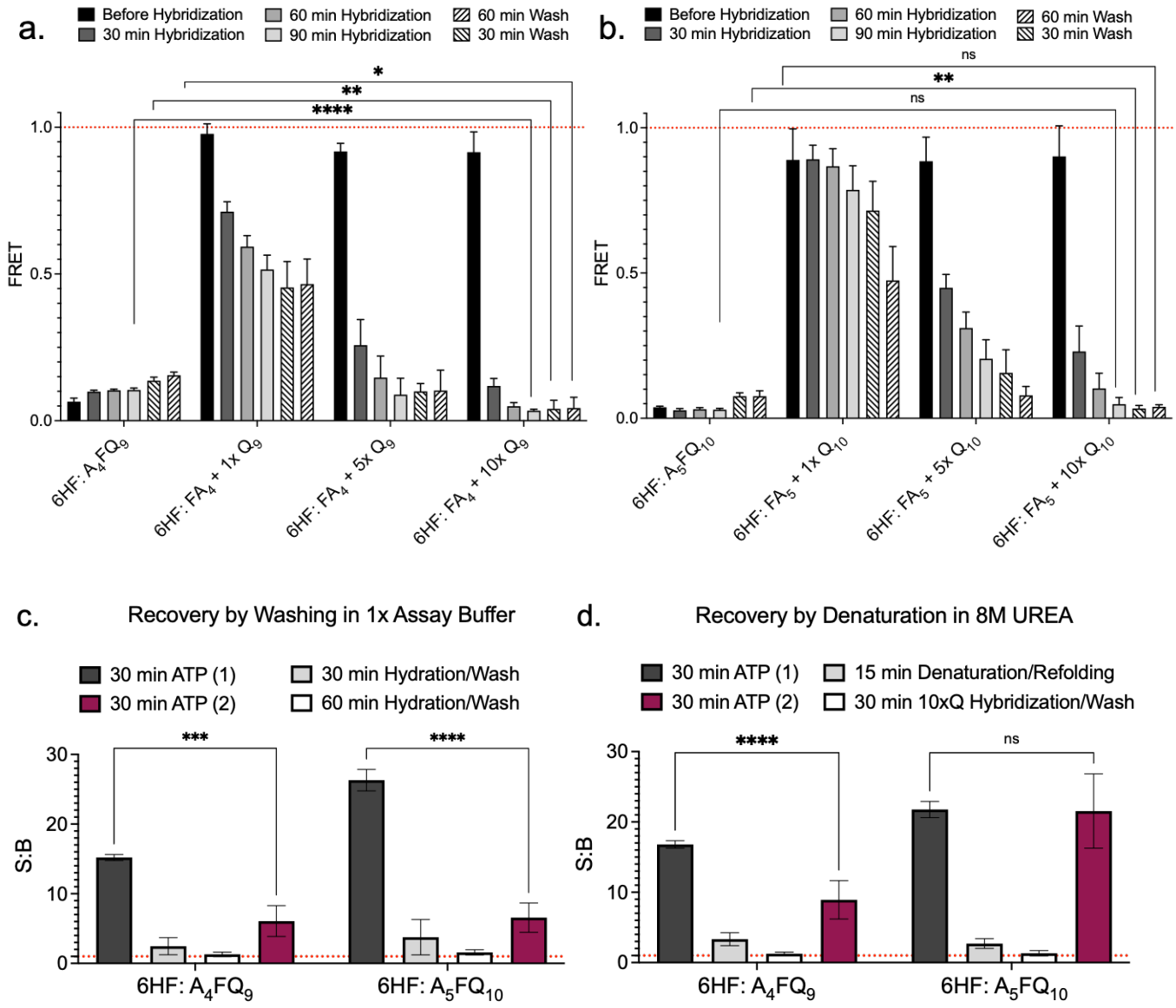

Figure S4.14 Reusability of hydrogel-based aptamer microarray assembled with 9- and 10-bp quencher stems in 6HF hydrogel. Optimization of Q-DNA hybridization to hydrogel-encapsulated fluorescent aptamer constructs and *in situ* assembly and stability against washing of (a) 9-bp (HF:FA_4 + Q_9) or (b) 10-bp (HF:FA_5 + Q_9) duplexed aptamers relative to encapsulated aptamer constructs (HF:AFQ). Following initial ATP incubation (1), the sensor was regenerated by (c) washing in 1xAssay buffer or (d) denaturing in 8 M urea accompanied by Q-DNA re-hybridization, with performance summarized by the S:B ratios measured after each step and following another exposure to ATP (2).

4.6.14. Hydrogel Microarray Aptamer Construct Assembly *via* In-Gel Hybridization of Very Short Q-DNAs (7-nt) to Encapsulated Fluorescent Aptamer Constructs

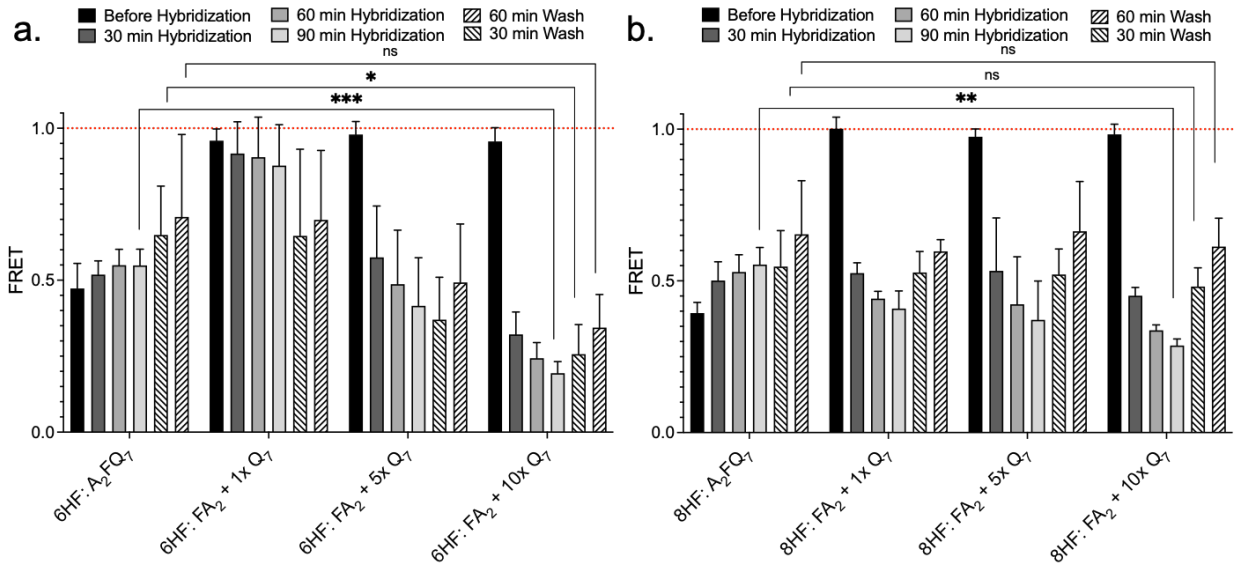

Figure S4.15 Optimization of Q-DNA hybridization to hydrogel-encapsulated fluorescent aptamer constructs and *in situ* assembly and stability against washing of 7-bp quencher stem long aptamer reporters in (a) 6HF and (b) 8HF hydrogel microarrays.

4.6.15. Qualitative Data on Printing Reproducibility

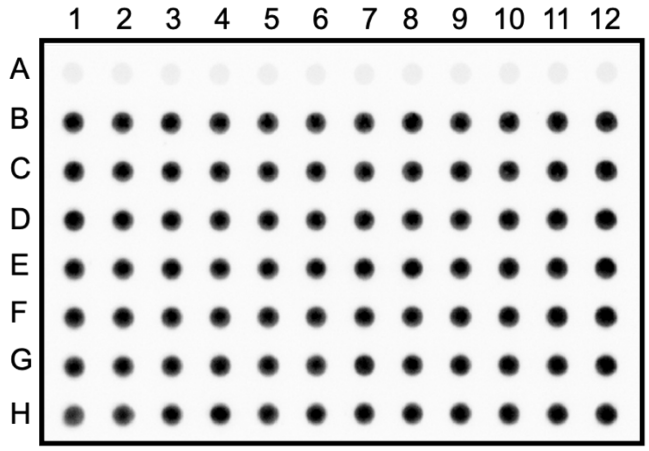

Figure S4.16 Fluorescent scan indicating the spot-to-spot uniformity of a printed hydrogel microarray encapsulating fluorescent aptamer construct (8HF:FA$_5$). Row A represents a hydrogel film (HF, blank) excluding the aptamer complex while rows B:H represent the printed hydrogel film encapsulating the fluorescent aptamer complex.

4.6.16. Supporting References

(1) Nutiu, R.; Li, Y. Structure-Switching Signaling Aptamers. *J. Am. Chem. Soc.* **2003**, *125* (16), 4771–4778. https://doi.org/10.1021/ja028962o.

(2) Carrasquilla, C.; Kapteyn, E.; Li, Y.; Brennan, J. D. Sol-Gel-Derived Biohybrid Materials Incorporating Long-Chain DNA Aptamers. *Angew. Chem. Int. Ed.* **2017**, *56* (36), 10686–10690. https://doi.org/10.1002/anie.201702859.

(3) Huizenga, D. E.; Szostak, J. W. A DNA Aptamer That Binds Adenosine and ATP. *Biochemistry* **1995**, *34* (2), 656–665. https://doi.org/10.1021/bi00002a033.

(4) Smeets, N. M. B.; Bakaic, E.; Patenaude, M.; Hoare, T. Injectable and Tunable Poly(Ethylene Glycol) Analogue Hydrogels Based on Poly(Oligoethylene Glycol Methacrylate). *Chem. Commun.* **2014**, *50* (25), 3306. https://doi.org/10.1039/c3cc48514e.

(5) Smeets, N. M. B.; Bakaic, E.; Patenaude, M.; Hoare, T. Injectable Poly(Oligoethylene Glycol Methacrylate)-Based Hydrogels with Tunable Phase Transition Behaviours: Physicochemical and Biological Responses. *Acta Biomaterialia* **2014**, *10* (10), 4143–4155. https://doi.org/10.1016/j.actbio.2014.05.035.

(6) Pikula, M.; Ali, M. M.; Filipe, C.; Hoare, T. Single-Step Printable Hydrogel Microarray Integrating Long-Chain DNA for the Discriminative and Size-Specific Sensing of Nucleic Acids. *ACS Appl. Mater. Interfaces* **2021**, *13* (2), 2360–2370. https://doi.org/10.1021/acsami.0c21061.

5. Conclusions and Recommendations

In this thesis, nucleic-acid-based molecular-recognition phenomena in hydrogel assemblies for biosensing applications were investigated across a range of potential analyte targets. To this end, a printable nitrocellulose-based hydrazone crosslinked hydrogel microarray was developed to physically entrap an RCA product that was utilized for the high-throughput detection of fluorophore-tagged oligonucleotides. The developed hydrogel technology was subsequently adapted for use in an aptamer-sensing system in which a hydrogel array assembled in microtiter plates was applied for a high-throughput investigation of the thermal stability of the developed hydrogel-encapsulated structure-switching aptamer constructs. In addition, adenosine-binding FRET-based structure-switching aptamer constructs were assembled with varying quencher stem lengths to assess their ability to enhance sensitivity once embedded in the highly hydrophilic polymeric matrix, which can exert a thermodynamic stabilizing effect on short DNA duplexes and thus supports a reduction of the fluorescence background signal while enabling a solution-like ligand binding dynamic response. Finally, the developed hydrogel-based aptamer technology was applied in a nitrocellulose-based microarray format with the aim of fabricating printable, portable, and multiplexed diagnostic devices for the detection of small molecules. The configuration of the aptamer reporters was optimized with respect to the quencher stem length and location vis-à-vis the ligand binding site to further enhance the sensitivity of the assay. Within these broad themes, the main technical contributions of this work are summarized below.

The hydrogel-printed RCA-product microarray described in Chapter 2 enabled size-selective and sequence-specific sensing of small oligonucleotides, with the particular benefit of improving the detection of very short (i.e., 10-nt long) DNA molecules that typically bind with low affinity and thus have low signaling capacity. These results can be primarily attributed to the confined and hydrophilic microenvironment provided by the hydrogel that can improve RCA product immobilization, stabilize the immobilized RCA product against various denaturing agents, and reduce the non-specific adsorption of biomolecules onto the nitrocellulose substrate. Additionally, a co-localization study showed that the long-chain DNA molecules were fully encapsulated inside the hydrogel film and uniformly distributed across each microarray spot, further preventing DNA binding sites from drying out and helping to generate a uniform fluorescence signal upon hybridization. This work is the first to develop DNA hybridization microarrays by entrapping RCA products in printable covalent crosslinked films affixed to a substrate without the need for external gelation initiators or post-gelation processing and using mild synthetic conditions. The developed sensing platform may be used in diagnostic situations in which discrimination between targets with different sizes but the same affinity is necessary to obtain the desired selectivity.

The analysis of the thermal stabilization of the hydrogel-trapped structure-switching aptamers (Chapter 3) revealed another functional benefit of the developed POEGMA hydrogel technology that can directly improve assay sensitivity: the thermodynamic stabilization of short DNA duplexes that enables the use of more ligand-responsive FRET aptamer constructs assembled with shorter quencher stems ($\leq$ 10-nt). By moderately increasing the melting temperature of more responsive quencher stems, hydrogels induce a reduction in background fluorescence, overcoming a major disadvantage of conventional aptamer assemblies. The encapsulated aptamer reporters remained ligand-responsive while maintaining signaling magnitudes and kinetics similar to hydrogel-free systems, with the solution-like, deformable, and swollen hydrogel network facilitating the quick distribution of analytes and aptamer renaturation upon molecular recognition. Furthermore, these functional benefits enable the use of low volumes of analytes and accurate dose-response curve quantification, suggesting that the utilized hydrogel configuration does not restrict affinity interactions despite keeping the binding sites entrapped. Compared to previously reported hydrogel technologies for immobilizing aptamers, the developed POEGMA system offers the benefits of

easier fabrication, avoiding the need for complex aptamer anchoring, and significantly reduced DNA consumption, thus establishing it as a simple and low-cost option in the design of small-molecule diagnostic devices.

The translation of the hydrogel-based aptamer technology described in Chapter 3 to a nitrocellulose-based printable microarray format (Chapter 4) created the possibility of fabricating portable, miniaturized devices for the high-throughput and sensitive detection of small molecules. The ligand-binding affinity constant can be modulated to levels comparable to the native aptamer by optimizing the hydrogel concentration, the surface density of the immobilized aptamer constructs, and/or the configuration of the aptamer constructs. Reduced affinity is a common issue following the translation of DNA aptamers from a native to a FRET-based signaling state; however, by truncating the quencher stem to 7-bp, rationally positioning it to hybridize with a single base of a ligand-binding site, and stabilizing it within an optimally concentrated hydrogel assembly under moderate aptamer surface density, high-affinity interactions could be maintained. Moreover, the hydrogel microarray enabled high immobilization capacity, accurate dose-response curve determination, protection against nucleolytic denaturation, and effective ligand detection in concentrated human serum. Significantly, the hydrogel microarray is also demonstrated to be amenable to fabrication by printing, representing a scalable process for manufacturing of the microarrays. The additional demonstrated capacity of the aptamer construct to be assembled *via* the in-gel hybridization of quencher-tagged oligonucleotides adds further versatility to the sensor, unlocking the potential for high-throughput screening of optimal signaling oligonucleotides in the design of structure-switching aptamer constructs.

The work presented herein is the first documented example of a miniaturized and printable high-throughput device that provides effective and facile immobilization of both long-chain DNA-sensing units and functional nucleic acids and improves the affinity and sensitivity of encapsulated structure-switching DNA aptamers based on the moderate thermal stabilization and effective aptamer configuration supported by the hydrophilic microenvironment. Ultimately, the results strongly suggest that the developed hydrogel microarray possesses great potential for practical sensor applications.

Moving forward, the developed hydrogel-based DNA hybridization microarray can be validated in more specific applications by adapting it to detect micro-RNA molecules (miRNA), which have been identified as important biomarkers for a variety of pathological conditions such as cancer and cardiovascular and inflammatory diseases.[1,2] miRNAs are involved in disease origin and development, and the ability to identify their altered expression could aid in early detection, classification, and predictive diagnostics.[1] As such, there has been a surge in research aimed at developing sensitive, specific, and cost-effective miRNA-detection methods that are also label- and amplification-free.[3,4] One issue with the detection of miRNA, which are typically between 19- and 23-nt long, is the existence of their longer precursor (*i.e.*, premature miRNA),[5] which usually contains 60-70-nt. Since the miRNA sequence is present in premature miRNA precursors,[1] detection methods that do not include size selection prior to detection are unable to avoid signal interference from the pre-miRNA and thus may falsely report higher miRNA values in samples containing different RNA forms.[5] Fu *et al.*[6] recently attempted to address this issue by integrating a FRET-based molecular beacon into a DNA molecular sieve (DNA-nanocage) constructed from a cavity-tunable nucleic acid framework. By using an appropriately-sized DNA-nanocage, the authors were able to successfully distinguish miRNA molecules from their longer analogues with the desired specificity while also avoiding nuclease-degradation and non-specific protein binding. Physically entrapping Fu *et al.*'s molecular beacon probe into the printable hydrogel microarray developed in Chapter 2 should enable size-selectivity by controlling the hydrogel pore size while also minimizing the amount of DNA consumed during sensor construction, hypothesized to enable accurate molecular

recognition in a high-throughput fashion. Moreover, given hydrogel's proven thermal stabilizing effect on short DNA duplexes, it is expected that molecular beacon probes will be characterized by lower fluorescence background, reinforced hybridizing stems to govern higher signaling magnitude, and better discrimination towards perfectly matched targets relative to imperfect miRNA isoforms. In addition, the proposed strategy would also be cost-effective and relatively facile compared to conventional miRNA-detection methods such as Northern Blotting[1], reverse-transcription quantitative PCR (RT-qPCR), or methods based on advanced molecular beacon designs combined with locked nucleic acids (MB-LNA)[4] or hybridization chain reactions (HCR).[7]

The integration of concatemeric DNA aptamers based on RCA product could further improve the sensitivity of hydrogel-based aptamer sensors, as several reports have demonstrated that amplified functional nucleic acids anchored on surfaces retain their molecular recognition capacity (based on a structure-switching model) while also exhibiting enhanced sensitivity.[8,9] The thermal stabilization of short DNA duplexes, better RCA spot-to-spot uniformity, and higher retention of sensing units provided by the POEGMA hydrogel material would enable the synthesis of more ligand-responsive aptamer constructs that are also amenable to printable fabrication and facile application. The fabrication of such sensors could be conducted following the protocols detailed in Chapters 2 or 4, in which aldehyde-functionalized precursor and hydrazide-functionalized precursor co-dissolved with RCA product functionalized with ATP DNA aptamer binding motifs would be sequentially deposited onto the nitrocellulose substrate using a layer-by-layer technique and assembled into a structure-switching construct utilizing very short quencher stems (≤ 9-nt). Alternatively, the protocols described in Chapters 2 and 4 could be employed to hybridize quencher-tagged oligonucleotides into hydrogel microarrays containing fluorescent RCA concatemers to explore the possibility of assembling even more responsive aptamer reporters in a high-throughput setting.

In addition to DNA aptamers, the integration of RNA aptamers into hydrogel film microarrays for biosensing applications can be explored. Although RNA aptamers exhibit excellent binding affinity and specificity, they have limited practical applicability due to their poor chemical stability and susceptibility to RNase degradation.[10] Li's lab developed a general approach to creating structure-switching reporters from RNA aptamers[10,11] that were subsequently entrapped in sol-gel-derived materials.[12,13] The sol-gel-entrapped RNA aptamers not only retained their functionality but they were also protected against nuclease and chemical degradation, thereby providing the long-term stability that is so critical for surface biosensors. However, the translation of this proof-of-concept study into a more clinically and commercially relevant format (*e.g.,* interfacial thin-film coating and microarrays) remains a challenge, as the nature of the sol-gel material causes problems for the printing process and automatic dispensing systems.[14] The protocol for integrating hydrogel films detailed in Chapter 4 may offer a solution to this issue, as the functional benefits, printability, and good immobilizing ability of POEGMA hydrogel can provide higher sensitivity, faster ligand response, and the consumption of lower volumes of analytes compared to sol-gel technology.

Finally, research exploring the incorporation of other types of functional nucleic acids—particularly DNAzymes—able to support colorimetric read outs and improve the commercialization potential of developed hydrogel technology is strongly encouraged. One strategy for producing a DNA-based colorimetric sensor that can provide equipment-free analysis is the incorporation of horseradish-peroxidase-mimicking DNAzymes.[15] The ability to couple colorimetric DNAzyme with DNA or RNA

[1] **NB** is the technique used for visualizing miRNA expression of all sizes (long primal miRNA and mature forms). This technique is based on the size-separation of RNA samples using denaturing gel-electrophoresis and the hybridization of radio-labeled nucleic acid probes complementary to the RNA-targets.

aptamers and RCA reactions to produce paper-based sensors makes it a good fit for in integration into the hydrogel system developed in this thesis. Indeed, adapting these elements would enable the detection and interpretation of the signal using the naked eye while significantly broadening the scope of prospective applications of POEGMA hydrogel technology.

5.1. References

(1) Dave, V. P.; Ngo, T. A.; Pernestig, A.-K.; Tilevik, D.; Kant, K.; Nguyen, T.; Wolff, A.; Bang, D. D. MicroRNA Amplification and Detection Technologies: Opportunities and Challenges for Point of Care Diagnostics. *Lab Invest* **2019**, *99* (4), 452–469. https://doi.org/10.1038/s41374-018-0143-3.

(2) Dong, H.; Lei, J.; Ding, L.; Wen, Y.; Ju, H.; Zhang, X. MicroRNA: Function, Detection, and Bioanalysis. *Chem. Rev.* **2013**, *113* (8), 6207–6233. https://doi.org/10.1021/cr300362f.

(3) Bidar, N.; Oroojalian, F.; Baradaran, B.; Eyvazi, S.; Amini, M.; Jebelli, A.; Hosseini, S. S.; Pashazadeh-Panahi, P.; Mokhtarzadeh, A.; de la Guardia, M. Monitoring of microRNA Using Molecular Beacons Approaches: Recent Advances. *TrAC Trends in Analytical Chemistry* **2020**, *131*, 116021. https://doi.org/10.1016/j.trac.2020.116021.

(4) James, A. M.; Baker, M. B.; Bao, G.; Searles, C. D. MicroRNA Detection Using a Double Molecular Beacon Approach: Distinguishing Between miRNA and Pre-miRNA. *Theranostics* **2017**, *7* (3), 634–646. https://doi.org/10.7150/thno.16840.

(5) Chugh, P.; Dittmer, D. P. Potential Pitfalls in microRNA Profiling: Potential Pitfalls in microRNA Profiling. *WIREs RNA* **2012**, *3* (5), 601–616. https://doi.org/10.1002/wrna.1120.

(6) Fu, X.; Ke, G.; Peng, F.; Hu, X.; Li, J.; Shi, Y.; Kong, G.; Zhang, X.-B.; Tan, W. Size-Selective Molecular Recognition Based on a Confined DNA Molecular Sieve Using Cavity-Tunable Framework Nucleic Acids. *Nat Commun* **2020**, *11* (1), 1518. https://doi.org/10.1038/s41467-020-15297-7.

(7) Yang, F.; Cheng, Y.; Cao, Y.; Dong, H.; Lu, H.; Zhang, K.; Meng, X.; Liu, C.; Zhang, X. Sensitively Distinguishing Intracellular Precursor and Mature microRNA Abundance. *Chem. Sci.* **2019**, *10* (6), 1709–1715. https://doi.org/10.1039/C8SC03305F.

(8) Liu, M.; Zhang, Q.; Kannan, B.; Botton, G. A.; Yang, J.; Soleymani, L.; Brennan, J. D.; Li, Y. Self-Assembled Functional DNA Superstructures as High-Density and Versatile Recognition Elements for Printed Paper Sensors. *Angew Chem Int Ed* **2018**, *57* (38), 12440–12443. https://doi.org/10.1002/anie.201806489.

(9) Carrasquilla, C.; Little, J. R. L.; Li, Y.; Brennan, J. D. Patterned Paper Sensors Printed with Long-Chain DNA Aptamers. *Chem. Eur. J.* **2015**, *21* (20), 7369–7373. https://doi.org/10.1002/chem.201500949.

(10) Lau, P. S.; Coombes, B. K.; Li, Y. A General Approach to the Construction of Structure-Switching Reporters from RNA Aptamers. *Angew Chem Int Ed* **2010**, *49* (43), 7938–7942. https://doi.org/10.1002/anie.201002621.

(11) Lau, P. S.; Lai, C. K.; Li, Y. Quality Control Certification of RNA Aptamer-Based Detection. *ChemBioChem* **2013**, *14* (8), 987–992. https://doi.org/10.1002/cbic.201300134.

(12) Carrasquilla, C.; Lau, P. S.; Li, Y.; Brennan, J. D. Stabilizing Structure-Switching Signaling RNA Aptamers by Entrapment in Sol–Gel Derived Materials for Solid-Phase Assays. *J. Am. Chem. Soc.* **2012**, *134* (26), 10998–11005. https://doi.org/10.1021/ja304064a.

(13) Hui, C. Y.; Lau, P. S.; Li, Y.; Brennan, J. D. Investigation of RNA Structure-Switching Aptamers in Tunable Sol–Gel-Derived Materials. *J Sol-Gel Sci Technol* **2019**, *89* (1), 234–243. https://doi.org/10.1007/s10971-018-4588-z.

(14) Li, Y.; Dahhan, O.; Filipe, C. D. M.; Brennan, J. D.; Pelton, R. H. Optimizing Piezoelectric Inkjet Printing of Silica Sols for Biosensor Production. *J Sol-Gel Sci Technol* **2018**, *87* (3), 657–664. https://doi.org/10.1007/s10971-018-4762-3.

(15) Hui, C. Y.; Liu, M.; Li, Y.; Brennan, J. D. A Paper Sensor Printed with Multifunctional Bio/Nano Materials. *Angew. Chem. Int. Ed.* **2018**, *57* (17), 4549–4553. https://doi.org/10.1002/anie.201712903.